

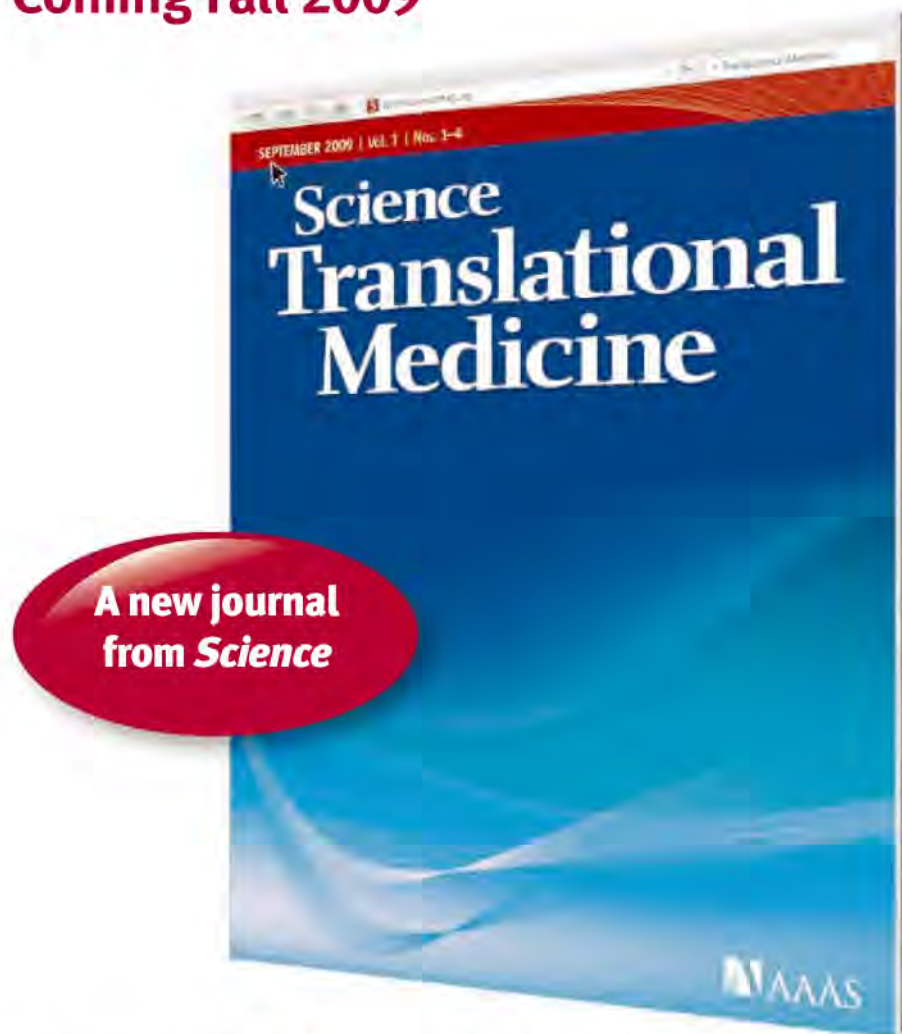
Science

16 January 2009 | \$10

International
Year of Astronomy

 AAAS

Coming Fall 2009



Integrating clinical medicine and science

AAAS, publisher of the world's leading general science journal, *Science*, is launching a new journal of translational medicine in the fall of 2009.

The journal's mission is to facilitate communication and cooperation among basic and preclinical researchers, physician scientists, regulators, policy makers, industry, and funding agencies in order to improve health around the world. It will present original, science-based peer-reviewed research that successfully moves the field closer to helping patients. Perspectives and reviews from basic and clinical viewpoints along with discussions about research funding and regulatory issues will be included.

With *Science Translational Medicine*, you can expect the same level of breakthrough research that is the hallmark of the journal *Science*. The journal will be edited by Katrina L. Kelner, Ph.D., and an international advisory group of clinician scientists and other experts.

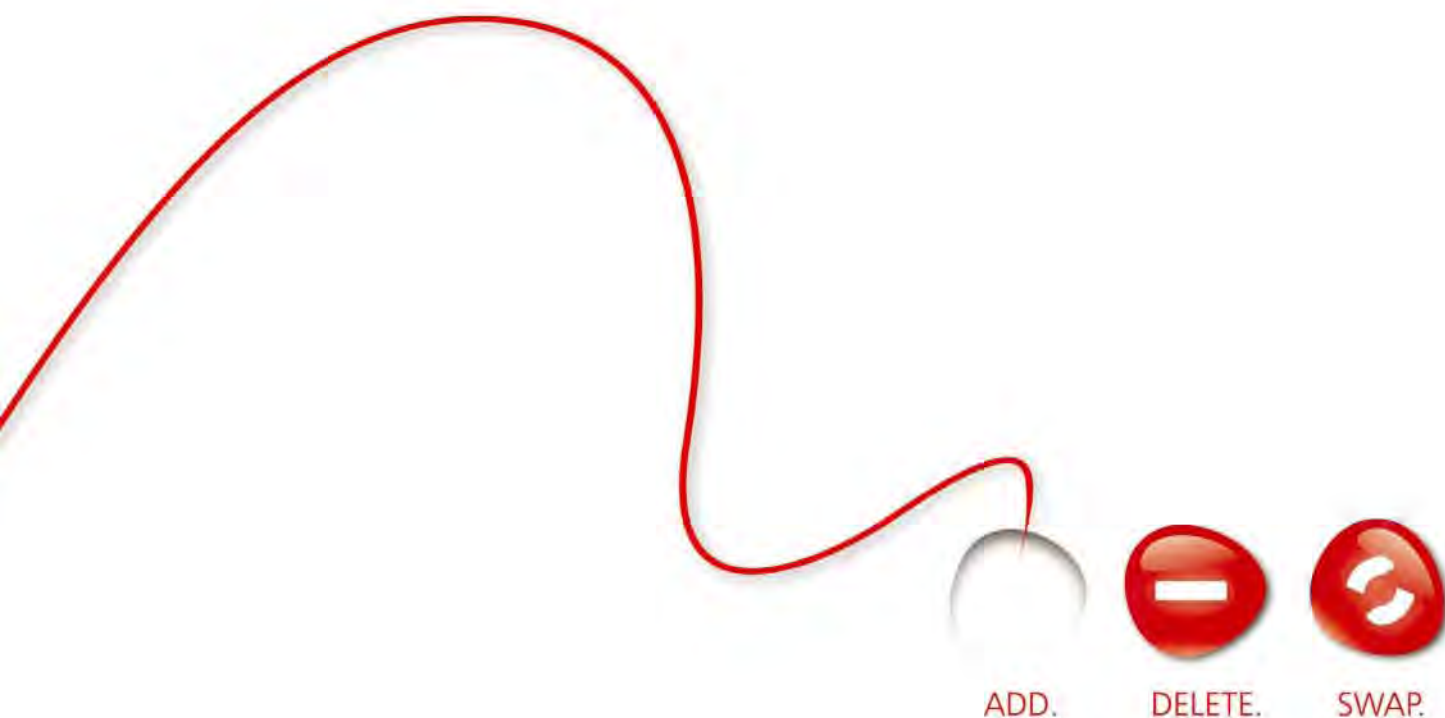
The monthly print edition, to be published 12 times a year, will be a compilation of the weekly online edition and sold exclusively to subscribers of the online edition. The print issues will include a selection of the online content and all primary peer-reviewed research. More subscription details will be available as the launch date approaches. For more information contact the editor and product manager at scitranslationalmed@aaas.org. For information on site licenses and subscriptions to print, please contact sciencemedicine@aaas.org.



YOUR NAME



Sigma and Sigma-Aldrich are registered trademarks belonging to Sigma-Aldrich Co. and its affiliate Sigma-Aldrich Biotechnology, L.P.
CompoZr is a trademark of Sigma-Aldrich Co. and its affiliate Sigma-Aldrich Biotechnology, L.P.



EDIT FOR THE BETTER.

**What would you do if you had the ability to craft
the future of genomic research?**

Now, it's all possible.

It's here. Introducing **CompoZr™ ZFN technology**, a breakthrough that enables simple and efficient genomic editing—exclusively from Sigma Life Science. Zinc Finger Nuclease (ZFN) technology, optimized over the years by Sangamo Biosciences, allows easy creation of novel cell lines and model organisms with precise and heritable gene additions, deletions or modifications. A proven technology with unimaginable potential.

*The future of genomic research is at your fingertips.
Discover ZFN technology at **compozrzfn.com***

SIGMA-ALDRICH®

Coming Fall 2009



Integrating clinical medicine and science

AAAS, publisher of the world's leading general science journal, *Science*, is launching a new journal of translational medicine in the fall of 2009.

The journal's mission is to facilitate communication and cooperation among basic and preclinical researchers, physician scientists, regulators, policy makers, industry, and funding agencies in order to improve health around the world. It will present original, science-based peer-reviewed research that successfully moves the field closer to helping patients. Perspectives and reviews from basic and clinical viewpoints along with discussions about research funding and regulatory issues will be included.

With *Science Translational Medicine*, you can expect the same level of breakthrough research that is the hallmark of the journal *Science*. The journal will be edited by Katrina L. Kelner, Ph.D., and an international advisory group of clinician scientists and other experts.

The monthly print edition, to be published 12 times a year, will be a compilation of the weekly online edition and sold exclusively to subscribers of the online edition. The print issues will include a selection of the online content and all primary peer-reviewed research. More subscription details will be available as the launch date approaches. For more information contact the editor and product manager at scitranslationalmed@aaas.org. For information on site licenses and subscriptions to print, please contact sciencemedicine@aaas.org.



Biacore systems



from inspiration ...to publication

Highest quality, information-rich interaction data from Biacore™ systems deepen your understanding of molecular mechanisms and interaction pathways and enable you to add function to structure.

Select the perfect solution for your application and draw conclusions with confidence – from the company that continues to set the standard for label-free protein interaction analysis.



Biacore T100
unmatched performance



Biacore X100
ready to run research system



Biacore Flexchip
array-based comparative profiling



www.biacore.com



imagination at work

EDITORIAL

- 309 **Pondering Astronomy in 2009**
Martin Rees
 >> *News Focus* section p. 326

NEWS OF THE WEEK

- 318 **Science Groups Emphasize Jobs in Push for More Research Funding**
 319 **Export Controls: Current System Hampers U.S. Innovation, Says Panel**
 321 **Can an Ecologist Push NOAA Up the Food Chain?**
 322 **A Human Trigger for the Great Quake of Sichuan?**
 323 **Waltzing Quasars Provide Signpost to Merging Galaxies**
 323 **Do Black Holes Seed the Formation of Galaxies?**
 324 **Infection Study Worries Farmers, Bird Lovers**
 324 **CDC's Gerberding Makes an Early Exit**
 325 **Tracking CO₂'s Comings and Goings From Space**

NEWS FOCUS

INTERNATIONAL YEAR OF ASTRONOMY

- 326 **Astronomy's Greatest Hits**
 330 **A Brief History of the Telescope**
 332 **Astronomy Hits the Big Time**
 >> *Editorial* p. 309; *Science Podcast*

LETTERS

- 337 **Grants on the Run**
S. Jeyaseelan
Fishing for More Effective Incentives
T. Smith et al.
Diverse Fisheries Require Diverse Solutions
N. C. Ban et al.
Response
J. Lynham et al.
A Question of Ethics
J. Boldt and O. Müller

Response
E. Parens et al.

CORRECTIONS AND CLARIFICATIONS

BOOKS ET AL.

- 340 **Insatiable Curiosity**
H. Nowotny, reviewed by E. J. Hackett
 341 **Browsings**

POLICY FORUM

- 342 **Racing Forward: The Genomics and Personalized Medicine Act**
S. S.-J. Lee and A. Mudaliar
 >> *Science Podcast*

PERSPECTIVES

- 343 **Animal Function at the Heart (and Gut) of Oceanography**
B. A. Seibel and H. M. Dierssen
 >> *Report* p. 359
 344 **Beyond Biomineralization**
W. Kunz and M. Kellermeier
 >> *Report* p. 362
 346 **New and Ancient Trace Makers**
S. Bengtson and B. Rasmussen
 347 **The Structure of Change**
C. A. M. Semple and M. S. Taylor
 >> *Report* p. 401
 348 **Excitons Surf Along Conjugated Polymer Chains**
J.-L. Brédas and R. Silbey
 >> *Report* p. 369
 350 **Origin of Species in Overdrive**
J. H. Willis
 >> *Reports* pp. 373 and 376

BREVIA

- 352 **Programmed Assembly of DNA-Coated Nanowire Devices**
T. J. Morrow et al.
 Electric fields help direct metal nanowires coated with different DNA sequences into specific positions on a substrate.

CONTENTS continued >>



page 326



page 340



COVER

Hot dust clouds in the center of the Milky Way, photographed by the Infrared Array Camera (IRAC) aboard the Spitzer Space Telescope. The International Year of Astronomy gets under way this week with opening ceremonies at UNESCO headquarters in Paris; *Science* marks the occasion with a special News Focus section beginning on page 326.

Image: NASA/JPL-Caltech/S. Stolovy (Spitzer Science Center/Caltech)

DEPARTMENTS

- 307 This Week in *Science*
 310 Editors' Choice
 312 *Science* Staff
 315 Random Samples
 317 Newsmakers
 405 New Products
 406 *Science* Careers

Automated sample and assay technologies by QIAGEN

Free up your time



Automated solutions from sample to result:

- The widest choice of sample processing protocols
- Low-, medium-, and high-throughput automation
- Leading solutions for molecular diagnostics
- Plug-and-play automated sample preparation
- Quantitative, real-time PCR detection
- Automated analysis of DNA fragments and RNA
- High-resolution sequence-based DNA detection and quantification
- HPV testing

Making improvements in life possible — www.qiagen.com



REPORTS

353 Dust Formation in a Galaxy with Primitive Abundances

G. C. Sloan et al.

A carbon star lacking many heavy elements produces abundant dust, perhaps explaining the origin of dust in the early universe.

356 Early Lunar Magnetism

I. Garrick-Bethell et al.

Remnant magnetism in minerals in an unshocked Apollo sample implies that the Moon had a molten core 4.2 billion years ago.

359 Contribution of Fish to the Marine Inorganic Carbon Cycle

R. W. Wilson et al.

Fish excrete large amounts of calcium carbonate and thus influence the carbon cycle in the ocean.

>> Perspective p. 343

362 Morphogenesis of Self-Assembled Nanocrystalline Materials of Barium Carbonate and Silica

J. M. García-Ruiz et al.

The growth of inorganic crystals in a chemically coupled system produces curved morphologies like those found in biology.

>> Perspective p. 344

366 Broadband Ground-Plane Cloak

R. Liu et al.

An automated design process arranges thousands of metamaterial components to cloak an object on a metal surface.

369 Coherent Intrachain Energy Migration in a Conjugated Polymer at Room Temperature

E. Collini and G. D. Scholes

Extended conformations of polymers in solution foster rapid energy transport along individual chains, but not between chains.

>> Perspective p. 348

373 A Mouse Speciation Gene Encodes a Meiotic Histone H3 Methyltransferase

O. Mihola et al.

A gene responsible for sterility in the offspring of two mouse species, and therefore important in speciation, regulates gene expression via methylation in chromatin.

>> Perspective p. 350

376 A Single Gene Causes Both Male Sterility and Segregation Distortion in *Drosophila* Hybrids

N. Phadnis and H. A. Orr

A *Drosophila* gene that causes sterility in the offspring of two species and may be important for speciation causes increased transmission of itself to progeny.

>> Perspective p. 350

379 The Dynamics and Time Scale of Ongoing Genomic Erosion in Symbiotic Bacteria

N. A. Moran et al.

Comparisons of strains of obligate symbionts reveal stepwise evolutionary changes leading to gene inactivation and DNA loss.

382 A Polymorphism in *npr-1* Is a Behavioral Determinant of Pathogen Susceptibility in *C. elegans*

K. C. Reddy et al.

Mutations in neuropeptide receptors prevent nematode worms from swimming away to avoid bacterial pathogens.

384 The Structure of Rat Liver Vault at 3.5 Angstrom Resolution

H. Tanaka et al.

The large, ribonucleotide proteins involved in resisting infection have domains that bind to lipid-raft regions of the cell membrane.

388 Draxin, a Repulsive Guidance Protein for Spinal Cord and Forebrain Commissures

S. M. Islam et al.

A protein cue guides the formation of bundles of nerve fibers that connect the cerebral hemispheres.

393 Recombination of Retrotransposon and Exogenous RNA Virus Results in Nonretroviral cDNA Integration

M. B. Geuking et al.

With the help of an endogenous retrovirus, RNA virus sequence can be incorporated into mouse chromosomes.

396 Molecular Mechanisms of HipA-Mediated Multidrug Tolerance and Its Neutralization by HipB

M. A. Schumacher et al.

A persistence factor similar to a eukaryotic kinase regulates bacterial dormancy and contributes to antibiotic resistance in *E. coli*.

401 Chromatin-Associated Periodicity in Genetic Variation Downstream of Transcriptional Start Sites

S. Sasaki et al.

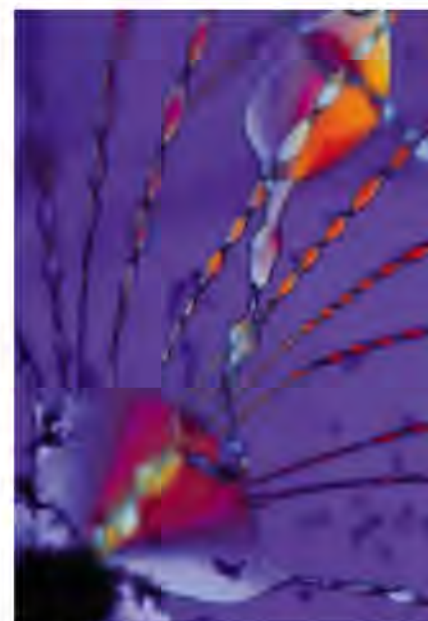
The periodic wrapping of DNA around nucleosomes in chromatin determines a periodic variation in mutation type and frequency around transcription start sites in a fish.

>> Perspective p. 347

CONTENTS continued >>



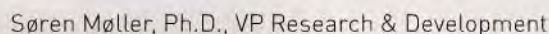
pages 350, 373, & 376



pages 344 & 362



page 388



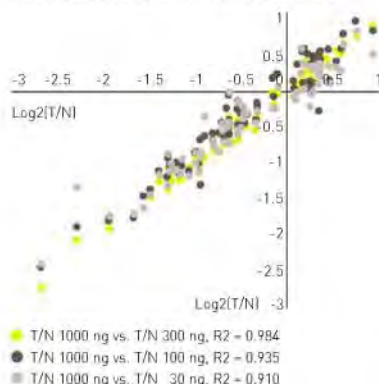
miRCURY LNA™ tools from Exiqon give you the reliability and specificity you need to trust your results. And we've got the data to prove it.



Søren Møller, Ph.D., VP Research & Development

Log2 ratios for tumor vs. normal (oesophagus)
- correlation between various RNA input amounts

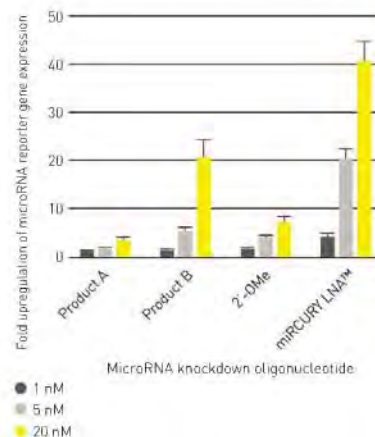
Exiqon's miRCURY LNA™
Arrays produce highly
reliable microRNA profiles
from just 30 ng total RNA.



Learn more at:
exiqon.com/array

Determination of microRNA function

With Exiqon's miRCURY
LNA™ Knockdown
Probes, you can achieve
comprehensive inhibition
of microRNA activity.



Learn more at:
exigon.com/knockdown

Visualization of miR-206 expression in the skeletal precursors of a *Gallus Gallus* embryo.

Learn more at:
exiqon.com/insitu

Figure 1 is a line graph showing the cycle number (Y-axis, ranging from 15 to 45) versus HeLa S3 total RNA concentration (X-axis, ranging from 1 pg to 100 ng). The graph displays the results of a quantitative PCR assay for various primers. The cycle number decreases as the RNA concentration increases. An arrow points to the line for primer 1, which is labeled "Corresponding to RNA from one cell".

With our new miRCURY LNA™ PCR System, your discovery starts from just 10 pg total RNA – you only need a single cell.

Learn more at:
exiqon.com/pcr

Dilution series of 6 different miRCURY LNA™ PCR assays showing accurate quantitation from total RNA amounts equivalent to a single cell.

[Learn more](#)

Visit exigon.com

NEW! view a 3-D animation of LNA™ on exiqon.com

[illegible]

EXIQON
Seek Find Verify

SCIENCEONLINE

SCIENCEEXPRESS

www.scienceexpress.org

The Formation of Massive Star Systems by Accretion

M. R. Krumholz et al.

Numerical simulations show that instabilities can channel gas into growing massive stars despite their high radiation pressure.

>> *Science Podcast*

10.1126/science.1165857

Strong Release of Methane on Mars in Northern Summer 2003

M. J. Mumma et al.

Earth-based spectrometers have detected seasonal variations of methane emissions from certain locations on Mars in 2003.

10.1126/science.1165243

Sensing Chromosome Bi-Oriented Separation by Spatial Separation of Aurora B Kinase from Kinetochore Substrates

D. Liu et al.

The mechanism for sensing tension across chromosome pairs before mitotic separation relies on the distance between enzyme and substrate.

10.1126/science.1167000

Effects of Genetic Perturbation on Seasonal Life History Plasticity

A. M. Wilczek et al.

Interactions among mutation, germination timing, and climate alter flowering patterns in *Arabidopsis*.

10.1126/science.1165826

A Genetic Defect Caused by a Triplet Repeat Expansion in *Arabidopsis thaliana*

S. Sureshkumar et al.

A strain of *Arabidopsis* provides a plant model for the harmful effects of repeat nucleotide expansions in populations.

10.1126/science.1164014

SCIENCENOW

www.sciencenow.org

Highlights From Our Daily News Coverage

The Flashiest Dino of Them All

Researchers find oldest example of feathers used for display.

Are You a Moneymaker? Look at Your Hands

Financial traders with relatively long ring fingers bring home the dough.

The Fastest Way to Change a Species: Start Eating It

Human hunting alters organisms' size and breeding schedule three times faster than natural forces.

SCIENCE SIGNALING

www.sciencesignaling.org

The Signal Transduction Knowledge Environment

PERSPECTIVE: Growth and Patterning in the Limb—Signaling Gradients Make the Decision

Y. Yang

Signaling gradients coordinately regulate proliferation and cell fate determination in the developing limb.

PODCAST

J. D. Scott et al.

The scaffold protein MAKAP localizes factors important for the cellular response to hypoxia.

NETWATCH: Cytoscape

Cytoscape is an expandable, open-source network analysis software platform; in Bioinformatics Resources.

NETWATCH: The Human Protein Atlas

An antibody-based proteomics database provides tissue-specific expression data for a growing list of human proteins; in Protein Databases.

NETWATCH: Science Webinar Series

Watch live and archived online seminars sponsored by Science/AAAS; in Web Broadcasts.

SCIENCE CAREERS

www.sciencereers.org/career_development

Free Career Resources For Scientists

Tooling Up: The Job Seeker's Lexicon

D. Jensen

Job seekers need to interpret the jargon used in job ads and interviews.

Astronomer Finds Rewards in Outreach

L. Laursen

Cameron Hummels is a student ambassador representing NASA during the International Year of Astronomy.

>> *Editorial p. 309*

SCIENCEPODCAST

www.sciencemag.org/multimedia/podcast

Free Weekly Show

Download the 16 January *Science* Podcast to hear about how massive stars may form, setting an agenda for personalized medicine, the culture of astronomy, and more.

ORIGINSBLOG

blogs.sciencemag.org/origins

A History Of Beginnings

SCIENCEINSIDER

blogs.sciencemag.org/scienceinsider

Science Policy News And Analysis



SCIENCE SIGNALING

Limb formation.



SCIENCE CAREERS

Reaching out for NASA.

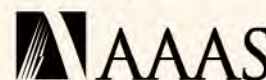


SCIENCENOW

Fashion statement.

SCIENCE (ISSN 0036-8075) is published weekly on Friday, except the last week in December, by the American Association for the Advancement of Science, 1200 New York Avenue, NW, Washington, DC 20005. Periodicals Mail postage (publication No. 484460) paid at Washington, DC, and additional mailing offices. Copyright © 2009 by the American Association for the Advancement of Science. The title SCIENCE is a registered trademark of the AAAS. Domestic individual membership and subscription (51 issues): \$146 (\$74 allocated to subscription). Domestic institutional subscription (51 issues): \$835; Foreign postage extra: Mexico, Caribbean (surface mail) \$55; other countries (air assist delivery) \$85. First class, airmail, student, and emeritus rates on request. Canadian rates with GST available upon request. GST #1254 88122. Publications Mail Agreement Number 1069624. Printed in the U.S.A.

Change of address: Allow 4 weeks, giving old and new addresses and 8-digit account number. Postmaster: Send change of address to AAAS, P.O. Box 96178, Washington, DC 20090-6178. Single-copy sales: \$10.00 current issue, \$15.00 back issue prepaid includes surface postage; bulk rates on request. Authorization to photocopy material for internal or personal use under circumstances not falling within the fair use provisions of the Copyright Act is granted by AAAS to libraries and other users registered with the Copyright Clearance Center (CCC) Transactional Reporting Service, provided that \$20.00 per article is paid directly to CCC, 222 Rosewood Drive, Danvers, MA 01923. The identification code for Science is 0036-8075. Science is indexed in the Reader's Guide to Periodical Literature and in several specialized indexes.

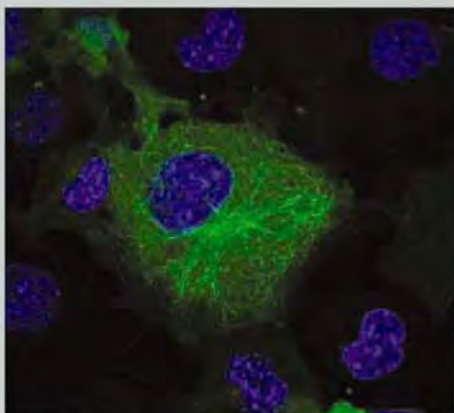


ADVANCING SCIENCE. SERVING SOCIETY

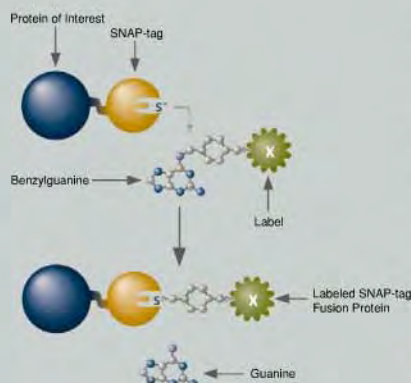
INFINITE POSSIBILITIES

Cellular Imaging & Analysis

NEB introduces SNAP-tag™ and CLIP-tag™ protein labeling systems. These innovative technologies provide simplicity and extraordinary versatility to the imaging of mammalian proteins *in vivo*, and to protein capture experiments *in vitro*. The creation of a single genetic construct generates a fusion protein which, when covalently attached to a variety of fluorophores, biotin, or beads provides a powerful tool for studying the role of proteins in living and fixed cells.



Live COS-7 cells transiently transfected with pSNAPm-Tubulinβ. Cells were labeled with SNAP-Cell TMR-Star (green pseudocolor) for 30 minutes and counterstained with Hoechst 33342 (blue) for nuclei.



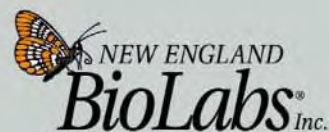
SNAP-tag Technology: SNAP-tag (gold) fused to the protein of interest (blue) self labels releasing guanine.

Advantages:

Versatile - Compatible systems enable dual labeling

Flexible - Multiple fluorophores allow for choice & flexibility

Innovative - A range of applications is possible with a single construct



CLONING & MAPPING

DNA AMPLIFICATION
& PCR

RNA ANALYSIS

PROTEIN EXPRESSION
& ANALYSIS

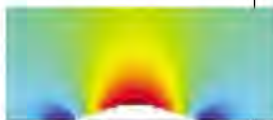
GENE EXPRESSION
& CELLULAR ANALYSIS

Galactic Dust

Dust is detected in galaxies as far back as 870 million years after the Big Bang. How the universe became dusty at such early times is a matter of debate. Carbon stars are an important source of dust in the local universe, but their contribution is less clear in the early universe, where supernovae are thought to dominate the production of dust. **Sloan *et al.*** (p. 353) used data from the Spitzer Telescope to study a nearby star that resembles what carbon stars would look like in the early universe. Despite containing fewer heavy elements than the Sun, this star is producing dust, showing that its primordial composition is not an obstacle to dust production.

Seeing Nothing on the Surface

Transformation optics provides a recipe to manipulate Maxwell's equations, and, when used in conjunction with metamaterials, provides the possibility of having light do "tricks" that cannot be achieved with naturally available materials. One such application is cloaking, where light is coaxed around a certain region, with an object placed within that region being concealed from view. **Liu *et al.***



(p. 366) demonstrate production of a cloak for an object placed on a metal surface. The metamaterial cloak was constructed from thousands of individual units of anisotropic, nonresonant metamaterial elements, each designed and fabricated by an automated process. A successful cloak was fabricated that was operational over a broad range of frequencies.

"Missing" Carbonate Source Found

Most of the calcium carbonate production in the oceans usually is attributed to marine plankton, specifically the coccolithophores and foraminifera. **Wilson *et al.*** (p. 359; see the Perspective by **Seibel and Dierssen**) reveal that another very important source has been overlooked: teleost fish. These fish—the ones with bony skeletons—produce large quantities of calcium carbonate in their guts as an osmoregulatory response to their continuous ingestion of calcium- and magnesium-rich seawater, which they then excrete as waste. This calcium carbonate, richer in magne-

Vaults in View >>

An intriguing but poorly understood structure, broadly distributed in eukaryotic cells, is a large ribonucleoprotein particle termed a vault—so named because electron microscopy revealed a complex morphology resembling the multiple arches of cathedral vaults. Now **Tanaka *et al.*** (p. 384) report the structure of the rat liver vault that shows how the cage-like structure is assembled from 78 subunits with 39-fold dihedral symmetry. One domain has structural similarity to a lipid-raft binding domain, consistent with a previous finding that vaults are recruited to lipid rafts where they may play a role in pathogen clearance.



sium than that produced by plankton and thus more soluble, may constitute more than a quarter of the marine carbonate budget, and could be a missing piece in the ocean's carbonate budget that explains many of the puzzling aspects surrounding the distribution of carbonate in the upper 1000 meters of the ocean.

Unshocked Apollo

Although many of the rocks collected from the Moon during the Apollo missions have a magnetic signature, whether the magnetic fields were produced during impacts or are intrinsic to the Moon has been uncertain. **Garrick-Bethell *et al.*** (p. 356) have analyzed the oldest known unshocked Apollo sample, which dates to about 4.2 billion years ago. Their analysis required reconstructing the temperature history of the sample and associating specific remnant magnetic signatures in different minerals with that history. The data imply that there was a strong, persistent magnetic field at that time, which would most likely have been produced by a con-
ducting iron core in the Moon.

Forming Inorganic Biomorphs

In the growth of crystals from a solution of barium or strontium carbonate in the presence of silica, there is a chemical coupling between the for-

mation carbonate and the formation of silica. This coupling causes pH oscillations at the growth front and wavelike alternating precipitation of the two species. **García-Ruiz *et al.*** (p. 362; see the Perspective by **Kunz and Kellermeier**) track these oscillations and observe a variety of stunning curved morphologies, termed "biomorphs." All of these complex inorganic forms emanate initially from a typical twinned pseudohexagonal witherite crystal that experiences noncrystallographic branching due to crystal growth poisoning by silica species. This observed complexity may mimic the growth of certain primitive organisms.

Gene Genie

Few speciation genes have been identified and those that have, appear to be involved in the reinforcement processes that occur during the later stages of speciation. **Phadnis and Orr** (p. 376, published online 11 December; see the Perspective by **Willis**) identify a speciation gene that causes reproductive isolation between populations of *Drosophila pseudoobscura* in the United States and Colombia. This gene, named *Overdrive*, causes hybrid sterility between two closely related subspecies of *Drosophila* and also causes hybrid segregation distortion—a bias in Mendelian segregation that favors transmission of the distorter gene to progeny. Thus, genetic conflict may be an important evolutionary force in speciation.

Continued on page 308



SETTING THE GOLD STANDARD IN DISCOVERY CHEMISTRY

PORTFOLIO

- 700,000 Screening Compounds
- Discovery chemistry research services

EXPERIENCE

- 15 years excellence in chemistry
- Top tier chemists: lead discovery libraries & med chem support

SUCCESS

- 400 international clients: biotech industry & academic
- Major, multi-year alliances with top pharma
- Proven results in literature citations

CHEMBRIDGE CORPORATION IS A LEADING GLOBAL DISCOVERY CHEMISTRY CRO AND PROVIDER OF ADVANCED SCREENING LIBRARIES FOR SMALL MOLECULE DRUG DISCOVERY.

CHEMBRIDGE CORPORATION
San Diego, California
1-800-964-6143 | sales@chembridge.com

WWW.CHEMBRIDGE.COM

This Week in *Science*

Continued from page 307

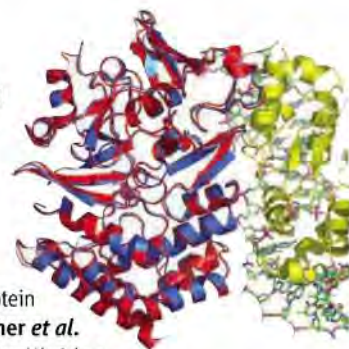
Nematodes Behaving Badly

Pathogenic and commensal microorganisms can trigger immune responses and control host behavior, revealing complex communication between host and microbe. Natural variations in pathogen susceptibility between different strains of the nematode worm *Caenorhabditis elegans* has been linked to a polymorphism in the *npr-1* gene, which encodes a homolog of the mammalian neuropeptide Y receptor. **Reddy et al.** (p. 382) studied the mechanism of NPR-1-mediated pathogen susceptibility and found that behavioral changes in the nematodes in response to altered oxygen levels caused by the presence of bacteria resulted in an increased exposure to pathogen, thus causing increased sensitivity. These data underscore the important contribution of behavioral avoidance to nematode survival in the presence of pathogenic bacteria.

Escape Artists

Bacterial multidrug tolerance (MDT) is an increasingly alarming phenomenon caused by the inability of antibiotics to eradicate infections completely. Most antibiotics target rapidly dividing cells. MDT is caused by a small population of bacterial cells, called persisters, which somehow become dormant and then switch back to growth phase after antibiotic removal, and resume the infection. The biochemical basis for persistence is unknown, but the *Escherichia coli* HipA (high persistence A) protein has been identified as a bona fide persistence factor. **Schumacher et al.**

(p. 396) studied the structural mechanisms behind HipA function. HipA is a Ser/Thr kinase that phosphorylates the essential translation factor EF-Tu, potentially halting translation and leading to cell stasis. The DNA binding protein HipB, which neutralizes HipA, was found to do so by locking HipA into an inactive state and by sequestering it away from its EF-Tu target.



Draxin and Axon Guidance

The developing nervous system is assembled with the help of a variety of signals and morphogens that guide the trajectory of growing neurons. **Islam et al.** (p. 388) have identified an axon guidance protein which they call draxin. Experiments in chick and mouse indicate that draxin, which appears to inhibit neurite outgrowth, is required for neurons to successfully cross the midline and form the major commissures of the brain.

Insider RNA Job

Retroviruses are well known for their ability to acquire host cell-derived genetic sequences by accident after their integration into the host genome, but, because of the very different mechanisms of replication, nonretroviral RNA viruses, which lack a DNA-integrated phase, have not been thought to be able to hijack extraneous sequences so easily. Now **Geuking et al.** (p. 393) have found that a nonretroviral RNA virus of mice can join forces with an endogenous retrotransposon, which allows reverse transcription of the viral RNA and integration into the host genome. Lymphocytic choriomeningitis virus forms a recombinant with the endogenous intracisternal A-type particle to yield a complementary DNA molecule that is able to integrate into the mouse chromosomes together with the retrotransposon. These findings may have implications for the use of RNA virus vectors in gene therapy.

Chromatin, DNA Repair, and Variation

Genomic DNA is wrapped up in chromatin. The principle components of this packaging are the nucleosomes, consisting of histone protein complexes around which roughly 150 base pairs of duplex DNA can be wound. Chromatin can influence the access of effector proteins to the genome, such as transcription and DNA repair factors. Can chromatin then also influence genetic variation? **Sasaki et al.** (p. 401; published online 11 December; see the Perspective by **Semple and Taylor**) compare the genomes of two Japanese killifish (medaka) and show that the mutation rate around the start of transcription shows a periodic pattern of peaks and valleys correlating with nucleosome occupancy, with insertions and deletions at a maximum and substitutions at a minimum. It is likely that transcription-coupled repair contributes to this pattern of mutation.

CREDIT: SCHUMACHER ET AL.



Martin Rees is professor of Cosmology and Astrophysics at Cambridge University and holds the title of Astronomer Royal.

Pondering Astronomy in 2009

THIS WEEK IN PARIS, AN OPENING CEREMONY HELD BY THE UNITED NATIONS EDUCATIONAL, Scientific and Cultural Organization and the International Astronomical Union proclaims 2009 as the International Year of Astronomy. The year marks the 400th anniversary of Galileo's first observations with his telescope, when he detected the moons of Jupiter; and of Kepler's great book *Astronomia Nova*, which showed that the planets move in elliptical orbits.

People in all eras and cultures have gazed at the night sky, though it has been interpreted in many different ways. Astronomy is the oldest science, except for medicine. Through its role in timekeeping and navigation, it's perhaps the first to have done more good than harm. But its scope has expanded hugely in recent decades. The cosmos is now being explored at the cutting edge of technology, on the ground and in space. Often, it is through cooperative international ventures, such as the European Southern Observatory's giant array of telescopes in Chile and the Atacama Large Millimeter Array in Chile, a collaboration involving Europe, Japan, and the United States. Powerful instruments have revealed a vaster and more intricate universe than our forbears envisaged. But the subject remains accessible to a wide public.

Black holes, dark matter, and the Big Bang have entered the common vocabulary. Millions have followed the progress of probes to Mars, Jupiter, and Saturn and admired images from the Hubble Telescope. The Internet allows scientists worldwide to access and analyze huge digitized data sets. Sophisticated amateurs can pursue projects that were once the province of professionals with large telescopes.

During 2009, astronomers will step up their campaign against the ever more pervasive light pollution that degrades their observations. But the campaign to preserve dark skies deserves support from a wide public. Everyone's environment is diminished if they can't see a starry sky. It's not just astronomers who care about this, just as it's not only keen ornithologists who would feel deprived if songbirds disappeared from our gardens. 2009 also marks 200 years since Charles Darwin's birth and 150 years since the publication of his great book *On the Origin of Species*. So it's an appropriate time to highlight a fascinating question of where astronomy and biology overlap: Does life exist elsewhere?

Within the past decade, we've realized that most stars are orbited by retinues of planets. The planets so far discovered are mainly large, comparable to Jupiter and Saturn, the giants of our solar system. But an astronomical highlight of 2009 will be the launch, by the U.S. National Aeronautics and Space Administration, of the Kepler spacecraft, which should reveal planets no bigger than Earth by detecting the slight dimming of a star when a planet transits in front of it.

There are many steps between detecting an Earthlike planet and reliably assessing whether it has a biosphere. Life's origin on Earth is still a mystery, so we cannot lay firm odds on its likelihood elsewhere. But we may learn, in the coming decades, whether biological evolution is unique to the pale blue dot in the cosmos that is our home, or whether Darwin's writ also runs in the wider universe.

Darwin closes *On the Origin of Species* with these famous words: "whilst this planet has gone cycling on according to the fixed law of gravity, from so simple a beginning, forms most beautiful and most wonderful have been, and are being, evolved." This "simple" beginning—the young Earth, orbiting a rather ordinary star—is itself very complicated, geologically and chemically. Astronomers aim to probe further back and set our entire solar system in a broader expanse of space and time.

Science is the one truly global culture, and it is surely a cultural deprivation to be unaware of the chain of events through which some mysterious genesis nearly 14 billion years ago triggered the emergence of atoms, galaxies, stars, and planets, and whereby, on at least one planet, Darwinian selection led to the emergence of creatures able to ponder their origins. The details are sharpening up faster than ever. The International Year of Astronomy is our opportunity to proclaim this immense story worldwide.

— Martin Rees



DEVELOPMENT

Hand Over Heart

Although each of us likes to feel unique, many of the physical characteristics that define us are not all that different from those of our neighbors. In particular, the size of one's body and the relative sizes of the component parts vary within a narrow range, but the guiding mechanisms are not well understood. For instance, after hepatectomy, the remaining liver cells divide only until the organ is fully regenerated and not beyond. How are the boundaries between individual organs and appendages controlled during development and regeneration? Evidence suggesting that cross talk between organs contributes to size determination comes from heritable congenital syndromes that affect multiple organs. Retinoic acid, a derivative of vitamin A, is part of a universal pathway involved in many aspects of vertebrate organogenesis. In zebrafish embryos, defective retinoic acid signaling causes an expansion of the heart and a reduction of the forelimb, but whether these two processes are coordinately regulated is unknown; although the heart and forelimbs are far apart in the adult, they are juxtaposed during early stages of development. Waxman *et al.* show that retinoic acid signaling in the developing

forelimb restricts the size of the adjacent cardiac progenitor field; the downstream factor *hoxb5b*, which is expressed in response to retinoic acid in the forelimb, mediates this restrictive effect on the heart. The coordinated development of heart and limbs would explain their correlated defects in some syndromes and suggests a mechanism whereby communication between adjacent organs helps to regulate size. — HP*

Dev. Cell **15**, 923 (2008).

BIOCHEMISTRY

No Hydrolysis Needed

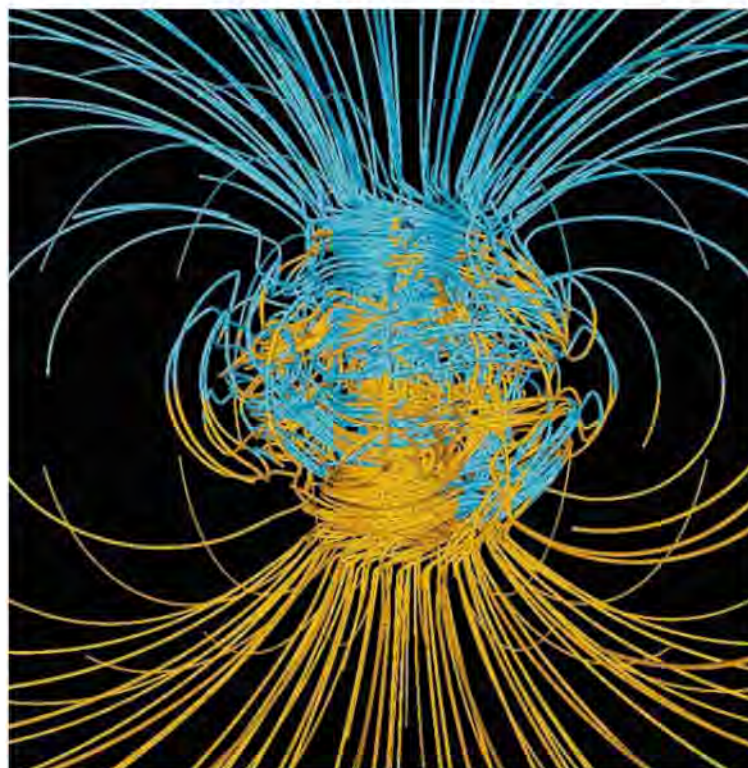
DEAD-box proteins facilitate RNA rearrangements that locally disrupt secondary or tertiary structure or RNA/protein interactions. They are structurally similar to DNA helicases that use the energy from ATP hydrolysis to unwind double-stranded DNA, but they do not appear to move very far along the RNA, although they can pry apart short duplex regions. Two groups show that RNA strand separation depends directly on ATP

binding rather than hydrolysis. Chen *et al.* report that the DEAD-box proteins CYT-19, Mss116p, and Ded1p achieve complete separation of short RNA duplexes with the hydrolysis of one or, under some conditions, even less than one ATP. Strand separation depends on ATP binding, which probably stabilizes a protein conformation that favors strand separation. Consistent findings are obtained by Liu *et al.*, who report that Ded1p, Mss116p, and eIF4A can separate short duplexes upon binding the ATP analog ADP-BeF₃, which is a mimic of the prehydrolysis state of ATP. They go on to show that ATP hydrolysis promotes dissociation of the protein from the RNA

and thus is required for efficient enzyme recycling. Intriguingly, even though ATP hydrolysis does not fuel translocation in these DEAD-box proteins, the related DEXD/H helicase RIG-1, which detects viral RNA and elicits an antiviral signaling cascade, undergoes ATP-dependent translocation on double-stranded RNA without unwinding it (see Myong *et al.*, Reports, *Science Express*, 1 January 2009). — VV

Proc. Natl. Acad. Sci. U.S.A. **105**, 20203; 20209 (2008).

*Helen Pickersgill is a locum editor in *Science's* editorial department.



GEOLOGY

Magnetic Perseverance

Earth currently has a strong magnetic field generated from fluid motion in its outer core, thought to be driven by heat released from the solidification of its inner core. This field (depicted graphically above) helps shield Earth from harmful cosmic rays. The timing of the formation of the inner core and the nature of the field in the Archean (before 2.7 billion years ago) are debated but important for understanding the origin and early evolution of life. Selkin *et al.* were able to obtain more than 100 paleointensity measurements from the Stillwater layered intrusion, a large late Archean magma reservoir in Montana. The data imply that Earth's field then was as strong as it is today. Considering these data with the albeit sparse other Archean data, there is no clear indication that the field's strength has decreased or increased greatly over time. — BH

Geochim. Geophys. Geosyst. **9**, Q12023 (2008).

BIOTECHNOLOGY

Lighting the Way Forward

The controlled expression of foreign genes has enabled all sorts of pyrotechnic displays, from the creation of carotene-rich golden rice to the riotous palette of neuronal arbors revealed via Brainbow by combinatorial derivatives of green fluorescent protein. In most instances, genes from the microbial world are identified, modified, and then packaged for delivery and expression in plant or animal tissues, sometimes for purposes completely unrelated to the specific aims for which the original research was funded. Berndt *et al.* describe one of the latest such endeavors, in which light-activated channelrhodopsin-2 (ChR2)—a cation-conducting protein from green algae—was engineered, on the basis of detailed structure-function analyses of the bacteriorhodopsin photocycle, and converted into a switch. Changing a single cysteine residue yielded a neuronally expressible ChR2 variant that turned on (and stayed on) when illuminated with 470-nm light for 10 ms, and could then be turned off with a 50-ms pulse of 530-nm light. These properties allow for non-invasive modulation of the membrane conductances of individual neurons with innocuous illumination. — GJC

Nat. Neurosci. 10.1038/nn.2247 (2008).



Expressed ChR2-C128T.

BIOMEDICINE

An Active Participant

In degenerative disorders of the central nervous system, inflammation at the site of neuronal injury is common, but it has not been clear whether this reaction is a primary factor in subsequent disease pathogenesis or a secondary response to the condition. Brochard *et al.* report that a particular subpopulation of T cells is critical for the development of Parkinson's disease (PD), a disorder characterized by the loss of brain neurons that use dopamine. The authors report the accumulation of CD4⁺ and CD8⁺ T cells in the post-mortem brains of PD patients and also in the brains of a mouse model of PD during progression of the disease. However, in mice lacking CD4⁺ T cells that express the cell surface protein FasL, dopaminergic neuronal injury was reduced, as was the activation of proinflammatory microglial cells in the brain. FasL could either mediate the activation of microglial cells, thereby promoting inflam-

mation and neurodegeneration, or it could mediate cell-cell contact that somehow allows T cells to destroy neurons directly. — LC

J. Clin. Invest. 119, 182 (2009).

CHEMISTRY

Clean Coupling

Alcohol oxidation is a crucial step in the preparation of many drugs and fine chemicals, but it often requires large amounts of toxic reagents. Zweifel *et al.* present a rhodium catalyst that can dehydrogenatively couple a range of alcohols with water, methanol, or various amines (including ammonia, a generally recalcitrant substrate) to afford the corresponding acid, ester, or amide directly.

The reactions proceed in a few hours at room temperature, driven by transfer of the liberated hydrogen to a cyclohexanone acceptor that can subsequently be recycled by reaction with hydrogen peroxide. Primary alcohols are oxidized selectively, and the catalyst tolerates olefin, thioether, and pyridine substituents. Simulations support a mechanism involving the transfer of a hydride to the Rh center, with accompanying protonation of a coordinated nitrogen ligand. — JSY

Angew. Chem. Int. Ed. 48, 559 (2009).

PHYSICS

Weaving a Quantum Computer

Quantum matter can be described by a quantum-mechanical wave function. Correlated phases of such matter can give rise to excitations that have been proposed to be useful for quantum computation. Of particular interest are those excitations that exhibit Abelian or non-Abelian statistics. Anyons fall into this category and are particle-like excitations. Compared with bosons or fermions, where swapping two will respectively keep the wave function as it is or introduce a negative sign, swapping two anyons is quite different—the action imposes a nontrivial phase shift on the wave function so that when a number of anyon swaps have been performed, measurement of the phase can tell you exactly which particles have been swapped. Such a braiding technique is at the heart of some quantum computation schemes, but exactly how these states would be manipulated experimentally is still up for grabs. Aguado *et al.* propose that a lattice of atoms held in an optical trap could be one such realization, showing how the manipulation of atoms in their respective lattice sites can affect the wave function describing the whole ensemble, which can be read out quantitatively. — ISO

Phys. Rev. Lett. 101, 260501 (2008).

2009

SARDINIA

for Plant Enthusiasts!

April 17-29, 2009

Explore Capo Caccia, a hotspot for endemic plants and the Gallura region. Cross to the unspoiled island of Caprera, and explore the island's prehistoric Nuraghe culture. Visit the Sinis peninsula, the remarkable Phoenician and Roman site of Tharros, and the basalt plateau of Giara di Gesturi. \$3,850 + air.



AEGEAN HERITAGE

by Yacht

May 1-9, 2009

Explore the heritage of the Aegean, including the Cyclades Islands and the Aegean Coast of Turkey, on board the 170-passenger sailing yacht, *Star Clipper*. See Rhodes, Bodrum Castle, Caunos, Santorini, and Hydra. From \$3,295 + air.

Wild & Prehistoric

FRANCE

May 22-June 4, 2009

Join Mark Walters and discover wild areas and prehistoric sites in Haute Provence, the Massif Central, and the Dordogne. See images of the greatest cave paintings in Europe at Lascaux II. See the cave art by train at Rouffignac. Visit the Vézère Valley, Font de Gaume, Arles, and Les Baux. \$3,895 + air.

ALASKA

May 31-June 7, 2009

Explore Southeast Alaska's coastal wilderness aboard the *National Geographic Sea Lion*. From \$5,390 plus free air from Seattle.

For a detailed brochure,
please call (800) 252-4910

AAAS Travels

17050 Montebello Road
Cupertino, California 95014

Email: AAASInfo@belchartexpeditions.com

1200 New York Avenue, NW
Washington, DC 20005

Editorial: 202-326-6550, FAX 202-289-7562

News: 202-326-6581, FAX 202-371-9227

Bateman House, 82-88 Hills Road
Cambridge, UK CB2 1LQ

+44 (0) 1223 326500, FAX +44 (0) 1223 326501

SUBSCRIPTION SERVICES For change of address, missing issues, new orders and renewals, and payment questions: 866-434-AAAS (2227) or 202-326-6417, FAX 202-842-1065. Mailing addresses: AAAS, P.O. Box 96178, Washington, DC 20090-6178 or AAAS Member Services, 1200 New York Avenue, NW, Washington, DC 20005

INSTITUTIONAL SITE LICENSES please call 202-326-6755 for any questions or information

REPRINTS: Author Inquiries 800-635-7181

Commercial Inquiries 803-359-4578

PERMISSIONS 202-326-7074, FAX 202-682-0816

MEMBER BENEFITS AAAS/Barnes&Noble.com bookstore www.aaas.org/bn; AAAS Online Store www.apisource.com/aaas/ code MKB6; AAAS Travels: Betchart Expeditions 800-252-4910; Apple Store www.apple.com/store/aaas; Bank of America MasterCard 1-800-833-6262 priority code FAA3YU; Cold Spring Harbor Laboratory Press Publications www.cshlpress.com/affiliates/aaas.htm; GEICO Auto Insurance www.geico.com/landingpage/go51.htm?logo=17624; Hertz 800-654-2200 CDP#343457; Office Depot https://bsd.officedepot.com/portalLogin.do; Seabury & Smith Life Insurance 800-424-9883; Subaru VIP Program 202-326-6417; VIP Moving Services www.vipmayflower.com/domestic/index.html; Other Benefits: AAAS Member Services 202-326-6417 or www.aaasmember.org.

science_editors@aaas.org (for general editorial queries)

science_letters@aaas.org (for queries about letters)

science_reviews@aaas.org (for returning manuscript reviews)

science_bookrevs@aaas.org (for book review queries)

Published by the American Association for the Advancement of Science (AAAS), *Science* serves its readers as a forum for the presentation and discussion of important issues related to the advancement of science, including the presentation of minority or conflicting points of view, rather than by publishing only material on which a consensus has been reached. Accordingly, all articles published in *Science*—including editorials, news and comment, and book reviews—are signed and reflect the individual views of the authors and not official points of view adopted by AAAS or the institutions with which the authors are affiliated.

AAAS was founded in 1848 and incorporated in 1874. Its mission is to advance science, engineering, and innovation throughout the world for the benefit of all people. The goals of the association are to: enhance communication among scientists, engineers, and the public; promote and defend the integrity of science and its use; strengthen support for the science and technology enterprise; provide a voice for science on societal issues; promote the responsible use of science in public policy; strengthen and diversify the science and technology workforce; foster education in science and technology for everyone; increase public engagement with science and technology; and advance international cooperation in science.

INFORMATION FOR AUTHORS

See pages 634 and 635 of the 1 February 2008 issue or access www.sciencemag.org/about/authors

EDITOR-IN-CHIEF **Bruce Alberts**

EXECUTIVE EDITOR **Monica M. Bradford**

DEPUTY EDITORS

R. Brooks Hanson, Barbara R. Jasny, Colin Norman

Katrina L. Kelner

NEWS EDITOR

EDITORIAL SUPERVISORY SENIOR EDITOR Phillip D. Szuroni; **SENIOR EDITOR/PERSPECTIVES** Lisa D. Chong; **SENIOR EDITORS** Gilbert J. Chin, Pamela J. Hines, Paula A. Kiberstis (Boston), Marc S. Lavine (Toronto), Beverly A. Purnell, L. Bryan Ray, Guy Riddihough, H. Jesse Smith, Valda Vinson; **ASSOCIATE EDITORS** Kristen L. Mueller, Jake S. Yeston, Laura M. Zahn; **ONLINE EDITOR** Stewart Wills; **ASSOCIATE ONLINE EDITORS** Robert Frederick, Tara S. Marathe; **WEB CONTENT DEVELOPER** Martyn Green; **BOOK REVIEW EDITOR** Sherman J. Suter; **ASSOCIATE LETTERS EDITOR** Jennifer Sills; **EDITORIAL MANAGER** Cara Tate; **SENIOR COPY EDITORS** Jeffrey E. Cook, Cynthia Howe, Harry Jach, Barbara P. Ordway, Trista Wagoner; **COPY EDITORS** Chris Filiatreau, Lauren Kmeck; **EDITORIAL COORDINATORS** Carolyn Kyle, Beverly Shields; **PUBLICATIONS ASSISTANTS** Ramatoulaye Diop, Joi S. Granger, Jeffrey Hearn, Lisa Johnson, Scott Miller, Jerry Richardson, Jennifer A. Seibert, Brian White, Anita Wynn; **EDITORIAL ASSISTANTS** Carlos L. Durham, Emily Guise, Patricia M. Moore; **EXECUTIVE ASSISTANT** Sylvia S. Kihara; **ADMINISTRATIVE SUPPORT** Maryrose Madrid

NEWS DEPUTY NEWS EDITORS Robert Coontz, Eliot Marshall, Jeffrey Mervis, Leslie Roberts; **CONTRIBUTING EDITORS** Elizabeth Culotta, Polly Shulman; **NEWS WRITERS** Yudhijit Bhattacharjee, Adrian Cho, Jennifer Couzin, David Grimm, Constance Holden, Jocelyn Kaiser, Richard A. Kerr, Eli Kintisch, Andrew Lawler (New England), Greg Miller, Elizabeth Pennisi, Robert F. Service (Pacific NW), Erik Stokstad; **INTERN** Jackie D. Grom; **CONTRIBUTING CORRESPONDENTS** Jon Cohen (San Diego, CA), Daniel Ferber, Ann Gibbons, Robert Koenig, Mitch Leslie, Charles C. Mann, Virginia Morell, Evelyn Strauss, Gary Taubes; **COPY EDITORS** Linda B. Felaco, Melvin Gatling, Melissa Raimond; **ADMINISTRATIVE SUPPORT** Scherraine Mack, Fannie Groom; **BUREAU NEW ENGLAND:** 207-549-7755, San Diego, CA: 760-942-3252, FAX 760-942-4979, Pacific Northwest: 503-963-1940

PRODUCTION DIRECTOR James Landry; **SENIOR MANAGER** Wendy K. Shank; **ASSISTANT MANAGER** Rebecca Doshi; **SENIOR SPECIALISTS** Steve Forrester, Chris Redwood; **SPECIALIST** Anthony Rosen; **PREFLIGHT DIRECTOR** David M. Tompkins; **MANAGER** Marcus Spiegler

ART DIRECTOR Yael Kats; **ASSOCIATE ART DIRECTOR** Laura Creveling;

ILLUSTRATORS Chris Bickel, Katharine Suttill; **SENIOR ART ASSOCIATES** Holly Bishop, Preston Huey, Nayomi Kevitigagala; **ART ASSOCIATE** Jessica Newfield; **PHOTO EDITOR** Leslie Blizard

SCIENCE INTERNATIONAL

EUROPE (science@science-int.co.uk) **EDITORIAL: INTERNATIONAL MANAGING EDITOR** Andrew M. Sugden; **SENIOR EDITOR/PERSPECTIVES** Julia Fahrenkamp-Uppenbrink; **SENIOR EDITORS** Caroline Ash, Stella M. Hurtle, Ian S. Osborne, Peter Stern; **ASSOCIATE EDITOR** Maria Cruz; **EDITORIAL SUPPORT** Deborah Dennison, Rachel Roberts, Alice Whaley; **ADMINISTRATIVE SUPPORT** John Cannell, Janet Clements; **NEWS: EUROPE NEWS EDITOR** John Travis; **DEPUTY NEWS EDITOR** Daniel Cleary; **CONTRIBUTING CORRESPONDENTS** Michael Balter (Paris), John Bohannon (Vienna), Martin Enserink (Amsterdam and Paris), Gretchen Vogel (Berlin); **INTERN** Sara Coelho

ASIA Japan Office: Asca Corporation, Eiko Ishioka, Fusako Tamura, 1-8-13, Hirano-cho, Chuo-ku, Osaka-shi, Osaka, 541-0046 Japan; +81 (0) 6 6202 6272, FAX +81 (0) 6 6202 6271; asca@os.gulf.or.jp; **ASIA NEWS EDITOR** Richard Stone (Beijing: rstone@aaas.org); **CONTRIBUTING CORRESPONDENTS** Dennis Normile (Japan: +81 (0) 3 3391 0630, FAX +81 (0) 3 5936 3531; dnormile@gol.com); Hao Xin (China: +86 (0) 10 6307 4439 or 6307 3676, FAX +86 (0) 10 6307 4358; cindyhao@gmail.com); Pallava Bagla (South Asia: +91 (0) 11 2271 2896; pbagla@vsnl.com)

EXECUTIVE PUBLISHER **Alan I. Leshner**

PUBLISHER **Beth Rosner**

FULFILLMENT SYSTEMS AND OPERATIONS (membership@aaas.org); **DIRECTOR** Waylon Butler; **SENIOR SYSTEMS ANALYST** Jonny Blaker; **CUSTOMER SERVICE SUPERVISOR** Pat Butler; **SPECIALISTS** Latoya Casteel, LaVonda Crawford, Vicki Linton, April Marshall; **DATA ENTRY SUPERVISOR** Cynthia Johnson; **SPECIALISTS** Eintou Bowden, Tarrika Hill, William Jones

BUSINESS OPERATIONS AND ADMINISTRATION DIRECTOR Deborah Rivera-Wienhold; **ASSISTANT DIRECTOR, BUSINESS OPERATIONS** Randy Yi; **MANAGER, BUSINESS ANALYSIS** Michael LoBue; **MANAGER, BUSINESS OPERATIONS** Jessica Tierney; **FINANCIAL ANALYSTS** Priti Pannani, Celeste Troxler; **RIGHTS AND PERMISSIONS:** **ADMINISTRATOR** Emilie David; **ASSOCIATE** Elizabeth Sandler; **MARKETING DIRECTOR** Ian King; **MARKETING MANAGER** Allison Pritchard; **MARKETING ASSOCIATES** Aimee Aponte, Alison Chandler, Mary Ellen Crowley, Julianne Wielga, Wendy Wise; **INTERNATIONAL MARKETING MANAGER** Wendy Sturley; **MARKETING EXECUTIVE** Jennifer Reeves; **MARKETING/MEMBER SERVICES EXECUTIVE** Linda Rusk; **DIRECTOR, SITE LICENSING** Tom Ryan; **DIRECTOR, CORPORATE RELATIONS** Eileen Bernadette Moran; **PUBLISHER RELATIONS, eRESOURCES SPECIALIST** Kiki Forsythe; **SENIOR PUBLISHER RELATIONS SPECIALIST** Catherine Holland; **PUBLISHER RELATIONS, EAST COAST** Phillip Smith; **PUBLISHER RELATIONS, WEST COAST** Philip Tsolakis; **FULFILLMENT SUPERVISOR** Iquo Edim; **FULFILLMENT COORDINATOR** Laura Clemens; **ELECTRONIC MEDIA:** **MANAGER** Elizabeth Harman; **PROJECT MANAGER** Trista Snyder; **ASSISTANT MANAGER** Lisa Stanford; **SENIOR PRODUCTION SPECIALISTS** Christopher Coleman, Walter Jones; **PRODUCTION SPECIALISTS** Nichole Johnston, Kimberly Oster

ADVERTISING DIRECTOR, WORLDWIDE AD SALES Bill Moran

PRODUCT (science_advertising@aaas.org); **MIDWEST/WEST COAST/W. CANADA** Rick Bongiovanni: 330-405-7080, FAX 330-405-7081; **EAST COAST/E. CANADA** Laurie Faraday: 508-747-9395, FAX 617-507-8189; **UK/EUROPE/ASIA** Roger Goncalves: TEL/FAX +41 43 243 1358; **JAPAN** Masahiko Yoshikawa: +81 (0) 3 3235 5961, FAX +81 (0) 3 3235 5852; **SENIOR TRAFFIC ASSOCIATE** Delandra Simms

COMMERCIAL EDITOR Sean Sanders: 202-326-6430

PROJECT DIRECTOR, OUTREACH Brianna Blaser

CLASSIFIED (advertise@sciencecareers.org); **INSIDE SALES MANAGER:** **MIDWEST/CANADA** Daryl Anderson: 202-326-6543; **INSIDE SALES REPRESENTATIVE** Karen Foote: 202-326-6740; **KEY ACCOUNT MANAGER** Jorihab Able; **NORTHEAST** Alexis Fleming: 202-326-6578; **SOUTHEAST** Tina Burks: 202-326-6577; **WEST** Nicholas Hintibidze: 202-326-6533; **SALES COORDINATORS** Rohan Edmonson, Shirley Young; **INTERNATIONAL SALES MANAGER** Tracy Holmes: +44 (0) 1223 326525, FAX +44 (0) 1223 326532; **Sales** Susanne Kharraz, Dan Pennington, Alex Palmer; **SALES ASSISTANT** Louise Moore; **JAPAN** Masahiko Yoshikawa: +81 (0) 3 3235 5961, FAX +81 (0) 3 3235 5852; **ADVERTISING PRODUCTION OPERATIONS MANAGER** Deborah Tompkins; **SENIOR PRODUCTION SPECIALIST/GRAPHIC DESIGNER** Amy Harcastle; **SENIOR PRODUCTION SPECIALIST** Robert Buck; **SENIOR TRAFFIC ASSOCIATE** Christine Hall; **PUBLICATIONS ASSISTANT** Mary Lagnaoui

AAAS BOARD OF DIRECTORS **RETIRED PRESIDENT, CHAIR** David Baltimore; **PRESIDENT** James J. McCarthy; **PRESIDENT-ELECT** Peter C. Agre; **TREASURER** David E. Shaw; **CHIEF EXECUTIVE OFFICER** Alan I. Leshner; **BOARD** Lynn W. Enquist, Susan M. Fitzpatrick, Alice Gast, Linda P. B. Katehi, Nancy Knowlton, Cherry A. Murray, Thomas D. Pollard, Thomas A. Woolsey



ADVANCING SCIENCE, SERVING SOCIETY

SENIOR EDITORIAL BOARD

John I. Brauman, Chair, Stanford Univ.
Richard Losick, Harvard Univ.
Robert May, Univ. of Oxford
Marcia McNitt, Monterey Bay Aquarium Research Inst.
Linda Partridge, Univ. College London
Vera C. Rubin, Carnegie Institution
Christopher R. Somerville, Univ. of California, Berkeley

BOARD OF REVIEWING EDITORS

Joanna Aizenberg, Harvard Univ.
David Altshuler, Broad Institute
Arturo Alvarez-Buylla, Univ. of California, San Francisco
Richard Amasino, Univ. of Wisconsin, Madison
Angelika Amon, MIT
Meinrat O. Andreae, Max Planck Inst., Mainz
Kristi S. Anseth, Univ. of Colorado
John A. Bargh, Yale Univ.
Cornelia I. Bargmann, Rockefeller Univ.
Ben Barnes, Stanford Medical School
Marisa Bartolomei, Univ. of Penn. School of Med.
Facundo Batista, London Research Inst.
Ray H. Baughman, Univ. of Texas, Dallas
Stephen J. Benkovic, Penn State Univ.
Ton Bisseling, Wageningen Univ.
Mina Bissell, Lawrence Berkeley National Lab
Peer Bork, EMBL
Robert W. Boyd, Univ. of Rochester
Paul M. Brakley, Leiden Univ.
Dennis Bray, Univ. of Cambridge
Stephen Burdowski, Harvard Medical School
Joseph A. Burns, Cornell Univ.
William P. Butz, Population Reference Bureau
Mats Carlsson, Univ. of Oslo
Peter Carmeliet, Univ. of Leuven, VIB
Mildred Cho, Stanford Univ.
David Clapham, Children's Hospital, Boston
David Clary, Oxford University
J. M. Claverie, CNRS, Marseille
Jonathan D. Cohen, Princeton Univ.


Andrew Cossins, Univ. of Liverpool
Robert H. Crabtree, Yale Univ.
Wolfgang Cramer, Potsdam Inst. for Climate Impact Research
F. Fleming Crim, Univ. of Wisconsin
William Cumberland, Univ. of California, Los Angeles
Jeff L. Dangl, Univ. of North Carolina
Stanislav Dehaene, Collège de France
Edward DeLong, MIT
Emmanouil T. Dermatzakis, Wellcome Trust Sanger Inst.
Robert Desimone, MIT
Dennis Discher, Univ. of Pennsylvania
Scott Doney, Woods Hole Oceanographic Inst.
W. Ford Doolittle, Dalhousie Univ.
Jennifer A. Doudna, Univ. of California, Berkeley
Julian Downward, Cancer Research UK
Denis Duboule, Univ. of Geneva/EPFL Lausanne
Christopher Dye, WHO
Gerhard Ertl, Fritz-Haber-Institut, Berlin
Mark Estelle, Indiana Univ.
Barry Everitt, Univ. of Cambridge
Paul G. Falkowski, Rutgers Univ.
Ernst Fehr, Univ. of Zurich
Toni Fenchel, Univ. of Copenhagen
Alain Fischer, INSERM
Scott E. Fraser, Cal Tech
Chris D. Frith, Univ. College London
Wulfraam Gerstner, EPFL Lausanne
Charles Godfrey, Univ. of Oxford
Diane Griffin, Johns Hopkins Bloomberg School of Public Health
Christian Haass, Ludwig Maximilians Univ.
Niels Hansen, Technical Univ. of Denmark
Dennis L. Hartmann, Univ. of Washington
Chris Hawkesworth, Univ. of Bristol
Martin Heimann, Max Planck Inst., Jena
James A. Hendler, Rensselaer Polytechnic Inst.
Ray Hilborn, Univ. of Washington
Ove Hoegh-Guldberg, Univ. of Queensland
Bridget L. M. Hogan, Duke Univ. Medical Center
Ronald R. Hoy, Cornell Univ.
Orli Ikkala, Helsinki Univ. of Technology
Meyer B. Jackson, Univ. of Wisconsin Med. School
Stephen Jackson, Univ. of Cambridge
Steven Jacobsen, Univ. of California, Los Angeles

Peter Jonas, Universität Freiburg
Barbara B. Kahn, Harvard Medical School
Daniel Kahne, Harvard Univ.
Gerard Karsenty, Columbia Univ. College of P&S
Bernhard Keimer, Max Planck Inst., Stuttgart
Elizabeth A. Kellog, Univ. of Missouri, St. Louis
Alan B. Krueger, Princeton Univ.
Lee Kump, Penn State Univ.
Mitchell A. Lazar, Univ. of Pennsylvania
Virginia Lee, Univ. of Pennsylvania
Olle Lindvall, Univ. Hospital, Lund
Marcia C. Lin, Univ. of California, Berkeley
John Lis, Cornell Univ.
Richard Losick, Harvard Univ.
Ke Lu, Chinese Acad. of Sciences
Andrew P. MacKenzie, Univ. of St Andrews
Raul Madariaga, Ecole Normale Supérieure, Paris
Anne Magurran, Univ. of St Andrews
Charles Marshall, Harvard Univ.
Virginia Miller, Washington Univ.
Yasushi Miyashita, Univ. of Tokyo
Richard Morris, Univ. of Edinburgh
Edward Moser, Norwegian Univ. of Science and Technology
Naoto Nagaosa, Univ. of Tokyo
James Nelson, Stanford Univ. School of Med.
Timothy W. Nilsen, Case Western Reserve Univ.
Roeland Nolte, Univ. of Nijmegen
Helga Nowotny, European Research Advisory Board
Eric N. Olson, Univ. of Texas, SW
Stuart H. Orkin, Dana-Farber Cancer Inst.
Erin O'Shea, Harvard Univ.
Elinor Ostrom, Indiana Univ.
Jonathan T. Overbeck, Univ. of Arizona
John Penry, Imperial College
Simon Philpot, Univ. of Florida
Philippe Poulin, CNRS
Molly Power, Univ. of California, Berkeley
Molly Przeworski, Univ. of Chicago
Colin Renfrew, Univ. of Cambridge
Trevor Robbins, Univ. of Cambridge
Barbara A. Romanowicz, Univ. of California, Berkeley
Michael M. Rubin, Lawrence Berkeley National Lab
Shimon Sakaguchi, Kyoto Univ.
Jürgen Sandkühner, Medical Univ. of Vienna

David W. Schindler, Univ. of Alberta
Georg Schulz, Albert-Ludwigs-Universität
Paul Schulze-Lefert, Max Planck Inst., Cologne
Christine Seidman, Harvard Medical School
Terrence J. Sejnowski, The Salk Institute
David Sibley, Washington Univ.
Joseph Silk, Univ. of Oxford
Montgomery Slatkin, Univ. of California, Berkeley
Davor Solter, Inst. of Medical Biology, Singapore
Joan Steitz, Yale Univ.
Elisbeth Stern, ETH Zürich
Jerome Strauss, Virginia Commonwealth Univ.
John Tschopp, Univ. of Lausanne
Derek van der Kooy, Univ. of Toronto
Bert Vogelstein, Johns Hopkins Univ.
Ulrich H. von Andrian, Harvard Medical School
Bruce D. Walker, Harvard Medical School
Christopher A. Walsh, Harvard Medical School
Graham Warren, Yale Univ. School of Med.
Colin Watts, Univ. of Dundee
Detlef Weigel, Max Planck Inst., Tübingen
Jonathan Weissman, Univ. of California, San Francisco
Ellen D. Williams, Univ. of Maryland
Ian A. Wilson, The Scripps Res. Inst.
Jerry Workman, Stowers Inst. for Medical Research
Xiaoling Sunney Xie, Harvard Univ.
John R. Yates III, The Scripps Res. Inst.
Jan Zaenen, Leiden Univ.
Huda Zoghbi, Baylor College of Medicine
Maria Zuber, MIT

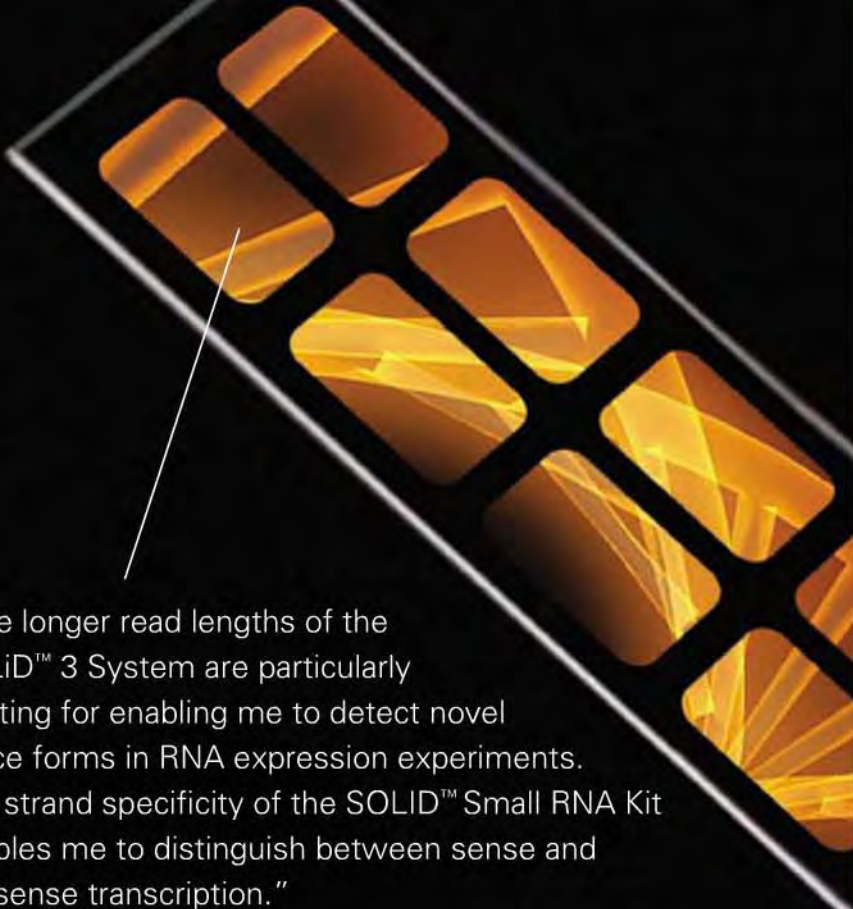
BOOK REVIEW BOARD

John Aldrich, Duke Univ.
David Bloom, Harvard Univ.
Angela Creager, Princeton Univ.
Richard Sweder, Univ. of Chicago
Ed Wasserman, DuPont
Lewis Wolpert, Univ. College London



NEED PROOF? HERE'S SOLID PROOF.

For more SOLID PROOF, visit
solid.appliedbiosystems.com



"The longer read lengths of the SOLiD™ 3 System are particularly exciting for enabling me to detect novel splice forms in RNA expression experiments. The strand specificity of the SOLiD™ Small RNA Kit enables me to distinguish between sense and antisense transcription."



Jesse Gray –
*Children's Hospital Boston,
Harvard Medical School*

New!

Flexible methods offer labs full control

Personal Automation™ Accelerates Research



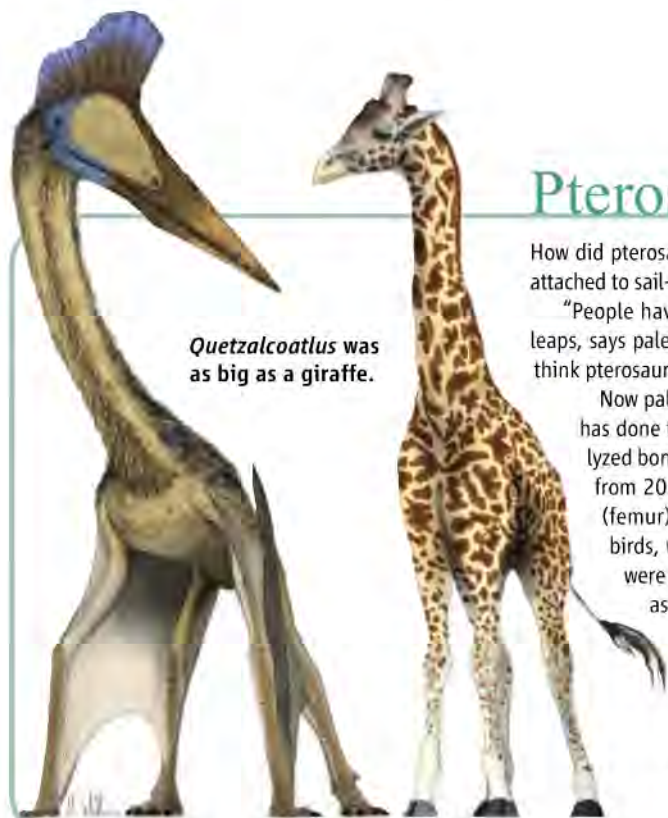
The NEW Flexi Method Firmware provides you flexibility to modify Maxwell® 16. You're in control to create, save and run your own automated methods.

The new Maxwell 16 Flexi Method Firmware enables you to modify, create, save and run your own automated methods for purification of DNA, RNA or recombinant proteins. It's automation at the bench that processes up to 16 samples. It gives you the flexibility and control to optimize your success.

**To get yourself more flexibility and control
visit: www.promega.com/maxwellflexi**

**TODAY COULD
BE THE DAY.**





Pterosaur Liftoffs

How did pterosaurs get off the ground? The giant flying reptiles had four legs, the front ones attached to sail-like wings, and could weigh 70 kilograms or more—far more than any bird.

“People have tried to fit pterosaur into a birdlike model,” taking flight with two-legged leaps, says paleontologist David Unwin of the University of Leicester, U.K. But some scientists think pterosaurs must have pushed off with all four feet, as modern vampire bats do.

Now paleontologist Michael Habib of Johns Hopkins University in Baltimore, Maryland, has done the math to show that a “quadrupedal launch” is indeed plausible. Habib analyzed bone strength by comparing measurements from three pterosaur species with those from 20 bird species. In a paper in the journal *Zitteliana*, he reports that the leg bone (femur) becomes proportionately thicker than the wing bone (humerus) in heavier birds, which need more leg muscle to take off. In pterosaurs, however, the forelimbs were more robust, supporting the notion that they helped propel the animals—some as big as giraffes—into flight without the aid of winds or jump-off points.

James Cunningham, an engineer in Collierville, Tennessee, who studies vertebrate flight mechanics, says the quadrupedal takeoff (which he thought of years ago) makes sense because the animals didn’t have enough shoulder muscle to take off by just running and flapping. Now, Unwin says, it’s time to see whether fossil pterosaur footprints support the theory. “Birds dig in just before takeoff,” he notes. “We can predict what a takeoff print would look like.”

A Finger for Profit

Financial traders who make the biggest bucks got more testosterone in the womb, judging by their index-to-ring-finger ratio, according to a new study by a former Wall Street trader.

There is evidence that men with lower 2D:4D ratios—that is, relatively long ring fingers compared with index fingers—were exposed to more male hormones in the womb. So cognitive scientist John Coates and colleagues at the University of Cambridge in the United Kingdom decided to see if sex hormones had anything to do with success on the stock market floor. They measured finger ratios of 44 young male traders from a fast-paced “noisy” London trading floor and compared the data with 20 months of individual profit and loss sheets. Traders with the

lowest ratios made the most money, even with years of experience controlled for, averaging £828,480 compared with £154,440 for the highest-ratio group.

The connection? High gestational androgen exposure has powerful organizational effects on the developing brain and affects traits such as increased risk-taking and quick reactions, as well as sensitivity to circulating testosterone, the researchers reported last week in *The Proceedings of the National Academy of Sciences*.

Psychologist Johannes Hönokopp of Northumbria University in Newcastle, U.K., says the notion that prenatal hormones contribute to noise traders’ skill is “plausible but speculative.” The fetal testosterone and finger-length relationship is weak, he says, so until they are replicated, the findings appear to be “too good to be true.”

Power Walking

Soon, Tokyo’s harried train commuters may not only have to buy their tickets but also generate the energy needed to punch them. East Japan Railway is testing a floor system that harvests energy from the footsteps of people walking through ticket gates.



The flooring is fitted with piezoelectric elements that convert the mechanical stress from pedestrians’ weight into little blips of electricity. Twenty-five square meters of piezoelectric flooring are expected to generate 1400 kilowatt-seconds of power per day, enough to light a 40-watt LED bulb for 17 hours. “It’s not much,” admits railway spokesperson Makoto Yasuhara. But the company hopes more-efficient future equipment will power automated ticket gates and information boards. A 2-month pilot system is being tested at Tokyo Station, where 70,000 train riders surge through ticket gates daily.

COOL COSMOS

It’s the International Year of Astronomy, and astronomers in Toronto, Canada, are driving the fact home with eye-catching ads on buses and subways. “We’re trying to make a point that it’s really not that remote—in some sense, the universe is right around you; it’s in you,” says University of Toronto astronomer Ray Jayawardhana. Ads, in addition to the one below, point out that our bodies are made up of material from dead stars, that neutrinos from the sun are constantly zinging through us, and that Earth’s slowing rotation makes each day a tiny bit longer. (Science, meanwhile, greets the year with a special News Focus section starting on page 324.)



I know you'll like what we came up with.

Get your best GEICO rate on auto insurance as an AAAS member.

- ✓ Visit **geico.com** for your FREE, no-obligation rate quote.
- ✓ Be sure to select AAAS when asked for your affiliation.
- ✓ New customers report an average savings of \$500 when they switch.

Go to **geico.com**, contact your local office, or call 1-800-368-2734.

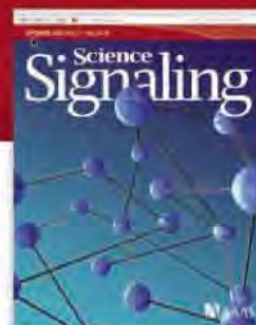
GEICO
geico.com

AAAS
ADVANCED SCIENCE ADJUDICATING SOCIETY

Some discounts, coverages, payment plans, and features are not available in all states or in all GEICO companies. Discount amount varies in some states. Discount is not available in all states or in all GEICO companies. One group discount applicable per policy. In New York a premium reduction is available. AAAS is compensated for allowing GEICO to offer this auto insurance program to AAAS members. GEICO auto insurance is not available in Mass. Government Employees Insurance Co. • GEICO General Insurance Co. • GEICO Indemnity Co. • GEICO Casualty Co. These companies are subsidiaries of Berkshire Hathaway Inc. GEICO: Washington, DC 20076. GEICO Gecko image © 1999 – 2008. © 2008 GEICO

Call for Papers

Science Signaling



From the publishers of *Science*, *Science Signaling*, formerly known as *Science's* STKE, now features top-notch, peer

reviewed, original research. Each week the journal will publish leading-edge findings in cellular regulation including:

- Molecular Biology
- Development
- Physiology and Medicine
- Immunology
- Neuroscience
- Microbiology
- Pharmacology
- Biochemistry
- Cell Biology
- Bioinformatics
- Systems Biology

Subscribing to *Science Signaling* ensures that you and your lab have the latest cell signaling resources. For more information visit sciencesignaling.org

Announcing Chief Scientific Editor for *Science Signaling* –

Michael B. Yaffe, M.D., Ph.D.

Associate Professor, Department of Biology
Massachusetts Institute of Technology

Now accepting original research submissions at:
sciencesignaling.org/about/help/research.dtl

Science Signaling

AAAS



Off Campus

ROAD TRIP. Plant geneticist Paul Porter of the University of Minnesota is taking his class on the road. For the next 4 months, the 52-year-old triathlete will be bicycling 11,300 kilometers across Africa and teaching agroecology to 34 undergraduate and graduate students. The students in Minneapolis will watch lectures via satellite as Porter explores local food production in 10 countries. Porter is joining a group of 50 riders on holiday, but he'll be working. Porter will also be blogging at paulporter.wordpress.com.

AWARDS

ENGINEERING GLORY. The National Academy of Engineering (NAE) doled out \$1.5 million last week, divided equally among three prestigious prizes. Retired chemical engineer Elmer Gaden of the University of Virginia, Charlottesville, snagged NAE's biannual Russ Prize for pioneering efforts to mass-produce penicillin and other drugs; he learned how to calibrate the oxygen needed for yeast to grow in giant fermentation tanks, a lesson quickly transferred to the penicillin mold. Robert Dennard of IBM received the academy's annual Draper Prize, for significant societal impact, for his invention of dynamic random-access memory, the most common type of working memory used by computers. Finally, Tom Byers and Tina Seelig, both of Stanford University in Palo Alto, California, received the Gordon Prize in education for teaching entrepreneurship to engineering students.

ON CAMPUS

BUY THE BOOK. Every graduate student accumulates a few textbooks, but Jaideep Singh, who is studying physics at the University of Virginia, Charlottesville, has collected 350 physics texts. His collection, which includes a textbook written by his father,

retired theorist Surjit Singh, got him named one of the country's top collegiate collectors by *Fine Books & Collections* magazine. "I didn't start thinking of myself as a collector until I had a couple hundred books," says Singh, who began seeking useful books as an undergraduate at the California Institute of Technology. "It just sort of happened."

The books provide an unusual perspective on the history of physics, Singh notes. Early texts on quantum mechanics were almost apologetic in describing the theory's weird principles, and advances in radar and related

technologies during World War II appear to have prompted texts on electricity and magnetism to include radiation and antenna theory, Singh says.

"He's driven by a deep interest in science and physics," says Gordon Cates Jr., Singh's graduate adviser. The



library has also been a boon to Cates, who says that "on more than one occasion" he's borrowed a book from Singh.

Got a tip for this page? E-mail people@aaas.org

Four Q's >>

After 13 years as executive director of the American Mathematical Society, **John Ewing** is moving from Providence, Rhode Island, to New York City to run Math for America. The 5-year-old nonprofit strives to boost math education in U.S. high schools by enticing talented new teachers into the classroom and keeping them there. The new job is a blast from the past for Ewing: He briefly taught middle school math in Attleboro, Massachusetts, while a grad student 40 years ago.



Q: What makes Math for America different from other math-education efforts?

After 3 years, roughly 40% of the teachers of mathematics [in U.S. schools] are gone. ... You can't sustain a profession if you have that kind of attrition. ... What Math for America does is concentrate on that one part of the problem. ... At the moment, it's bringing through something like 40 to 50 new teachers a year. Our hope is to double that number in the next couple of years.

Q: What are the prospects for improving high school math teaching?

I think the prospects are pretty good. ... The money you invest in a teacher, ... when you spread that money out over the thousands of students [taught during his or her career], it's actually very cheap.

Q: What can professional mathematicians do for school mathematics?

Be interested. ... The biggest thing that's missing in secondary education ... is that teachers often are not inspired about mathematics. And what research mathematicians can do [is] tell them about the beauty, the power, and what's going on [in the field].

Q: What was high school math like for you?

I had the greatest teacher; ... his name was Mr. Latino. He was funny; he told terrible jokes; he came strutting into the classroom; he would sometimes make fun of students. But he loved mathematics.



Steering NOAA
through choppy
waters

321



A trigger for
the Sichuan
earthquake?

322



U.S. ECONOMIC RECOVERY

Science Groups Emphasize Jobs in Push for More Research Funding

As the United States struggles with its worst economic crisis since the Great Depression, lobbyists for basic research are offering one more reason the federal government should boost its investment in science: Science means jobs.

Specifically, they want Congress to spend billions on a long list of existing research projects and programs at several federal agencies as part of a massive economic recovery plan legislators are cobbling together this month. To their surprise, that message has received a warm reception from President-elect Barack Obama, his aides, and the Democratic congressional leaders who are shaping a plan that could cost more than \$800 billion over 2 years.

The American Physical Society (APS), for example, is circulating a \$3.5 billion wish list that covers research and training efforts funded by the U.S. Department of Energy (DOE), the National Science Foundation (NSF), and the National Institute of Standards and Technology (NIST). The list proposes upgrades and new activities at DOE's national laboratories, investments in a range of renewable energy technologies, and bump-ups in competitive grants programs at all three agencies. The society's initial list, drawn up right

after the November elections, totaled \$1.5 billion; it was revised after Obama transition team officials "told us we should think bigger," says APS's Michael Lubell.

Some of the projects are also listed in a \$2.7 billion proposal from the Association of American Universities, which includes \$1.8 billion for NSF and the U.S. National Institutes of Health (NIH) to help scientists setting out to become independent investigators. A similar compilation of projects from NASULGC, an association of public and land-grant universities, also calls for an additional \$1.2 billion in NIH's bread-and-butter investigator grants and \$200 million for competitive research at the U.S. Department of Agriculture.

Maria Zuber, a geophysicist at the Massachusetts Institute of Technology (MIT) in Cambridge, says House Speaker Nancy Pelosi (D-CA) delivered the same message to a panel of academic and industry leaders who met with legislators at a December roundtable in Princeton, New Jersey, to discuss the role of science in reviving the economy. "In my wildest dreams, I thought that the best we could hope for would be full funding of the America COMPETES Act [2007 legislation that authorizes a 7-year budget doubling for

NSF, DOE's Office of Science, and NIST]," says Zuber, a member of the panel, which was arranged by Representative Rush Holt (D-NJ), a former physicist. "But when we got there, the speaker told us, 'The COMPETES Act is good. But ask for all of it now, and think bigger.'"

Zuber, who reprised her role last week at a House Democratic leadership forum on Capitol Hill that Pelosi convened, doesn't expect everything on the societies' lists to be incorporated into bills being prepared separately by the House and Senate. But she also doesn't think lawmakers will turn a cold shoulder to the requests. One proposal before Senate appropriators would give DOE's Office of Science as much as \$500 million in construction funds, to be spent at the agency's discretion.

Advocates say the new focus on the literal nuts and bolts of modern science will not only put people back to work quickly but also make it less likely those jobs will disappear in a few years by keeping U.S. companies competitive in a global economy. With unemployment topping 7%, the highest rate in 16 years, that's an easy sell to politicians. In an 8 January speech billed as his first major address since his election, for example, Obama said that repairing the nation's tattered economy will require "investing in the science, research, and technology that will lead to new medical breakthroughs, new discoveries, and entire new industries" in addition to the traditional emphasis on "shovel-ready" construction projects. Extending his earlier commitment to renovate and connect up the nation's elementary and secondary schools, he also proposed "equipping tens of thousands of schools, community colleges, and public universities with 21st century classrooms, labs, and libraries."

That latter promise is music to the ears of academic scientists and administrators. Zuber, head of MIT's department of earth, atmospheric, and planetary sciences, says a new junior faculty member receives a \$1 million start-up package from the university for buying equipment, renovating existing space, and doing whatever else it takes to launch an experimental program. After that, the fledg-

CREDIT: LIZ LYNCH

ling scientist generally must fly solo.

Even if the faculty member wins a federal research grant, chances are it won't include money for lab upgrades. Most federal agencies award less than scientists request, and most scientists choose people over instrumentation when deciding what to eliminate. "NASA always says that things will be better in the out years, but it never happens," says Zuber, who is principal investigator for

GRAIL, an upcoming NASA mission to measure the moon's gravitational field. She says that doubling NSF's major research instrumentation program, which now receives triple the number of good proposals that its \$93 million budget can accommodate, "would be a really helpful" way to ease that crunch.

Pelosi said as much at last week's forum, when she noted Zuber's presence on a panel along with three eminent economists and

Norman Augustine, the former CEO of aerospace giant Lockheed Martin, who chaired a 2005 National Academies' report calling for a \$20 billion federal investment in research and education to strengthen U.S. innovation. "Having a scientist here emphasizes that [the recovery plan] must be about the future," Pelosi stated. "That's nothing new. ... It's about innovation, which begins in the classroom and in the lab."

—JEFFREY MERVIS

EXPORT CONTROLS

Current System Hampers U.S. Innovation, Says Panel

In a world in which economic and national security hinges on a country's technological and scientific prowess, the United States gains more than it loses from sharing information. That counterintuitive message comes from a U.S. National Academies' panel that heaped scorn on current rules that control access to sensitive technical information by non-U.S. citizens as well as the release or export of certain items.

The problem, the panel says in a report issued last week, is that the restrictions are bad for business, security, and science. The solution is to put restrictions on fewer technologies and tighten up on those technologies, such as nuclear weapons or chips to guide missiles, that are vital to U.S. security. "What we want is an open system," says study co-author Brent Scowcroft. "The [better] premise is that everything is open except those things you can justify [a] need to be [restricted]."

The study calls for President-elect Barack Obama to set up new White House bodies to simplify how scientists and companies obtain export licenses and resolve disputes between agencies that delay decisions. It says that export controls on specific items or technologies should last no longer than 1 year unless the government can recertify them. The report also calls for streamlining the process for providing visas for foreigners working in scientific areas. (The study, initiated by the academies, didn't deal with the issue of which information should be labeled as classified.)

Maintained by the State Department, Commerce Department, and the Pentagon, export-control rules determine what products and components can be exported, which concepts can be discussed in open scientific papers, and which subjects are acceptable to discuss with foreign nationals. In the past 2 years, the three agencies have set new time limits to reduce delays in issuing export licenses, removed items that pose no risk from protected lists, and eased restrictions on technical information or products that are readily available on the Internet or overseas. But report co-author John Hennessy, president of Stanford University in

Palo Alto, California, said such moves are just "incremental improvements."

Space scientist Thomas Zurbuchen of the University of Michigan, Ann Arbor, says the current rules are "an obstacle to universities in the United States ... from being the leaders in space research." The Swiss-born researcher was the lead scientist on a project to build a plasma sensor for a Mercury-bound NASA spacecraft called MESSENGER that was launched in 2004. But in 1999, Congress tightened export-control laws, and project managers restricted Zurbuchen's access to design documents he had created. Fortunately, Zurbuchen soon received a green card that exempted him from these restrictions. "We got lucky," he says.

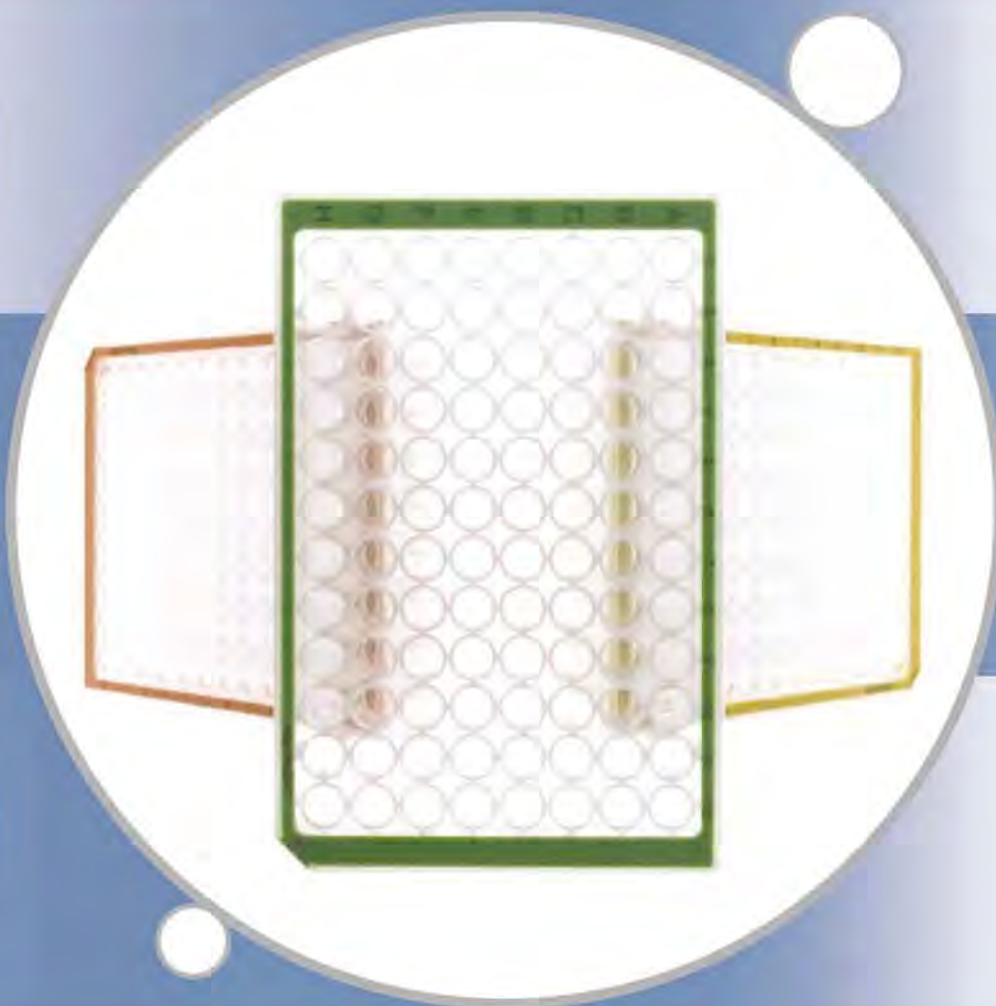
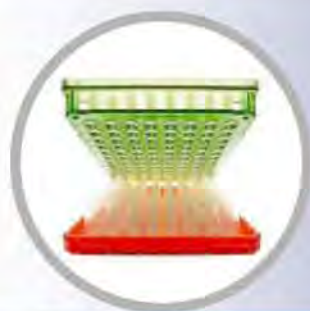
One member of the new Administration likely to be sympathetic to such changes is Defense Secretary Robert Gates, former director of central intelligence and a holdover from the Bush Administration. Gates was a member of the academies' panel before he joined the Cabinet in December 2006. In an e-mailed statement, his spokesperson said the report's recommendations "would have a significant, positive impact" on defense science, though it didn't specify how.

Congress has resisted previous calls for easing export controls, fearing that greater sharing would aid the country's enemies. Supporters worry that any attempt to implement the panel's recommendations could backfire: Legislators could instead pass even more restrictive laws.

—ELI KINTISCH



Killing the MESSENGER. Rules regulating satellite technology almost knocked out a plasma sensor on a 2004 NASA probe to Mercury.



Make the best of it!

Top quality for your sample.

Each of your valuable samples deserves the best treatment. See for yourself how the eppendorf Plate® will save time and reduce costs.

Sample loss in plates can be time consuming and expensive. Therefore, the close environment of each sample should be adapted to its specific quality and purity needs. This can involve a specific purity level or the absence of certain substances, but also stability, reliability, or geometry. The eppendorf Plate® is designed to cover all of the specific needs of your samples!

Bring out the best! Eppendorf Deepwell Plates:

- 30 % faster and easier well identification with the unique OptiTrack® Matrix
- High dimensional stability for efficient centrifugation and mixing
- Minimized sample loss with DNA or Protein LoBind quality and RecoverMax® well design

Learn more about Eppendorf Deepwell Plates:

www.eppendorf.com/dwp

eppendorf
In touch with life

THE TRANSITION

Can an Ecologist Push NOAA Up the Food Chain?

Marine ecologist Jane Lubchenco launched her career studying the complexity of the intertidal zone—who eats whom, for example, and how ecosystems are affected by internal dynamics and external forces. Her colleagues expect that intellectual background to serve her well in the turbulent waters of U.S. federal politics if, as expected, she's confirmed as head of the National Oceanic and Atmospheric Administration (NOAA), part of the Department of Commerce.

Nominated last month by President-elect Barack Obama, Lubchenco, 61, would assume the reins of a \$3.9 billion agency squeezed by cost overruns from a problematic satellite system and beset with aging research infrastructure. Her political bosses are also likely to ask it to play a bigger role in studying and preparing for climate change. "She's got a big job ahead of her," says Marcia McNutt, head of the Monterey Bay Aquarium Research Institute in Moss Landing, California. Although Lubchenco has less management experience than recent administrators, McNutt and other supporters say her tenacity and her experience in teaching scientists how to talk to policymakers augur well for her chances of success.

Lubchenco, a faculty member for 30 years at Oregon State University, Corvallis, has branched out beyond basic research into issues of ocean health and sustainable management. A turning point, says Pamela Matson of Stanford University in Palo Alto, California, was her participation in a strategic planning exercise for the Ecological Society of America (ESA). The effort led to a 1991 "Sustainable Biosphere Initiative" that identified global climate change as a priority research topic for ecologists and called for a focus on improving management of Earth's life support systems. "After that, she became much more engaged in scientific leadership and communication and more focused on the use of science in decision-making," Matson says.

During her leadership of ESA in the early 1990s, Lubchenco helped move the society's offices to Washington, D.C., and set up a policy staff. "She's not a caretaker leader," says Matson. Lubchenco continued to advocate for injecting more science into policymaking when she was president, then chair of the board, of AAAS (which publishes *Science*) from 1996 to 1998.

Lubchenco is a talented dealmaker as well, notes Andrew Rosenberg of the University of New Hampshire, Durham. While serving on the privately funded Pew Oceans Commis-

sion, Lubchenco helped broker a merger in 2005 with the publicly funded U.S. Commission on Ocean Policy. "I don't think it was a foregone conclusion that they would work together," says McNutt.

Lubchenco also has a knack for recognizing a need and filling it. In 1993, she founded the Aldo Leopold Leadership Program, which trains scientists to communicate with policymakers and others, and 6 years later she



Speaking up. Jane Lubchenco has spent her career explaining science to others, including policymakers.

began a similar organization, the Communication Partnership for Science and the Sea, to help publicize policy-relevant findings. Lubchenco's polished communication skills will help her build support for NOAA in Congress and among stakeholders, predicts David Fluharty of the University of Washington, Seattle, who chairs NOAA's Science Advisory Board. "This is where Jane is going to be very strong."

That strength will be needed in running an agency whose responsibilities span basic oceanographic and atmospheric research, the National Weather Service (NWS), fisheries management, and hurricane forecasting. The \$14 billion National Polar-orbiting Operational Environmental Satellite System, for which NOAA is the lead agency with NASA

and the Department of Defense, is behind schedule, over budget, and facing technical challenges. In addition, cost overruns in preparing for the 2010 census, managed by the Commerce Department, could affect NOAA and other departmental activities. Meanwhile, more and more research vessels and other facilities need to be upgraded or replaced. "There are very tough choices," says Conrad Lautenbacher, her predecessor, who resigned in October.

A likely priority is improving NOAA's ability to forecast regional climate change impacts, a cause that Lubchenco has endorsed. (Lubchenco declined to be interviewed, as is customary before nominees are confirmed by the Senate.) NOAA has recently begun considering how to create a National Climate Service (NCS), which would be analogous to NWS (*Science*, 3 October 2008, p. 31).

NCS would bring together NOAA activities now scattered across various branches. NOAA spends roughly \$300 million on climate research and outreach, but Richard Spinrad, head of NOAA's \$398-million-a-year Office of Oceanic and Atmospheric Research, says NCS will need a budget no smaller than the \$900 million that NWS receives. "The diversity of products and services is apt to be broader for an NCS," he says.

Lubchenco will also have to scramble to fund what she sees as needed changes in fisheries management, including setting up marine reserves. A decade ago, Lubchenco proposed putting 20% of the ocean in reserves by 2020, 40 times the current percentage. "I would expect her to be much more cautious at setting goals as an administrator," Fluharty says.

Those who know Lubchenco say her approach to understanding is relevant to managing NOAA: Gather lots of data, think deeply, figure out what needs to be done, and then be an advocate for action. "I think she will harness and energize NOAA's considerable resources to bring about enormous change for the good," says Nancy Baron, COMPASS Ocean Science Outreach Director. "It's an amazing opportunity."

—ERIK STOKSTAD

SEISMOLOGY

A Human Trigger for the Great Quake of Sichuan?

Natural disasters are often described as “acts of God,” but within days of last May’s devastating earthquake in China’s Sichuan Province, seismologists in and out of China were quietly wondering whether humans might have had a hand in it. Now, the first researchers have gone public with evidence that stresses from water piled behind the new Zipingpu Dam may have triggered the failure of the nearby fault, a failure that went on to rupture almost 300 kilometers of fault and kill some 80,000 people.

Still, no one is near to proving that the Wenchuan quake was a case of reservoir-triggered seismicity. “There’s no question triggered earthquakes happen,” says seismologist Leonardo Seeber of the Lamont-Doherty Earth Observatory in Palisades, New York. That fact and the new evidence argue that the quake-dam connection “is worth pursuing further,” he says, but proving triggering “is not easy.” And the Chinese government is tightly holding key data.

Seismologists have been collecting examples of triggered seismicity for 40 years. “The surprising thing to me is that you need very little mechanical disturbance to trigger an earthquake,” says Seeber. Removing fluid or rock from the crust, as in oil production or coal mining, could do it. So might injecting fluid to store wastes or sequester carbon dioxide, or adding the weight of 100 meters or so of water behind a dam.

Whatever the nature of the disturbance, it must bring a nearby fault to the point of failure to trigger a quake. In the case of reservoir-triggered seismicity, the water’s weight can weaken a fault by counteracting the stresses that are squeezing the two sides of the fault together and tightly locking it. Or, the added weight can increase the stress already tending to push opposing sides past each other and break the fault. In 1967, impoundment behind the Koyna Dam in India triggered the largest known reservoir-triggered quake, a magnitude-6.3 temblor that killed 200 people. Seismologists recognize dozens of other reservoir-triggered quakes in the range of magnitude 3 to 6.

So when the magnitude-7.9 Wenchuan earthquake struck, many scientists wondered

if a reservoir was to blame. Ruling out the much-maligned Three Gorges Dam as too distant, experts considered the Zipingpu Dam, just 500 meters from the fault that failed and 5.5 kilometers from the quake’s epicenter. The timing was right. The Zipingpu reservoir began filling in December 2004, and within 2 years the water level had rapidly risen by 120 meters, says Fan Xiao, a chief engineer of the Sichuan Geology and Mineral Bureau in Chengdu.

The several hundred million tons of water piled behind the Zipingpu Dam put just the wrong stresses on the adjacent Beichuan fault, geophysical hazards researcher Christian Klose of Columbia University said at a ses-

just the way the reservoir loading had encouraged it to, he noted.

Klose’s listeners were intrigued but far from convinced. They wanted to hear more details about changing water levels and local, lower-level seismicity. Fan, who was not at the meeting, provides some of those details, all of which favor a link between the Zipingpu Reservoir and the earthquake. Judging by the history of known reservoir-triggered quakes, the rapid filling of Zipingpu as well as its considerable depth would have favored triggering, he says. The delay between filling and the great quake would have given time for reservoir water to penetrate deep into the crust, where it can weaken a fault. And the greatest danger of triggering comes not at the time of maximum filling, he argues, but when the water level is falling. “As we now know, a week before the May 12 earthquake, the water level fell more rapidly than ever before,” says Fan.

A paper in last month’s issue of the Chinese journal *Geology and Seismology* arrives at a similar conclusion. Zipingpu’s impoundment “clearly affected local seismicity,” says lead author Lei Xinglin, a geophysicist at the China Earthquake Administration in Beijing and the National Institute of Advanced Industrial Science and Technology in Tsukuba, Japan. Lei emphasizes that a firm conclusion is premature, but he sees penetration of reservoir water into the fault and the reservoir decline between December 2007 and May 2008 as “major factors associated with the nucleation of the great Sichuan earthquake.”

Fan also does not see the Zipingpu-Wenchuan connection as proven yet, but he’s seen enough to urge caution. “We should readjust our existing plans and take a more cautious attitude when planning projects,” he says. “But I am pessimistic that many of these large-scale constructions will be canceled, because of the strong economic interests that benefit hydropower developers and local governments.”

Building a stronger case for restraint, researchers in and out of China say, will require access to even more detailed data. “Time-variation evidence for seismicity of small earthquakes near and surrounding the reservoir, as well as for the water levels and loading of the reservoir, are needed,” says geophysicist Wen Xue-ze of the Sichuan Seismological Bureau in Chengdu. Fan believes that researchers in the Chinese Academy of Sciences have preliminary results from such studies, “but they are reluctant to share them.”

—RICHARD A. KERR AND RICHARD STONE



Heavy. The several hundred million tons of water behind Sichuan’s Zipingpu Dam may have triggered a devastating earthquake.

sion last month at the Fall Meeting of the American Geophysical Union in San Francisco, California. In his talk, Klose coyly explained—without ever mentioning a dam—how the added water changed the stresses on the fault. According to his calculations, the added weight both eased the squeeze on the fault, weakening it, and increased the stress tending to rupture the fault. The effect was 25 times that of a year’s worth of natural stress loading from tectonic motions, Klose said. When the fault did finally rupture, it moved



Waltzing Quasars Provide Signpost to Merging Galaxies

Astronomers want to know how frequently galaxies merge to understand the broader evolution of the universe. A team reported here at the annual meeting of the American Astronomical Society that it has found a new way of spotting galaxy mergers: by looking for the dance of death of their central black holes. Julia Comerford of the University of California, Berkeley, and her colleagues claim their findings add strength to the idea that merged galaxies can form quasars.

Traditionally, astronomers find mergers by scanning the skies for oddly shaped galaxies or galaxies close together, apparently on the point of merger. Because most galaxies have a supermassive black hole at their center, Comerford and her team reasoned that galaxies that had merged recently would have two black holes spiraling inward. If the black holes had enough gas around them, the gas would collapse inward,

releasing energy and converting one or both black holes into active galactic nuclei (AGNs), or quasars.

So, the astronomers searched spectra from the DEEP2 Galaxy Redshift Survey—the most detailed picture of the universe from as far back as 8 billion years ago—to find the tell-tale light signature of AGNs. (They excluded galaxies with ongoing star formation because this mimics the AGN signature.) The researchers found 107 candidates and then examined their spectra for signs of a merger.

Comerford's team figured that in a recently merged galaxy, the two spiraling AGNs would be moving a lot quicker than the stars in the surrounding galaxies, and so the AGNs' emission lines would be Doppler-shifted out of step with the rest of the galaxy. Because the two AGNs would move in opposite directions, the emission lines of the first AGN would be shifted one way and the lines of the second the

Tell-tail. Astronomers currently spot merging galaxies such as this pair—known as the Mice Galaxies—by their anomalous shapes.

other, resulting in a double peak. That's exactly what the researchers found in two of the 107 galaxies, leading them to conclude that these were dual AGNs.

In another 35 galaxies, the emission lines appeared to be from a single AGN but were offset from the lines of the surrounding galaxy, suggesting an AGN spiraling around a black hole. So 37 galaxies in all—more than a third of the AGN-bearing galaxies in the study—seemed to have undergone a recent merger. From this, the researchers concluded that galaxies from between 4 billion and 7 billion years ago underwent three mergers every billion years. Although that's six times the rate predicted by theoretical models, Comerford says it is close to previous estimates of merger rates derived from observations. She says the discrepancy with the models is because they only consider mergers between two big galaxies.

Aaron Barth, an astronomer at the University of California, Irvine, says the new technique is "very useful because it's completely independent of other methods to estimate the merger rate." The surprisingly high percentage of AGNs showing "offset nuclei" points to "a very clear link between galaxy mergers and the buildup of black holes by accretion of gas," he says.

—YUDHIJIT BHATTACHARJEE

Do Black Holes Seed the Formation of Galaxies?

Which came first, the galaxy or the black hole? Astronomers have been pondering that question because most galaxies have massive black holes at their centers. Are the black holes the seeds around which galaxies grow, or do they form after the galaxies have already taken shape? The verdict from a study presented here at the annual meeting of the American Astronomical Association is that black holes come first. The findings could lead to a better understanding of how galaxies are born.

Galaxies in the nearby universe appear to be uniformly about 700 times as massive as the black holes at their core. Many view this ratio as a clue to the link between galaxy formation and black holes. To understand that link, a team led by Chris Carilli of the National Radio Astronomy Observatory in Socorro, New Mexico, and Dominik Riechers of the California Institute of Technology

in Pasadena set out to establish whether black holes lead to galaxy growth or vice versa.

The researchers looked at distant galaxies, as far back as 1 billion years after the big bang. Carilli and his colleagues, using the Very Large Array radio telescope in New Mexico and the Plateau de Bure Interferometer in France, looked at the radio signals from gas clouds in four such galaxies and deduced their masses. They then compared each mass with the mass of their black holes, which had been obtained using optical telescopes. They found that the galaxies were only about 30 times as massive as their central black holes. If galaxies in the early universe had less than 5% of the galactic flesh around their cores than galaxies of today, Carilli and his colleagues reasoned, then the black holes must have formed before the galaxies.

"It appears that the black holes come first and grow the galaxy around them," says

Carilli. Eventually, like a ripening fruit, the galactic mass grows until its ratio to the black hole mass reaches what astronomers observe in nearby galaxies. Carilli and his colleagues acknowledge that the results seem to contradict findings suggesting that the enormous energy emanating from active black holes inhibits galaxy growth around them.

Astronomer Andrew Fabian of the University of Cambridge, U.K., calls the results "very interesting" and says they are "bound to generate theoretical work" on how black holes and galaxies influence each other. But he's reserving judgment on whether black holes did indeed come first because the conclusions are "deduced from gas motions, not stars," and gas clouds can be affected by nongravitational forces such as magnetic fields, causing astronomers to underestimate the ancient galaxy's mass.

—YUDHIJIT BHATTACHARJEE

AVIAN INFLUENZA

Infection Study Worries Farmers, Bird Lovers

AMSTERDAM—Dutch researchers have embarked on a study in which they deliberately infect wild swans with avian influenza to study the effects on bird migration and viral spread. Although the researchers are using a virus that causes no detectable disease in birds and poses no risk to humans, the experiment has triggered consternation among poultry farmers and bird lovers, who worry that the virus could infect poultry or threaten wild birds. Concerns have reached all the way to the Dutch parliament.

The researchers insist that the risks are vanishingly small because the experiment involves a low-pathogenic influenza subtype called H4N6 that is already ubiquitous in nature. They also point out that the protocol was rigorously reviewed and deemed safe, and the scientific payoff could be considerable.

Scientists know relatively little about how avian influenza—including H5N1, the dangerous strain that has sparked fears of a worldwide pandemic—affects bird migration, which in turn is believed to influence the virus's epidemiology. In a 2007 study, researchers from the Netherlands Institute for Ecology (NIOO) in Heteren and the Erasmus Medical Center in Rotterdam showed that wild Bewick's swans naturally infected with low-pathogenic strains H6N2 and H6N8 fed less frequently and departed on their winter migration later than uninfected birds. But it wasn't clear whether being infected caused the birds to eat less, or vice versa.

In the new study, the same two groups hope to answer that question. The protocol calls for



Trial or error? An experiment in which Bewick's swans (*inset*) are infected with bird flu has veterinarian and Member of Parliament Henk Jan Ormel worried.



16 Bewick's swans to be caught at overwintering sites in the Netherlands, infected with H4N6, then released and tracked using a GPS collar for 18 months. Sixteen other birds serve as controls, while a third group will be injected with phytohemagglutinin, a compound that switches on the immune system in a way that mimics disease. Because H4N6 is so widespread, infecting 16 wild birds is like adding a drop of water to the ocean, says NIOO researcher Marcel Klaassen. Unlike the H5

and H7 strains, H4 has never been known to mutate to highly pathogenic versions or to pose a threat to humans.

Even so, realizing that "this would be very sensitive," the team cleared the study not just with an animal experimentation committee, as Dutch law requires, but also with officials at the Dutch health and agriculture ministries, says Albert Osterhaus, who leads the Erasmus group. The team also consulted independent virologists in the Netherlands and abroad.

"I must admit [that] when I was first asked for a review of this, I was unsure of the ethical considerations," says bird flu researcher Ian Brown of the Veterinary Laboratories Agency in Weybridge, U.K. But Brown became convinced that the study poses a negligible risk and has scientific merit.

Others are not so sure. "It's quite something to deliberately release a virus into the wild," says Henk Jan Ormel, a veterinarian and member of the Dutch House of Representatives. Ormel has asked Minister of Health Ab Klink whether he believes the study is safe for humans and poultry and if not, whether it can be banned. Trinus Haitjema, a Dutch amateur ornithologist who specializes in Bewick's swans, worries that the study may harm the species, whose numbers have dropped sharply the past 15 years.

For now, however, the study is on hold, although not for safety concerns. Because of unusually cold temperatures in January, the researchers decided not to catch any more birds to avoid putting more stress on the animals. Unless an interim analysis of the data later this year yields clear-cut results, researchers hope to complete the study next year. By then, they hope any public opposition will have subsided. —**MARTIN ENSERINK**

THE TRANSITION

CDC's Gerberding Makes an Early Exit

Julie Gerberding, the first woman to lead the U.S. Centers for Disease Control and Prevention (CDC), is stepping aside after more than 6 years of a sometimes rocky tenure at the agency's helm. Her resignation, announced last week, came early but was not a surprise, given that the new Democratic Administration is looking for its own CDC chief. President-elect Barack Obama is expected to nominate his choice shortly; in the meantime, Gerberding's deputy, Chief Operating Officer William Gimson, who has

a business degree and has spent more than 30 years at CDC, will fill in.

Gerberding, an infectious-disease specialist, came to CDC during a tumultuous time, less than a year after the 9/11 terrorist attacks and anthrax mail attacks. Like other agencies such as the U.S. National Institutes of Health, CDC received a massive increase in bioterror defense funding, which Gerberding focused on boosting surveillance of and response to possible biological attacks and other terrorist threats. She also juggled a

dizzying series of disease outbreaks and potential outbreaks, from SARS in China to monkeypox in the United States, to widespread fears of a global influenza pandemic that hasn't materialized.

All these shifts left CDC more "politically visible," says James Curran, dean of the Rollins School of Public Health at Emory University in Atlanta, Georgia, who spent years at CDC and helped lead the agency's response to HIV/AIDS in the early days of the epidemic. Several CDC experts noted that Gerberding was unusually adept at communicating with the public, an increasingly necessary task. "For those of us out in the field, far too often people from on high at

CREDITS: H. J. ORMEL; (INSET) DAVID A. NORTHCOTT/CORBIS

EARTH OBSERVATION

Tracking CO₂'s Comings and Goings From Space

Climate scientists trying to better understand Earth's carbon cycles have long been hampered by tunnel vision. Ground-based carbon dioxide (CO₂) monitoring is precise, but the 100-odd stations across the globe provide insufficient coverage, particularly in developing countries and over the oceans. Soon, however, there will be two eyes in the sky with all-encompassing views of this worrisome greenhouse gas. In the next few weeks, Japan and the United States plan to launch satellites to observe CO₂ from space.

The view from on high should lead to more accurate predictions of how rising CO₂ levels might affect global temperatures and climate change. "This will also contribute to political decisions on [acceptable levels] of CO₂ emissions," says Tatsuya Yokota, who heads the satellite observation office of Japan's National Institute for Environmental Studies (NIES) in Tsukuba. In addition, patchy data have been a "barrier to coloring in the maps of CO₂ sources and sinks," says Peter Reyner, a climate modeler at the Laboratoire des Sciences du Climat et de l'Environnement near Paris. "There are large parts of the globe where this will be our first look [at CO₂ data]."

Japan will launch its Greenhouse Gases Observing Satellite (GOSAT) on 21 January. NASA's Orbiting Carbon Observatory (OCO) will follow on 23 February. Both intend to answer a fundamental question: Where is CO₂ generated by human activities coming from and going to? Each year, humans dump about 9 billion tons of carbon into the atmosphere, but only half stays there, says David Crisp, principal investigator for the \$270 million OCO at NASA's Jet Propulsion Laboratory in Pasadena, California. Of CO₂ recycled from



Parallel views. Japan's GOSAT (left) and NASA's OCO will provide the first global views of CO₂.

the atmosphere, about one-quarter is absorbed by land vegetation and another quarter is somehow drawn into the oceans. "We don't know where the other half is going," Crisp says.

How these carbon sinks might evolve as climate shifts in response to rising CO₂ levels is also unclear. And scientists can't begin to fathom the missing sinks until they've been located.

There are other mysteries, such as large variations in atmospheric CO₂ concentrations from year to year. In 1973, virtually all of the 5 billion tons of carbon put into the atmosphere stayed there; but the following year, 4 billion out of 5 billion tons that were emitted got absorbed by sinks, Crisp says. In another riddle, in 1993, a major El Niño coincided with high rates of CO₂ absorption; the link and mechanism are unclear. GOSAT, a \$500 million joint effort of Japan's space and environment agencies and NIES, has a mission lifetime of 5 years (versus OCO's 2 years) because scientists want "to detect annual variations in CO₂ [resulting from] El Niño, La Niña, and other weather phenomena," Yokota says.

GOSAT will also measure methane, a

greenhouse gas for which there is even less data. Both missions might also contribute to understanding localized problems by helping pinpoint pollution sources.

The satellites grew out of ongoing Earth-observation programs. Crisp says that the CO₂ data gap was long recognized but that improved detection was beyond standard remote-sensing techniques. Previous satellite sensors for ozone worked at thermal or ultraviolet wavelengths, but thermal wavelengths don't work well for CO₂. The new satellites will observe in near-infrared. "The measurement technique is one of the real innovations that OCO and GOSAT have had to make in order to move forward," says Crisp.

The two satellites will observe in different patterns; OCO will be more sensitive to fortnightly or monthly rhythms, whereas GOSAT will be better able to correlate CO₂ levels with changing weather patterns. "The data will be highly complementary," says Yokota. That kind of stereovision might be just what it takes to spot those missing carbon sinks.

—DENNIS NORMILE

CDC have made statements that meant nothing [to us]. Julie really tried to connect CDC with the average person," says Michael Osterholm, director of the Center for Infectious Disease Research and Policy at the University of Minnesota, Minneapolis, and a longtime supporter of Gerberding—and, he hastens to note, of Barack Obama.

But Gerberding's leadership of CDC was also marked by tension and sharp criticism, especially after she launched an extensive reorganization of the agency. Morale among CDC scientists reportedly

Saying goodbye. Julie Gerberding is leaving CDC to make way for an Obama appointment.



plunged, and five former CDC directors wrote Gerberding a letter 3 years ago expressing "great concern" about the departure of top scientists from the agency. In a

sometimes testy interview with *Science* in late 2006, Gerberding defended the changes and expressed confidence that they were needed to help CDC tackle large-scale health threats (*Science*, 13 October 2006, p. 246).

The agency is "clearly at a crossroads" now, says James LeDuc, who spent 14 years at CDC before leaving at the end of 2006 to join the University of Texas Medical Branch at Galveston. Whoever takes over next will have to ensure that young, talented scientists come and stay. And, adds Curran, they must prove adept at another critical task—communicating with Congress and the White House.

—JENNIFER COUZIN

Astronomy's Greatest Hits

When Galileo first pointed his telescope at the moon in 1609, the light from some of the discoveries mentioned in these pages was just passing the Pleiades star cluster, some 400 light-years from Earth. (The moon's light took about 1.25 seconds to reach Galileo's telescope.) During those 400 years,

astronomers learned to capture light from ever-greater distances, revealing a universe that became (and continues to become) ever larger and stranger. Here is a sampler of what we've learned from 4 centuries of harvesting photons.

—TIM FOLGER

1600s



1609: Between 30 November and 19 December, Galileo trained his telescope on the moon and saw mountains, valleys, and "seas." His drawings of the moon appeared in *Sidereus Nuncius*, or "Starry Messenger," which Galileo published in Venice in 1610.

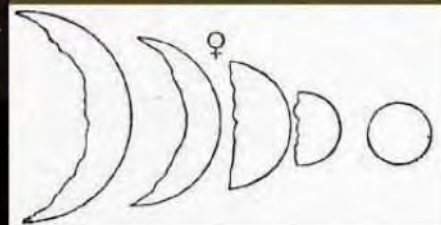


1610: A page from Galileo's journal with sketches of Jupiter and its moons. By 15 January, 3 months before the publication of *Sidereus Nuncius*, Galileo realized that four "stars" he had been tracking near Jupiter were in fact moons of the giant planet.

1610: On 30 July, Galileo wrote to his patron, Cosimo Medici, "I have discovered another very strange wonder. ... Saturn is not a single star, but is a composite of three." Galileo sketched Saturn's rings without knowing what they were. In 1659, Christian Huygens proposed that a ring surrounded Saturn, but he believed the ring was a solid object.

1610: In December, Thomas Harriot, an English polymath, made the first observations of sunspots.

1610: Galileo's drawings of the phases of Venus, which he observed in December. The discovery proved that Venus orbited the sun, not Earth.





1835: Man-bats on the moon! In August, *The New York Sun* falsely reported that John Herschel (William Herschel's son) had discovered life on the moon, including herds of bison, biped beavers, and humanoid bat-winged creatures.

(He also made the first telescopic drawings of the moon a month or so before Galileo's sketches but never published them.)

1639: A 20-year-old English astronomer named Jeremiah Horrocks became the first person to observe the transit of Venus. Horrocks, who died only 2 years after observing the transit, was also the first to hypothesize

that the moon's orbit was elliptical.

1687: Isaac Newton published *Philosophiæ Naturalis Principia Mathematica* (The Mathematical Principles of Natural Philosophy). The *Prin-*



cipia, arguably the most important scientific work ever written, presented Newton's laws of motion

and his theory of gravity, giving birth to modern physics and astronomy.

1700s

1705: Edmund Halley published *Synopsis of Cometary Astronomy* in 1705, which described the orbits of comets and predicted the periodic return of the comet now named for him.

1781: William Herschel discovered Uranus and wanted to

name the new planet after King George III.

1800s



1846: Neptune, the first planet whose existence was predicted on the basis of mathematical calculations, was discovered on 23 September.

1877: The Italian astronomer Giovanni Schiaparelli reported seeing *canali* (channels) on the surface of Mars. Percival Lowell, an American astronomer, later popularized the notion that intelligent beings on Mars had constructed an elaborate network of canals.

1900s

1908: Henrietta Swan Leavitt discovered that Cepheid variable stars

can be used as "standard candles" to measure interstellar distances with great accuracy.

1919: Arthur Eddington led an expedition to Principe, an island off the west coast of Africa, to observe a total solar eclipse. Eddington's observations confirmed Einstein's prediction that massive bodies can warp spacetime and bend light.

1930: Clyde Tombaugh discovered Pluto while working at Lowell Observatory in Flagstaff, Arizona.

1932: Karl Jansky invented radio astronomy with the discovery that the center of the Milky Way emits radio waves. His rotating antenna was mounted on wheels from an old Model T automobile.

1951–1953: James Van Allen launched a



1785: William Herschel and his sister Carolyn mapped the entire sky, proving that the Milky Way is a giant disk of stars with a central bulge.



Late 1920s: Edwin Hubble discovered the first galaxies outside the Milky Way. He also found something even more startling: The galaxies were all rushing away from us, proof that the universe is expanding.

series of “rock-oons”—balloon-borne rockets—and found the first evidence of radiation belts surrounding Earth.

1963: Maarten Schmidt, an astronomer at the California Institute of Technology, identified the first of what he dubbed quasi-stellar objects, or quasars, which can emit thousands of times more energy than the entire Milky Way. Quasars are now thought to be the cores of distant galaxies harboring enormous black holes, and their stupendous energy output is probably caused by radiation released by matter falling into the black hole.

1967: Jocelyn Bell detected the first



1964: Arno Penzias and Robert Wilson discovered the cosmic microwave background radiation, the big bang’s afterglow. At first they thought the signal was caused by heat released from pigeon droppings on the large horn of their radio antenna.

pulsar, a discovery that won a Nobel Prize for her thesis adviser, Antony Hewish. Bell initially wondered if the regular 1-per-second radio pulses she had

picked up might be a signal from an extraterrestrial civilization. The pulses are now known to be generated by the rapidly spinning, extremely dense cores of burned-out stars.

1968: Project Vela, a secret U.S. mission that used satellites to monitor nuclear testing done by the Soviet Union, discovered the first gamma ray bursts. Astronomers now believe the bursts mark the explosions of massive stars.

1971: The first black hole, Cygnus X-1, an x-ray emitting object discovered in 1964, was determined to be a black hole.

1972–1973: The Pioneer 10 and Pioneer 11 spacecraft were launched in March 1972 and April

1973. The spacecraft made the first images of Jupiter’s poles and returned close-ups of the Great Red Spot.

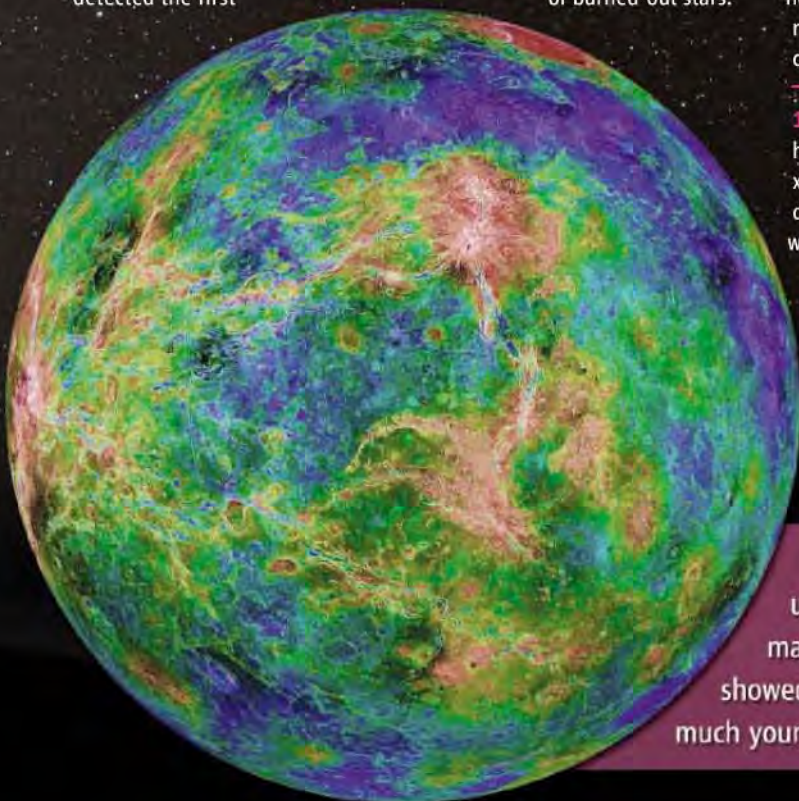
1974: Joseph Taylor and Russell Hulse discovered a binary pulsar system, with one pulsar orbiting the other at a rate approaching 10% of the speed of light. The orbit is so tight and the pulsars so compact that the entire binary system would fit within the sun. Gravitational waves emitted by the pulsars have enabled astronomers to rigorously test Ein-

stein’s general theory of relativity.



1977: The two Voyager space probes were launched and, over the next decade, produced spectacular images of the outer planets, including Saturn and its moons.

1988: Canadian astronomers announced the possible discovery of the first extrasolar planet around a star called Gliese 581; confirmation of the discovery came in 2003. Astronomers now believe that at least three planets orbit the star.



1990: The Magellan spacecraft used radar to make detailed 3D maps of the surface of Venus. They showed that the planet’s surface was much younger than researchers expected.



1995: Immense pillars of gas in this Hubble image of the Eagle nebula glow with the light from newborn stars.

1990–present: The Hubble Space Telescope has found dozens of gravitational lenses, parts of the sky where large concentrations of matter warp light, producing distorted images of distant galaxies.

1992: Aleksander Wolszczan, a Polish astronomer, made the first generally accepted discovery of extrasolar planets. The planets orbit a pulsar—the rapidly spinning remnant of a supernova—980 light-years from Earth.

1994: Between 16 and 22 July, comet Shoemaker-Levy 9,

which had been discovered just the year before, broke apart and collided with Jupiter.



1995: On 7 December, the Galileo spacecraft, launched in 1989, arrived at Jupiter and transmitted some 14,000 images of the planet and its moons back to Earth. Before plunging into Jupiter's

atmosphere in 2003, Galileo found evidence that a 100-kilometer-deep ocean of water may lie beneath the fractured, icy surface of Jupiter's moon Europa.

1995: For 10 consecutive days between 18 and 28 December, astronomers used the Hubble Space Telescope to make hundreds of exposures of a single, small region of the sky. The Hubble Deep Field image showed thousands of the youngest and most distant known galaxies.

1998: Observations of distant supernovas showed that the expansion of the universe is accelerating, driven by a mysterious "dark energy."

2000s

2001: The Wilkinson Microwave Anisotropy Probe spacecraft, launched on 30 June, surveyed the cosmic microwave background with unprece-



1999: The Chandra X-ray Observatory, launched on 23 July, is a satellite that has studied supernova remnants and x-rays from a gargantuan black hole at the center of the Milky Way. In this Chandra image, hot gases streaming into the Milky Way's central black hole release x-rays that light up surrounding clouds of gas.

dent resolution, enabling cosmologists to calculate the age and composition of the universe.

2003: In October, astronomers announced the discovery of the largest structure in the universe: the Sloan Great Wall. It is an

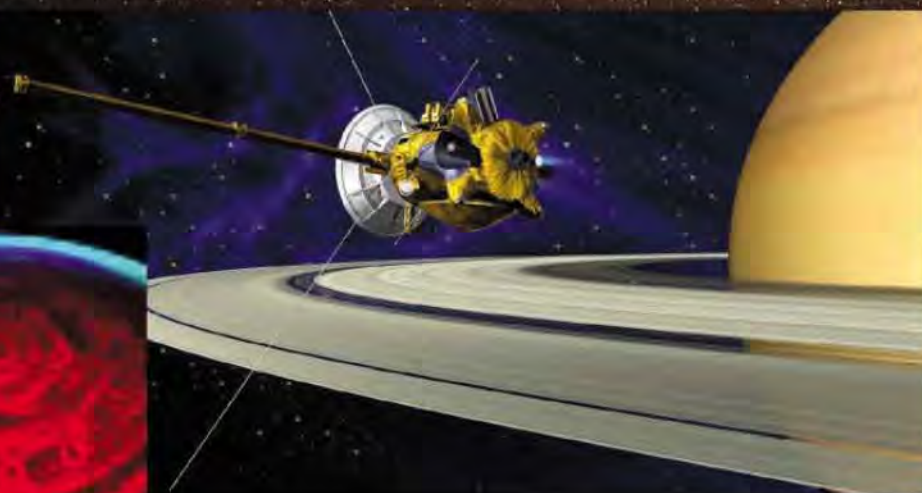
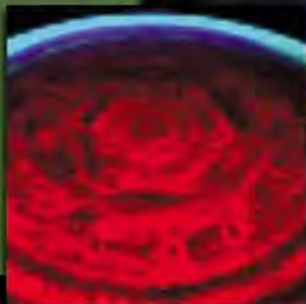
enormous collection of galaxies 1.37 billion light-years in length located about a billion light-years from Earth.

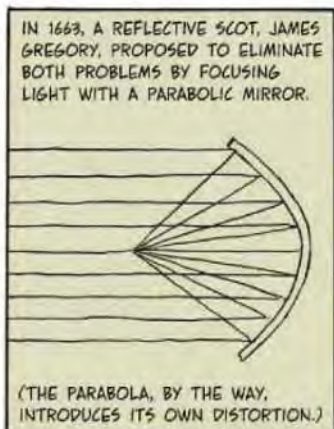
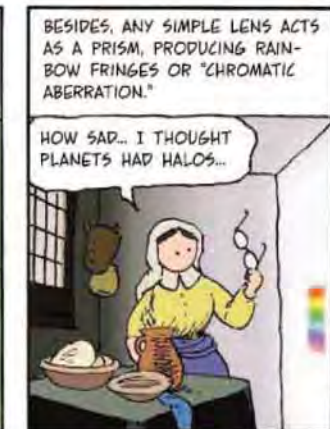
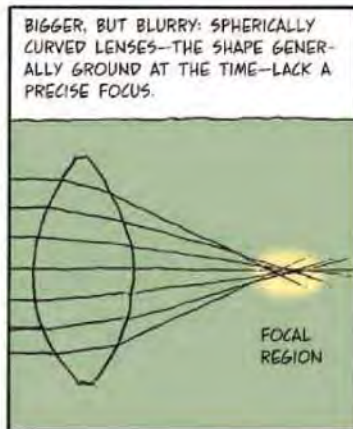
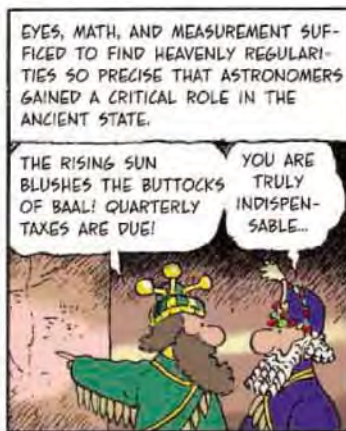
2005: In November, the Spitzer Space Telescope captured the faint infrared glow left from the first stars in the universe.

2008: In September, a Keck telescope on Mauna Kea, Hawaii, and the Hubble Space Telescope captured the first optical images of planets orbiting other stars.

Tim Folger is a contributing editor at *Discover* and *On Earth* magazines and lives in Gallup, New Mexico.

2004: Since the Cassini spacecraft settled into orbit around Saturn on 1 July, it has discovered new moons and hydrocarbon lakes on Titan, and observed wonders such as this strange hexagonal structure at Saturn's north pole.

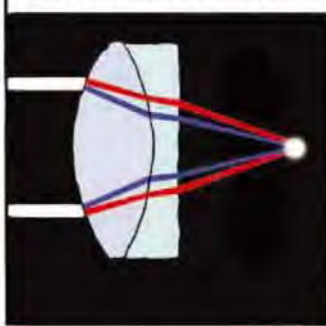




IN 1733, MATHEMATICIAN CHESTER HALL PROVED NEWTON WRONG.



HALL'S IDEA: ABOUT TWO LENSES OF DIFFERENT REFRACTIVE INDICES. ONE WOULD UNBEND THE CHROMATIC ABERRATION OF THE OTHER.



TO MASK HIS PLAN, HE HIRED TWO OPTICIANS, ONE FOR EACH LENS... BUT THEY BOTH USED THE SAME SUBCONTRACTOR, GEORGE BASS, AND BASS BLABBED.



HALL MOVED ON AND LEFT MASTER GRINDER JOHN DOLLOND TO PERFECT AND PATENT COMPOUND LENSES THAT ALL BUT ELIMINATED BOTH CHROMATIC AND SPHERICAL ABERRATION.



MIRROR SHAPING IMPROVED TOO. IN THE 1770S AND '80S, WILLIAM HERSCHEL MADE BIG REFLECTORS, EACH WITH A PARABOLIC MIRROR VIEWED FROM THE LIP OF THE TELESCOPE.



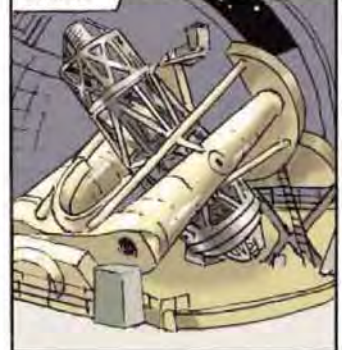
DESPITE SOME FINE REFRACTORS, THE FUTURE CLEARLY LAY WITH BIG REFLECTORS, THOUGH MAYBE NOT LORD ROSSE'S 1847 LEVIATHAN, STUPIDLY SITED IN MISTY IRELAND.



1917: THE GREAT 254-CM MT. WILSON REFLECTOR OPENED ITS EYE—UPON WHICH, ITS OBSESSIVE DESIGNER GEORGE HALE CHECKED INTO AN ASYLUM WITH AN IMAGINARY GREEN FRIEND...



AND FINALLY MT. PALOMAR'S MONSTER, WITH ITS 5-METER, 12-TON MIRROR.



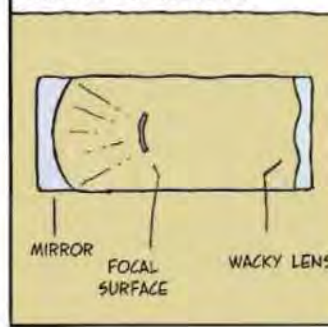
AND THEN WHAT? THESE GIANTS HAD LIMITS: THEIR NARROW FIELD OF VIEW HAMPERED SKY MAPPING... AND THEY HAD TO PEER THROUGH A FUZZY, FLUID BLANKET OF AIR LIKE EVERYONE ELSE.



IN THE 1920S, BERNHARD SCHMIDT SOLVED THE WIDE-ANGLE PROBLEM WITH VAST CALCULATIONS, ALL BY HAND (NOT SO EASY, SINCE HE HAD BLOWN OFF HIS HAND IN A YOUTHFUL EXPERIMENT)...



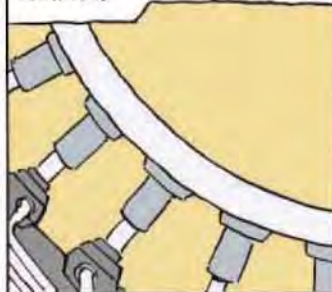
A SCHMIDT TELESCOPE USES A SPHERICAL MIRROR CORRECTED BY A WACKY LENS THAT DELIVERS NEAR-PERFECT GEOMETRY.



NOW ZIP AHEAD TO COMPUTERS AND ROCKETS... THE HUBBLE HURDLES THE ATMOSPHERE... CLEAR IMAGES AT LAST (ONCE THE ORIGINAL FAULTY OPTICS WERE FIXED)!



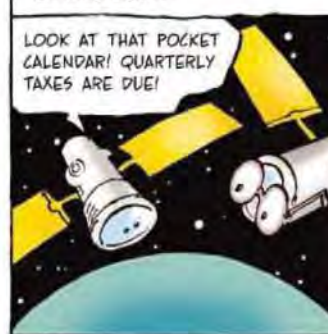
BIG TERRESTRIAL REFLECTORS NOW USE MULTIPLE MIRROR SEGMENTS: THIN, NEARLY FLOPPY THINGS SUPPORTED BY COMPUTER-CONTROLLED LIFTERS THAT MAINTAIN PERFECT CURVATURE.



COMPUTERS CAN EVEN TWEAK SECONDARY MIRRORS TO "DETWINKLE" THE EFFECT OF AIR TURBULENCE IN REAL TIME, FOR IMAGES NEARLY AS CRISP AS THE HUBBLE'S.



OF COURSE, NO GROUND-BASED TELESCOPE CAN COMPETE WITH THE NUMEROUS ORBITING EYES POINTING DOWN.



WHO KNOWS WHAT THE FUTURE MAY BRING? DON'T ASK US... THIS IS A HISTORY, NOT A PREDICTION!



CREDIT: ASTRONOMER WILLIAM ALSCHULER TEACHES AT CAL ARTS; HE GROUND HIS FIRST TELESCOPE LENS IN 8TH GRADE

Astronomy Hits the Big Time

Four hundred years after the invention of the telescope, astronomy is flourishing. But even as the discoveries keep coming, the field is rapidly evolving toward huge telescopes, large collaborations, and—alas—bigger headaches

Because anyone can search the sky, astronomy remains the most democratic of sciences—perhaps the only one in which an amateur can still make a bona fide discovery. In August 2007, Hanny van Arkel did just that. The primary-school teacher from Heerlen, the Netherlands, spotted a strange blue blob in the sky. The intergalactic ghost turned out to be an enormous cloud of gas that is reflecting the light lingering from a now-dead quasar in a nearby galaxy to create a never-before-seen “light echo.” The discovery of Hanny’s Voorwerp (Dutch for Hanny’s Object) earned Van Arkel, 25, a moment of fame. “My name was all over the world, and that’s fun,” she says.

At the same time, the discovery highlights dramatic changes within astronomy. Van Arkel made her find not by looking through a telescope—she doesn’t own one—

arrays spanning thousands of kilometers. Their costs will be measured in billions of dollars apiece. Meanwhile, some researchers are performing huge surveys that take a whole new approach to collecting data, spotting everything in sight and recording it all in vast computerized databases. Already considered “big science,” astronomy is rapidly growing much bigger. And with that growth comes some of the headaches that plague other fields: increasing competition for limited resources and longer times to see projects completed.

“We shouldn’t lose sight of the fact that it’s good to have this problem,” says Roger Blandford, a theoretical astrophysicist at Stanford University in Palo Alto, California. “It’s a sign that astronomy is as intellectually and scientifically exciting as it’s ever been.” Michael Turner, a cosmologist at the University of Chicago in Illinois, agrees:

“This is a very special time in astronomy, when you finally know enough about the universe to ask a variety of big questions, and you have the tools to go after the answers.”

Still, as astronomers reap an ever-greater understanding, they may be losing the romance of their craft. As computerized data streams and remote-controlled observatories become the norm, the lone astronomer trekking to the mountaintop for a night of observing is quickly becoming a quaint anachronism.

A variety of riches

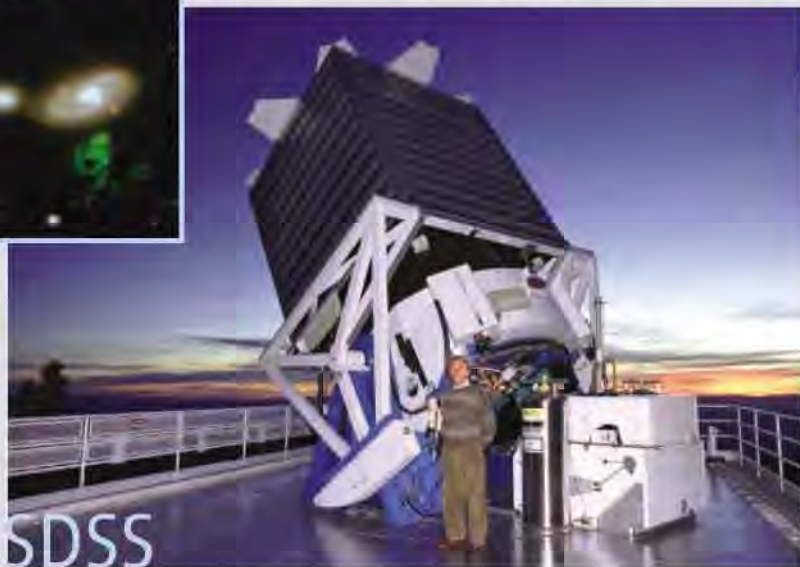
Strikingly, as astronomers have learned more, their field has continued to grow more diverse. Whereas scientists in fields such as particle physics have homed in on a few key conceptual questions—is there a Higgs boson?—astronomers find themselves blessed with an ever-longer list of mysteries ripe for exploration: What’s speeding up the expansion of the universe? How did the first galaxies form? Where do cosmic rays come from? What is the nature of the black hole in the middle of our galaxy?

Much of this progress has been driven by technology. Astronomers have continued to improve their ability to detect the electromagnetic radiation of various wavelengths that emanates from stars and galaxies, from the

advent of radio astronomy in the 1940s, to the birth of x-ray astronomy in the 1960s, to precision studies of the microwaves lingering from the big bang starting in the 1990s.

Most recently, the high-energy gamma-ray universe is coming into focus. These energetic photons are too rare to be picked up by the small telescopes of orbiting observatories and are blocked by the atmosphere. But when one strikes the atmosphere, it sets off an avalanche of electrons and other charged particles. As they zip through the air, these particles produce a pulse of light called Cerenkov radiation that special ground-based telescopes can detect. In 2004, the four telescopes of the High Energy Stereoscopic System (H.E.S.S.) in Gölleschau, Namibia, became the first to spot a source of high-energy gamma rays shining in the sky (*Science*, 3 September 2004, p. 1393; 5 November 2004, p. 956).

Other Cerenkov telescopes, including VERITAS in the United States and MAGIC in the Canary Islands, have joined the search, and astronomers now have more than 100 sources to study. Such high-



Data factory. The Sloan Digital Sky Survey’s 2.5-meter telescope catalogs all it can see. An amateur found the strange “light echo” known as Hanny’s Voorwerp (*inset*, green) in the mounds of data.

but by viewing on her computer some of the millions of images of galaxies captured by the Sloan Digital Sky Survey, an 8-year-old project cataloging everything that can be seen in a vast swath of sky with a 2.5-meter telescope on Apache Point in New Mexico. Van Arkel is one of more than 160,000 volunteers helping to classify 1 million galaxies as part of an outreach program called Galaxy Zoo.

Four hundred years after the invention of the telescope, the heavens continue to yield mind-bending surprises: stellar explosions called gamma-ray bursts that momentarily outshine the rest of the entire universe in gamma-ray light, the bizarre dark energy that is stretching space and speeding the expansion of the universe, and strange planets orbiting other stars.

But even as the science flourishes, the practice and culture of astronomy are changing. Telescopes have grown steadily over the centuries, but the ones now in planning are truly immense—optical behemoths with mirrors measuring 30 meters or more across, and radio-telescope

energy gamma rays are thought to originate in violent events such as supernovas, gamma-ray bursts, and supermassive black holes sucking in matter at the hearts of distant galaxies. "People are very, very excited about progress with the new telescopes," says astrophysicist Masahiro Teshima of the Max Planck Institute for Physics in Munich, Germany, who works on MAGIC. "Their information gives us a clear picture of what is happening in these violent sources."

Novel approaches have also opened realms of discovery. Michel Mayor of the University of Geneva, Switzerland, developed a way to search for parts-in-10-million variations in the color of starlight, such as those a planet can produce by tugging on its star. The frequency of the light increases as the star is pulled toward Earth and decreases as it is pulled away, just as the pitch of a siren rises as a police car approaches and falls as it speeds away.

In 1995, Mayor and colleagues detected the first planet beyond our solar system—a Jupiter-sized giant whizzing around its star once every 4.2 days. Astronomers have since discovered more than 300 extrasolar planets. Those often bizarre other worlds have brought with them more questions than answers, Mayor says, because "we have discovered that our own solar system is in no way typical of what can form in the universe."

Astronomy has also begun to attract more scientists from other fields. They include geologists interested in planet formation, biologists seeking the chemical precursors of life, and—perhaps most notably—particle physicists fascinated by the mystery of dark energy. Since 1998, astronomers have known that some sort of space-stretching energy is accelerating the expansion of the universe, and many physicists are determined to find out what that stuff is.

Stellar strip mining

Near the 2788-meter summit of Apache Point, a telescope juts above the spindly pines, its rectangular casing resembling a big cardboard box. With a 2.5-meter mirror, it isn't a large telescope. Yet perhaps no other is changing the practice of astronomy as dramatically as this one, which feeds the Sloan Digital Sky Survey, a \$150 million effort supported by the private Alfred P. Sloan Foundation, federal agencies, and the 25 participating institutions.

Traditionally, astronomers have taken turns using telescopes, with individuals or small teams applying for observing time to prospect for the astronomical gems that intrigue them. In contrast, since 2000, the 150 members of the Sloan team have worked together to spot all they can in a quarter of the celestial sphere, including 100 million galaxies. Smaller teams then sift through the data from this celestial

strip-mining operation before they are eventually made public.

"People giggled when we put out papers with 100 authors," says Michael Strauss of Princeton University. "But we showed that that many astronomers could get along without killing each other and [that] a large survey could be enormously scientifically productive." For example, Sloan has traced the distribution of galaxies, revealed the structure of our own Milky Way galaxy, and helped explain the origins of different types of asteroids.

The Sloan survey also melds scientific cultures. Particle physicists from Fermi National Accelerator Laboratory (Fermilab) in Batavia, Illinois, have provided key expertise in handling both large collaborations and huge data streams, says David Weinberg, an astronomer at Ohio State University in Columbus. "Without the resources that Fermilab had to bring, I don't think the project would have succeeded," he says.

The Sloan survey is just the first of several enormous surveys in the works. The proposed Panoramic Survey Telescope & Rapid Response System (Pan-STARRS), a \$100 million array of four 1.8-meter telescopes whose construction is funded by the U.S. Air Force, would mainly spot asteroids that menace Earth, but it would also do survey work surpassing Sloan in sensitivity. A prototype telescope is already working on Haleakala in Hawaii. And the planned Large Synoptic Survey Telescope (LSST), a \$400 million instrument that would be paid for by the U.S. National Science Foundation (NSF) and private contributors, would sit atop Cerro Pachón in Chile and use a 3.2-gigapixel camera to image an entire hemisphere of the sky once every 3 nights, spotting 2 billion objects. That's too

many images for humans to look at, so instead they'll have to be "viewed" by specially programmed computers.

To be sure, astronomers have surveyed the skies before. From 1948 to 1958, astronomers at the Palomar Observatory in southern California used a 1.22-meter telescope to produce 937 photographic plates that others used for decades to guide their searches. But the new surveys aim to not only provide better data but also tackle new types of statistical studies.

Following Sloan's lead, Pan-STARRS and LSST will trace the three-dimensional distribution of galaxies and their apparent orientations on the sky. Those measurements should reveal the interplay between space-stretching dark energy and dark matter, the mysterious stuff whose gravity holds galaxies together. Only digital cameras and high-power computing make that statistical approach practical, says LSST's project leader, Anthony Tyson of the University of California, Davis.

Some astronomers say that after such statistical measurements are finished, attention will move away from huge surveys. Others argue

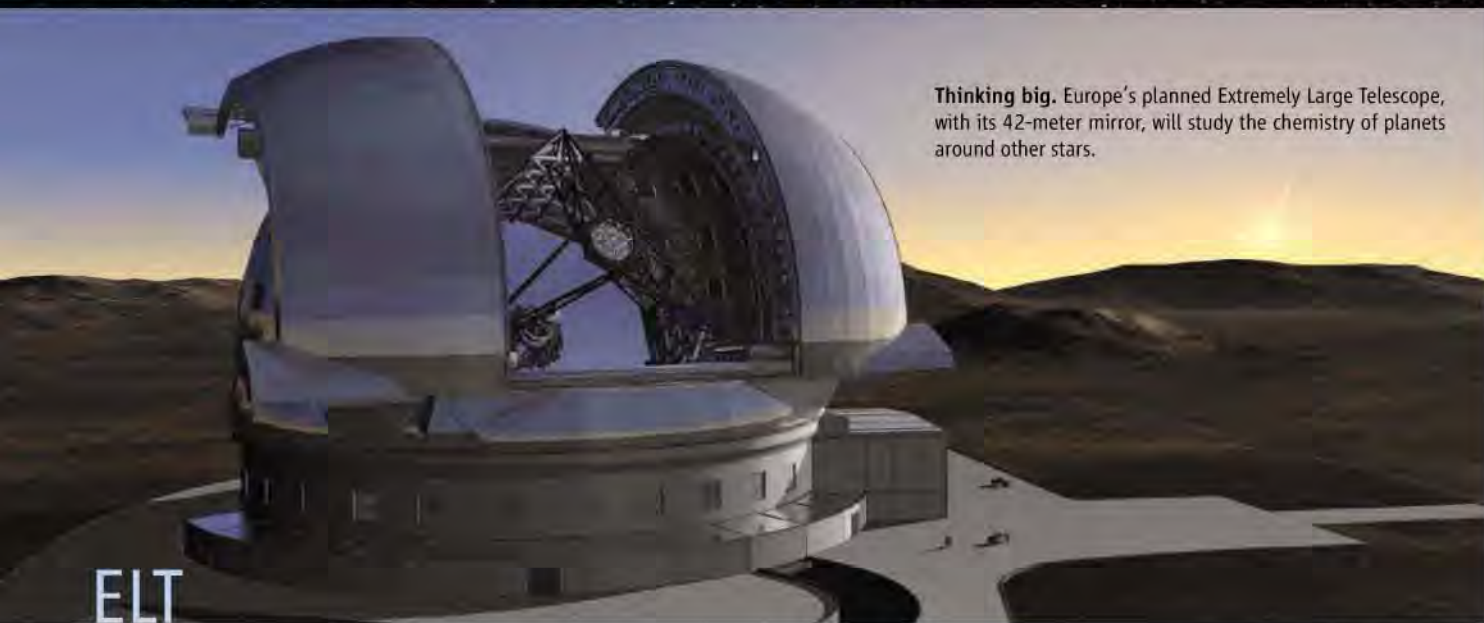


"People giggled when we put out papers with 100 authors. But we showed that that many astronomers could get along without killing each other and [that] a large survey could be enormously scientifically productive."

—MICHAEL STRAUSS
PRINCETON UNIVERSITY



Flash photography. The four telescopes of H.E.S.S. in Namibia look out for the flashes caused by gamma rays hitting the upper atmosphere.



Thinking big. Europe's planned Extremely Large Telescope, with its 42-meter mirror, will study the chemistry of planets around other stars.

that the push toward surveys will permanently change the character of astronomy. "It's here to stay, and it will grow as an overall fraction of the field," Weinberg says.

Watchful giants

Astronomers generally agree that in the future many of them will continue to work in smaller teams to seek out and study individual astronomical objects. That's because "often it is the best-case example [of an object] that tells you the most," says Britain's Astronomer Royal, Martin Rees of the University of Cambridge. But those observations may be made with gargantuan telescopes, and such giants will likely change the practice of observing the sky.

The size of optical telescopes has grown steadily over the past century, from the 60-inch (1.5-meter) telescope at Mount Wilson in California, inaugurated in 1908, to the Large Binocular Telescope at Mount Graham, Arizona, whose twin 8.4-meter mirrors saw first light in 2007. But the next growth spurt will be a big one, as telescope designers have mastered combining many small reflectors into one huge segmented mirror. In the United States, two such extremely large telescopes (ELTs) are in preparation. Grinding has begun on the seven 8.4-meter mirrors that will make up the equivalent of a 24.5-meter reflector for the Giant Magellan Telescope to be built at Las Campanas in Chile, and the Thirty Meter Telescope, with a single giant segmented mirror, is in its design phase. Meanwhile, European astronomers are designing their own European-ELT (E-ELT) with a 42-meter segmented mirror.

Although such gigantic telescopes may be shared in the traditional way, most astronomers won't enjoy the usual hands-on interaction with the machinery. For example, at the European Southern Observatory's Very Large Telescope—an array of four 8.2-meter telescopes on Cerro Paranal in Chile—40% of observations are carried out by astronomers who come to the site on allotted nights, says ESO's Roberto Gilmozzi, E-ELT principal investigator. With a giant such as E-ELT, that will be difficult.

Instead, with thousands of astronomers clamoring for observing time, the scheduling of observations and steering of the telescope are likely to

be fully automated to squeeze out every useful second. No astronomer will need to travel to the mountain—or will be encouraged to do so. In fact, Rees says, the largest optical telescopes will likely be run much like the orbiting Hubble Space Telescope, entirely by remote control.

The notion of a small observing team may also change. The competition for use of the telescope will push astronomers into larger and larger collaborations. Astronomers already gang together for projects that need a lot of observing time to gather large statistical samples. "These will evolve into even larger collaborations," says Gilmozzi, as researchers design elaborate campaigns to make the most of scarce time.

Radio astronomers are going through a similar process with plans for the Square Kilometer Array (SKA), whose thousands of networked dishes will include some more than 1000 kilometers from the array's compact core (*Science*, 18 August 2006, p. 910). Currently in its design stage, SKA will be built in either South Africa or Australia and will scan the sky more than 10,000 times faster than is currently possible. That ability means that large-scale surveys will become an even higher priority. "Surveys will be very big and will take up a lot of the telescope's time," says SKA Director Richard Schilizzi. This will lead to sociological changes, "but I don't know how we'll handle that yet," he says. "Will we have papers with 400 authors? I don't know."

—WENDY FREEDMAN
CARNegie INSTITUTION
OF WASHINGTON

Tighter budgets and stiffer competition

While the size and cost of big telescopes are soaring, national astronomy budgets aren't keeping pace. So the competition for limited resources is growing fiercer. Such budget constraints are already starting to pinch. In 2005, NSF, which funds ground-based efforts, requested that astronomers conduct a "senior review" to free up \$30 million in its \$200 million annual astronomy budget. Among other cuts, the 2006 review recommended that NSF stop funding the gigantic and storied Arecibo radio observatory in Puerto Rico in 2011.

The painful process was necessary, says Craig Foltz, acting director of NSF's division of astronomical sciences, because the agency did not have enough money to develop new projects such as LSST and an ELT or to pay the United States's share for operating the



Atacama Large Millimeter Array (ALMA), a \$1 billion international observatory under construction in Chile.

European astronomers may face similar decisions as they enter the era of E-ELT and SKA. Just 2 months ago, they completed a road map of desired projects for the next 2 decades; now they are waiting to see how funders react to the requested 20% funding increase over the next 10 years (*Science*, 28 November 2008, p. 1313). "Even if you closed all the smallest telescopes, it doesn't make any inroads into the cost of the E-ELT," says astrophysicist Michael Bode of Liverpool John Moores University (LJMU) in the U.K., who headed the road-map effort. "We'll need to increase budgets overall for the largest [projects]."

As telescopes get bigger, the time needed to complete them is stretching, too. Each decade, U.S. astronomers rank their top future projects in a "decadal survey" sponsored by the U.S. National Research Council. None of the four large ground-based projects in the 2001 decadal survey has been completed yet, notes Wendy Freedman, an astronomer with the Observatories of the Carnegie Institution of Washington in Pasadena, California, and chair of the NSF-NASA Astronomy and Astrophysics Advisory Committee. Compounding matters, large projects are often international efforts involving multiple funding agencies. "We need to find a mechanism for getting all these funding agencies and countries to work together," Freedman says. "That's a lot more complex" than working with a single funding agency.

Those complexities became apparent in the development of ALMA, an array of 66 millimeter-wave dishes taking shape 5000 meters up at Llano de Chajnantor, a plateau in Chile's Atacama Desert. Widely regarded as the first worldwide collaboration in astronomy, the project originated when U.S. and European astronomers merged two rival projects in 1999. Japan joined in 2001.

But getting the U.S.-European part of the project to work has not been easy. Early on, it was run by two management teams in Garching, Germany, and Charlottesville, Virginia, but that arrangement proved cumbersome and decision-making was slow. The project also found itself buffeted by factors outside its control, such as rapidly rising prices of steel, copper, and labor, and problems with prototype antennas provided by suppliers. As a result, in 2005, managers were forced to ask for a 40% budget increase to about \$1 billion (*Science*, 19 May 2006, p. 990).

U.S. and European funders eventually agreed to the increase. To streamline the project's management, the partners set up a joint team in Santiago, Chile's capital, to make day-to-day decisions. ALMA was then back on track, and the first of its dishes, most of them 12 meters across, was installed last month. Still, managers are feeling pressure to prove that such an effort can work. "We have a big burden on our shoulders," says ALMA Director Thijs de Graauw. "If ALMA works, it will neutralize many of the critical comments about the size and global nature of such projects."

Dreads and dreams

Some researchers have misgivings about the push toward huge telescopes and large collaborations. Astronomy may be starting down the "dinosaurs' path to extinction" taken by

Looking up. The first dish of 66 that will eventually make up the 16-kilometer-wide ALMA array in Chile, the first global observatory.

ALMA

particle physics, a field that now consists of a few huge experiments with hundreds or thousands of collaborators, says Simon White, a theorist at the Max Planck Institute for Astrophysics in Garching. Bigger telescopes aren't necessarily more productive, White says, but researchers push for them because it's clear how they improve on their predecessors. "You can't plan for scientific discovery, but you can plan for technological advances," he says.

White also worries that large collaborations encourage researchers to overspecialize. "More and more people are trained basically to develop software for a specific measurement and not to look for something new,"

he says. De Graauw sees a related problem. "Astronomers are getting so used to getting everything by computer that they're removed from reality," he says. "It's getting hard to find astronomers who are familiar with instruments."

Others say the push to bigger teams and increased specialization is inevitable if the science is to advance. "The whole field is becoming much more professional," says Bruno Leibundgut, ESO's science director. "If you want to build an instrument for a big telescope, you can't just go to a funding agency and say, 'Here's our idea, and if it doesn't work, too bad.' You need quality assurances and controls that four guys at an institute may not have."

Many say that small groups working with small telescopes still have plenty of opportunities to make real contributions. For a start, smaller observatories are important training grounds for younger astronomers and test beds for new ideas and techniques. "Training is a lot easier with a backyard instrument," Schilizzi says. But smaller scopes need to do more than that to justify their continued existence. "They're never going to compete with big telescopes in extracting a spectrum of a faint object," says LJMU's Bode, so instead they have to find niches that play to their strengths.

For example, small scopes are good for reacting quickly to fast-moving events in the sky. Such agility is the bread and butter of the 2-meter Liverpool Telescope operated by the Astrophysics Research Institute at LJMU. If, say, an orbiting observatory sends word that it has sighted a new gamma-ray burst, the fully automated scope drops what it is doing, swings to the patch of sky indicated in the message, and compares what it sees with an image from an online database. If something interesting is afoot, it will start snapping pictures. "This can be done within a minute or two of a gamma-ray burst," Bode says—probably faster than a bleary-eyed astronomer could react.

Although such uses may provide a role for smaller telescopes in the future, they still don't require an astronomer to make the long trip to a distant mountaintop and spend a cold night gazing at the stars. "An important romantic part of the field is disappearing," De Graauw says. Although astronomers are unlikely to complain as long as they can do the science they want, it's hard not to feel a pang of regret. Peer through your own telescope, and starlight millions of years old passes into your eye. It's an experience that inspires awe and wonder. With the advent of automated observatories and computerized data streams, it's also one that bears ever less resemblance to the practice of astronomy.

—ADRIAN CHO
AND DANIEL CLERY

Online sciencemag.org

Podcast interview
with authors

Adrian Cho and
Daniel Clery.



China's 2009 Eclipse

July 13-24, 2009



Visit three of China's most important cultural sites—**Beijing**, **Xi'an**, and **Hangzhou**—before seeing the **Total Solar Eclipse, July 22, 2009** at the mouth of the Qiantang River near Hangzhou.

In Beijing, visit landmarks like the Forbidden City, and Mutianyu, where the Great Wall winds sinuously along steep ridges that once formed the northern frontier of China's "Middle Kingdom."

Xi'an is our second major destination and was China's capital more than 2,000 years ago when the Qin Dynasty Emperor Huangdi interred several thousand life-sized horses and soldiers made of terra cotta clay. Xi'an is also the site of the recently-excavated Banpo neolithic culture site.

Experience the heritage of **Hangzhou**, in the lake country of Zhejiang, eastern China, which has been a resplendent city since the time of Marco Polo more than 700 years ago. Sample the heritage of Hangzhou and beautiful West Lake.



At Yanguan, which is on the coast of eastern China, the **Total Solar Eclipse of July 22, 2009** will have a duration of totality of **5 minutes and 48 seconds**, the longest there will be in our lifetimes.

Also visit **Shanghai**, the city which expresses China's futuristic vision most extravagantly. \$3,695 + air

For a detailed brochure, please call (800) 252-4910

AAAS Travels

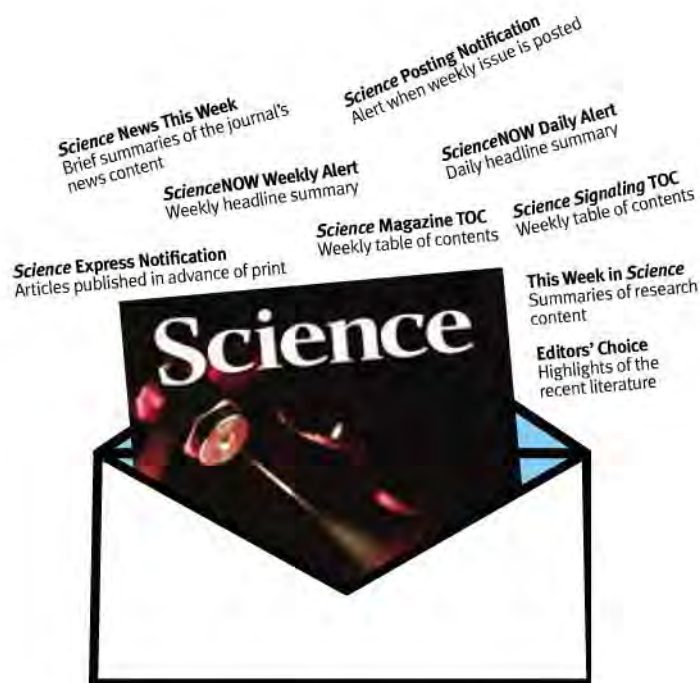
17050 Montebello Road
Cupertino, California 95014

Email: AAASInfo@betchartexpeditions.com

FREE
with registration

Science Alerts in Your Inbox

Get daily and weekly E-alerts on the latest breaking news and research!



Get the latest news and research from *Science* as soon as it is published. Sign up for our e-alert services and you can know when the latest issue of *Science* or *Science Express* has been posted, peruse the latest table of contents for *Science* or *Science Signaling*, and read summaries of the journal's research, news content, or Editors' Choice column, all from your e-mail inbox. To start receiving e-mail updates, go to:

sciencemag.org/ema



Innovation and
the future

340

Fish and
the carbon cycle

343



Organizing inorganics

344



LETTERS | BOOKS | POLICY FORUM | EDUCATION FORUM | PERSPECTIVES

LETTERS

edited by Jennifer Sills

Grants on the Run



EPSCoR states

THE EXPERIMENTAL PROGRAM TO Stimulate Competitive Research (EPSCoR) was designed to help U.S. states with limited facilities improve their research infrastructure in order to make them more competitive for nationwide grants, such as the R01. Twenty-seven states and territories (including Puerto Rico and the U.S. Virgin Islands) have been designated EPSCoR states (1). In a recent Letter ("Declines in NIH R01 research grant funding," 10 October

2008, p. 189), H. G. Mandel and E. S. Vesell presented the current funding statistics for R01 grants. These findings and other changes in policy (2) demonstrate the difficulty in getting R01 grants funded in the current climate. The existing funding situation encourages investigators from EPSCoR states to take their R01 grants and leave for better institutions because better institutions have the resources to obtain new R01 grants and renew R01 grants.

How can institutions in EPSCoR states retain their scientists with R01 grants under these difficult conditions? It may be necessary to offer extremely competitive financial packages to scientists from elsewhere with R01s or to change the promotion and tenure policies. Perhaps scientists who have R01s could receive early promotion and tenure, or the tenure clock could be extended to give scientists more time to obtain an R01.

SAMITHAMBY JEYASEELAN

Department of Pathobiological Sciences, Louisiana State University, Baton Rouge, LA 70803, USA. E-mail: jey@lsu.edu

References

1. EPSCoR Foundation, "What Is EPSCoR?" (www.epscorfoundation.org/WhatIsEPSCoR.htm).
2. NIH, "New NIH Policy on Resubmission (Amended) Applications" (<http://grants.nih.gov/grants/guide/notice-files/NOT-OD-09-003.html>).

Fishing for More Effective Incentives

IN THEIR REPORT "CAN CATCH SHARES PREVENT fisheries collapse?" (19 September 2008, p. 1678), C. Costello *et al.* present empirical evidence to support the view that providing incentives for fishers by allocating them shares in the catch [individual transferable quotas (ITQs)] can halt, or even reverse, the trend toward increasing collapse

of fisheries. We do not dispute that correct incentives are important in solving fishery problems, but we urge caution in interpreting and acting on these results.

Adoption of ITQs does not always prevent overfishing, as illustrated by several stocks managed by ITQs in Australia and New Zealand (1). ITQs are a blunt economic instrument and may actually create perverse incentives. For example, "high-grading" (discarding fish of lower market value to maximize returns from the catch share) is a

common feature of such systems. Partial rights allocation (a common feature where fish cross jurisdictional boundaries) can result in both misreporting and failure to control catches (2). In multispecies fisheries, restrictions on quota species can lead to targeting and overfishing on commercial species not in the quota system. Placing all species in the quota system leads to very expensive fishery management systems, and rights allocation tends to be an irreversible decision short of complete government buy-out of a fishery. Furthermore, like other management regimes based on strong property rights, ITQ management can lead to litigious behavior and attract speculators.

Costello *et al.* focus on overfishing of target species, but fishery managers now have to consider and manage broader ecological impacts of fishing (3), and it is not clear that catch shares create incentives to deal with these problems. For example, major global issues include both bycatch (catch and discarding of noncommercial species) and the impacts of fishing on benthic habitats and communities (4, 5). Once private property rights have been allocated, it may prove difficult for regulators to protect benthic habitats and associated and dependent noncommercial species (6).

Concerns about overfishing and wider ecological impacts of fishing have prompted a variety of solutions to the fisheries management problem. Those who despair of traditional approaches tend to favor alternatives such as widespread use of areas closed to fishing (e.g., marine protected areas) (7). Those

Letters to the Editor

Letters (~300 words) discuss material published in *Science* in the previous 3 months or issues of general interest. They can be submitted through the Web (www.submit2science.org) or by regular mail (1200 New York Ave., NW, Washington, DC 20005, USA). Letters are not acknowledged upon receipt, nor are authors generally consulted before publication. Whether published in full or in part, letters are subject to editing for clarity and space.

with more direct experience of fisheries tend to stress the importance of incentives, of which catch shares are the most common (but not only) example (2). We agree with the importance of incentives but distrust any single-factor solutions to overfishing and other fishery issues. In our experience, solutions to most real-world fisheries problems are likely to comprise a package of measures, including (where appropriate) ITQs, spatial management, effort and gear restrictions, as well as removal of excessive subsidies.

TONY SMITH,* MARK GIBBS, DAVID SMITH

Wealth from Oceans National Flagship and CSIRO Marine and Atmospheric Research, Australia.

*To whom correspondence should be addressed. E-mail: tony.d.smith@csiro.au

References

1. J. Larcombe, K. McLoughlin, Eds., "Fishery status reports 2006: Status of fish stocks managed by the Australian government" (Bureau of Rural Sciences, Canberra, 2007).
2. R. Q. Grafton *et al.*, *Can. J. Fish. Aquat. Sci.* **63**, 699 (2006).
3. E. K. Pikitch *et al.*, *Science* **305**, 346 (2004).
4. D. L. Alverson *et al.*, *FAO Fish. Tech. Pap.* **339** (1994).
5. J. B. C. Jackson *et al.*, *Science* **293**, 629 (2001).
6. M. T. Gibbs, *Mar. Pol.* **31**, 112 (2007).
7. C. M. Roberts *et al.*, *Science* **294**, 1920 (2001).

Diverse Fisheries Require Diverse Solutions

WE APPLAUD C. COSTELLO *ET AL.*'S REPORT "CAN catch shares prevent fisheries collapse?" (19 September 2008, p. 1678) for empirically evaluating one solution to fisheries collapses—individual transferable quotas (ITQs)—but worry about promoting a single, prescriptive solution for diverse global fisheries based on the overly simplistic premise of "getting incentives right" (1–3). Examples of ITQs considered by Costello *et al.* come from developed countries with strong governance and temperate or subtropical ecosystems with low relative diversity; these conditions favor single-species fisheries. Hence, the results do not represent catch shares generally and cannot be extrapolated globally to model the recovery of the world's predominantly small-scale and data-poor fisheries.

ITQs raise social issues that should not be ignored, such as the effects of consolidation, lost livelihoods, restricted resource access, allocation by historical privilege, and reduced local investment (4). These undermine the local stewardship and "individual incentives" necessary for successful implementation of ITQs (3). Without solutions to issues of equity, population growth coupled with increases in ITQ-managed fisheries could

lead fishers displaced from formerly open-access areas to pursue illegal, unregulated, and unreported fishing or to fish other species within ITQ zones.

To stem collapse and begin recovery, the world's fisheries need diverse and practical management measures, including ITQs as well as marine protected areas, traditional user rights, and minimum/maximum size limits, among others (5, 6).

NATALIE C. BAN,^{1,2*} IAIN R. CALDWELL,^{1,2} THOMAS L. GREEN,³ SIÂN K. MORGAN,² KERRIE O'DONNELL,^{1,2} JENNIFER C. SELGRATH^{1,2}

¹Project Seahorse, University of British Columbia, Vancouver, BC V6T 1Z4, Canada. ²Fisheries Centre, University of British Columbia, Vancouver, BC V6T 1Z4, Canada. ³Interdisciplinary Studies, University of British Columbia, Vancouver, BC V6T 1Z4, Canada.

*Present address: Australian Research Council Centre of Excellence for Coral Reef Studies, James Cook University, Townsville, QLD 4811, Australia.

†To whom correspondence should be addressed. E-mail: n.ban@fisheries.ubc.ca

References

1. J. R. Beddington, D. J. Agnew, C. W. Clark, *Science* **316**, 1713 (2007).
2. D. R. Griffith, *Frontiers Ecol. Env.* **6**, 191 (2008).
3. C. Costello, S. D. Gaines, J. Lynham, *Science* **321**, 1678 (2008).
4. J. D. Wingard, *Human Org.* **59**, 48 (2000).
5. J. M. Orensanz *et al.*, *Bull. Mar. Sci.* **76**, 527 (2005).
6. F. Berkes, R. Mahon, P. McConney, R. Pollnac, R. Pomeroy, *Managing Small-Scale Fisheries: Alternative Directions and Methods* (International Development Research Centre, Ottawa, 2001).

Response

OUR REPORT (BY J.L., C.C., AND S.D.G.) should not be read as a blinkered push for individual transferable quotas (ITQs). We agree that ITQs are not a panacea; we simply used them as a convenient subset of rights-based management to test whether Worm *et al.*'s prediction (1) of 100% collapse holds true for rights-based fisheries. The data used by Worm *et al.* are aggregated over large spatial areas, and ITQ fisheries are the only rights-based fisheries that are implemented on a similar scale.

We showed in our Report that, on average, ITQ-managed fisheries are significantly less prone to collapse than are non-ITQ fisheries. However, simply switching to ITQs does not guarantee ecological and social benefits: Total allowable catches (TACs) must still be set appropriately, and design must account for social objectives. Fisheries are complex interactions between ecosystems and human societies where market incentives can fail for a variety of reasons. For example, when enforcement is inadequate, species with little economic value may still be discarded. Quota holders may support the depletion rather than

the sustainable harvest of species with exceptionally low productivity. Separation between those who harvest the fish and those who set the quota can compromise the incentives for sustainable harvesting. Component populations may be depleted if the geographic scale of management exceeds the geographic scale of these populations.

Smith *et al.* raise a range of valid concerns about the ecological impacts of ITQs (such as bycatch and high-grading). However, ITQs can result in quota holders encouraging more restrictive TACs, reducing levels of bycatch, and supporting conservation measures such as marine protected areas (2–4). Branch *et al.* (5) found no evidence that ITQs cause an increase in high-grading. In Canada, multispecies ITQs were observed to be no more expensive to enforce than existing regulations (6). Learning from this rich range of experience is fundamental to improving fisheries management generally and to applying rights-based mechanisms in particular.

Similarly, Ban *et al.* raise justifiable concerns about the socioeconomic impacts of ITQ implementation. Potential for consolidation and lost livelihoods should be part of any discussion on implementing rights-based management and balanced against expected societal gains from enhanced management. As noted by our Report, there are many rights-based alternatives to ITQs.

Despite these caveats, we strongly disagree that "getting incentives right" is an overly simplistic premise. Our Report tested and validated Hilborn *et al.*'s (7) hypothesis that sustainable fishing will occur when institutional incentives encourage participants to behave in ways that society considers beneficial. Other premises (such as Ban *et al.*'s argument that equity is essential for sustainability) should also be tested with the same degree of rigor.

JOHN LYNHAM,^{1*} CHRISTOPHER COSTELLO,² STEVEN D. GAINES,³ R. QUENTIN GRAFTON,⁴ JEREMY PRINCE⁵

¹Department of Economics, University of Hawaii at Manoa, 2424 Maile Way, Honolulu, HI 96822, USA. ²Bren School of Environmental Science and Management, 4410 Bren Hall, University of California, Santa Barbara, CA 93106, USA. ³Marine Science Institute, University of California, Santa Barbara, CA 93106, USA. ⁴Crawford School, Australian National University, Ellery Crescent, Canberra, ACT 0200, Australia. ⁵Biospherics P/L, Post Office Box 168, South Fremantle, WA 6162, Australia.

*To whom correspondence should be addressed. E-mail: lynham@hawaii.edu

References

1. B. Worm *et al.*, *Science* **314**, 787 (2006).
2. R. Q. Grafton *et al.*, *Can. J. Fish. Aquat. Sci.* **63**, 699 (2006).
3. D. Griffith, *Front. Ecol. Environ.* **6**, 191 (2008).
4. D. Festa, D. Regas, J. Boomhauer, *Issues Sci. Tech.* **75**, Winter (2008).

5. T. Branch, K. Rutherford, R. Hilborn, *Mar. Pol.* **20**, 281 (2006).
6. D. Burke, G. Brander, *FAO Fisheries Techn. Pap.* **401/1** (2000).
7. R. Hilborn, A. E. Punt, J. Orensanz, *Bull. Mar. Sci.* **74**, 493 (2004).

A Question of Ethics

IN "DO WE NEED 'SYNTHETIC BIOETHICS'?" (Policy Forum, 12 September 2008, p. 1449), E. Parens *et al.* warn of a further "balkanization" of bioethics: the tendency to divide bioethics into ever more subfields (such as gen-ethics and neuro-ethics), each of which lacks awareness of the general ethical questions common to all areas. According to the Policy Forum, the ethics of synthetic biology is just the latest offspring in a line of ethical enterprises of debatable value. Parens *et al.* use our commentary on synthetic biology's ethical implications (1) as an example of this trend.

We did not call for the inauguration of "synthetic bioethics" as a new field of inquiry. However, we do claim that the ethical issues raised by synthetic biology differ from those raised by genetic engineering. Synthetic biology constitutes a shift from

manipulation (the optimization of known organisms) to creation (the vision of nature as blank space to be filled with whatever organisms one might devise). We must integrate synthetic biology's specific characteristics with the thornier questions of general ethical provenance.

JOACHIM BOLDT* AND OLIVER MÜLLER

Department of Medical Ethics and History, University of Freiburg, Freiburg, Germany.

*To whom correspondence should be addressed. E-mail: joachim.boldt@uniklinik-freiburg.de

Reference

1. J. Boldt, O. Müller, *Nat. Biotechnol.* **26**, 387 (2008).

Response

WE REGRET THAT BOLDT AND MÜLLER INTERPRETED our Policy Forum as charging them with balkanizing bioethics and calling for such a subfield; they do not call for this, nor did we say that they do.

Boldt and Müller do claim that synthetic biology raises new ethical issues, and on this we differ. We think that "creating" life in the context of synthetic biology raises the same ethical question that is raised by "manipulat-

ing" life in the context of genetic engineering (and in contexts such as assisted human reproduction, embryonic stem cell research, or animal-human chimeras). The question is: Should there be any in-principle limits on our capacity to transform ourselves and the rest of the natural world?

If Boldt and Müller are right and synthetic biology raises fundamentally new ethical issues, then someone would have solid ground on which to argue for a new bioethical subfield. If we are right, it makes better sense to just drill down with this thorny old question.

ERIK PARENS,* JOSEPHINE JOHNSTON,
JACOB MOSES

The Hastings Center, Garrison, NY 10524, USA.

*To whom correspondence should be addressed. E-mail: parens@thehastingscenter.org

CORRECTIONS AND CLARIFICATIONS

News of the Week: "European Union floats tighter animal-research rules" by G. Vogel (14 November 2008, p. 1037). The article referred to lampreys as invertebrates. Lampreys, however, have backbones. The new European Union regulations regarding animal research list Cyclostomes as "invertebrate species" that should be regulated. Cyclostomes include hagfish (which lack a vertebral column) and lampreys.



Genomics of Energy & Environment is the topic of the 2009 Department of Energy Joint Genome Institute (DOE JGI) User Meeting, which will be held March 25-27 in Walnut Creek, California. This year's meeting will specifically emphasize the **genomics of renewable energy strategies, biomass conversion to biofuels, environmental gene discovery, and engineering of fuel-producing organisms**. The meeting will feature presentations by leading scientists advancing these topics. The meeting will also include informatics workshops and tutorials for the analysis of prokaryotic and eukaryotic genomes, and the evaluation of new sequencing platforms and their applications. Poster submissions are encouraged. Pre-registration is required as interest is expected to exceed meeting capacity again this year. Registration and a preliminary agenda can be found at: www.jgi.doe.gov.

ScienceClassic

The complete
Science archive
1880-1996

Fully integrated with
Science Online
(1997-today)

Available to institutional
customers through a site license.
Contact ScienceClassic@aaas.org
for a quote.

Information: www.sciencemag.org/classic



SCIENCE, TECHNOLOGY, AND SOCIETY

Reflections for Looking Forward

Edward J. Hackett

"[T]echnology is always disruptive of traditional social forms and creates a crisis for culture. The ground on which the battle is fought is nature."

—Daniel Bell (2)

Bell's ringing call to action is one voice in a choir of concern about the potentially unsettling consequences of technological innovation, harmonizing with those of Lewis Mumford (megatechnics), Joseph Schumpeter (creative destruction), Langdon Winner (technological somnambulism), and the many scholars concerned with varieties of technological determinism (3). Their voices create an essential counterpoint to melodies of technological optimism. With *Insatiable Curiosity*, her latest book about innovation, Helga Nowotny (vice president of the European Research Council and an eminent scholar of science, technology, and society) has added a voice of distinctive elegance, clarity, and sophistication to the choir. Her central motif is the paradox of innovation: Innovations arise from the past, take form in the present, and shape the future. They are at once a source of societal advantage and vulnerability, certain to unsettle us in unpredictable ways. With this slim volume, Nowotny invites us to contemplate "innovation in a fragile future" and provides the means and occasion for doing so.

The invitation is timely, welcome, and consequential: Despite the predictable disruptions and disorders it brings, technological innovation is avidly pursued as a matter of national policy and cultural commitment in the United States and elsewhere. Federal agencies and private foundations that support science, technology, and medicine have sought to catalyze transformative ideas and now seek systematic tools for promoting, managing, and measuring the performance of the national innovation system. Marking a stage in the journey new technologies travel from policy through laboratory

to popular consciousness, the 14 December 2008 *New York Times Magazine* celebrated the "Year in Ideas," the eighth in an annual series of reflections on innovations. This year, the ideas ranged from an automated anesthesia system and a cloth car to strategies for educating, investing, taxing, and deciding whether to wait for the bus or walk. (Many of them were based on behavioral, economic, or social science.) The issue's spirit is captured by a seasonal red cover featuring the famous photographic portrait of Albert Einstein with his tongue sticking

Insatiable Curiosity

Innovation in a Fragile Future

by Helga Nowotny

Translated from the German (1)
by Mitch Cohen, MIT Press,
Cambridge, MA, 2008. 193 pp.
\$30, £19.95. ISBN 9780262141031.

effect through an intricate negotiation with existing social forms and cultural understandings: Transformatively new innovations "have to be emplaced in already existing organizational forms, social structures, and biographies. ... they must be accepted and altered in such a way that they identify and meet latently present needs." So the shock of the new is conveyed and modulated through the arrangements and understandings of the old. Innovation is a process of mutual accommodation, its success dependent

as much on societal receptivity and the quality of communication and integration with existing social forms as on the sacred spark of its inventor. Darwin knew this surpassingly well, as Gillian Beer has shown (4), and Nowotny extends the process to characterize the socio-cultural negotiations through which a society makes the "collective wager on the future" that is called innovation.

"Paths of curiosity," the topic of the second chapter, are the routes people travel in pursuit of epistemic things (the "objects of knowledge," such as reaction mechanisms, ecological processes, and biological structures and functions, that science aims to understand) that are attained through the application of research technologies. (These are experimental systems, model organisms, assays, instruments, and such that range in scale from tabletop procedures and microscopes to the Laser Interferometer Gravitational-Wave Observatory and the Large Hadron Collider.) Research technologies and the knowledge they yield are necessary but not sufficient for innovation. Also crucial are the institutional context and socio-cultural environment that motivate, shape, integrate, regulate, deploy, and lend meaning to new ideas and new ways of doing things. For example, the structure of the DNA molecule certainly implies a mechanism of replication. But innovations employing that mechanism arose from decades of related studies (some strikingly original in their own right) and from an institutional context that joins transformative ideas and technologies to social purposes, cultural values, and capital in its various forms (cultural, economic, human, and social).

For decades the U.S. government has sought, through legislation, policy, funding, and other means, to accelerate and guide the innovation system. After thinking things over, aided by this book, I remain an open-minded



Patricia Piccinini's *Nest* (2006).

out. Innovation, serious and playful, is central to our strategies, our cultures, and our selves: we need it yet we fear it.

A little book full of big ideas, *Insatiable Curiosity* is something to think with and through. It is not a book to skim for a sense of central claims and arguments, but one that rewards rumination and reflection. Nowotny offers a meditation, in three parts, on the nature and origins of innovation and its place in the human future.

The first chapter, concerned with "the emergence of the new," explains how radically original ideas and technologies—Darwin's theory is given as an example—take form and

The reviewer is at the School of Human Evolution and Social Change, Arizona State University, Box 872402, Tempe, AZ 85287-2402, USA. E-mail: ehackett@asu.edu

skeptic about the likely success of the endeavor. Precisely because new ideas and technologies become innovations through a process of rich interactions with diverse social groups, cultural values, and institutional arrangements, investments in the supply side of originality must be complemented by deeper engagement with users, patients, customers, and others of the general public in order to shape technologies to human needs. We are still inventing ways to accomplish and benefit from such engagements.

"Innovation in a fragile future," the theme of the third chapter, aptly describes our mission and our fate. We are driven to innovate, not only by virtue of innate and institutionalized "insatiable curiosity" but also by necessity: sustaining our existence and our fragile planet depend on it. Yet innovation will occur in circumstances of growing complexity and consequent uncertainty because the shape, character, and effect of an innovation are determined by forces beyond the imagining of its inventor. In a self-exemplifying fashion that the author could not have anticipated, this lesson is powerfully conveyed in a passage near the end of the book:

By betting on human action, innovation should broadcast the calming message that the unforeseeable will nonetheless be manageable. Dealing with risks? Not a real problem, for if needed, there is the precautionary principle. Instead of being intimidated by the apocalyptic warnings of the risk society, the decision can be made in favor of a "modern risk culture," as prevails in the global financial markets.

The risk culture of global financial markets has been exposed as flawed in various ways—some systemic, some tragic, some venal. An observer as wise, knowledgeable, and well positioned as the author could not foresee the unraveling interdependencies that undermined the risk calculus of the modern risk culture. Yet innovation is still the best bet around; we must remain calm, and the unforeseeable will, somehow, be managed.

References

1. H. Nowotny, *Unersättliche Neugier: Innovation in einer fragilen Zukunft* (Kulturverlag Kadmos, Berlin, 2005).
2. D. Bell, *Am. Scholar* 42, 385 (1973).
3. M. R. Smith, L. Marx, Eds., *Does Technology Drive History? The Dilemmas of Technological Determinism* (MIT Press, Cambridge, MA, 1994).
4. G. Beer, in *Innovation: Kreativität in Kunst und Wissenschaft. Ergebnisse des Initiative-Workshops*, H. Nowotny, Ed. (IFK Materialien, Vienna, 1994), pp. 15–19.

BROWSINGS

Chocolate: Pathway to the Gods. Meredith L. Dreiss and Sharon Edgar Greenhill. University of Arizona Press, Tucson, 2008. 208 pp + 60-minute DVD. \$30. ISBN 9780816524648.

The generic name of the cacao tree, *Theobroma cacao*, means "food of the gods." However, the tree's fresh seeds are bitter and astringent and do not taste like chocolate. In the traditional, manual preparation of that delicacy, the beans (seeds) are removed from cacao pods, fermented for three days, dried, roasted, and ground on a stone metate. Drawing on archaeological and ethnographic research, the authors discuss the religious, social, cultural, and medicinal roles that chocolate has played in the lives of Mesoamericans for some 3500 years. For example, this clay figurine of a warrior clad in cacao armor (Late Classic Maya from Campeche, Mexico; right) reflects beliefs that one is energized and strengthened by chocolate. The profusely illustrated book grew out of the authors' 2005 documentary film (provided on the DVD): They had gathered far too many striking still photographs of ceramics, carvings, murals, monuments, and codices to incorporate in the film.



The Princeton Companion to Mathematics. Timothy Gowers, Ed.; June Barrow-Green and Imre Leader, Associate Eds. Princeton University Press, Princeton, NJ, 2008. 1056 pp. \$99, £60. ISBN 9780691118802.

Focusing on "modern, pure mathematics," the editors and their 132 authors aim to provide "a large and representative sample of the ideas that mathematicians are grappling with ... in as attractive and accessible a way as possible." Four introductory articles sketch mathematics' main branches, its language and grammar, fundamental definitions, and research goals. Seven historical chapters trace developments from numbers and number systems through the 1920s crisis in the foundations of mathematics. The next three sections of the volume cover 99 concepts (e.g., the axiom of choice); 26 branches of mathematics (e.g., operator algebras); and 35 theorems, paradoxes, and problems (e.g., the Weil conjectures). Brief biographies summarize the lives and accomplishments of 96 famous mathematicians, from the legendary Pythagoras through the collective "Nicolas Bourbaki." Fourteen chapters explore the influence of mathematics on other fields, such as chemistry, biology, economics, philosophy, music, and art. The volume concludes with several "reflections about the nature of mathematics and mathematical life"—which might be the best place for many readers to start. Although the editors' original goal of text that could be understood by anyone with a good background in high school mathematics proved short-lived, this wide-ranging account should reward undergraduate and graduate students and anyone curious about math as well as help research mathematicians understand the work of their colleagues in other specialties. The editors note some advantages a carefully organized printed reference may enjoy over a collection of Web pages, and this impressive volume supports their claims.

Where Our Food Comes From: Retracing Nikolay Vavilov's Quest to End Famine.

Gary Paul Nabhan. Island, Washington, DC, 2008. 251 pp. \$24.95, £21.50. ISBN 9781597263993.

The renowned botanist and geneticist Vavilov ran afoul of T. D. Lysenko, was made a scapegoat for Stalin's disastrous farm policies, and died of starvation in a Soviet prison during World War II. Before his downfall, he had traveled the world collecting hundreds of thousands of samples of seeds, roots, and fruits in his efforts to identify the centers of agricultural diversity and to improve food security. Following in Vavilov's footsteps, ethnobotanist and conservationist Nabhan journeys to nine agricultural landscapes, including the grain fields of the Pamirs, the farms of Italy's Po Valley, date palm oases of North Africa's Maghreb, and the maize and beans *milpas* of Mexico's Sierra Madre. He discusses how the traditional practices described by Vavilov have been affected by irrigation, mechanized agriculture, urban sprawl, changing climate, and political turmoil. Noting the drawbacks of global standardization of agriculture, the author argues that preserving a diversity of crop varieties and the accompanying practices of land use and food preparation is essential to shielding humanity from widespread hunger.

10.1126/science.1167600

MEDICINE

Racing Forward: The Genomics and Personalized Medicine Act

Sandra Soo-Jin Lee* and Ashwin Mudaliar

In 2006, then-U.S. Senator Barack Obama introduced the Genomics and Personalized Medicine Act (GPMA) as S.3822 (1) and again, with the cosponsorship of U.S. Senator Richard Burr (R-North Carolina), in 2007 as S.976 (2). Broad in scope, the bill outlines measures that bolster governmental oversight and create economic incentives to catalyze translation of research into clinical care. However, in the transition from S.3822 to S.976, there were omissions that decouple consideration of the implications of human genetic diversity from legislation aimed at building the infrastructure for genomic medicine. This represents a missed opportunity to engage critical issues with deep scientific, social, and ethical implications.

Pharmacogenomic testing of individuals may prevent adverse drug reactions and save both lives and money. However, personalized medicine remains in its nascency, and populations identified by race and ethnicity, rather than individuals, remain the focus of current pharmacogenomic research despite the dominant view in anthropological genetics that race is a poor predictor of genotype. A central question in pharmacogenomics is which populations have greater frequencies of alleles associated with drug-metabolizing enzymes, drug transporters, or drug targets. Although scientists suggest that “race” in the context of genetic research will be rendered obsolete once genetic markers for the relevant phenotypes are found, recent developments reflect growing use of racial categories in efforts to translate basic research into clinical practice (3, 4).

In 2005, the U.S. Food and Drug Administration (FDA) approved BiDil as an antihypertensive combination therapy for use in “self-identified Blacks” (5). Scholars have challenged the scientific justification (6, 7) of setting a precedent for race-specific drugs, cautioning that conflation of genes, race, and drugs undermines what many scientists insist—that the sociopolitical concepts of race and ethnicity are not genetic (8, 9). This nuance is quickly lost in clinical translation and mar-

ket segmentation when race becomes a “category of convenience” (10). The roughly 700 drugs in the development pipeline aimed at African Americans (11) signal an emerging landscape of race-based therapeutics and underline the risk of prematurely jumping from genotype to phenotype.

A strength of S.3822 was its direct engagement with the issue of genetic variation and the rationale for using racial and ethnic categories in pharmacogenomic research. In a dedicated section entitled, “Race, Genomics, and Health,” the bill mandated that within 1 year of its passage, a newly formed Genetics and Personalized Medicine Interagency Working Group (IWG) would be charged with (i) determining appropriate definitions and use of categories of race and ethnicity, (ii) determining ways to increase access to pharmacogenomic and related clinical genetic services for minority populations, (iii) providing research opportunities and funding support in the area of race and genomics, (iv) enhancing integration of federal wide effort and activities, and (v) recommending privacy protection of genetic information.

The IWG was charged with leading a national discussion that would have addressed fundamental questions including the following: What constitutes racial and ethnic difference in the context of human genetic variation research? How are individuals designated as members of a racial and ethnic group? What should be the standards for evaluating claims of race-based therapeutics? Perhaps most important, how will guidelines regarding use of racial and ethnic categories affect health disparities among minority populations?

However, when S.3822 was revised and reintroduced to Congress in 2008 as S.976, the entire section of “Race, Genomics, and Health” and its provisions were deleted from the bill. In S.976, there is no mention of “race,” “ethnicity,” or “diversity,” and “minority” is mentioned only once.

Many of the measures addressing genetic variation and population diversity outlined in S.3822 were added to the current version of Minority Health Improvement and Health Disparity Elimination Act S.1576 (12), an overarching bill to enhance efforts to eliminate health disparities. Race and ethnicity are

A key section was eliminated from a bill supporting research and development in pharmacogenomics.

clearly defined in S.1576 by the census categories of the Office of Budget and Management, but the appropriateness of these categories in the context of pharmacogenomics remains a key question for the field. In building an infrastructure for personalized medicine, such questions are best addressed in the context of the GPMA.

A feature outlined in S.3822 and S.976 is the National DNA Biobanking Research Initiative, which would facilitate collection and integration of genomic data with environmental and clinical health information. A mandate in S.3822 was aimed at ensuring diverse representation of the individuals included, which would allow analysis of population subgroups. In S.976, this provision has been dropped. This has implications for pharmacogenomics, where population stratification issues and challenges to recruitment of minority populations persist.

An opportunity to provide clarity and leadership on critical issues of human genetic variation from “bench” to “bedside” is lost in the current GPMA. Direct engagement on these problems within the context of specific legislation on pharmacogenomics is necessary in setting a scientifically valid and ethically responsible agenda for personalized medicine.

References and Notes

1. Genomics and Personalized Medicine Act of 2006, 109th Cong., 2d Sess. [introduced in the Senate (IS)], S.3822.IS.
2. Genomics and Personalized Medicine Act of 2007, 110th Cong., 1st Sess., S.976.IS.
3. C. N. Rotimi, *Nat. Genet.* **36**, 543 (2004).
4. C. W. Yancy, *Curr. Hypertens. Rep.* **10**, 276 (2008).
5. FDA Approves BiDil Heart Failure Drug for Black Patients, www.fda.gov/bbs/topics/news/2005/new01190.html.
6. J. Kahn, *Yale J. Health Policy Law Ethics* **4**, 1 (2004).
7. S. S. Lee, *Am. J. Publ. Health* **95**, 2133 (2005).
8. C. D. M. Royal, G. M. Dunston, *Nat. Genet.* **36**, 55 (2004).
9. S. S. Lee, *Genome Biol.* **9**, 404 (2008).
10. *Today's Topics in Health Disparities—Race and Genetics: The Future of Personalized Medicine* (Kaiser Family Foundation, Menlo Park, CA, 20 August 2008); www.kaisernetnetwork.org/health_cast/hcast_index.cfm?display=detail&hc=2884.
11. *Medicines in Development for Major Diseases Affecting African Americans* (Pharmaceutical Research and Manufacturers Association of America, Washington, DC, September 2007).
12. Minority Health Improvement and Health Disparity Elimination Act of 2007, 110th Cong., 1st Sess., S.1576.IS.
13. S.S.-J.L. was supported by the Ethical, Legal, and Social Implications Research Program, National Human Genome Research Institute, NIH, grants K01 HL72465 and P50 HG003389.

Stanford Center for Biomedical Ethics, Stanford University Medical School, Palo Alto, CA 94304-1703, USA.

*Author for correspondence. E-mail: sandra.lee@stanford.edu

10.1126/science.1165768

OCEAN SCIENCE

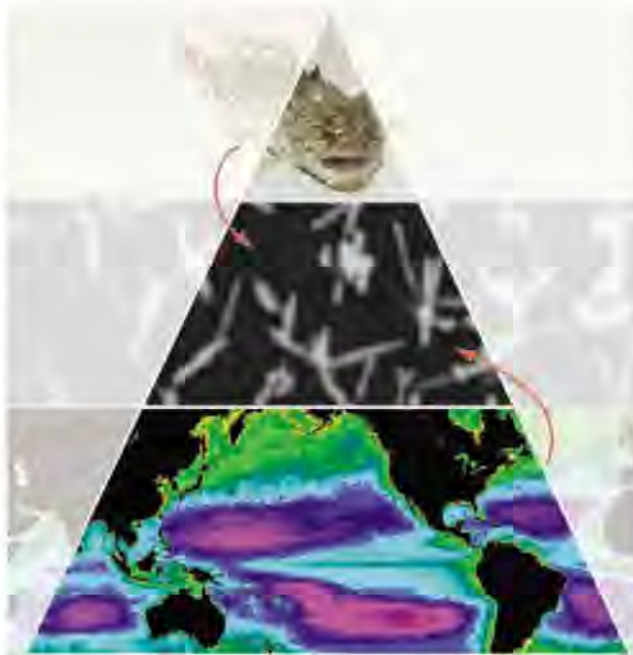
Animal Function at the Heart (and Gut) of Oceanography

Brad A. Seibel¹ and Heidi M. Dierssen²

Far more biomass is contained in marine primary producers than in marine animals at higher levels of the food chain. This relation suggests that animals—particularly secondary consumers such as fishes—must play a negligible role in elemental cycling in the world's oceans (1). However, given that the midwater ecosystem is the largest on Earth, with over 99.5% of the habitable space (2), the activity and metabolism of oceanic animals across great depth ranges, especially in productive regions, should perhaps not be discounted (3, 4). Unfortunately, marine animal biomass, distribution, and function are not sufficiently well known to fully reconcile these opposing views (5). On page 359 of this issue, Wilson *et al.* (6) elucidate a physiological pathway, common to all marine bony fishes, that seems to contribute substantially to the marine inorganic carbon cycle.

The first clue to a possible role of fish in the marine inorganic carbon cycle came from studies of toadfish, *Opsanus beta*. In 1991, while investigating the fate of urea-derived carbon, Walsh *et al.* observed pellets in the toadfish's gut (7), which were later found to be a metastable form of calcite that contains large amounts of magnesium. The source of these "gut rocks" was not immediately obvious, but Walsh *et al.* reasoned that if common to all fish, they might contribute to the inorganic carbon cycle.

More than a decade of detailed physiology has revealed how and why gut rocks form. As far as is known, all bony fishes regulate their internal osmolarity at a level considerably lower than that of seawater and, in seawater, must drink to remain hydrated. However, absorption of the imbibed fluid by the intestine is osmotically limited by the concentrated ions in sea-



An unexpected role. Fishes at the top of the trophic pyramid are traditionally considered unimportant for biogeochemical cycles because of the loss of energy as one moves from low to higher levels in the food chain. This stylistic pyramid shows how marine fish, as first discovered in the toadfish *Opsanus beta* (top), produce precipitated carbonates ("gut rocks") within their intestines (middle) (6) and make a substantial contribution to the global calcium carbonate cycle (bottom) (estimated CaCO_3 concentrations for the world oceans).

water. Active acid-base regulation facilitates precipitation of the divalent ions as gut rocks and promotes fluid absorption. This appears to be a universal phenomenon critical to the survival of all marine-adapted bony fishes.

For most of the past century, substantial dissolution of calcium carbonate (CaCO_3) was believed to occur only in the deep waters that are undersaturated with respect to the various phases of calcium carbonate. However, more recent observations of water column alkalinity reveal that substantial dissolution of calcium carbonate must be occurring at depths well above this "chemical lysocline" (8). The most likely explanation is dissolution of more soluble forms of calcium carbonate, such as the aragonitic shells of pteropod mollusks. More studies on CaCO_3 are needed, particularly in remote regions like the Southern Ocean (9), but current estimates of such sources fail to explain all of the mysterious

Animal physiology has a substantial impact on the marine inorganic carbon cycle, for example, through the formation of calcium carbonate "gut rocks" in bony fish.

alkalinity. One possible source is the high-magnesium calcite from which gut rocks are formed; its lysocline is shallower than that for other forms of carbonate, and gut rocks would therefore dissolve at shallower depths. However, few oceanographers took note of Walsh's gut rock hypothesis.

Wilson *et al.* have now modeled the size, composition, and abundance of marine fish across the global ocean using two different approaches. Each relies on satellite-derived estimates of global primary productivity from phytoplankton and the conversion of organic matter from one trophic level or link in the food chain to the next (10) (see the figure). It is thus imperative, particularly in this era of climate change, that satellite assets be maintained and expanded via consistent national investment to produce quality imagery (11) that can be used not only to assess traditional phytoplankton concentrations but also to model top-down linkages in the food chain (6, 12, 13). Because of the immensity of the oceans, small

variations in model assumptions can swell into vastly different global results. Nevertheless, when coupled with global models and estimates of sea surface temperature, the present analysis predicts substantial fish carbonate production across the world ocean—enough to explain at least one-quarter of the increased alkalinity, or 3 to 15% of total oceanic carbonate production.

Comparative physiology is a thriving field, but is rarely applied to oceanographic problems. Wilson *et al.* (6) show convincingly that animals, even in the upper trophic levels, can affect elemental cycles via their physiological manipulations. Previous studies have recognized several mechanisms by which animals may contribute to such cycles. For example, many oceanic animals undergo diel vertical migrations from their shallow feeding grounds to depths of several hundred meters, where they continue to excrete respi-

¹Biological Sciences, University of Rhode Island, Kingston, RI 02891, USA. ²Marine Sciences Geography, University of Connecticut, Groton, CT 06340, USA. E-mail: seibel@uri.edu, heidi.dierssen@uconn.edu

ratory carbon dioxide, effectively pumping carbon out of the atmosphere to the deep sea (3). Metabolic suppression and anaerobic metabolism, used by some migrators during daytime forays into expansive oxygen minimum zones, may reduce the efficiency of this biological carbon pump in some regions (14). The efficiency of carbon pumping is similarly reduced in the Southern Ocean, where air-breathing mammals and birds are a key component of the food chain. They respire massive amounts of photosynthetically derived carbon back into the atmosphere (13). In contrast, larvaceans increase carbon flux by concentrating particles in their mucus feeding webs that then sink rapidly to depth (15). All these processes depend on the demand for energy, which varies between species by up to three orders of magnitude [see supporting online material (6)].

Despite their potential importance, these and similar phenomena remain

poorly constrained for most oceanic taxa. It is thus difficult to estimate or predict the role of animal function in biogeochemical cycles. The relevant processes must be recognized and quantified, their rates scaled up, and put in the context of global elemental budgets. Wilson *et al.*'s important contribution to our knowledge of the inorganic carbon cycle will hopefully infuse a new appreciation for the role of higher trophic levels in ocean dynamics. Clearly, the field is moving beyond the dismissive viewpoint described by Horne, in which animals were merely a source of "heterogeneity in the sea" [(16), p. 239]. As he noted, "Our element of seawater may well contain an important second phase we have not mentioned—a fish" [(16), p. 3].

References

1. P. A. Del Giorgio, C. M. Duarte, *Nature* **420**, 379 (2002).
2. B. H. Robison, *J. Exp. Mar. Biol. Ecol.* **300**, 253 (2004).

3. K. O. Buesseler *et al.*, *Science* **316**, 567 (2007).
4. H. G. Dam, X. Zhang, M. Butera, M. R. Roman, *Deep-Sea Res. II* **42**, 732 (1995).
5. A. J. Richardson, E. S. Poloczanska, *Science* **320**, 1294 (2008).
6. R. W. Wilson *et al.*, *Science* **323**, 359 (2009).
7. P. J. Walsh, P. Blackwelder, K. A. Gill, E. Danulat, T. P. Mommensen, *Limnol. Oceanogr.* **36**, 1227 (1991).
8. C. L. Sabine *et al.*, in *Toward CO₂ Stabilization: Issues, Strategies, and Consequences*, C. B. Field, M. R. Raupach, Eds. (Island Press, Washington, DC, 2003), pp. 7–44.
9. W. M. Balch, H. R. Gordon, B. C. Bowler, D. T. Drapeau, E. S. Booth, *J. Geophys. Res.* **110**, C07001 (2005).
10. J. H. Ryther, *Science* **166**, 72 (1969).
11. E. Kintisch, *Science* **319**, 886 (2008).
12. M. E. Huntley, M. D. Lopez, D. M. Karl, *Science* **253**, 64 (1991).
13. R. Rosa, H. M. Dierssen, L. Gonzalez, B. A. Seibel, *Ecology* **89**, 3449 (2008).
14. R. Rosa, B. A. Seibel, *Proc. Natl. Acad. Sci. U.S.A.* **105**, 10107 (2008).
15. B. H. Robison, K. R. Reisenbichler, R. E. Sherlock, *Science* **308**, 1609 (2005).
16. R. A. Horne, *The Structure of Water and the Chemistry of the Hydrosphere* (Wiley Interscience, New York, 1969).

10.1126/science.1161618

MATERIALS SCIENCE

Beyond Biomineralization

Werner Kunz and Matthias Kellermeier

Modern strategies to design advanced materials are often inspired by nature. For instance, during biomineralization, living organisms can impose highly complex shapes and textures with remarkable structural hierarchy upon solid inorganic matter to produce materials that often far exceed the performance of human-made counterparts (1, 2). However, crystallization in purely inorganic systems can also yield smoothly curved forms that resemble those of biomaterials (3). These so-called "biomorphs" are obtained by coprecipitation of barium carbonate (witherite) and silica from alkaline media. A concerted self-assembly process yields nanosized carbonate crystallites that arrange in a highly ordered manner over micrometer lengths, thereby shaping morphologies such as regular helicoids on scales up to millimeters—all in the absence of any complex organic additive or surface scaffold. On page 362 of this issue, García-Ruiz *et al.* use video microscopy to provide insight into several steps decisive for structure evolution and identify a chemical feed-

back process as the driving force for the observed self-organization (4).

A striking similarity between these abiotic biomorphs and most actual biominerals is their mode of construction, with hierarchical structuring over many length scales and preferential crystallographic orientation. In turn, the chemistry and preparation of the biomorphs are rather simple, thus rendering them excellent model systems to study multiscale interactive self-organizing phenomena.

One of the principles of self-organization explored by García-Ruiz *et al.* is a dynamic, pH-based coupling of equilibria, which induces alternating precipitation of the components. The sensitivity of silicate and carbonate speciation to pH fluctuations in alkaline media, together with pH gradients close to the mineralizing fronts and opposite pH trends in solubility of silica and barium carbonate, are fundamental prerequisites in this context. In other words, an acid and a base (i.e., hydrogen carbonate and silicate) are alternately subject to local neutralization, the latter being directly linked to precipitation. Neutralizing one leads to local conditions under which the other is suddenly out of equilibrium—a situation somewhat reminiscent of the famous

Self-assembly of purely inorganic components can also give rise to complex structures and morphologies once thought restricted to biological materials.

Belousov-Zhabotinsky reaction (5). Silica thereby acts, via precipitation, as an inhibitor for continued carbonate crystal growth first, to stimulate renewed carbonate nucleation later on.

This concept has obvious potential for the design of systems that spontaneously self-assemble to yield highly organized materials. An interesting challenge will be to look for other "acid-base" pairs that would engage in a similar coupled process if conditions are adjusted properly. Simple substitutions such as replacement of barium by one of its alkaline-earth homologs have already been done with success (6, 7). However, the search for alternative reagent pairs should also extend to phenomena beyond those related to pH effects and precipitation; such pairs may be based on a principle analogous to the pH-mineralization feedback. This feedback process teaches us an important lesson: Oscillating precipitation does not necessarily imply periodic structures. The latter arise as a consequence of spatial oscillation, as observed in common banded Liesegang patterns (8). In the present case, oscillation is only of a temporal nature, resulting mainly in encapsulation of carbonate crystallites by silica rather than formation of

Institute of Physical and Theoretical Chemistry, University of Regensburg, Regensburg 93040 Germany. E-mail: werner.kunz@chemie.uni-regensburg.de

alternating layers. Nevertheless, the oscillatory nature of chemical coupling can become manifest as periodicity in space if initial conditions are chosen appropriately.

The chemical coupling described by García-Ruiz *et al.* nicely explains the origin of the nanocrystals and their uniformity, as well as their sheathing by silica (see the figure, panel A). It also sheds light on the dynamics behind their formation (3). However, details on molecular-scale interactions remain to be clarified, such as how silicate species adsorb or precipitate on the surfaces of growing carbonate crystals.

The circumstances leading to the orientational order of crystallites over mesoscopic

ance of attractive and repulsive forces varies between the tips and the lateral faces of the silica-coated carbonate crystallites, possibly as a result of different charge densities.

Further intriguing questions arise at larger length scales where the global morphology of aggregates evolves. García-Ruiz *et al.* convincingly explain why carbonate undergoes a transition in its mode of growth in the presence of silica, from self-similar branching of one single crystal to continuous formation of nanocrystals toward a polycrystalline assembly. When silica has entirely blocked the initial fractal crystal, new carbonate precipitation is expected to occur as three-dimensional nucleation creat-

ety of complex curved morphologies to a basic mechanism in which the relative directionality of the curling rim segments, as well as their respective growth velocities and height, determine whether helicoids, braids, or worm-like shapes are formed.

But what is the reason for the leaves curling? Is this near-macroscopic curling a consequence of interfacial tension between the medium and the solid surface? Obviously, the crystal assembly starts to turn back at a certain time and grow on itself—which might be an expression of its tendency to minimize overall surface. Or do parameters such as species concentrations or pH change enough in the course of precipita-

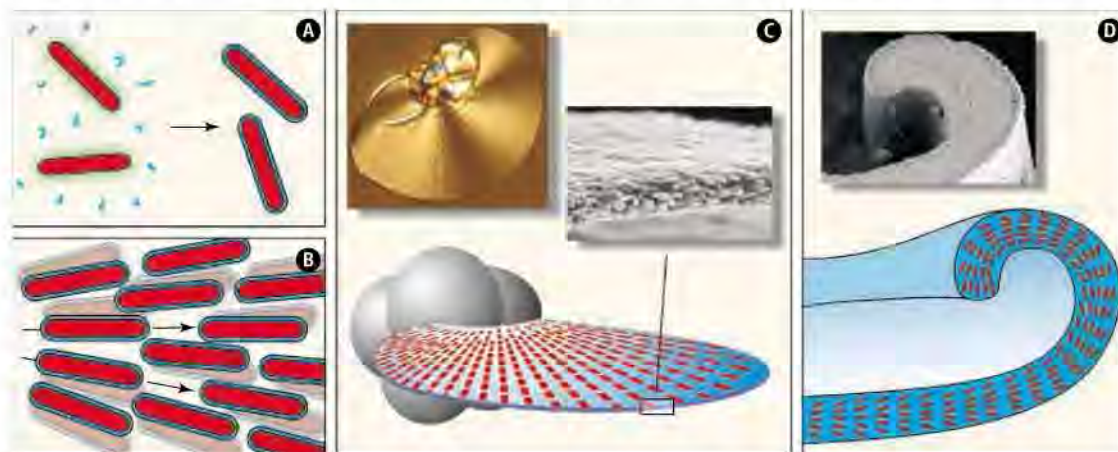
tion to favor curved growth? Varying interparticle interactions at lower pH could alter slightly the preferential co-orientation of nanocrystallites in such a way that their assembly inevitably describes a curved surface.

The lessons learned from biomorphs will help to shed more light on the principles nature uses to construct hierarchical architectures. Synergy and intergrowth between components over many length scales are properties innate to both biomorphs and biominerals. Beyond this conceptual similarity, the role of silica as a struc-

ture-inducing additive that itself evolves dynamically during mineralization—rather than being a simple static template—could be the basis for new pathways to fascinating novel materials.

References

1. H. A. Lowenstam, S. Weiner, *On Biomineralization* (Oxford Univ. Press, New York, 1989).
2. N. Kröger, S. Lorenz, E. Brunner, M. Sumper, *Science* **298**, 584 (2002).
3. J. M. García-Ruiz *et al.*, *Science* **302**, 1194 (2003).
4. J. M. García-Ruiz, E. Melero-García, S. T. Hyde, *Science* **323**, 362 (2009).
5. A. N. Zaikin, A. M. Zhabotinsky, *Nature* **225**, 535 (1970).
6. A. E. Voinescu *et al.*, *Cryst. Growth Des.* **8**, 1515 (2008).
7. T. Terada, S. Yamabi, H. Imai, *J. Cryst. Growth* **253**, 435 (2003).
8. R. E. Liesegang, *Z. Phys. Chem.* **88**, 1 (1914).
9. S. Mann, H. Cölfen, *Angew. Chem. Int. Ed.* **42**, 2350 (2003).



Silica-witherite biomorphs. (A) Rod-like carbonate nanocrystallites (red) become enveloped in a silica skin (blue) as pH gradients around the growing crystallites (green) provoke local silica precipitation. As a result of “chemical coupling” of carbonate and silicate chemistry, nucleation and sheathing occur alternately and coated particles are continuously formed. (B) Coated nanocrystals arrange with an incremental tilt, establishing long-range orientational order throughout their assembly. (C) On global scales, the self-assembly of nanoparticles proceeds at first by developing quasi-2D leaf-like sections. Witherite rods in the leaf describe a radial orientation field, as indicated by distinct interference patterns in polarized optical micrographs. (D) Laminar growth continues until the leaves become scrolled at certain points around their border. The emergent curvature is fueled by propagation of the initial curl along the rim.

lengths remain a mystery: Why do adjacent nanorods arrange with a certain twist with respect to each other (see the figure, panel B), and how is that twist kept constant throughout the assembly? Coated nanoparticles with high aspect ratio, such as rods, have been shown to be versatile building blocks for constructing higher-order superstructures, if the adsorbed layers maintain specific interactions to one another (9). However, the interactions between layers of sheathing silica are by nature quite complicated because of its inherent reactivity. Mutual repulsion results from the negative charges that silica species bear at high pH, whereas attraction can be caused either by hydrogen bonding between protonated groups or direct covalent linking via condensation. The slight misalignment of rods observed in biomorphs suggests that the bal-

ancing numerous crystallites all over the surface (4). Attachment of further nanocrystallites is then, however, observed only along a thin path over the surface, which results in two-dimensional extrusions (see the figure, panel C). This observed two-dimensionality may arise as a result of the sudden precipitation of expanded silica layers on the fractal carbonate crystal and later on the growing leaves. This could effect large-area inhibition of carbonate crystallization, thereby imposing selective growth directions.

The second mystery about the morphological evolution of the crystalline assembly on global scales refers to the actual origin of curvature. According to García-Ruiz *et al.*, leaves continue to grow flat until they curl at certain points around their rim (see the figure, panel D) (4). They describe a physical model that reduces the emergence of a vari-

PALEONTOLOGY

New and Ancient Trace Makers

Stefan Bengtson¹ and Birger Rasmussen²

Giant globular amoebas have been found to make traces up to 50 cm in length on the sea floor off the Bahamas at a depth of nearly 800 m. The discovery, reported by Matz *et al.* in *Current Biology* (1), will force a reevaluation of putative animal traces in the early fossil record and provide a fresh view on controversial two-billion-year-old trace fossils.

Trace fossils are a key source of information about ecological interactions and animal behavior. Unlike body fossils, they presumably reflect the direct conditions of the place where they are found. They have not been transported or redeposited in the way that body fossils often have. Also, traces are easily preserved because they are formed in sediment or rock.

Yet in one important respect they fail us. The sedimentological conditions for trace fossil preservation are different from those conducive to preserving most body fossils; indeed, trace-producing activities are usually detrimental to the preservation of body fossils. This is why the bodies of the trace makers are rarely found with the traces, and hence the makers typically remain unknown. The international commission that regulates zoological nomenclature has endorsed a system of names for traces that is decoupled from the identity of the trace maker.

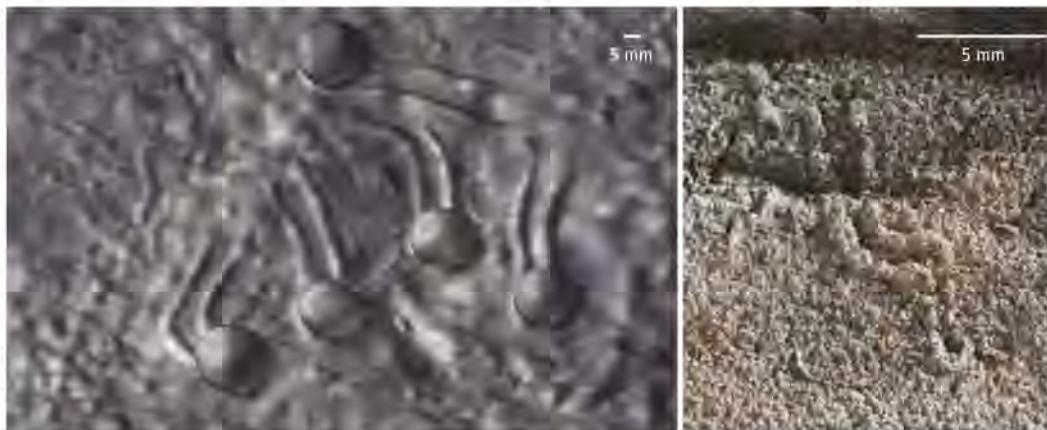
Knowing the trace maker is thus at best difficult, even in the Phanerozoic (the past 545 million years), where body fossils abound. A few animals may leave unique and recognizable traces, but most trace fossil “taxa” can be produced by several organisms that may not be closely related. Trace fossils thus reflect behavior, not biological affinity.

The sudden appearance of animal fossils at the beginning of the Cambrian period, now dated to 542 million years ago, has long been recognized as an ecological revolution involv-

ing the rampant radiation of multicellular taxa, not the artifact of preservation that was surmised by the great scientists of former centuries, such as Charles Darwin and Charles Doolittle Walcott. Trace fossils played a great role in this insight: They show a rapid evolution of behavior at this time, demonstrating that the appearance of a diverse fauna was a real biological event, not merely the effect of improved conditions for fossilization. The famous soft-bodied impressions of the Edi-

Trace fossils that are older than known animal fossils may have been formed by large unicellular organisms such as amoebas.

almost universal consensus that large traces of motile organisms implicate animals, evidence of older traces has been seen as spurious. Accepting them as traces, given an underlying assumption that they must have been made by animals, would clash with the general absence of animal body fossils before the Ediacaran. Reports of motile multicellularity in the early rock record (5, 6) have thus met with one of two responses: The rocks have been misdated, or the fossils have been misinterpreted (7, 8).



Making traces. (Left) Reconstruction of *Gromia* making traces on the sea floor. (Right) Trace fossils of *Myxomitodes* dated at 1.8 to 2 billion years (9).

acara “fauna” that precede the Cambrian are, with few exceptions, not accepted as animal fossils. But simultaneously occurring traces have been taken as independent evidence that among the exotic Ediacarans there crawled advanced, bilaterally symmetrical animals (bilaterians) (2). This is probably an oversimplification, however. Some alleged traces have turned out to be body fossils of what have been interpreted as giant sedentary amoebas (3). Amoebas are not closely related to animals—being unicellular eukaryotes, they are usually microscopic in size, although in rare instances they can become larger. Other alleged bilaterian traces are so simple that they could have been produced also by simple nonbilaterians that moved along self-made mucus tracts with the help of cilia (4). Trace fossils thus have less to contribute to the early evolution of animals than previously believed.

If Ediacaran trace-like fossils have too readily been interpreted as the products of advanced bilaterian animals, the inverse is true for older occurrences. Because of the

This is akin to a paleontological version of the Heisenberg uncertainty principle.

Healthy skepticism is in order when interpreting such often obscure structures as traces of simple organisms. The perceived anomaly only exists, however, under the assumption that trace fossils were always made by animals, which are always multicellular. Are there alternatives? Although unicellular organisms are commonly motile, they are generally too small to leave megascopic traces. Even those unicellulars that occasionally aggregate into “slugs,” like slime molds, are not known to leave durable traces. Some amoebas attain the large size of multicellulars by having a syncytial (multinucleated) organization and/or by incorporating inert material in their cytoplasm, but they tend to be immobile.

Matz *et al.* may now have resolved the anomaly by demonstrating that a common type of trace fossil need not have been made by animals at all. They observed large balls, up to 3 cm in diameter, slowly moving (possibly rolling) in different directions on the ocean

¹Nordic Center for Earth Evolution and Department of Palaeozoology, Swedish Museum of Natural History, Box 50007, SE-10405 Stockholm, Sweden. E-mail: stefan.bengtson@nrm.se ²Department of Applied Geology, Curtin University of Technology, GPO Box U1987, Perth, WA 6845, Australia.

floor and leaving behind a sinuous groove bordered by two low lateral ridges (see the figure, left panel). Near a ball there was usually a central ridge between the lateral ones. The balls turned out to be giant shelled amoebas, *Gromia sphaerica*, previously known from the Arabian Sea. The traces look like regular animal trace fossils, but Matz *et al.* also note that they are quite similar to the almost two-billion-year-old trace fossil *Myxomitodes* (see the figure, right panel).

Myxomitodes have been interpreted as traces formed by multicellular or syncytial organisms gliding along a mucus band. These were far too ancient for animals, but not for simpler eukaryotes, to have formed them (9). The discovery of *Gromia* traces now provides an extant example of the kind of nonanimal megascopic motile eukaryote that was previously only hypothesized. Similarity is not

identity, however. Both *Gromia* and the *Myxomitodes* trail maker move across the sediment surface in short forays rather than burrow, but the differences are still considerable. *Gromia* is larger than *Myxomitodes*, and the latter shows evidence of shape change and copious mucus production that appear unlikely for an encased organism like *Gromia*.

The real significance of the *Gromia* traces lies not in their resemblance to *Myxomitodes* but in the direct demonstration that large traces need not have been made by animals. With that interpretive restraint gone, the time may have come for a more general acceptance of the possibility that the long Proterozoic Eon (which began 2.5 billion years ago) saw more and larger organisms moving on the sea floor than is currently recognized. The long-standing questions of how, when, and why large organisms emerged from the placid

microbial biosphere may then be seen in a wider temporal, environmental, and taxonomic perspective.

References

1. M. V. Matz, T. M. Frank, N. J. Marshall, E. A. Widder, J. Sönke, *Curr. Biol.* **18**, 1849 (2008).
2. T. P. Crimes, in *The Palaeobiology of Trace Fossils*, S. K. Donovan, Ed. (Johns Hopkins Univ. Press, Baltimore, MD, 1994), pp. 105–133.
3. A. Seilacher, D. Grazhdankin, A. Legouta, *Paleontol. Res.* **7**, 43 (2003).
4. A. G. Collins, J. H. Lipps, J. W. Valentine, *Paleobiology* **26**, 47 (2000).
5. A. Seilacher, P. K. Bose, F. Pflüger, *Science* **282**, 80 (1998).
6. B. Rasmussen, S. Bengtson, I. R. Fletcher, N. J. McNaughton, *Science* **296**, 1112 (2002).
7. R. J. Azmi, *Science* **282**, 627 (1998).
8. S. Conway Morris, *Science* **298**, 57 (2002).
9. S. Bengtson, B. Rasmussen, B. Krapež, *Paleobiology* **33**, 351 (2007).

10.1126/science.1168794

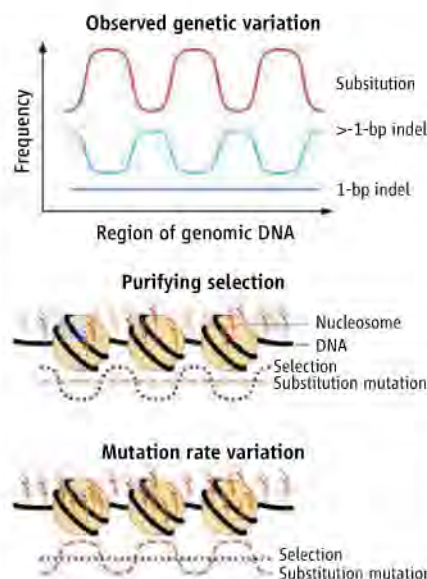
MOLECULAR BIOLOGY

The Structure of Change

Colin A. M. Semple¹ and Martin S. Taylor²

Spatial patterns in the rate of genetic variation are often interpreted as the footprints of natural selection. On page 401 of this issue, Sasaki *et al.* (1) report oscillating patterns in the rate of genetic variation around the start sites of transcription in the medaka (Japanese killifish, *Oryzias latipes*) genome. The patterns correspond to the positions of nucleosomes, the protein-DNA complexes that are the fundamental building blocks of chromosomes. But is this correlation best explained by the action of selection, or as the authors contend, could it represent a difference in the rate of mutation between nucleosome-bound DNA and that of intervening linker sequence? The answer could have major implications for the study of genome evolution.

The genome of eukaryotic cells is an intricately structured environment organized in hierarchical layers. Each layer is based on interactions between DNA and proteins to achieve compaction of the linear DNA helix, and the term “chromatin structure” encompasses all of these layers up to the chromosome. The basic unit of this



Position and effect. The frequencies of nucleotide substitutions and indels that are >1 nucleotide in length fluctuate along a region of DNA (top) and mirror the positioning of nucleosomes along the DNA (middle and bottom). Two models could explain the periodic substitution-rate fluctuations. (Middle) Mutations (red) occur randomly along the DNA, but natural selection acts to preferentially remove those located in linker regions (pink). (Bottom) Substitution mutations preferentially occur in DNA wrapped in nucleosomes rather than linker regions between nucleosomes. In this model, the selection pressure is constant across the region.

The organization of DNA and proteins into chromatin influences the location and rates of mutations across eukaryotic genomes.

packaging is the nucleosome, a ~147-base pair (bp) section of DNA tightly wound around an octamer of histone proteins. Nucleosomes are arranged along DNA like beads on a string, with an intervening, variable length of linker DNA between them (see the figure) (2).

The spacing of nucleosomes, covalent modification of histones, and the nature of higher-order chromatin packaging are all dynamically regulated and can influence the expression of genes (3), timing of DNA replication, and the rate of genetic recombination. Chromatin structure has also been implicated in the variation of mutation rate across the genome (4), and particular structures vary in their accessibility to homology-directed DNA repair processes (5). Unfortunately, most of the data relevant to chromatin structure and evolution have accumulated gradually, over different organisms, cell types, and samples. What has been lacking is a comparative study of chromatin structure and gene expression in a common, ideally germline tissue, combined with measurements of evolutionary rates between species separated by an appropriate phylogenetic distance (close enough to align noncoding sequences reliably but divergent enough to provide adequate variation for statistical analysis). Sasaki *et al.* have provided exactly this kind of study.

¹MRC Human Genetics Unit, Institute of Genetics and Molecular Medicine, Edinburgh EH4 2XU, UK. ²European Molecular Biology Laboratory European Bioinformatics Institute, Wellcome Trust Genome Campus, Hinxton, Cambridge CB10 1SD, UK. E-mail: colins@hgu.mrc.ac.uk, mst@ebi.ac.uk

To investigate the relationship of DNA sequence variation to genome structure and function, Sasaki *et al.* obtained genetic variation data by comparing the whole-genome sequences from two divergent strains of medaka. They also produced high-quality functional genomic data to define 11,654 transcription start sites, and map 37.3 million genomic nucleosome positions. When nucleotide substitution and indel (insertion and deletion) rates were examined around transcription start sites, they observed a ~200-bp periodicity corresponding to nucleosome positions. Nucleosomes were most consistently spaced downstream of the transcription start sites, which coincided with the most pronounced oscillation of substitution and indel rates. Unexpectedly, indels and substitutions showed an opposing periodicity: In the linker sequence, where the indel rate peaked, the substitution rate reached a minimum. The authors conclude that the divergence patterns are best explained by the differences in mutational spectra or mutation repair processes encountered by nucleosomes and linker regions.

Two recent studies in yeast also found substantially lower substitution rates in nucleosome linker regions than in core regions (6, 7), and showed that this variation (and by inference chromatin structure) is maintained over considerable evolutionary time scales (6), which is in itself a remarkable observation. There are two possible (nonexclusive) explanations for this pattern: Either the mutation rate varies between linker and core regions; or natural selection has acted to eliminate more mutations from the linker than from the core regions, indicating functional constraint on linker regions.

Both Sasaki *et al.* and Washietl *et al.* (6) favor discordance in mutation rate between core and linker regions as an explanation, and they have shown that this is not simply a result of the differences in average nucleotide composition between these regions (1, 6, 7). Warnecke *et al.* suggest that the lower substitution rate in linker regions is a consequence of purifying selection for the preservation of nucleosome spacing. A similar controversy has arisen in the field of promoter evolution in primates (8, 9). The rate of nucleotide substitution in primate promoter regions exceeds that in neighboring and selectively neutral control sequences (10). Again, this could be principally explained by either the frequent action of (diversifying) selection, or a higher rate of mutation in promoter regions than in other regions of the genome.

So are these observations best explained by the predominant action of selection or mutation? The proposition that nucleosomes are precisely placed to allow or restrict the binding of the transcription machinery seems plausible for promoter regions. But the periodic fluctuation in mutation rates is not confined to promoter regions; it is observed over most of the yeast genome, including coding sequence (6, 7), and substitution rate oscillations are most pronounced downstream rather than upstream of the transcription start sites in both medaka (1) and yeast (7). The observation that indels are enriched in linker relative to core sequence is also difficult to reconcile with a model of linker sequence conservation, because sites that are constrained for substitutions are also likely to be constrained for indel events (11).

Although the action of purifying selection at many sites within linkers cannot be excluded on the basis of current data, the evidence seems to favor chromatin-mediated mutational bias as the main cause of

periodic divergence patterns around consistently positioned nucleosomes. This suggests that the physical structure of the genome can directly influence the rate of mutation down to the single-nucleotide level, with far-reaching implications for genome evolution.

References and Notes

1. S. Sasaki *et al.*, *Science* **323**, 401 (2009); published online 11 December 2008 (10.1126/science.1163183).
2. T. J. Richmond, C. A. Davey, *Nature* **423**, 145 (2003).
3. ENCODE Project Consortium, *Nature* **447**, 799 (2007).
4. J. G. Prendergast *et al.*, *BMC Evol. Biol.* **7**, 72 (2007).
5. W. J. Cummings *et al.*, *PLoS Biol.* **5**, e246 (2007).
6. S. Washietl, R. Machne, N. Goldman, *Trends Genet.* **24**, 583 (2008).
7. T. Warnecke, N. N. Batada, L. D. Hurst, *PLoS Genet.* **4**, e1000250 (2008).
8. R. Haygood *et al.*, *Nat. Genet.* **39**, 1140 (2007).
9. M. S. Taylor *et al.*, *Nat. Genet.* **40**, 1262 (2008).
10. M. S. Taylor *et al.*, *PLoS Genet.* **2**, e30 (2006).
11. G. Lunter, C. P. Ponting, J. Hein, *PLoS Comput. Biol.* **2**, e5 (2006).
12. C.A.M.S. is supported by the UK Medical Research Council, and M.S.T. is funded by the Wellcome Trust (Program grant GR078968).

10.1126/science.1169408

CHEMISTRY

Excitons Surf Along Conjugated Polymer Chains

Jean-Luc Brédas¹ and Robert Silbey²

The energy carriers in an organic polymer semiconductor stay in phase when they move along a single polymer chain at room temperature.

An electron excited by light in organic semiconductors does not move about freely; it is bound to a positively charged carrier, or hole, left behind in the valence band. This bound state of an electron and hole—or exciton—can move through the material, and the performance of organic solar cells, photodiodes, and sensors (1–3) largely depends on the efficiency of their migration (4, 5). On page 369 of this issue, Collini and Scholes (6) show that an exciton can preserve its quantum coherence as it diffuses along the chain of a conjugated polymer (intrachain diffusion) at room temperature; the exciton can glide from one chain segment to an adjacent chain segment while maintain-

ing the phase relation of its quantum mechanical wave function. These features are in marked contrast to the traditional view that excitons in organic semiconductors move between well-separated chain segments through a series of independent hops, and that any quantum coherence would survive only at low temperatures.

The electronic and optical properties of conjugated polymers lie in the p orbitals of the backbone atoms, which overlap to form delocalized π molecular orbitals. In π -conjugated systems, any change in electronic state caused by excitation or ionization modifies the π -bond electron densities, thereby modifying the bond lengths and torsion angles between repeat units. This strong connection between electronic and geometric structure is referred to as strong electron-vibration (phonon) coupling.

Once promoted to an excited state, the conjugated system relaxes. When it reaches

¹School of Chemistry and Biochemistry and Center for Organic Photonics and Electronics, Georgia Institute of Technology, Atlanta, GA 30332, USA. ²Department of Chemistry, Massachusetts Institute of Technology, Cambridge, MA 02139, USA. E-mail: jean-luc.bredas@chemistry.gatech.edu; silbey@mit.edu

its equilibrium geometry, a relaxed exciton has formed; the corresponding geometry relaxation generally extends over some 15 to 20 bonds, or 2.0 to 2.5 nm. The energy needed to keep the electron and hole bound as an exciton is typically on the order of 0.5 eV (7), about 20 times the thermal energy at room temperature. The corresponding energy in an inorganic semiconductor such as silicon is only a few millielectron volts, and thermal energy is then sufficient to create free carriers.

This high exciton binding energy of π -conjugated organic materials arises not only from the weak screening of charges (reflected in their low dielectric constant) but also from substantial electron correlation and geometry relaxation effects present in

states (sometimes completely). In this case, the fluctuations will cause the exciton to “hop” incoherently from site 1 to site 2; thus, no memory of the quantum mechanical phase information of the initial excitonic state on site 1 is preserved after the exciton has jumped to site 2. Incoherent hopping is the standard description of exciton transport in conjugated polymers. The only exception reported has been the case of a perfectly crystalline polydiacetylene chain, where coherent exciton motion was observed at very low temperature (8).

Collini and Scholes compared exciton transfer in two distinct morphologies of a derivative of the conjugated polymer poly(*p*-phenylenevinylene). When dissolved in a good solvent, the polymer chains are sepa-

observed to be correlated (for at least 250 fs) for intrachain transfer.

These results suggest that an intermediate coupling description, where Δ is similar to V , is appropriate. The preservation of coherence in the energy transfer along the chain is caused by correlations in fluctuations of E_1 and E_2 or in V that occur because sites 1 and 2 share a common structural framework. These correlations may arise because a vibrational mode, strongly coupled to the excitation, has a correlation length longer than the donor-acceptor spacing along the conjugated chain. Such a mode could be related to phenylene ring rotations along the chains, because the E_1 and E_2 energy levels strongly depend on the extent of chain planarity.



Surf, don't hop. Pictorial representation of exciton transfer from site 1 to site 2 along a poly(*p*-phenylenevinylene) conjugated polymer chain. Coherence could be preserved upon exciton transfer by coupling of the excitation to a vibrational

mode (taken here for the sake of illustration to be a rotational mode, as suggested by the arrows) with a correlation length longer than the spacing between sites 1 and 2.

these materials. Photon absorption results in exciton formation in organic solar cells and photodiodes, so these devices must have an interface between an electron donor and an electron acceptor, where the excitons can dissociate into free carriers. For such a device to be useful, the excitons must migrate fast enough to reach the donor-acceptor interface before undergoing other unproductive decay processes.

In a simple model for exciton migration, two structurally relaxed excitonic states, quasi-localized on sites 1 and 2, have different energies E_1 and E_2 . Moving the exciton from site 1 to site 2 (see the figure) requires substantial coupling V between the states. All of these quantities can fluctuate because of thermal noise and interactions with the surroundings. When the difference in energy $\Delta = E_1 - E_2$ is small relative to V (called the strong coupling limit), the excitonic states are largely delocalized over the two sites. The description of the states as delocalized remains correct as long as the fluctuations introduce only small perturbations. Thus, an exciton initially formed on site 1 can oscillate coherently between sites 1 and 2 before the fluctuations eventually lead to the decay of the coherence.

In the opposite limit, $\Delta \gg V$ (weak coupling), the fluctuations further localize the

exciton, and the dominant exciton motion should be along the chain backbone (intrachain diffusion). In contrast, polymer nanoparticles suspended in a poor solvent have collapsed chains, and the dominant motion should be between chains (interchain diffusion). In their ultrafast polarization experiment, exciton motion along the extended conjugated chains was coherent at short times (~ 250 fs, which might correspond to a motion over some 5 to 10 monomer units), whereas interchain exciton motion in collapsed chains exhibited no coherence signal.

Recently, Fleming and co-workers saw coherence in energy transfer at 77 K between closely spaced chromophores in protein light-harvesting complexes that lasted for 440 fs—considerably longer than the estimated exciton transfer time, ~ 250 fs—and inferred correlated fluctuations in the protein surrounding the chromophores (9). To understand how coherence can be preserved in their system even at room temperature, Collini and Scholes performed a two-dimensional photon echo experiment that reveals the time dependence of the correlation between initial and final states by changing the population time in the echo pulse sequence. The fluctuations in the energies E_1 and E_2 between sites 1 and 2 were

It is perhaps not surprising that the bonding structure in conjugated systems can induce long-range coherences. The strong electron-vibration coupling, responsible for so many of the properties of conjugated polymers, might also play a role in preserving quantum coherences. Thus, in combination with the results for polydiacetylene chains at low temperature (8), the results of Collini and Scholes on poly(*p*-phenylenevinylene) chains at room temperature imply that the efficiency of exciton migration in organic polymeric systems can be improved by strengthening intrachain transfer, in particular by promoting extended conformations.

References

1. G. D. Scholes, G. Rumbles, *Nat. Mater.* **5**, 683 (2006).
2. N. S. Saricic, Ed., *Primary Excitations in Conjugated Polymers: Molecular Exciton Versus Semiconductor Band Model* (World Scientific, Singapore, 1997).
3. J. L. Brédas, D. Beljonne, V. Coropceanu, J. Cornil, *Chem. Rev.* **104**, 4971 (2004).
4. S. W. Thomas III, G. D. Joly, T. M. Swager, *Chem. Rev.* **107**, 1339 (2007).
5. S. S. Sun, N. S. Saricic, Eds., *Organic Photovoltaics: Mechanisms, Materials and Devices* (Taylor & Francis, Boca Raton, FL, 2005).
6. E. Collini, G. D. Scholes, *Science* **323**, 369 (2009).
7. L. Sebastian, G. Weiser, *Phys. Rev. Lett.* **46**, 1156 (1981).
8. F. Dubin et al., *Nat. Phys.* **2**, 32 (2006).
9. H. Lee, Y.-C. Cheng, G. R. Fleming, *Science* **316**, 1462 (2007).

10.1126/science.1168821

GENETICS

Origin of Species in Overdrive

John H. Willis

This year is both the 200th anniversary of Charles Darwin's birth and the 150th anniversary of the publication of his masterwork, *On the Origin of Species* (1). This work established the facts of biological evolution: Species change over time, and new species arise by the splitting of ancestral species into two or more descendant species. Darwin also argued that natural selection is the mechanism by which species adapt to their environment. The great discoveries of 20th-century biology, including genetics and molecular biology, have confirmed and strengthened

species to arise remain mysterious. Two papers in this issue, one by Mihola *et al.* on page 373 (2) and the other by Phadnis and Orr on page 376 (3), advance our understanding of the evolution and molecular basis of hybrid sterility (see the figure).

The evolution of hybrid sterility and lethality, in contrast to other forms of reproductive isolation between species, was difficult for Darwin and early evolutionary biologists to understand because natural selection should not favor the production of dead or sterile offspring. Early 20th-century geneticists postu-

The genes that cause the sterility of hybrids between species should reveal the molecular genetic and evolutionary mechanisms that drive speciation.

was located to a region of chromosome 17 in a cross between house mouse subspecies (*Mus musculus musculus* and *Mus musculus domesticus*) (5). The "hybrid sterile" version of this gene functioned perfectly well within the genetic background of its own subspecies, but in hybrids from crosses between these subspecies, it interacted with other genes to cause early meiotic arrest in sperm-producing cells in testes, resulting in sterile hybrid male mice. Recently, investigators narrowed the region containing the hybrid sterility factor to a stretch of chromosome containing only a few



Speciation genes in mice and flies. Molecular genetic studies of hybrids formed by crosses between subspecies of the mouse *Mus musculus* by Mihola *et al.* and the fruit fly *Drosophila pseudoobscura* by Phadnis and Orr have identi-

fied genes causing hybrid male sterility. These new findings provide insight into the molecular, genetic, and evolutionary causes of hybrid incompatibilities, an important barrier to reproduction between species.

Darwin's theses. Comparisons of genes and genomes have revealed the evolutionary relationships of all life forms through a history of descent from common ancestors, and have pin-pointed changes in DNA that are driven by natural selection and underlie important adaptive traits in humans and many other species. But how have we progressed in understanding speciation, Darwin's "mystery of mysteries" (1)? Modern biology has shown that biological species are reproductively isolated either because ecological adaptations prevent them from interbreeding with other species in the wild, or because genetic incompatibilities cause the interspecific hybrids to be inviable or sterile. However, the molecular, genetic, and evolutionary mechanisms that cause new

species to arise remain mysterious. Two papers in this issue, one by Mihola *et al.* on page 373 (2) and the other by Phadnis and Orr on page 376 (3), advance our understanding of the evolution and molecular basis of hybrid sterility (see the figure). The evolution of hybrid sterility and lethality, in contrast to other forms of reproductive isolation between species, was difficult for Darwin and early evolutionary biologists to understand because natural selection should not favor the production of dead or sterile offspring. Early 20th-century geneticists postulated that two or more genetic changes in incipient species, while remaining functional within species, might become nonfunctional when paired in a hybrid. This model, though supported by numerous genetic mapping studies of hybrid incompatibilities in plants, animals, and fungi (4), predicts neither the nature of the genetic changes nor the evolutionary mechanisms that lead to hybrid incompatibilities. Are the new forms of the genes beneficial and thus divergent as a result of positive selection, or do the new mutations have no fitness effect and simply accumulate by random genetic fluctuations? What sort of molecular changes in genes are tolerated or even favored within species while causing severe developmental problems in hybrid genetic backgrounds?

Thirty-five years ago, the first hybrid sterility gene to be genetically mapped in a mammal

genes. Mihola *et al.* have now identified the hybrid sterility gene. They cloned a series of overlapping DNA fragments derived from the narrow chromosomal region of mice that carried the "hybrid fertile" version of the hybrid sterility gene, and individually engineered them into hybrid mice that would normally be sterile. By comparing the overlap of fragments that rescued the sterility to those that did not, they show that a single gene, *Prdm9*, causes the hybrid sterility.

To confirm the functional identity of *Prdm9*, the authors compared the cellular and molecular phenotypes of the sterile hybrid mice to those of normal mice genetically engineered to lack the gene ("knock-out" mice). The *Prdm9* gene encodes a methyltransferase that epigenetically modifies a chromatin structural protein, histone H3. This activates the promoters of genes

Department of Biology, Duke University, Durham, NC 27708, USA. E-mail: jwillis@duke.edu

essential for meiosis (6). *Prdm9* knockout mice exhibit defects in meiosis and produce sterile mice of both sexes. The meiotic defects include abnormalities in gene expression, chromosomal pairing, double-strand break repair, and male meiotic sex chromosome inactivation. But male hybrid mice resulting from crosses between the subspecies had defects related to their sterility that were identical to those of the knockout mice, even though the hybrid female mice had normal fertility. The *Prdm9* gene network functions normally within each subspecies, interacting with other components of the “genetic network” to promote meiosis. But what genes does *Prdm9* interact with in the hybrid animals to cause male sterility? In hybrids, the normal functional form of the gene from one subspecies now finds itself in a genetic background that contains the genetic network (related to meiosis; in this case, likely one or more genes that are yet to be identified) from another subspecies. Apparently, the gene does not work within the latter situation. In other words, whether or not the subspecies’ version of the *Prdm9* gene functions depends on the context—if the genetic background is from its own subspecies, the mice are fertile, whereas if one or more unknown genes from the other subspecies are present, the male mice are sterile. Important clues should emerge once it is determined which genes are modified and thus activated by *Prdm9*. Furthermore, when the complete hybrid sterility gene network is revealed, it may also be possible to discover why this incompatibility system has arisen in the first place. Interestingly, the hybrid sterile form of *Prdm9* is polymorphic within the mouse subspecies in which it was found originally (7). Perhaps experimental studies of the fitness effects of these alleles in the wild, or population genetic analyses of the DNA sequence variations around this gene (8), will show whether positive natural selection is acting on this hybrid sterility gene.

The classical view of the evolution of hybrid incompatibilities is that each successive genetic change increases individuals’ Darwinian fitness (or has no effect within species), but together they are incompatible in the hybrid genetic background (4). An alternative, and controversial, view is that hybrid incompatibilities evolve because “intra-genomic conflict” enables so-called selfish genes to distort the normal Mendelian mechanism of inheritance

“On the theory of natural selection the case [of hybrid sterility] is especially important, inasmuch as the sterility of hybrids could not possibly be of any advantage to them, and therefore could not have been acquired by the continued preservation of successive profitable degrees of sterility ... I hope, however, to be able to show that sterility is not a specially acquired or endowed quality, but is incidental on other acquired differences.”

—DARWIN [(1), P. 245]

to their own advantage, perhaps by eliminating gametes that carry the alternative allele. Theory suggests that such “meiotic drive” genes can invade a species even if they reduce individuals’ fertility. Such genes are especially likely to evolve if they are located on a sex chromosome, and by inactivating gametes with the alternative sex chromosome, lead to highly biased sex ratios. This process can be followed by the evolution of unlinked genes (those on different chromosomes) that suppress the sex ratio distorter’s detrimental effects, and restore Mendelian inheritance and sex ratios to 50:50. Later, if such a species interbreeds with another species that lacks the suppressed system, meiotic drive can be unleashed in the resulting hybrids, potentially leading to hybrid sterility (9, 10).

The discovery by Phadnis and Orr that a gene that causes sterility in male hybrids from crosses between subspecies of a fruit fly (*Drosophila pseudoobscura*) profoundly distorts the normally Mendelian inheritance of sex chromosomes directly challenges the classical view. Previous research had shown that crosses between female flies from the Bogotá, Columbia, subspecies of *D. pseudoobscura* and males from the United States subspecies result in fertile female hybrids and hybrid males that are almost completely sterile. These hybrid males have almost no functional sperm when young, but as they age, they occasionally produce enough to make a few offspring. The hybrid male sterility is caused by incompatibilities between the Bogotá versions of two genes on the X chromosome and the U.S. versions of two other genes (11). Notably, when the almost sterile hybrid male flies are able to reproduce, they produce nearly all daughters.

Is the sex-ratio distortion related to the hybrid sterility? Mapping of the hybrid sterility genes showed that one of them resided in a region of the X chromosome that also caused

extreme sex-ratio distortion in the rare offspring of hybrid males (12). Was this linkage merely a coincidence? Not according to Phadnis and Orr. They first isolated a tiny region of the X chromosome harboring both the hybrid sterility gene and the sex-ratio distorter (by many generations of genetic crossing). Like Mihola *et al.*, they then used a series of transgenic experiments coupled with genetic crosses to see which of the five genes in this interval was responsible for the hybrid sterility and sex-ratio distortion. Remarkably, they show that a single gene, of previously unknown function, encodes a product that causes both hybrid traits, and hence they name the gene *Overdrive*. DNA sequence comparisons of the two subspecies in the vicinity of *Overdrive* indicate rapid evolution in the Bogotá lineage, consistent with an evolutionary history of sex-ratio distortion. How *Overdrive* interacts with other genes to cause meiotic drive and hybrid male sterility remains uncertain, but these dual effects suggest that in this case, hybrid sterility has evolved by genetic conflict, rather than as a side-effect of adaptive evolution.

Further genomic studies should reveal many more genes underlying hybrid sterility and lethality in different species. Like *Prdm9*, will such genes appear to have evolved while maintaining important functions for survival or fertility within species? Or, like *Overdrive*, will they appear to have evolved through conflicting, antagonistic selection pressures between genes in different regions of the genome? Darwin was struck by how antagonistic ecological interactions between species can drive adaptation. He would have been fascinated to see how analogous processes between genes within genomes can drive speciation.

References

1. C. Darwin, *On the Origin of Species* (Murray, London, 1859).
2. O. Mihola, Z. Trachtulec, C. Vlcek, J. C. Schimenti, J. Forejt, *Science* **323**, 373 (2009); published online 11 December 2008 (10.1126/science.1163601).
3. N. Phadnis, H. A. Orr, *Science* **323**, 376 (2009); published online 11 December 2008 (10.1126/science.1163934).
4. J. A. Coyne, H. A. Orr, *Speciation* (Sinauer, Sunderland, MA, 2004).
5. J. Forejt, P. Ivanyi, *Genet. Res.* **24**, 189 (1974).
6. K. Hayashi, K. Yoshida, Y. Matsui, *Nature* **438**, 374 (2005).
7. J. M. Good, M. A. Handel, M. W. Nachman, *Evolution* **62**, 50 (2008).
8. Z. Trachtulec *et al.*, *Genetics* **178**, 1777 (2008).
9. S. A. Frank, *Evolution* **45**, 262 (1991).
10. L. D. Hurst, A. Pomiankowski, *Genetics* **128**, 841 (1991).
11. H. A. Orr, S. Irving, *Genetics* **158**, 1089 (2001).
12. H. A. Orr, S. Irving, *Genetics* **169**, 1089 (2005).

10.1126/science.1169442

Programmed Assembly of DNA-Coated Nanowire Devices

Thomas J. Morrow,¹ Mingwei Li,² Jaekyun Kim,² Theresa S. Mayer,^{2*} Christine D. Keating^{1*}

Fabricating electronic devices using multi-level photolithography provides excellent control of feature geometry and registration between layers (1), but each deposition step incorporates just one material, from a limited set, over the entire chip. Alternatively, device components such as nanowires can be synthesized from many different materials and even coated with biological molecules before assembling them onto a chip. However, it is still challenging to accurately position the various nanowires in different locations on the chip (2, 3).

We present a hybrid approach that uses forces generated by electric fields to direct different populations of biofunctionalized nanowires to specific regions of the chip while providing accurate registry between each individual nanowire and the photolithographic features within that region. We synchronized sequential injections of nanowires carrying different DNA sequences with a programmed, spatially confined electric-field profile that directs nanowire assembly. Nanowire-bound DNA was able to selectively bind complementary targets after assembly and device fabrication, which makes this process compatible with conventional integrated circuit manufacturing.

DNA oligonucleotides complementary to sequences found in human pathogens were attached covalently to different batches of nanowires (8 μm long, $\sim 10^9$ wires per ml) (4). Aliquots were sequentially injected across a dense two-dimensional array

of photolithographically defined microwells superimposed across gaps separating guiding electrodes used for programmed assembly (Fig. 1A). Electric-field calculations with sinusoidal voltages applied between specific pairs of guiding electrodes showed that the field strength is highest in the microwells that span the biased electrodes and negligible elsewhere (Fig. 1B). These field gradients induced long-range dielectrophoretic

forces that directed individual nanowires to the biased microwells in <1 min. Fields were shielded in occupied wells, preventing additional nanowires from entering. Electrostatic forces centered the wires across the gaps, and capillary forces pushed them against the sides of the wells; this fixed the position of nanowire tips and their pitch, respectively. After all batches were assembled, we generated an array of nanowire resonator devices (5) by forming contacts to each wire (Fig. 1C).

In this proof of concept, we assembled nanowires carrying different DNA sequences into three separate columns. We used ~ 300 -nm-diameter wires, with a 20-nm SiO_2 shell to facilitate verification of DNA function by fluorescence. After device integration, the entire chip was incubated with a mixture of DNA target sequences, each complementary to one of the nanowire-bound probes and labeled with a different dye. Each labeled target bound to wires in a different column (Fig. 1D), indicating successful nanowire assembly and retention of DNA binding selectivity despite exposure to electric fields, photoresist coatings, and solvents.

Almost no nanowires assembled in the wrong column ($\leq 1\%$). The array had a 71% yield of individual nanowire devices in 750 potential sites (2.4×10^4 devices per cm^2); defects included vacancies (19%) and multiples of the same nanowire type (9%). Submicrometer placement accuracy was achieved across the entire array. This would allow direct electrical connection between each nanowire device and a dedicated transistor on an integrated circuit chip. This assembly approach, which is also compatible with smaller-diameter nanowires, could be extended to more diverse materials or coatings and alternative device structures, such as field effect transistors that enable not only detection but also stimulation of biological events (6, 7).

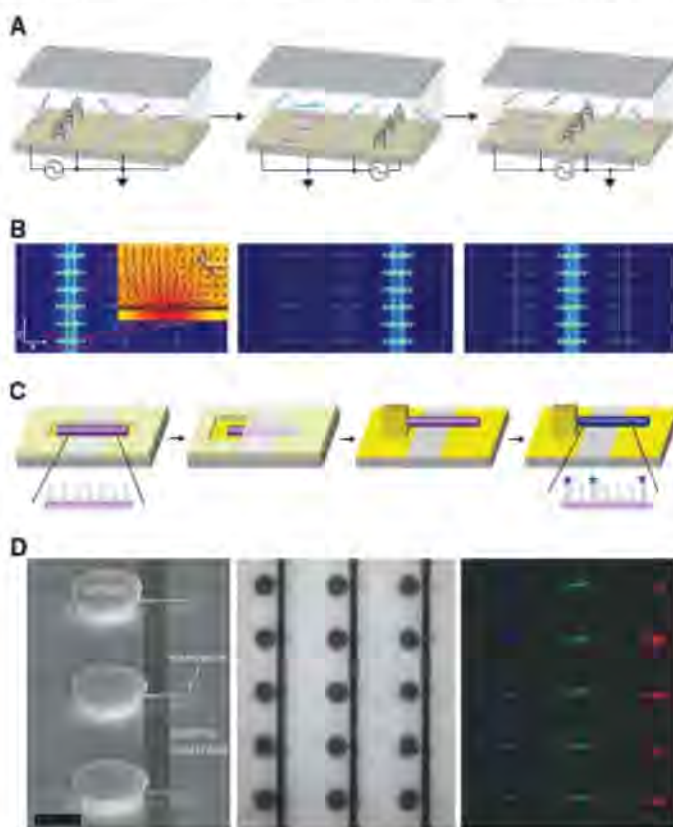


Fig. 1. Fabrication of multisequence DNA-coated nanowire device array. (A) Assembly process. Suspensions of nanowires carrying different DNAs were injected sequentially, while 4.2-V, 1-MHz voltages were applied between guiding electrodes. Nanowires were directed to microwells in a particular column. (B) Simulated spatial electrical-field gradient during assembly. Contour plots show $\nabla|\mathbf{E}|^2$ measured at the surface of the microwells for the peak value of voltage applied in (A), where \mathbf{E} is the electric field; scale is 10^{10} (blue) to 10^{18} (red) V^2/m^3 . (Inset) Cross-sectional view of one microwell, plotted as $\log \nabla|\mathbf{E}|^2$; scale is 10^{13} (yellow) to 10^{20} (red) V^2/m^3 ; arrows indicate the dielectrophoretic force. (C) Postassembly device integration. Windows registered to microwells were opened in photoresist. Au contacts were electrodeposited; additional processing, for example, oxide removal, is possible. Dissolving photoresist left nanowire resonator devices; these were incubated with DNA. (D) Scanning electron microscope (left), optical reflectance (center), and fluorescence (right) images after incubation with labeled complementary targets. Scale bar indicates 5 μm .

References and Notes

1. T. Ito, S. Okazaki, *Nature* **406**, 1027 (2000).
2. J.-H. Ahn et al., *Science* **314**, 1754 (2006).
3. W. Lu, C. M. Lieber, *Nat. Mater.* **6**, 841 (2007).
4. Materials and methods are available as supporting material on Science Online.
5. M. Li et al., *Nat. Nanotechnol.* **3**, 88 (2008).
6. F. Patolsky et al., *Science* **313**, 1100 (2006).
7. T.-T. Ho et al., *Nano Lett.* **8**, 4359 (2008).
8. Supported by NIH, NSF, and Semiconductor Research Corporation–Nanoelectronics Research Initiative.

Supporting Online Material

www.sciencemag.org/cgi/content/full/323/5912/352/DC1
Materials and Methods

Fig. S1

Table S1

References

15 September 2008; accepted 17 November 2008
10.1126/science.1165921

¹Department of Chemistry, Pennsylvania State University, University Park, PA 16802, USA. ²Department of Electrical Engineering, Pennsylvania State University, University Park, PA 16802, USA.

*To whom correspondence should be addressed. E-mail: tsm2@psu.edu (T.S.M.); keating@chem.psu.edu (C.D.K.)

Dust Formation in a Galaxy with Primitive Abundances

G. C. Sloan,^{1*} M. Matsuura,^{2,3} A. A. Zijlstra,⁴ E. Lagadec,⁴ M. A. T. Groenewegen,⁵ P. R. Wood,⁶ C. Szyszka,⁴ J. Bernard-Salas,¹ J. Th. van Loon⁷

Interstellar dust plays a crucial role in the evolution of galaxies. It governs the chemistry and physics of the interstellar medium. In the local universe, dust forms primarily in the ejecta from stars, but its composition and origin in galaxies at very early times remain controversial. We report observational evidence of dust forming around a carbon star in a nearby galaxy with a low abundance of heavy elements, 25 times lower than the solar abundance. The production of dust by a carbon star in a galaxy with such primitive abundances raises the possibility that carbon stars contributed carbonaceous dust in the early universe.

Dust is an important astrophysical constituent. It regulates the cooling of the interstellar medium, attenuates light emitted by galaxies, and fragments collapsing molecular clouds into intermediate- and low-mass stars. The detection of dust in the early universe (1, 2) raises questions about its composition and origin. Primordial dust may differ substantially from dust in the Milky Way because it formed when the abundances of refractory elements were low. Polycyclic aromatic hydrocarbons (PAHs), a carbon-rich dust component, have been detected as far back as a redshift of 2.7, or 2.5 billion years after the Big Bang (3), but galaxies with low metallicities (that is, with little enrichment from elements heavier than helium) have a deficit in PAH emission (4, 5). The 2200 Å bump seen in ultraviolet extinction curves and associated with carbonaceous interstellar dust is also largely absent in both metal-poor galaxies (6) and distant quasars (7). The extinction curves of these galaxies still require carbon-rich dust (8), but the nature of that carbon-rich dust is changing with metallicity.

The main sources of dust are the winds of evolved stars and supernovae (SNe). In the Milky Way, stars on the asymptotic giant branch (AGB) dominate the injection of dust into the interstellar medium (ISM) (9). The chemistry of this dust depends on the C/O ratio in the photosphere of the star, which in turn depends on how much carbon produced by triple- α burning in the interior of the star has been dredged to the surface.

The stable CO molecule will form until either C or O is exhausted. Solids form from the remainder, resulting in either oxygen-rich dust dominated by silicates or carbonaceous dust. Both observations (10, 11) and theory (12) show that the fraction of AGB stars that become carbon-rich increases in more metal-poor systems.

There are reasons to expect reduced dust production at low metallicity. Radiation pressure on dust grains cannot drive the winds from oxygen-rich AGB stars at metallicities below 0.1 of the solar value, which could lead to higher SN rates in primitive galaxies (13) and make SNe the dominant source of dust in the early universe (14). However, observational evidence that SNe produce sufficient dust, and produce more than they destroy, remains controversial (15, 16).

Studies with the Infrared Spectrograph (IRS) (17) on the Spitzer Space Telescope (18) of the

Large Magellanic Cloud (LMC) and Small Magellanic Cloud (SMC) (19–21) and the Fornax Dwarf Spheroidal (22) have revealed dust-forming carbon stars at metallicities as low as ~ 0.1 that of the Sun. As the metallicity of the sample decreases, the amount of dust produced by oxygen-rich AGB stars decreases; but for carbon stars, the amount of dust remains unchanged (23, 24). Other properties of the outflows from carbon stars do depend on metallicity. As the metallicity of the sample drops, carbon stars produce less trace dust components such as SiC and MgS, even though the production of amorphous carbon does not change. There is evidence for increasing abundances of acetylene (C_2H_2) at lower metallicity. Acetylene is the fundamental building block of larger carbon-rich structures such as PAHs (25). Thus, mass loss and dust formation in carbon stars do not appear to depend on the abundances with which the star formed. Instead, free carbon (after the formation of CO) needed by these stars to form dust is produced by the stars themselves and then dredged to the surface. It follows that even the most metal-poor carbon stars should produce dust.

To test this hypothesis, we observed a carbon star in the direction of the Sculptor Dwarf Spheroidal galaxy with the IRS on Spitzer. The Sculptor Dwarf is a satellite of the Milky Way, with a metallicity only 0.04 that of the Sun (26). A study of carbon stars in the Galactic Halo detected a candidate, MAG 29, in the field of the Sculptor Dwarf (27). This study assumed that the absolute magnitude in the narrow K filter (K_s) of MAG 29 was -6.9 , but noted that it could be brighter by half a magnitude or more. The apparent K_s magnitude of MAG 29 is 11.60 (28). Thus, the assumed absolute K_s magnitude (M_K) implies a distance of 50 kpc, in the foreground of the

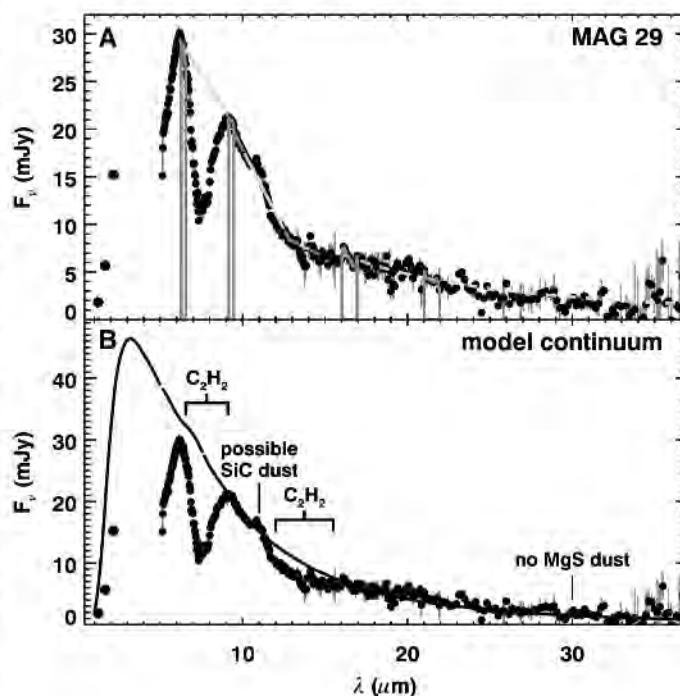


Fig. 1. The IRS spectrum of MAG 29. F_ν , flux density per unit of frequency; λ , wavelength. The three points at 1.2 to 2.2 μm represent older, ground-based 2MASS observations (28). (A) The Manchester method determines the [6.4] – [9.3] and [16.5] – [21.5] colors (boxes), fits line segments over the C_2H_2 bands at 7.5 and 13.7 μm and under the SiC emission feature at $\sim 11 \mu\text{m}$ (solid lines), and extrapolates a Planck function from the [16.5] – [21.5] color under any possible MgS emission in the 30- μm vicinity (dashed line). (B) A radiative transfer model of the dust continuum (solid curve).

¹Department of Astronomy, Cornell University, Ithaca, NY 14853-6801, USA. ²National Optical Astronomical Observatory of Japan, Osawa 2-21-1, Mitaka, Tokyo 181-8588, Japan. ³Department of Physics and Astronomy, University College London, Gower Street, London WC1E 6BT, UK. ⁴School of Physics and Astronomy, University of Manchester, Post Office Box 88, Manchester M60 1QD, UK. ⁵Royal Observatory of Belgium, Ringlaan 3, B-1180 Brussels, Belgium. ⁶Research School of Astronomy and Astrophysics, Australian National University, Cotter Road, Weston Creek Australian Capital Territory 2611, Australia. ⁷Astrophysics Group, Lennard-Jones Laboratories, Keele University, Staffordshire ST5 5BG, UK.

*To whom correspondence should be addressed. E-mail: sloan@isc.astro.cornell.edu

Sculptor Dwarf, which is 87 kpc away (29). However, calibrations of near- and mid-infrared color magnitude relations (23) make MAG 29 a likely member of the Sculptor Dwarf. The $J - K_s$ color (difference between apparent J and K_s magnitudes) of MAG 29 is 3.24 (28). The linear relation between $J - K_s$ and M_K implies $M_K = -7.90 \pm 0.51$ and a distance of 80 ± 19 kpc. Measuring the magnitude of MAG 29 at 6.4 and 9.3 μm (9.3) and applying the relation between $[6.4] - [9.3]$ color and $M_{9.3}$ provides a second estimate of the distance. The $[6.4] - [9.3]$ color is 0.494 ± 0.012 , which gives an absolute magnitude at 9.3 μm ($M_{9.3}$) = -11.38 ± 0.59 . The apparent magnitude at 9.3 μm is 8.35, implying that the distance is 88 ± 18 kpc. The two color-based distances are consistent with each other and the distance to the Sculptor Dwarf, but both are inconsistent with the previous provisional estimate of 50 kpc. Combining the two new distances gives 84 ± 13 kpc, confirming the association between the star and the galaxy and making MAG 29 the most metal-poor, carbon-rich AGB star studied spectroscopically in the infrared.

The mid-infrared spectrum of MAG 29 shows a continuum, with strong molecular absorption bands (Fig. 1A). We analyzed the spectrum by applying the Manchester method (19), which uses the $[6.4] - [9.3]$ color to diagnose the continuum

temperature in this spectral region. Radiative transfer models show that this color varies linearly with the logarithm of the mass-loss rate (24). The calibration of $[6.4] - [9.3]$ color to dust mass-loss rate (23), which assumes an outflow velocity of 10 km s^{-1} , implies that MAG 29 is producing dust at the rate of 8×10^{-9} solar masses (M_\odot) year^{-1} , with an uncertainty of $\sim 16\%$.

We tested this conclusion by fitting a radiative transfer model (30) to the IRS spectrum and to the 2MASS data of Skrutskie *et al.* (28) (Fig. 1B). The 2MASS data were best fitted with a model in which the stellar temperature was 4000 K, higher than found for Galactic mass-losing stars. Metal-poor AGB stars are bluer and hotter than their metal-rich counterparts (31). The dust shell around MAG 29 has a temperature of 1600 K at its inner radius. Although below the condensation temperature of amorphous carbon, it is higher than what is typically found for Galactic carbon stars, indicating that the dust in MAG 29 forms close to the star and that graphite may be a component. The fitted model implies that MAG 29 is producing dust at a rate of $2.5 \times 10^{-8} M_\odot \text{ year}^{-1}$. This value is larger than that estimated with the Manchester method by a factor of ~ 3 because the radiative transfer model leads to a higher outflow velocity (35 versus 10 km s^{-1}). Assuming a gas-to-dust ratio of 200, the total mass-loss rate of

MAG 29 is in the range of $1.6 \times 10^{-6} M_\odot \text{ year}^{-1}$ to $4.9 \times 10^{-6} M_\odot \text{ year}^{-1}$. These results point to substantial mass loss and dust production.

In most carbon stars, amorphous carbon dominates the dust, but trace amounts of SiC and MgS produce emission features at ~ 11.3 and 26 to 30 μm , respectively. We used the Manchester method to fit a line segment to the continuum on either side of the SiC feature. We found a possible emission feature centered at 10.9 μm , similar to that found in two carbon stars in the SMC (19), with a strength of $3 \pm 1\%$ that of the continuum. However, it is possible that what appears to be emission is simply continuum between a suspected absorption band at 10 μm (20) and acetylene absorption between 11 and 16 μm . Therefore, the measured SiC strength is an upper limit of 4%. The MgS emission extends beyond 37 μm , outside the wavelength coverage of the IRS. We extrapolated the continuum under the MgS emission feature by fitting a Planck function at 16.5 and 21.5 μm and found no evidence of MgS emission.

The spectrum of MAG 29 shows a deep absorption band at 7.5 μm . It is substantially deeper and broader than the acetylene bands in carbon stars in the LMC (32). Thus, we modified the Manchester method by fitting a continuum at 6.14 to 6.44 μm and 9.12 to 9.42 μm . The band's equivalent width is $0.79 \pm 0.02 \mu\text{m}$, almost twice as strong as that measured in any other carbon star. We compared it to that of a typical carbon star in the SMC and to a synthetic spectrum of acetylene with an excitation temperature of 1750 K (Fig. 2). The synthetic spectrum reproduces the general shape of the band, demonstrating that acetylene is the primary absorber. The synthetic spectrum does not match the details of the absorption core, but it is limited by the available line lists, which do not include the higher-order transitions that will be populated at these high temperatures and column densities (33).

MAG 29 shows another acetylene feature centered at 13.7 μm . The Manchester method is not useful to study this feature because it measures the Q branch of this transition, but not the P and R branches that can extend from ~ 11 to $\sim 16 \mu\text{m}$ (33). Matches between the data and a model of the continuum over this wavelength range show that the band's equivalent width is $0.990 \pm 0.022 \mu\text{m}$. Only one carbon star, MSX SMC 093 in the SMC, has a stronger band (34), whereas IRAS 04496-6958 in the LMC, another carbon star, has a band of comparable strength (Fig. 3).

We compared the acetylene strength and the SiC strength of MAG 29 with those observed in Local Group samples (Fig. 4). We limited the comparison sample to those sources with colors similar to those of MAG 29; that is, those with $0.35 \leq [6.4] - [9.3] \leq 0.65$. The data for the 7.5- μm feature and SiC strength are from previously published studies of the Magellanic Clouds (19–21, 23) and new analysis of spectra from the Fornax Dwarf (22). The 11- to 16- μm data are taken directly from a recent study (34). We adopted $[Z/H] = 0.00 \pm 0.10$ for the Galaxy (Z is the metal

Fig. 2. The 7.5- μm absorption band in the spectrum of MAG 29, compared to the spectrum of MSX SMC 036, a typical carbon star in the SMC (19) (top) and to a synthetic absorption spectrum from acetylene (C_2H_2) (bottom).

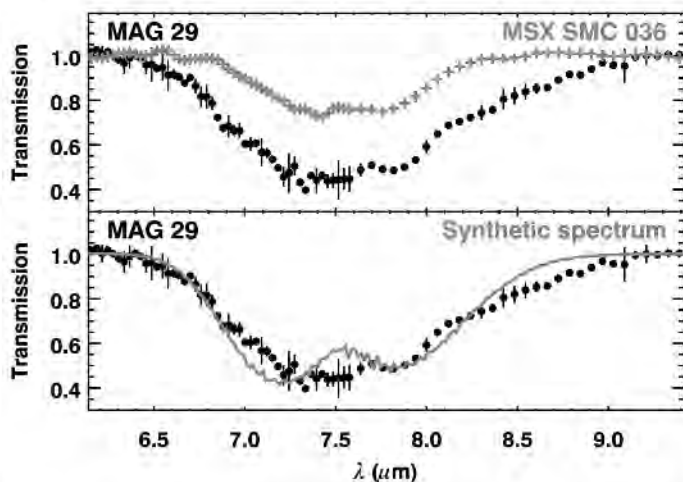


Fig. 3. The 11- to 16- μm absorption band in the spectrum of MAG 29, plotted as transmission by dividing by the continuum as estimated from the radiative transfer model in Fig. 1 and compared to the IRS spectrum of IRAS 04496-6958 (33) (top) and a synthetic acetylene spectrum (bottom).

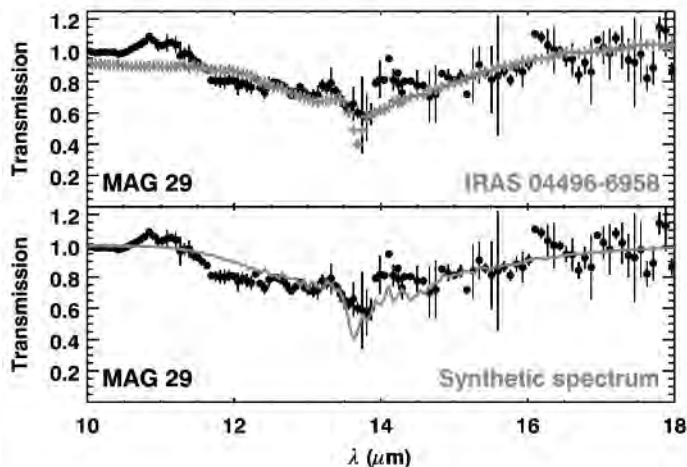
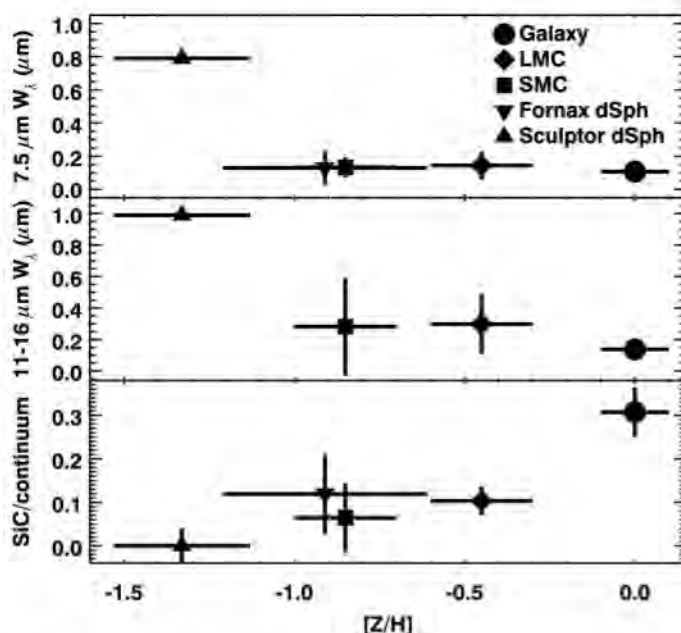


Fig. 4. The metallicity dependence of the acetylene equivalent widths at 7.5 μm (top) and 11 to 16 μm (middle) and the SiC/continuum flux ratio (bottom) for sources with $0.35 \leq [6.4] - [9.3] \leq 0.65$. The error bars are the standard deviation of the populations, except for MAG 29. We have considered the SiC strength in MAG 29 to be $0 \pm 4\%$ of the continuum, although it could be as large as $3 \pm 1\%$.



abundance), -0.45 ± 0.15 for the LMC, and -0.85 ± 0.15 for the SMC (35). We adopted $[Z/H] = -1.33 \pm 0.20$ for the Sculptor Dwarf (26) and $[Z/H] = 0.93 \pm 0.30$ for Fornax [based on $[\text{Fe}/\text{H}] = -1.0 \pm 0.3$ (36) and assuming the same $[\alpha/\text{Fe}]$ as for the Sculptor Dwarf]. The weak trend of increasing acetylene absorption with decreasing metallicity is more readily apparent when the data are examined over a larger color range (23). The spectrum of MAG 29 shows that the previously observed trends extend to metallicities as low as that of the Sculptor Dwarf.

In the Galactic environment, radiation pressure on carbon-rich dust can drive high mass loss from carbon stars (37). A carbon star self-produces its carbon via the triple- α reaction; if it can dredge up enough excess carbon, compared to oxygen, to allow the formation of carbonaceous dust, this high-mass-loss phase becomes inevitable (38). The spectrum of MAG 29 shows that metallicity is not a hurdle for the formation of dust around carbon stars. Metal-poor stars have an increased carbon dredge-up efficiency and lack the intrinsic oxygen that offsets dredged-up carbon, leading to a higher amount of excess carbon after the formation of CO (39, 40).

Once enough time has elapsed after a galaxy has formed for stars to reach the AGB and dredge up carbon, its ISM should be seeded with carbon-rich dust. Dust has been detected in galaxies to a redshift of 6.4 (1), or only 870 million years after the Big Bang. Recent modeling (41) shows that as soon as trace amounts of metals (10^{-3} of the solar amount) appear in the ISM, intermediate-mass stars can form. Thus, precursors of carbon stars will form almost immediately after the formation of galaxies, which should have occurred by a redshift of ~ 10 , or ~ 480 million years after the Big Bang (42). Thus, carbon stars have ~ 390 million years to evolve from their birth to the AGB. Models of stars at 0.01 solar metallicity (43) be-

come carbon-rich over the full mass range studied (2.5 to $5 M_{\odot}$). Similarly, all models from 2 to $6 M_{\odot}$ at half that metallicity also become carbon-rich (44). These models will evolve from the zero-age main sequence to the AGB in only 70 million years for the most massive stars. The $3-M_{\odot}$ models require only 280 to 310 million years. These time scales are less than the 500-million-year time scale used previously to rule out carbon stars as contributors to the dust at these redshifts (14, 45).

How much dust carbon stars can contribute at these redshifts depends on variables that are more difficult to quantify. The amount of carbon formed and dredged up differs by an order of magnitude in the models referred to above. The star formation rate and the initial mass function will determine how many stars form in the appropriate mass range. The star formation rates needed for carbon stars to explain the dust observed at high redshift may be consistent with observed luminosities (46). All of these quantities need to be better understood before we can quantify how much dust carbon stars contributed in the early universe.

The relative contributions of SNe and carbon stars to dust in the early universe is a problem of great interest. Core-collapse SNe appear well before the first carbon stars, whereas type Ia SNe require white dwarfs, which appear only after AGB stars have evolved. Core-collapse SNe can produce both silicates and carbonaceous dust; it is difficult to determine which would dominate (47). Current measurements of the dust around observed SNe fall short of what is needed to account for the dust observed at high redshifts (45), but we lack direct observations of SNe at low metallicity. A recent study of dust extinction at a redshift of 6.2 found evidence for carbonaceous dust (48). In the light of the observations reported here, the presence of such dust could be explained, at least in part, by the mass loss from carbon stars in the early universe.

References and Notes

1. F. Bertoldi et al., *Astron. Astrophys.* **406**, L55 (2003).
2. D. C. Hines et al., *Astrophys. J.* **641**, L85 (2006).
3. H. I. Teplitz et al., *Astrophys. J.* **659**, 941 (2007).
4. C. W. Engelbracht et al., *Astrophys. J.* **628**, L29 (2005).
5. Y. Wu et al., *Astrophys. J.* **639**, 157 (2006).
6. K. D. Gordon, G. C. Clayton, K. A. Missell, A. U. Landolfi, M. J. Wolff, *Astrophys. J.* **594**, 279 (2003).
7. K. M. Pitman, G. C. Clayton, K. D. Gordon, *Publ. Astron. Soc. Pac.* **112**, 537 (2000).
8. J. S. Mathis, *Astrophys. J.* **497**, 824 (1998).
9. R. Gehr, in *Proceedings of IAU Symposium 135*, L. J. Allamandola, A. G. G. M. Tielens, Eds. (Kluwer Academic, Dordrecht, Netherlands, 1989), pp. 445–453.
10. B. M. Blanco, V. M. Blanco, M. F. McCarthy, *Nature* **271**, 638 (1978).
11. V. M. Blanco, B. M. Blanco, M. F. McCarthy, *Astrophys. J.* **242**, 938 (1980).
12. A. Renzini, M. Voli, *Astron. Astrophys.* **94**, 175 (1981).
13. G. H. Bowen, L. A. Willson, *Astrophys. J.* **375**, L53 (1991).
14. E. Dwek, *Astrophys. J.* **501**, 643 (1998).
15. B. E. K. Sugerman et al., *Science* **313**, 196 (2006).
16. W. P. S. Meikle et al., *Astrophys. J.* **508**, 106 (2007).
17. J. R. Houck et al., *Astrophys. J. Suppl.* **154**, 18 (2004).
18. M. W. Werner et al., *Astrophys. J. Suppl.* **154**, 1 (2004).
19. G. C. Sloan et al., *Astrophys. J.* **645**, 1118 (2006).
20. A. A. Zijlstra et al., *Mon. Not. R. Astron. Soc.* **370**, 1961 (2006).
21. E. Lagadec et al., *Mon. Not. R. Astron. Soc.* **376**, 1270 (2007).
22. M. Matsuura et al., *Mon. Not. R. Astron. Soc.* **382**, 1889 (2007).
23. G. C. Sloan et al., *Astrophys. J.* **686**, 1056 (2008).
24. M. A. T. Groenewegen et al., *Mon. Not. R. Astron. Soc.* **376**, 313 (2007).
25. M. Frenklach, E. D. Feigelson, *Astrophys. J.* **341**, 372 (1989).
26. C. Babusiaux, G. Gilmore, M. Irwin, *Mon. Not. R. Astron. Soc.* **359**, 985 (2005).
27. N. Mauron, M. Azzopardi, K. Gigoyan, T. R. Kendall, *Astron. Astrophys.* **418**, 77 (2004).
28. M. F. Skrutskie et al., *Astron. J.* **131**, 1163 (2006).
29. J. Kaluzny et al., *Astron. Astrophys.* **112**, 407 (1995).
30. M. Elitzur, Ž. Ivezić, *Mon. Not. R. Astron. Soc.* **327**, 403 (2001).
31. E. M. Levesque et al., *Astrophys. J.* **628**, 973 (2005).
32. M. Matsuura et al., *Mon. Not. R. Astron. Soc.* **371**, 415 (2006).
33. A. K. Speck et al., *Astrophys. J.* **650**, 892 (2006).
34. J. M. Leisenring, F. Kemper, G. C. Sloan, *Astrophys. J.* **681**, 1557 (2008).
35. J. Th. van Loon, *Astron. Astrophys.* **354**, 125 (2000).
36. E. Tolstoy et al., *Mon. Not. R. Astron. Soc.* **327**, 918 (2001).
37. P. Woitke, *Astron. Astrophys.* **460**, L9 (2006).
38. E. Lagadec, A. A. Zijlstra, *Mon. Not. R. Astron. Soc.* **390**, L59 (2008).
39. J. Th. van Loon, A. A. Zijlstra, M. A. T. Groenewegen, *Astron. Astrophys.* **346**, 805 (1999).
40. M. Matsuura et al., *Astron. Astrophys.* **434**, 691 (2005).
41. P. C. Clark, S. C. O. Glover, R. S. Klessen, *Astrophys. J.* **672**, 757 (2008).
42. T. H. Greif, J. L. Johnson, R. S. Klessen, V. Bromm, *Mon. Not. R. Astron. Soc.* **387**, 1021 (2008).
43. P. Ventura, F. D'Antona, I. Mazzitelli, *Astron. Astrophys.* **393**, 215 (2002).
44. F. Herwig, *Astrophys. J. Suppl.* **155**, 651 (2004).
45. E. Dwek, F. Galliano, A. P. Jones, *Astrophys. J.* **662**, 927 (2007).
46. H. L. Morgan, M. G. Edmunds, *Mon. Not. R. Astron. Soc.* **343**, 427 (2003).
47. R. Schneider, A. Ferrara, R. Salvaterra, *Mon. Not. R. Astron. Soc.* **351**, 1379 (2004).
48. R. Maiolino et al., *Nature* **431**, 533 (2004).
49. Support for G.C.S. was provided by NASA through contract number 1257184 issued by the Jet Propulsion Laboratory, California Institute of Technology, under NASA contract 1407. The Australian Research Council provided support to P.R.W., and M.M. was supported by a Japan Society for the Promotion of Science fellowship.

8 September 2008; accepted 2 December 2008
10.1126/science.1165626

Early Lunar Magnetism

Ian Garrick-Bethell,^{1*} Benjamin P. Weiss,¹ David L. Shuster,² Jennifer Buz¹

It is uncertain whether the Moon ever formed a metallic core or generated a core dynamo. The lunar crust and returned samples are magnetized, but the source of this magnetization could be meteoroid impacts rather than a dynamo. Here, we report magnetic measurements and $^{40}\text{Ar}/^{39}\text{Ar}$ thermochronological calculations for the oldest known unshocked lunar rock, troctolite 76535. These data imply that there was a long-lived field on the Moon of at least 1 microtesla ~4.2 billion years ago. The early age, substantial intensity, and long lifetime of this field support the hypothesis of an ancient lunar core dynamo.

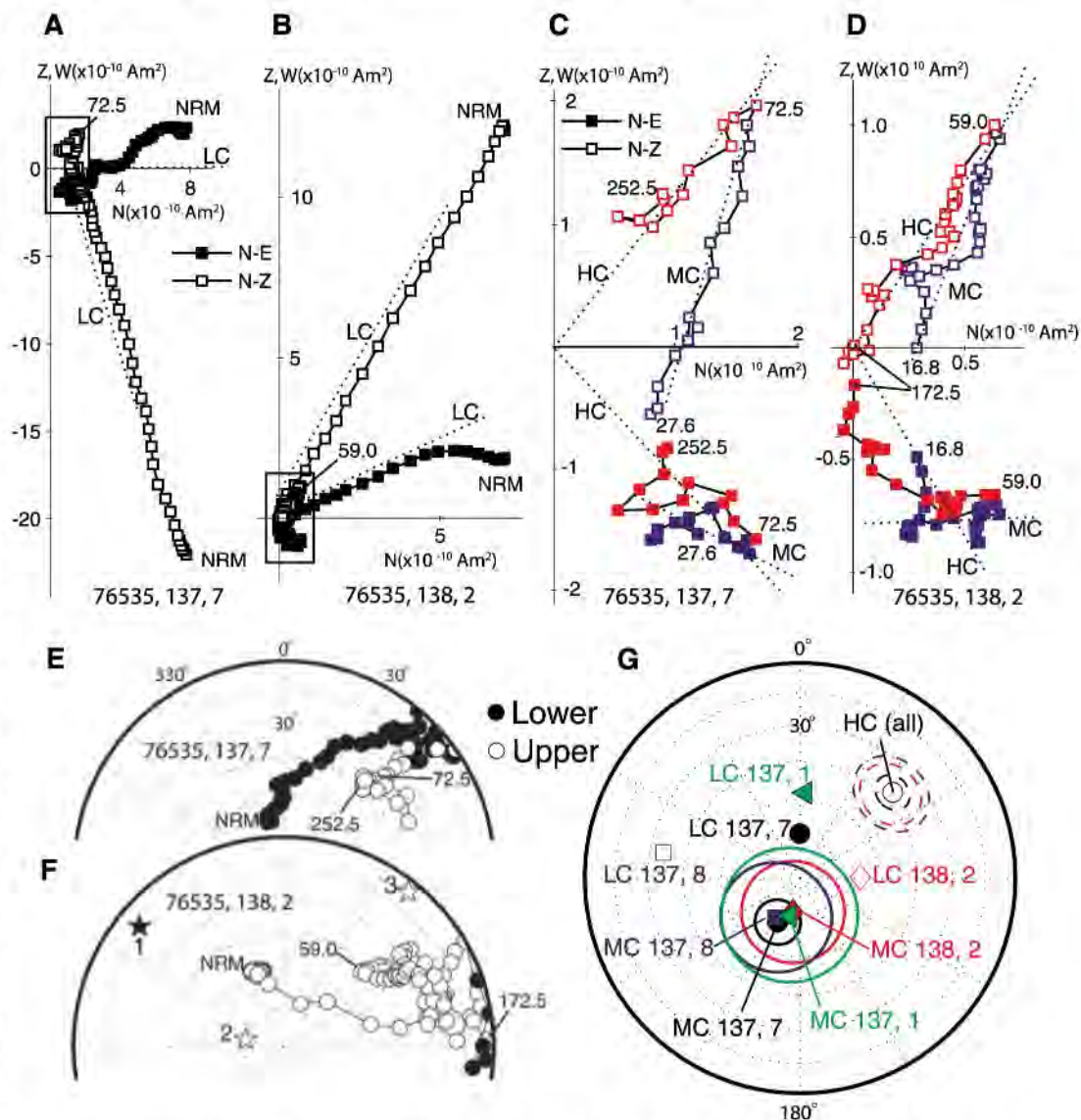
Before the Apollo missions, the Moon was often thought to be a primordial undifferentiated relic of the early solar system (1) that had never formed a core or generated a magnetic dynamo. Because it was well known that the Moon presently has no global magnetic field (2), it was a surprise when the Apollo subsatellites and surface magnetometers detected magnetic fields originating from the lunar crust (3), and paleo-

magnetic analyses of returned samples identified natural remanent magnetization (NRM) (4). The magnetization of many samples must have been produced by ancient magnetic fields, but the association of crustal magnetization with impact structures (5, 6) and the identification of NRM in <200-million-year-old impact glasses (7) suggest that the field sources could have been impact-generated plasmas (8–11) rather than a core dynamo

(12). Determining the source of lunar paleofields is critical for understanding the thermal evolution of the Moon, the limits of dynamo generation in small bodies, and, by implication, the magnetization of asteroids and meteorites.

A key difficulty is that available lunar rocks are often poor recorders of magnetic fields (13, 14). Most highlands samples are brecciated and/or shocked, making it difficult to distinguish between NRM acquired instantaneously during shock-magnetization or from long-lived dynamo fields (11). A further complication is that the precise thermal histories of most lunar rocks are unknown. Their magnetization ages have often been assumed to be equal to their radiometric ages (14), even

Fig. 1. NRM in troctolite 76535. (A to D) Two-dimensional projection of the NRM vector during AF demagnetization. Closed symbols represent end points of magnetization projected onto the horizontal N and E planes, and open symbols represent end points of magnetization projected onto the vertical N and Z planes. Peak fields for selected AF steps are labeled in mT. Dashed lines are component directions determined from principal component analyses (PCA). (A) AF demagnetization of 76535,137,7 up to 252.5 mT and its LC component. (B) AF demagnetization of 76535,138,2 up to 172.5 mT and its LC component. (C) Zoom of boxed region in (A), showing data for the MC (blue) and HC (red) components. Data points are from averages of a total of 185 AF measurements. The HC direction is anchored to the origin. (D) Zoom of boxed region in (B), showing data for the MC (blue) and HC (red) components. Data points are from averages of a total of 1450 AF measurements. The HC direction is anchored to the origin. (E) Equal-area projection of the remanence directions shown in (A). (F) Equal-area projection of the remanence directions shown in (B) and first, second, and third principal axes of the anisotropy of remanence ellipsoid (stars), calculated with a 100- μT bias field ARM in a peak AF field of 57 mT. (G) LC, MC, and HC components obtained from PCA of four subsamples studied (four symbols/colors), rotated so that all HC directions overlap with the HC direction of 137,7. Circles indicate maximum angular deviations.



¹Department of Earth, Atmospheric, and Planetary Sciences, Massachusetts Institute of Technology, 54-521, 77 Massachusetts Avenue, Cambridge, MA 02139, USA. ²Berkeley Geochronology Center, 2455 Ridge Road, Berkeley, CA 94709, USA.

*To whom correspondence should be addressed. E-mail: iang@mit.edu

though thermal events that can remagnetize rocks may have no effect on most geochronometers.

Here, we report a magnetic study of an unshocked ancient rock with a well-constrained thermal history, troctolite 76535. We applied $^{40}\text{Ar}/^{39}\text{Ar}$ thermochronological constraints (15) in conjunction with paleomagnetism to determine when 76535 was last remagnetized and to constrain the nature and duration of the recorded paleofields. Because of the putative late heavy bombardment at ~ 3.9 billion years ago (Ga), there are few lunar rocks with $^{40}\text{Ar}/^{39}\text{Ar}$ ages older than ~ 4.0 billion years and no paleomagnetic analyses from before this time. However, it is during this early epoch when a convecting core dynamo is most thermally plausible (16). 76535 is the only known unshocked (17–19) whole rock from this epoch (20).

76535 was found in a rake sample from the ejecta blanket of a 10-m-diameter impact crater (21). Four different chronometers (U/Pb, Th/Pb, Sm/Nd, and $^{40}\text{Ar}/^{39}\text{Ar}$) yielded indistinguishable ages of 4.2 to 4.3 billion years (22–26). Its Rb/Sr age is less certain because of spurious effects associated with olivine separates, ranging between 4.61 to 4.38 Ga (24, 27). The rock contains the ferromagnetic Fe-Ni-Co minerals kamacite and taenite as free grains and as inclusions of oriented linear arrays and needles (with axial ratios up to 45:1) in plagioclase (17–19). An unsuccessful Thellier-Thellier paleointensity experiment on 76535 (14) indicated that it contains a highly stable NRM composed of at least two components and that its Curie point is $>780^\circ\text{C}$. The Co content of its iron metal, up to 6 weight percent, among the largest measured for any lunar sample (17, 28), would indicate a Curie point of $\sim 850^\circ\text{C}$ (29).

To determine if 76535 has a record of lunar magnetic paleofields, we conducted nondestructive alternating field (AF) demagnetization of six unoriented polycrystalline chips. AF data for our four most carefully controlled samples (137.1; 137.7;

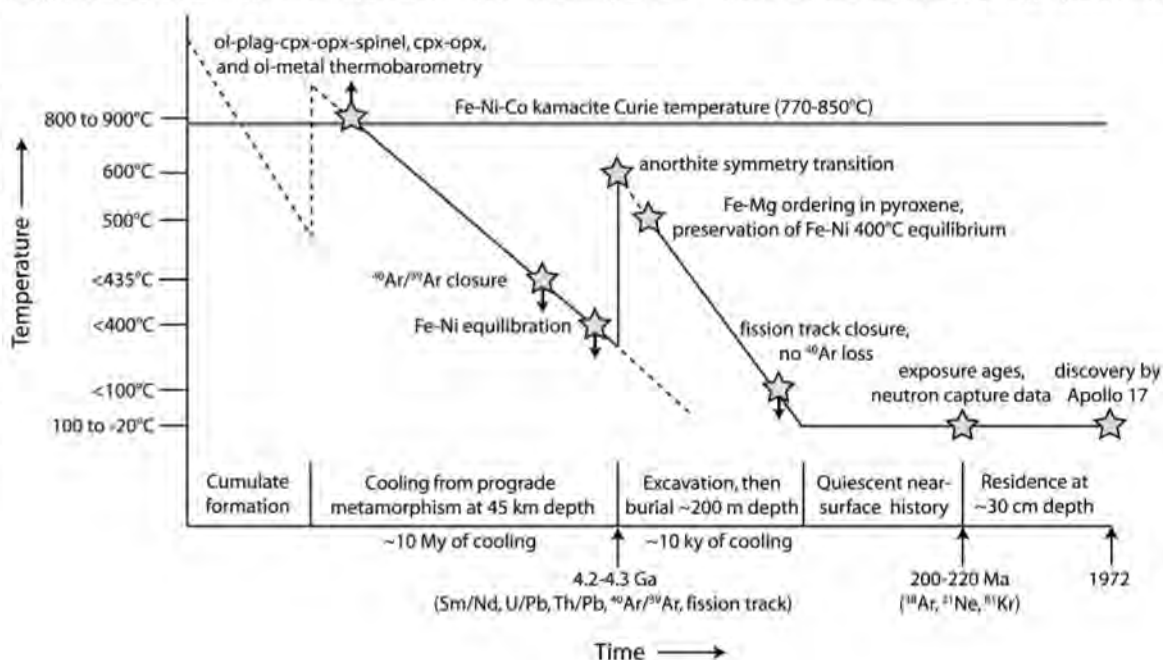
137.8; and 138.2) demonstrate that the NRM consists of low coercivity (LC), medium coercivity (MC), and hard coercivity (HC) components [supporting online material (SOM) text]. The LC component, blocked below ~ 12 mT, is apparently a combination of viscous remanent magnetization and an isothermal remanent magnetization (IRM) with a non-unidirectional orientation relative to the MC and HC components (Fig. 1, A and B, and figs. S1 and S2), resembling that observed in many other Apollo samples (14, 30) and meteorites (31). The MC component is much weaker than the LC component and extends from ~ 15 mT to between 45 and 83 mT (Fig. 1, C and D, and figs. S1 and S2, blue). A final HC component trends to the origin from 45 to between 83 and >250 mT, suggesting that it is the final primary component (Fig. 1, C and D, and figs. S1 and S2, red). The angular distances between the MC and HC components for all four subsamples after correction for anisotropy of remanence are similar (142° to 149°) and are consistent with the two components being unidirectional across the 76535 parent rock (Fig. 1G). The high coercivities of NRM are also consistent with the pseudo-single-domain state of the iron in plagioclase-rich subsamples (fig. S11). The inferred paleointensities (SOM text) for the MC and HC components obtained using the anhysteretic remanent magnetization (ARM) and IRM methods are at least 0.3 to 1 μT and possibly an order of magnitude larger (for comparison, the intensity of Earth's dynamo field at the Earth's surface is ~ 50 μT). Such paleointensities are far larger than that expected from external sources like the Earth, sun, protoplanetary disk, or galaxy from 4.3 to 4.2 Ga (SOM text) but are consistent with fields generated by meteoroid impacts and a lunar core dynamo.

The latter two possibilities can be distinguished by use of a diversity of petrologic and geochronologic data on 76535. The complete lack

of shock features in 76535 [peak shock pressures of <5 GPa (17)] argues against isothermal shock remanent magnetization (SRM) [which for these pressures typically blocks below coercivities of <30 mT (32, 33)], as well as the possibility of shock-produced thermoremanent magnetization (TRM) [the temperature increase for any shock of <5 GPa is negligible (34, 35)]. The low ratio of NRM to saturation IRM above 15 mT rules out magnetization by impact-generated (36) and artificial IRM fields. These data indicate that nonshock TRM is the most likely explanation for the MC component and much of the HC component (37).

Petrologic analyses suggest that 76535 experienced only two cooling events that could have blocked TRM (Fig. 2). The rock crystallized as a cumulate at ~ 45 km depth (17, 18, 38), and multiple thermobarometers indicate that it later experienced prograde metamorphism to peak temperatures of $>800^\circ$ to 900°C (38–42). The observed equilibrium compositions of kamacite and taenite indicate that it then cooled slowly (at $\sim 10^\circ\text{C}$ per million years) to at least $\sim 400^\circ\text{C}$ (17), over which time five independent geochronometers closed to yield radiometric ages that are indistinguishable within their uncertainties of 50 to 100 million years ago (Ma). Observations of Fe-Mg ordering in 76535 orthopyroxene indicate that after excavation, it was heated again to at least 500°C and then cooled more rapidly to $\sim 20^\circ\text{C}$ (the lunar near-surface temperature) over a period of $\sim 10,000$ years, probably in an ejecta blanket at ~ 200 m depth (39). Extrapolation of measurements of the diffusivity of Ni in taenite (43, 44) and the observation that the 400°C kamacite equilibrium composition was preserved after excavation imply that the peak temperature reached during burial was $<500^\circ$ to 600°C . This prediction is also in agreement with the 600°C temperature inferred from symmetry transitions in 76535 anorthite that formed during rapid cooling

Fig. 2. Thermal history of troctolite 76535, as inferred from a variety of petrologic and geochronometric measurements. Stars and solid lines indicate relatively well-constrained times and temperatures. Dashed lines indicate less-certain time-temperature histories. References for the various data sets described here are found in the main text. Axes are not linearly scaled. My, million years; ky, thousand years.



(19, 45). A final event excavated the rock to a depth of ~30 cm where it remained for much of the last ~220 million years (23).

Fission track data (46), in conjunction with our calculations using $^{40}\text{Ar}/^{39}\text{Ar}$ data (25), demonstrate that initial excavation took place at ~4.2 Ga. Because the rock was heated to 500° to 600°C after initial excavation, its fission track age (~4.2 billion years, when corrected for annealing at ambient lunar surface temperatures) must have been completely reset at this time [see (47, 48)]. The lack of evidence for Ar loss after 4.2 Ga places a conservative upper bound of heating for ~50 years at 500°C at 3.9 Ga, the time of major basin formation, or several hours at 800°C (Fig. 3) (SOM text). Limits placed on events since 3.9 Ga are even more stringent (Fig. 3C). Therefore, a simple interpretation of these magnetic data are that the HC component was acquired during slow cooling in the deep crust at ~4.2 Ga and the MC component was acquired just after excavation during cooling in an ejecta blanket over ~10,000 years. The cooling rates experienced by 76535 during both events require that the magnetizing fields persisted for far longer than expected for the

longest-lived impact-generated fields [just ~1 day for the largest basins (10)]. The slow cooling rate for the HC component indicates that the field was stable over millions of years, comparable to superchrons on Earth during the last several hundred million years (49).

Although the Ar data are permissive of extremely brief ad hoc heating events (such as those from deposition in shallow ejecta blankets) after 4.2 Ga, we can demonstrate that even if such events took place, the durations of the magnetic fields from such impacts are too short to be a plausible source of the magnetization in 76535. Conductive heating from a hot ejecta blanket would raise the temperature of the ~5-cm-diameter rock (conservatively assuming it has always been no larger than its size as sampled by Apollo 17) from ~20°C (ambient subsurface) to 770°C (the minimum Curie temperature) in approximately 1000 s (fig. S12). However, spontaneously generated fields due to plasma currents or motion of charged ejecta are believed to disappear in $<10^2$ s for craters <100 km in diameter (8, 9), before the rock could even begin to cool and acquire TRM. Such short thermal events are also unlikely to have occurred

during the last 4 billion years because they would require the rock to be in a thin ejecta blanket unrealistically close to the surface (<10 cm) (fig. S12), in contradiction with its exposure age of 220 million years and neutron capture data (23, 50). Even the day-long impact-generated fields that may have been present during major basin formation ~3.9 Ga would require an unrealistically small <1-m-thick ejecta blanket to permit 76535 to acquire TRM (SOM text). Therefore, the most reasonable remaining origin for the high-coercivity NRM in 76535 is from long-lived magnetic fields like those expected from a core dynamo.

The plausibility of a lunar dynamo has been questioned because of the unconfirmed existence of a fluid metallic core (51), the difficulty of sustaining a dynamo at least 600 million years after accretion (16, 52), and large paleointensities of ~100 μT that are difficult to reconcile with theoretical predictions (51, 53). However, recent predictions of the effect of dissipation at a liquid-core mantle boundary on the orientation of the lunar spin axis (54) and refined measurements of the tidal Love number (55) have provided growing evidence that the Moon even today has a small

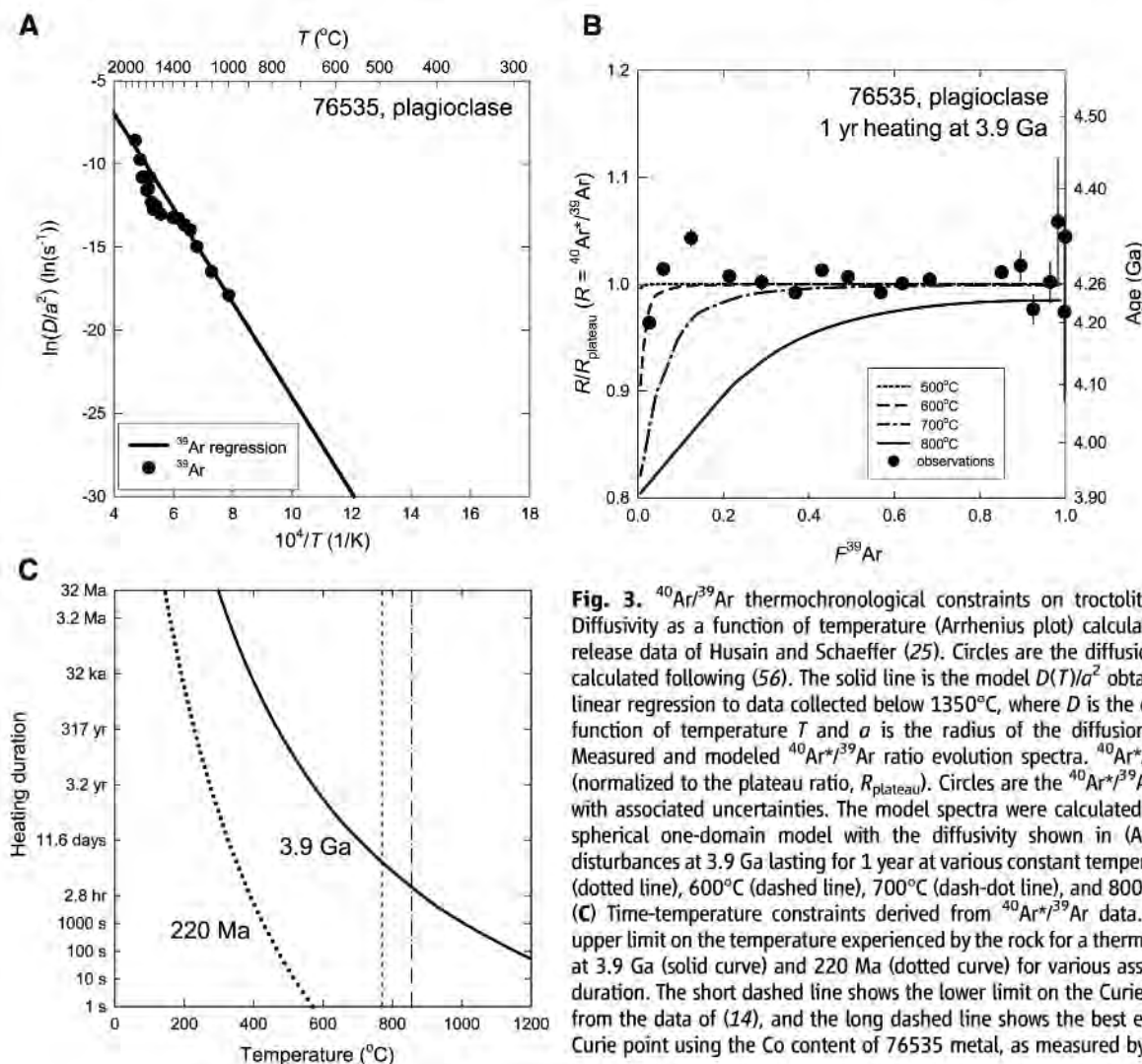


Fig. 3. $^{40}\text{Ar}/^{39}\text{Ar}$ thermochronological constraints on troctolite 76535. (A) Diffusivity as a function of temperature (Arrhenius plot) calculated from ^{39}Ar release data of Husain and Schaeffer (25). Circles are the diffusion coefficients calculated following (56). The solid line is the model $D(T)/a^2$ obtained from the linear regression to data collected below 1350°C, where D is the diffusivity as a function of temperature T and a is the radius of the diffusion domain. (B) Measured and modeled $^{40}\text{Ar}^*/^{39}\text{Ar}$ ratio evolution spectra. $^{40}\text{Ar}^*/^{39}\text{Ar}$ ratios, R (normalized to the plateau ratio, R_{plateau}). Circles are the $^{40}\text{Ar}^*/^{39}\text{Ar}$ data of (25) with associated uncertainties. The model spectra were calculated with use of a spherical one-domain model with the diffusivity shown in (A) for thermal disturbances at 3.9 Ga lasting for 1 year at various constant temperatures: 500°C (dotted line), 600°C (dashed line), 700°C (dash-dot line), and 800°C (solid line). (C) Time-temperature constraints derived from $^{40}\text{Ar}^*/^{39}\text{Ar}$ data. Shown is an upper limit on the temperature experienced by the rock for a thermal disturbance at 3.9 Ga (solid curve) and 220 Ma (dotted curve) for various assumed heating duration. The short dashed line shows the lower limit on the Curie point derived from the data of (14), and the long dashed line shows the best estimate of the Curie point using the Co content of 76535 metal, as measured by (17).

(~350-km radius) partially liquid core. Furthermore, the field that magnetized 76535, which is ~300 million years older than that recorded by all previously studied lunar samples, is from the early epoch when the Moon would have most likely had a convecting core due to enhanced heat flow and a possible cumulate overturn event (52). Finally, the NRM in 76535 indicates that minimum paleointensities were of order microteslas, consistent with the theoretical expectations for a lunar core dynamo (53). Our data and these considerations suggest that at 4.2 Ga, the Moon possessed a dynamo field, and by implication a convecting metallic core.

References and Notes

- H. C. Urey, *Geochim. Cosmochim. Acta* **1**, 209 (1951).
- N. F. Ness, K. W. Behannon, C. S. Seacore, S. C. Cantarano, *J. Geophys. Res.* **72**, 5769 (1967).
- P. Dyal, C. W. Packer, C. P. Sonett, *Science* **169**, 762 (1970).
- S. K. Runcorn et al., *Science* **167**, 697 (1970).
- J. S. Halekas, R. P. Lin, D. L. Mitchell, *Meteorit. Planet. Sci.* **38**, 565 (2003).
- D. L. Mitchell et al., *Icarus* **194**, 401 (2008).
- N. Sugiura, Y. M. Wu, D. W. Strangway, G. W. Pearce, L. A. Taylor, *Proc. Lunar Planet. Sci. Conf.* **10**, 2189 (1979).
- L. J. Srnka, *Proc. Lunar Sci. Conf.* **8**, 785 (1977).
- D. A. Crawford, P. H. Schultz, *Int. J. Impact Eng.* **23**, 169 (1999).
- L. L. Hood, N. A. Artemieva, *Icarus* **193**, 485 (2008).
- R. R. Doell, C. S. Gromme, A. N. Thorpe, F. E. Sentele, *Science* **167**, 695 (1970).
- S. K. Runcorn, *Nature* **275**, 430 (1978).
- M. Fuller, S. M. Ciesowski, in *Geomagnetism*, vol. 2, J. A. Jacobs, Ed. (Academic Press, New York, 1987), pp. 307–456.
- K. P. Lawrence, C. L. Johnson, L. Tauxe, J. Gee, *Phys. Earth Planet. Int.* **10.1016/j.pepi.2008.05.007** (2008).
- D. L. Shuster, B. P. Weiss, *Science* **309**, 594 (2005).
- D. J. Stevenson, *Rep. Prog. Phys.* **46**, 555 (1983).
- R. Gooley, R. Brett, J. R. Smyth, J. Warner, *Geochim. Cosmochim. Acta* **38**, 1329 (1974).
- R. F. Dymek, A. L. Albee, A. A. Chodos, *Proc. Lunar Sci. Conf.* **6**, 301 (1975).
- G. L. Nord, *Proc. Lunar Sci. Conf.* **7**, 1875 (1976).
- D. E. Wilhelms, "The Geologic History of the Moon" [Professional Paper 1348, U.S. Geological Survey (USGS), Government Printing Office, Washington, DC, 1987].
- E. W. Wolfe, "The Geologic Investigation of the Taurus-Littrow Valley: Apollo 17 Landing Site" (Professional Paper 1080, Government Printing Office, Washington, DC, 1981).
- J. C. Huneke, G. J. Wasserburg, *Lunar Sci.* **VI**, 417 (1975).
- G. W. Lugmair, K. Marti, J. P. Kurtz, N. B. Scheinin, *Proc. Lunar Sci. Conf.* **7**, 2009 (1976).
- W. R. Premo, M. Tatsumoto, *Proc. Lunar Planet. Sci. Conf.* **22**, 381 (1992).
- L. Husain, O. A. Schaeffer, *Geophys. Res. Lett.* **2**, 29 (1975).
- D. Bogard, L. E. Nyquist, B. M. Bansal, H. Wiesmann, C.-Y. Shih, *Earth Planet. Sci. Lett.* **26**, 69 (1975).
- D. A. Papanastassiou, G. J. Wasserburg, *Proc. Lunar Sci. Conf.* **7**, 2035 (1976).
- G. Ryder, M. D. Norman, R. A. Score, *Proc. Lunar Planet. Sci. Conf.* **11**, 471 (1980).
- R. M. Bozorth, *Ferromagnetism*. (IEEE Press, New York, 1951), pp. 968.
- G. W. Pearce, D. W. Strangway, "Apollo 16: Preliminary Science Report" (SP-315, NASA, 1972), chap. 7C, pp. 7–55.
- J. Gattacceca, P. Rochette, *Earth Planet. Sci. Lett.* **227**, 377 (2004).
- J. Gattacceca et al., *Phys. Earth Planet. Inter.* **166**, 1 (2008).
- J. Pohl, A. Eckstaller, *Lunar Planet. Sci.* **12**, 851 (1981).
- A. Bischoff, D. Stoffler, *Eur. J. Mineral.* **4**, 707 (1992).
- N. Artemieva, B. Ivanov, *Icarus* **171**, 84 (2004).
- L. Carporzen, S. A. Gilder, R. J. Hart, *Nature* **435**, 198 (2005).
- Because some kamacite would have exsolved from taenite during slow-cooling in the deep lunar crust, the HC component is probably a mixture of nonshock TRM and phase-transformation crystallization remanent magnetization (SOM text).
- I. S. McCallum, J. M. Schwartz, *J. Geophys. Res.* **106**, 27969 (2001).
- I. S. McCallum et al., *Geochim. Cosmochim. Acta* **70**, 6068 (2006).
- D. H. Lindsley, D. J. Andersen, *Proc. Lunar Planet. Sci. Conf.* **13**, A887 (1983).
- C. T. Herzberg, *Lunar Planet. Sci.* **10**, 537 (1979).
- R. H. Hewins, J. I. Goldstein, *Lunar Planet. Sci.* **6**, 356 (1975).
- K. Richter, A. J. Campbell, M. Humayun, *Geochim. Cosmochim. Acta* **69**, 3145 (2005).
- A. Meibom et al., *Science* **288**, 839 (2000).
- J. R. Smyth, *Proc. Lunar Planet. Sci. Conf.* **17**, E91 (1986).
- D. Braddy, I. D. Hutcheon, P. B. Price, *Proc. Lunar Sci. Conf.* **6**, 3587 (1975).
- C. W. Naeser, H. Faul, *J. Geophys. Res.* **74**, 705 (1969).
- R. A. Ketchum, R. A. Donelick, W. D. Carlson, *Am. Mineral.* **84**, 1235 (1999).
- R. B. Merrill, M. W. M. McElhinny, *The Magnetic Field of the Earth: Paleomagnetism, the Core, and the Deep Mantle* (Academic Press, San Diego, 1998), p. 531.
- It is plausible that a small (<10 cm), highly localized, magmatic dike could heat a sample for short timescales; however, such an event would be highly fortuitous, and even more fortuitous to have taken place simultaneously with an impact event.
- D. W. Collinson, *Surv. Geophys.* **14**, 89 (1993).
- D. R. Stegman, M. A. Jellinek, S. A. Zatzman, J. R. Baumgardner, M. A. Richards, *Nature* **421**, 143 (2003).
- M. A. Wiczkorek et al., *Rev. Mineral. Geochem.* **60**, 221 (2006).
- J. R. Williams, D. H. Boggs, C. F. Yoder, J. T. Ratcliff, *J. Geophys. Res.* **106**, 27933 (2001).
- S. Goossens, K. Matsumoto, *Geophys. Res. Lett.* **35**, L02204 (2008).
- H. Fechtig, S. T. Kalbitzer, in *Potassium Argon Dating*, O. A. Schaeffer, J. Zähringer, Eds. (Springer-Verlag, New York, 1966), pp. 68–107.
- We thank the Johnson Space Center staff and the Curation and Analysis Planning Team for Extraterrestrial Materials for allocating 76535; V. Fernandes for insights into lunar $^{40}\text{Ar}/^{39}\text{Ar}$ geochronology; I. S. McCallum for discussions about thermobarometry; S. Slotznick and S. Pedersen for help with the paleomagnetic analyses; M. Zuber and T. Bosak for suggestions; and K. Willis for administrative help. B.P.W., D.L.S., and I.G.-B. thank the NASA Lunar Advanced Science and Exploration Research Program; B.P.W. thanks the Charles E. Reed Faculty Initiatives Fund for support; and D.L.S. thanks the Ann and Gordon Getty Foundation.

Supporting Online Material

www.sciencemag.org/cgi/content/full/323/5912/356/DC1
SOM Text
Figures S1 to S12
Tables S1 to S3
References

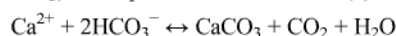
6 October 2008; accepted 3 December 2008
10.1126/science.1166804

Contribution of Fish to the Marine Inorganic Carbon Cycle

R. W. Wilson,^{1*} F. J. Millero,^{2*} J. R. Taylor,² P. J. Walsh,^{2,3} V. Christensen,⁴ S. Jennings,⁵ M. Grosell^{2*}

Oceanic production of calcium carbonate is conventionally attributed to marine plankton (coccolithophores and foraminifera). Here we report that marine fish produce precipitated carbonates within their intestines and excrete these at high rates. When combined with estimates of global fish biomass, this suggests that marine fish contribute 3 to 15% of total oceanic carbonate production. Fish carbonates have a higher magnesium content and solubility than traditional sources, yielding faster dissolution with depth. This may explain up to a quarter of the increase in titratable alkalinity within 1000 meters of the ocean surface, a controversial phenomenon that has puzzled oceanographers for decades. We also predict that fish carbonate production may rise in response to future environmental changes in carbon dioxide, and thus become an increasingly important component of the inorganic carbon cycle.

The inorganic half of the marine carbon cycle includes biogenic reaction of seawater calcium (Ca^{2+}) with bicarbonate (HCO_3^-), producing insoluble calcium carbonate (CaCO_3) in the process of calcification (1):



The vast majority of oceanic calcification is by planktonic organisms (2). Coccolithophores are considered to be the major contributor, but foraminifera are also included in global carbonate budgets (3). Upon death, their carbonate "skeletons" are released and rapidly sink to deeper ocean layers. Based on observations and models, estimates of global production of new CaCO_3

range from 0.7 to 1.4 Pg $\text{CaCO}_3\text{-C year}^{-1}$ (4–7) (Fig. 1).

It is less widely known that all marine teleosts (bony fish) produce and excrete carbonate pre-

¹School of Biosciences, University of Exeter, Exeter EX4 4PS, UK. ²Rosenstiel School of Marine and Atmospheric Science, University of Miami, Miami, FL 33149–1098, USA. ³University of Ottawa, Ottawa, ON K1N 6N5, Canada. ⁴Fisheries Centre, University of British Columbia, Vancouver, BC V6T 1Z4, Canada. ⁵Centre for Environment, Fisheries and Aquaculture Science, Lowestoft, and School of Environmental Sciences, University of East Anglia, Norwich NR4 7TJ, UK.

*To whom correspondence should be addressed. E-mail: r.w. wilson@ex.ac.uk (R.W.W.), fmillero@rsmas.miami.edu (F.J.M.), and mgrosell@rsmas.miami.edu (M.G.)

cipitates. Walsh *et al.* (8) originally suggested that this might be quantitatively significant on a large scale, an idea not previously considered within a global carbonate budget framework. Carbonate precipitates are excreted by fish via the intestine as a by-product of the osmoregulatory requirement to continuously drink calcium- and magnesium-rich seawater, and they are produced whether or not fish are feeding (9). As imbibed seawater passes through the intestine, it is alkalized (to pH 8.5 to 9.2) along with substantial secretion of HCO_3^- ions, typically reaching 50 to 100 mM in gut fluid (8–11), well in excess of concentrations in seawater (~2.5 mM). These conditions cause precipitation of imbibed Ca^{2+} (and some Mg^{2+}) ions as insoluble carbonates (8–11). This process has physiological importance in facilitating water absorption by the gut (10), and it reduces calcium absorption, which secondarily protects the kidney by minimizing renal stone formation (12). Carbonate precipitates formed in the gut are excreted either within discrete mucus-coated tubes or pellets, or incorporated with feces when fish are feeding (8–10). The organic mucus-matrix is rapidly degraded in natural seawater, leaving only inorganic crystals of CaCO_3 with high magnesium content (Mg:Ca ratio ranging from 10 to 33 mol %) (8) (fig. S1).

A striking visual indication of the high rate of carbonate production in marine fish is provided by x-rays of European flounder (*Platichthys flesus*) after acute transfer from fresh water (in which they do not produce carbonates) to seawater (Fig. 2). Accumulations of the precipitates (more x-ray opaque than some of the surrounding bones) can be seen forming inside the intestine within 3 hours of fish initiating drinking after transfer. Excreted carbonates have been collected and titrated to reveal production rates in the temperate European flounder and subtropical Gulf toadfish (*Opsanus beta*) ranging from 18 to 40 $\mu\text{mol C}$ per kg of fish per hour (8–13). This range is explained by differences in metabolic rate, which are determined by body mass and temperature within a species, as well as by interspecific life-style differences. In aquatic organisms, mass-specific metabolism scales inversely with body size, increasing ~1.6-fold with every 10-fold decrease in body mass, and increases exponentially with temperature typically by 1.83-fold for every 10°C rise (14). Thus, smaller fish at higher temperatures produce proportionally more carbonate per unit body mass (fig. S2).

To calculate the teleostean contribution to oceanic carbonate budgets requires knowledge of global marine fish biomass. We used two entirely independent models to describe the size composition and abundance of marine fish across the global oceans, one by using a size-based macroecological approach (15) and the other by using Ecopath software (16). The fish biomass estimates generated for each size-class and the relevant average local sea temperatures were then combined with individual fish carbonate excretion rates to predict global fish CaCO_3 production

ranging from 3.2×10^{12} to 8.9×10^{12} mol year^{-1} (0.04 to 0.11 Pg of $\text{CaCO}_3\text{-C year}^{-1}$). This range accounts for 2.7 to 15.4% of estimates for total global new CaCO_3 production in the surface oceans.

Several potentially biasing assumptions are made in these calculations, but we adopted a conservative approach that, if anything, underestimates fish carbonate production. Adopting the more liberal of these realistic assumptions would yield estimates almost three times as high, i.e., 9 to 45% of total global new CaCO_3 production (see Supporting Online Material for details of the above calculations and assumptions). Despite this conservatism, our estimate shows that fish are a major but previously unrecognized source of oceanic carbonate and contribute substantially to the marine inorganic carbon cycle (Fig. 1).

An important question following from this discovery is how the nature and fate of piscine carbonates compares with those from traditionally accepted sources. At the higher pressure and colder temperatures of the deep ocean, seawater becomes undersaturated with respect to CaCO_3 , leading to dissolution as it sinks, in a reversal of reaction 1; thus, the concentration of dissolved HCO_3^- and CO_3^{2-} increases with depth [measured as an increase in the total alkalinity (TA) of seawater]. Pelagic CaCO_3 particles from traditional sources are predicted to dissolve once they reach the chemical lysoclines for either calcite (~4300 and 750 m) or aragonite (~1500 and 500 m), respectively, in the North Atlantic and Pacific Oceans (1, 17–20). However, contrary to this view, recent carbonate budgets suggest that the majority (50 to 71%) of carbonates exported

from surface waters dissolve at much shallower depths (4, 5, 21). This results in an increase in TA from ~2400 μM to 2480 and 2500 μM at 1000-m depth, in the North Atlantic and Pacific oceans, respectively (1) (Fig. 3), a controversial phenomenon that has puzzled oceanographers for decades (7).

The causes of CaCO_3 dissolution above the lysocline (7) are subject to debate and have been attributed to (i) dissolution in zooplankton guts (22–26); (ii) dissolution in microenvironments where bacterial oxidation of organic matter enhances this process (27); and (iii) dissolution of more soluble forms of CaCO_3 , including pteropods and high-magnesium calcite (28, 29). However, dissolution in copepod guts can account for only a small portion of the increase of TA (27). The sharp increase in TA in the Pacific indicates that a more soluble phase may be dissolving (28, 29), such as high-magnesium calcites that are twice as soluble as aragonite (30, 31). We suggest that a large portion of the increasing TA in surface waters is indeed related to the dissolution of high-magnesium calcites produced by fish. Given their high magnesium content (8) (fig. S1) and solubility, we predict that dissolution of piscine carbonates will make a major contribution (up to 26%) to the increase in TA in the shallower oceanic depths and helps at least partially explain this currently perplexing observation (7) (Fig. 3).

The above estimate is a global average for fish-derived carbonates and does not take into account the potential for regional hot spots of piscine carbonate production (figs. S4 and S5). Indeed, 50% of fish biomass is predicted to occur

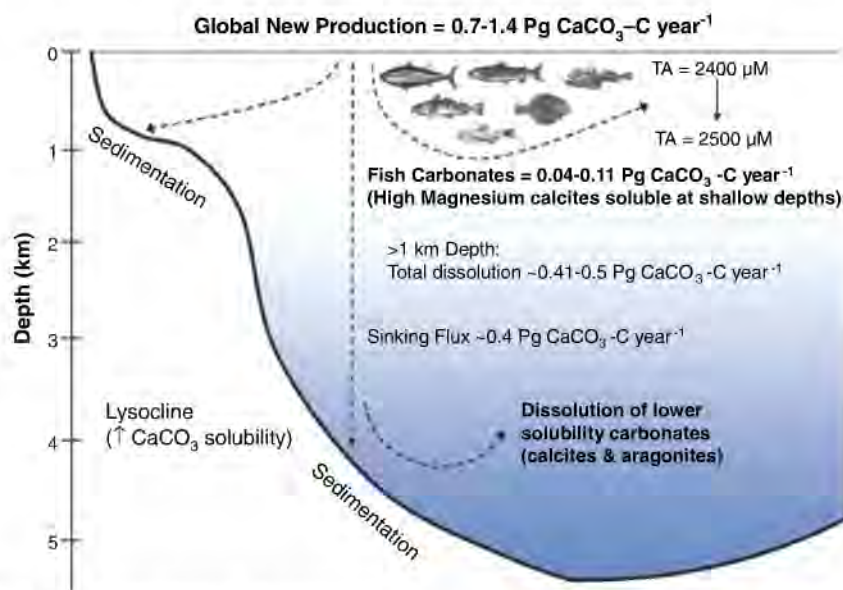


Fig. 1. A modified schematic diagram of ocean CaCO_3 budget showing the potential contribution of high-magnesium calcite produced by marine teleost fish. The fish images represent teleosts from a wide range of species and habitats, because all teleosts (but not elasmobranchs) are thought to produce carbonates as part of their osmoregulatory strategy (8–13). All values except the fish production rate are previously published estimates for total global production or dissolution in the upper ocean (2, 5–7).

in only 17% of ocean area (15) (fig. S4). Furthermore, such hot spots are largely found over continental shelves and in upwellings where the water is mostly shallow (100 to 200 m deep). This raises the possibility that fish could be the major source of carbonate production in the surface ocean in these areas. Also, dissolution of fish carbonates at such shallow depths may not occur if the carbonates are buried within sediments. Thus, we suggest that the localized high production rates and fate of fish carbonates in some parts of the ocean (and correspondingly low production areas elsewhere) require further investigation. In addition, most carbonates collected in sediment traps cannot be visually identified and accurately assigned to traditional planktonic sources. Intriguingly, some of these collected carbonate particles strongly resemble those found in the intestines of marine fish (fig. S3). The Mg:Ca ratio of fish carbonates (10 to 33 mol %) overlaps with the range for the finest-sized fraction ($<37\ \mu\text{m}$) of magnesian calcite particles collected in sediment traps in the Sargasso Sea (9 to 12 mol %) (32). At that time, this magnesian calcite phase of carbonate was assumed to originate from bryozoan skeletons attached to floating Sargassum. It is now tempting to suggest that fish may be the source of this carbonate phase.

So far, we have concentrated on production of carbonates, their excretion, and potential disso-

lution in the ocean, ignoring a subtle process that further links fish production and distribution to oceanic acid-base chemistry. HCO_3^- ions secreted by intestinal cells into the intestinal lumen of fish are derived largely from metabolic CO_2 reacting with water within intestinal epithelial cells, under the catalytic influence of carbonic anhydrase (11). This reaction produces H^+ , which is exported into the blood and ultimately excreted into the external seawater via ion-transporting cells in the gills of fish (12, 13). Thus, there is an anatomical separation of, and physical distinction between, the acid and base components of this reaction and its excretory products; i.e., insoluble CaCO_3 excreted via the gut, and dissolved H^+ ions excreted via the gills. Furthermore, solid CaCO_3 will rapidly sink and only redissolve at depth (raising TA at this point), whereas H^+ ions excreted via the gills will remain in the surface ocean (decreasing TA). Regular vertical migrations of many pelagic fish species, often daily and over several hundred meters, may complicate interpretation of the expected acid-base effects, but the principle is worth noting.

Postindustrial oceanic acidification due to elevated atmospheric CO_2 is now well recognized and is predicted to have major impacts on calcifying organisms (33), raising questions about how such future environmental changes may influence piscine global carbonate production.

We predict that production of carbonate precipitates by fish will accelerate as a result of both increasing seawater temperatures and CO_2 concentrations. First, metabolic rate increases exponentially with temperature in ectothermic fish, thus increasing metabolic CO_2 production and intestinal carbonate excretion at the individual level (fig. S7). However, for communities, the model of Jennings *et al.* (15) suggests that community fish biomass will decrease with temperature (for a given rate of primary production) and that this will offset the accompanying increase in carbonate production owing to temperature effects on individual metabolism. Second, rising ambient levels of dissolved CO_2 will cause a corresponding increase in CO_2 partial pressures in the blood of fish (34, 35). In vitro studies show that increasing blood CO_2 concentrations stimulate intestinal cells to produce more HCO_3^- (36), and thus intestinal excretion of precipitated carbonates is predicted to rise with ambient CO_2 . This contrasts with the commonly cited view that CaCO_3 production rates decrease in calcifying marine plankton and corals as ambient CO_2 increases [(2, 33); but see Supporting Online Material and (37)]. The biomineralization mechanisms in these organisms are not well understood (37) but are dependent upon the ambient concentrations of CO_3^{2-} or HCO_3^- in seawater, which change with pH as CO_2 concentration increases (2). Distinct from this, fish use endogenous CO_2 to produce HCO_3^- ions that rise to very high concentrations within the microenvironment of the gut lumen (typically 50 to 100 mM) (8–11). Thus, the contribution of fish to marine carbonate production seems likely to increase in the future and become an even more important component of the inorganic carbon cycle.

Fig. 2. Digital x-ray photographs of live European flounder (*Platichthys flesus*) showing formation of gut carbonates in unfed fish after transfer from fresh water to seawater. Note the absence of bones (apart from the overlying pectoral fin) over the abdominal area (bounded by dashed line) where the viscera (including intestine) are situated. (A) Flounder acclimated to fresh water for 1 week to allow clearance of previously produced carbonates from the intestine. (B) X-ray photo taken 3 hours after a freshwater flounder was transferred to seawater. In seawater, the fish rapidly initiates drinking and high rates of intestinal HCO_3^- secretion. This results in the formation of CaCO_3 precipitates that form x-ray opaque structures within the intestine (indicated by solid white arrows). X-ray images were taken with Siemens multix-TOP x-ray equipment and a Konica regus computed radiography system.

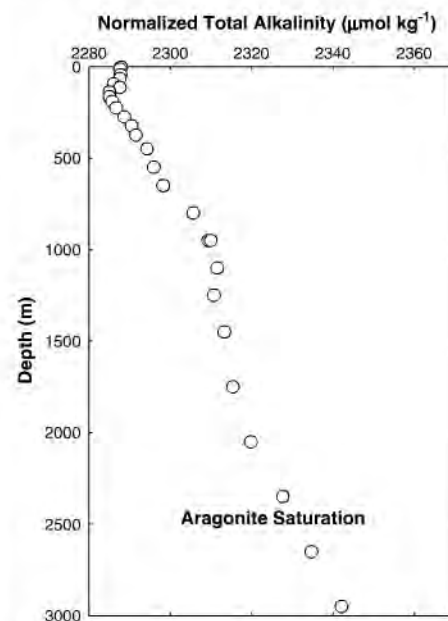
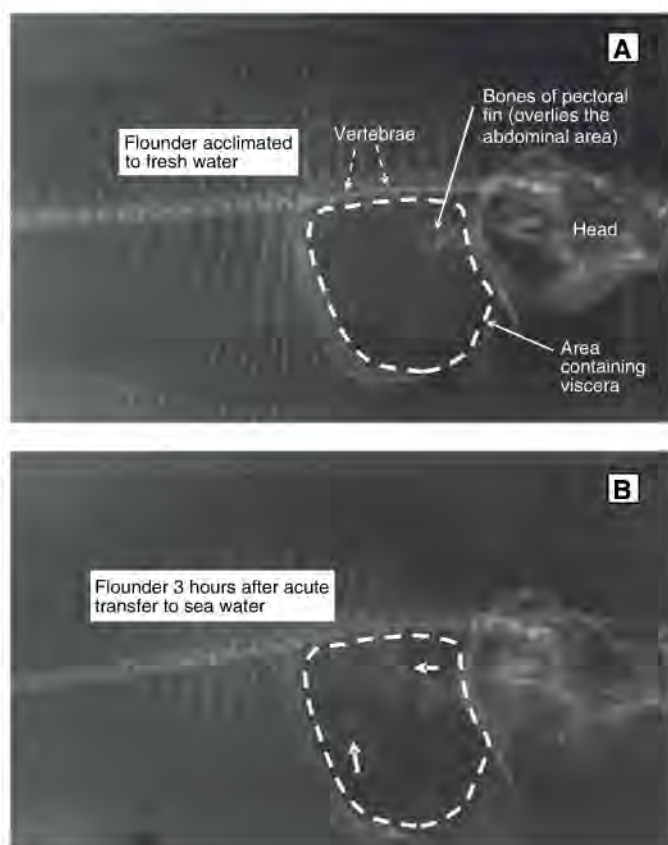


Fig. 3. The normalized total alkalinity of seawater as a function of depth for North Atlantic Waters (30°N and 23°E) (18, 20).

References and Notes

1. F. J. Millero, *Chemical Oceanography* (CRC Press, Boca Raton, FL, ed. 3, 2006).
2. R. A. Feely et al., *Science* **305**, 362 (2004).
3. R. Schiebel, *Global Biogeochem. Cycles* **16**, 1065 (2002).
4. J. D. Milliman, A. W. Droxler, *Geol. Rundsch.* **85**, 496 (1996).
5. K. Lee, *Limnol. Oceanogr.* **46**, 1287 (2001).
6. D. Iglesias-Rodriguez et al., *Eos Trans. AGU* **83**, 365 (2002).
7. J. D. Milliman et al., *Deep Sea Res. Part I Oceanogr. Res. Pap.* **46**, 1653 (1999).
8. P. J. Walsh, P. Blackwelder, K. A. Gill, E. Danulat, T. P. Mommensen, *Limnol. Oceanogr.* **36**, 1227 (1991).
9. R. W. Wilson, K. M. Gilmour, R. P. Henry, C. M. Wood, *J. Exp. Biol.* **199**, 2331 (1996).
10. R. W. Wilson, J. M. Wilson, M. Grosell, *Biochim. Biophys. Acta* **1566**, 182 (2002).
11. M. Grosell, *J. Exp. Biol.* **209**, 2813 (2006).
12. R. W. Wilson, M. Grosell, *Biochim. Biophys. Acta* **1618**, 163 (2003).
13. J. Genz, J. R. Taylor, M. Grosell, *J. Exp. Biol.* **211**, 2327 (2008).
14. A. Clarke, N. M. Johnstone, *J. Anim. Ecol.* **68**, 893 (1999).
15. S. Jennings et al., *Proc. R. Soc. London B. Biol. Sci.* **275**, 1375 10.1098/rspb.2008.0192 (2008).
16. V. Christensen et al., *Models of the World's Large Marine Ecosystems. GEF/LME Global Project Promoting Ecosystem-Based Approaches to Fisheries Conservation and Large Marine Ecosystems* (IOC Technical Series No. 80, UNESCO, 2008).
17. W. S. Broecker, in *The Fate of Fossil CO₂ in the Oceans*, N. R. Anderson, A. Malahoff, Eds. (Plenum, New York, 1977), p. 207.
18. R. A. Feely et al., *Global Biogeochem. Cycles* **16**, 1144 (2002).
19. C. L. Sabine, R. M. Key, R. A. Feely, D. Greeley, *Global Biogeochem. Cycles* **16**, 1067 (2002).
20. S. Chung et al., *Global Biogeochem. Cycles* **17**, 1093 (2003).
21. C. L. Sabine et al., in *The Global Carbon Cycle: Integrating Humans, Climate, and the Natural World*, C. B. Field, M. R. Raupach, Eds. (Island Press, Washington, DC, 2004), pp. 17–44.
22. T. Takahashi, *Spec. Publ. Cushman Found. Foraminiferal Res.* **13**, 11 (1975).
23. J. K. B. Bishop, J. C. Stepien, P. H. Wiebe, *Prog. Oceanogr.* **17**, 1 (1986).
24. R. P. Harris, *Mar. Biol. (Berlin)* **119**, 431 (1994).
25. P. Van der Wal, R. S. Kempers, M. J. W. Veldhuis, *Mar. Ecol. Prog. Ser.* **126**, 247 (1995).
26. D. W. Pond, R. P. Harris, C. A. Brownlee, *Mar. Biol. (Berlin)* **123**, 75 (1995).
27. H. Jansen, D. A. Wolf-Gladrow, *Mar. Ecol. Prog. Ser.* **221**, 199 (2001).
28. R. H. Byrne, J. G. Acker, P. R. Betzer, R. A. Feely, M. H. Cates, *Nature* **312**, 321 (1984).
29. R. A. Feely et al., *Mar. Chem.* **25**, 227 (1988).
30. J. W. Morse, F. T. Mackenzie, *Geochemistry of Sedimentary Carbonates* (Elsevier, New York, 1990).
31. J. W. Morse, D. K. Gledhill, F. J. Millero, *Geochim. Cosmochim. Acta* **67**, 2819 (2003).
32. V. J. Fabry, W. G. Deuser, *Deep-Sea Res.* **38**, 713 (1991).
33. J. C. Orr et al., *Nature* **437**, 681 (2005).
34. H. O. Pörtner, M. Langenbuch, A. Reipschläger, *J. Oceanogr.* **60**, 705 (2004).
35. B. A. Seibel, P. J. Walsh, *Science* **294**, 319 (2001).
36. M. Grosell et al., *Am. J. Physiol. Regul. Integr. Comp. Physiol.* **288**, R936 (2005).
37. V. J. Fabry, *Science* **320**, 1020 (2008).
38. R.W.W. acknowledges support from the UK Biotechnology and Biological Sciences Research Council (awards BB/D005108/1, BB/F009364/1, and ISIS 1766) and The Royal Society (award RSRG 24241). F.J.M. acknowledges the Oceanographic Section of the U.S. National Science Foundation (NSF). P.J.W. is supported by the Natural Sciences and Engineering Research Council (NSERC) of Canada and the Canada Research Chair program. V.C. acknowledges support from NSERC, the Global Environment Facility's UNEP/UNESCO/IOC (Intergovernmental Oceanographic Commission) LME (Large Marine Ecosystem) activities, and from the Sea Around Us Project, initiated and funded by The Pew Charitable Trusts. S.J. thanks the European Commission and the UK Department of Environment, Food, and Rural Affairs for funding support, and A. Clarke (British Antarctic Survey, Cambridge) for providing a compilation of fish oxygen consumption data. M.G. and S.J. are supported by the NSF (awards 0416440, 0714024, and 0743903). We also thank referees for their insightful comments; K. Knapp (School of Physics, University of Exeter) for the fish x-ray images (Fig. 2); R. Walton (University of Warwick, UK) for the powder x-ray diffraction analysis (fig. S1); H. Stoll (Department of Geoscience, Williams College, Williamstown, MA) and A. Pritchard (University of Exeter, Biosciences) for the scanning electron micrographs of sediment trap samples and fish carbonates, respectively (fig. S3); R. Forster (Centre for Environment, Fisheries and Aquaculture Science, Lowestoft) for plotting fig. S4; FishBase (www.fishbase.org) for providing fish species' information; J. Whittamore for preparation of flounder for x-ray imaging; J. Corcoran and C. Cooper for the sheephead minnow experiments in the Supporting Online Material; and R. van Aarle for assistance with graphical illustrations.

Supporting Online Material

www.sciencemag.org/cgi/content/full/323/5912/359/DC1

Materials and Methods

SOM Text

Figs. S1 to S6

Tables S1 and S2

18 March 2008; accepted 16 June 2008

10.1126/science.1157972

Morphogenesis of Self-Assembled Nanocrystalline Materials of Barium Carbonate and Silica

Juan Manuel García-Ruiz,¹ Emilio Melero-García,¹ Stephen T. Hyde²

The precipitation of barium or strontium carbonates in alkaline silica-rich environments leads to crystalline aggregates that have been named silica/carbonate biomorphs because their morphology resembles that of primitive organisms. These aggregates are self-assembled materials of purely inorganic origin, with an amorphous phase of silica intimately intertwined with a carbonate nanocrystalline phase. We propose a mechanism that explains all the morphologies described for biomorphs. Chemically coupled coprecipitation of carbonate and silica leads to fibrillation of the growing front and to laminar structures that experience curling at their growing rim. These curls propagate in a surflike way along the rim of the laminae. We show that all observed morphologies with smoothly varying positive or negative Gaussian curvatures can be explained by the combined growth of counterpropagating curls and growing laminae.

The theoretical morphology of classical crystals is well accommodated within conventional crystal growth theory, where the development of various crystal faces is accounted

for by the relative crystallographic surface energies at the atomic scale, and the overall symmetry is imposed by the atomic-scale packing. The relation between nonequilibrium crystal shapes and their physical and chemical growth conditions is also part of the general picture (1). In contrast, despite numerous observations over the years (2) that life is able to make precise, smooth, differentiable shapes made of polycrystalline minerals (shells, teeth, bones, etc.), we have a limited understanding of the morphogenetical mechanisms

leading to the formation of these fascinating architectures. The laboratory synthesis of actual self-assembled structures mimicking the ability of life to create sinuous noncrystallographic morphologies with crystalline materials is still a challenge. Among the few examples of synthetic self-organized nanocrystalline materials known to display a wealth of morphologies comparable to that of biominerals are silica/carbonate biomorphs (3–5). Biomorphs, like biominerals, exhibit nanoscale atomic ordering but lack long-range positional order. As a consequence, no characteristic faces or edges are expressed; rather, they are bounded by smoothly curved surfaces. Thus biomorphs, whose morphogenetic mechanism has remained unknown (5–7), display a zoo of curvilinear morphologies, often indistinguishable from the forms of biomaterials found in vivo.

Silica/barium carbonate biomorphs can be grown routinely by mixing barium chloride solutions with silica solutions and gels within a pH range from 8.5 to 11, at atmospheric pressure and temperature (8). Under alkaline conditions, carbonate from dissolved atmospheric CO₂ reacts with Ba²⁺ to precipitate crystalline barium carbonate (witherite) in the form of pseudohexagonal prismatic crystals tapered by bipyramidal faces (9). However, it has been shown (3–7, 10, 11) that when barium carbonate crystallizes from silica-rich solutions or from silica gels, it forms polycrystalline aggregates displaying a variety of

¹Laboratorio de Estudios Cristalográficos, Instituto Andaluz de Ciencias de la Tierra, Consejo Superior de Investigaciones Científicas–Universidad de Granada, Avenida del Conocimiento, Parque Tecnológico, Ciencias de la Salud, 18100 Armilla, Spain. ²Department of Applied Mathematics, Research School of Physical Sciences, Australian National University, Canberra, Australian Capital Territory 0200, Australia.

micrometer- to millimeter-sized morphologies with noncrystallographic symmetry shaped by “differentiable” surfaces of well-defined and smoothly varying Gaussian curvature. Its sub-micrometer structure has been shown to be composed of nanometer-sized rods of witherite, whose mutual arrangement is characterized by a high degree of orientational order but no translational order. The carbonate nanocrystals are coated by amorphous silica (SiO_2) that also cements the structure, thus forming a composite material, as demonstrated by the ability to selectively dissolve the crystalline or amorphous phase with either dilute HCl or NaOH solutions, respectively (12).

We used time-lapse video microscopy and electron microscopy to monitor the formation, growth development, and final morphology and textures of witherite biomorphs (8). Our observations have established that the core of all these morphologies is a pseudohexagonal twinned prismatic crystal of witherite that grows preferentially along the *c* axis (Fig. 1A). The morphologies seem

to arise from the breaking of the crystallographic symmetry of this crystal core of carbonate that occurs along two consecutive but different routes. The first of these routes goes from crystallographic symmetry toward dilation symmetry, whereas the second continues toward rotational symmetry. The dilation route ends in fractal cauliflowerlike morphologies, whereas the rotational route ends in three-dimensional (3D) microstructures displaying a wealth of smoothly curved surfaces of uniformly varying Gaussian curvature.

The crystallographic symmetry is initially broken toward dilation symmetry by the splitting of the basal pinacoid {001} or the pseudohexagonal bipyramidal faces of the growing crystal core. Because of pioneering work by Keith and Paden (13), crystal splitting at noncrystallographic angles can be explained by the concentration at the growth front of nonabsorbable polymeric impurities, which are pushed ahead of the growing crystal and cause the formation of 2D islands that are slightly misoriented with respect to the crystalline lattice (13–15). These islands continue to

grow, forming a tilted outgrowth displaying a noncrystallographic angle with the initial seed (Fig. 1, B to D). Under alkaline conditions, as a result of the chemical coupling between the precipitation of carbonate and silica, the precipitation process of the crystalline carbonate phase triggers the formation of polymeric impurities at the crystallization front, which in turn triggers the precipitation of carbonate. This chemical feedback process occurs as follows: During the crystallization of barium carbonate, there is a continuous removal of carbonate groups, which decreases the pH of the local environment surrounding the growing crystals according to the reactions $\text{Ba}^{2+} + \text{CO}_3^{2-} \rightleftharpoons \text{BaCO}_3$ and $\text{HCO}_3^- + \text{H}_2\text{O} \rightleftharpoons \text{H}_3\text{O}^+ + \text{CO}_3^{2-}$.

On the other hand, the precipitation of amorphous silica occurs exclusively by the condensation of molecules of silicic acid $\text{Si}(\text{OH})_4$ (16). At alkaline pH, the silicic acid deprotonates according to $\text{Si}(\text{OH})_4 \rightleftharpoons \text{SiO}(\text{OH})_3^- + \text{H}_3\text{O}^+$ at pH = 9 and $\text{SiO}(\text{OH})_3^- \rightleftharpoons \text{SiO}_2(\text{OH})_2^{2-} + \text{H}_3\text{O}^+$ at pH = 10.7.

Therefore, the decrease of pH caused by the precipitation of carbonate increases the local super-

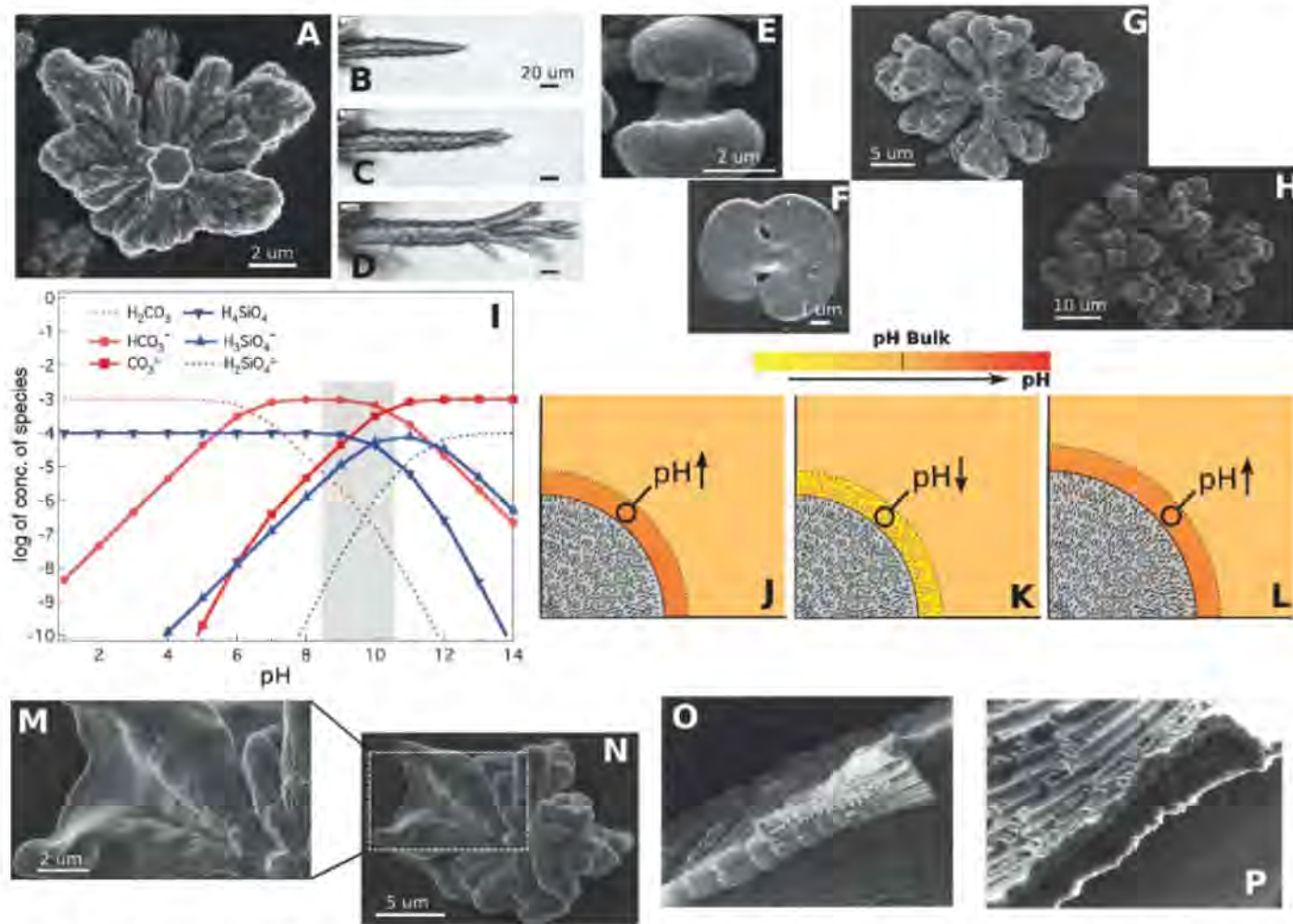


Fig. 1. The breaking of the crystallographic symmetry and chemical coupling. (A to H) illustrate the transition from a single pseudohexagonal crystal core shown in (A) to sheaf-of-wheat [(E) and (F)] and globular [(G) and (H)] structures, through splitting of the pinacoidal or bipyramidal tip of the crystal core [(B) to (D)]. [(B) to (D)] are frames of a video (movie S4). (I) shows the con-

centration of the chemical species as a function of pH (29) and the pH region (gray) at which these structures form. (J to L) show schematically the growing of the fibrillated front due to the local oscillations of pH driven by the coupled precipitation of silica and carbonate. The last four panels show the beginning of the formation (M and N) and details of the laminar structures (O and P).

saturation of silicic acid in the vicinity of the growing carbonate crystals, thus provoking the adsorption and precipitation of silica on their positively charged surfaces (17), poisoning crystal growth and causing bifurcation of the crystals. This chemical coupling ensures continuous splitting at noncrystallographic angles, leading to the formation of sheaf-of-wheat structures and, on further growth, to space-filling cauliflowerlike structures (Fig. 1, E to H) (18, 19).

At elevated pH values, typical of biomorph growth conditions, the silica solubility is more sensitive to changes in pH value (Fig. 1I). Therefore, the amount of silica coating the nanocrystals is large enough to provoke the cessation of carbonate crystal growth. In turn, the precipitation of amorphous silica increases the local pH by converting the acidic $-OH$ groups into siloxane bonds. This increase in pH promotes the formation of additional carbonate ions, increasing the barium carbonate supersaturation and leading to a further round of carbonate nucleation in the form of 3D nuclei (Fig. 1, J to L). This process causes the single-crystal growth front to fragment, creating a polycrystalline front of nanocrystals co-oriented with the single crystal. We call this transformation fibrillation. Despite the fibrillation mechanism being due to the oscillatory behavior of pH at the growth front, this does not necessarily yield oscillatory dynamics of the growth front.

Subsequent silica precipitation prevents these nuclei from growing larger than the size of a few tens to hundreds of nanometers before they become almost fully coated with silica, therefore bearing an overall negative charge at alkaline pH. Mutual repulsion between these witherite-silica particles is screened by the cations (Na^+ and excess Ba^{2+}) in solution. As a consequence, the nanocrystals of witherite-silica experience only weak interaction forces that must be attractive to account for the observed near co-orientation of the particles along their long axis. Co-orientation can be stabilized by the condensation of silanol groups and the formation of siloxane bonds between neighbor witherite-silica particles (16). However, the absence of strict translational order between the nanocrystals is also suggestive of a weak interparticle interaction.

Eventually, via fibrillation, a transition from continuously splitting crystals to laminar nanocrystalline aggregates with macroscopic radial symmetry occurs (Fig. 1, M to P). The final voluptuous morphologies characteristic of biomorphs grow in the absence of crystallographic constraints by the following mechanism. The growth front of the lamina advances linearly with time, and because the radial growth rate is independent of the azimuthal angle φ , the lamina initially forms a circular disc with an arced growth edge. Time-lapse microscopy reveals the forma-

tion of a small curled lip at some single point of the growth edge. The curling induces the following at this single point: (i) the cessation of growth along the radial direction, and (ii) the formation of two new growth fronts located on the right and left of the curl (movie S1). The growth fronts propagate the curling along the perimeter of the lamina, much as a surfing wave forms a quasi-tubular rim (Fig. 2A). As the curling advances along the rim of the circular lamina, it arrests the radial propagation of the structure: The curling front propagates at constant velocity tangentially to the circular perimeter, while the radial velocity of the curled perimeter becomes zero. As a result, the point at which the flat lamina starts to curl follows a trajectory that is the result of orthogonal growth fronts: the radial growth velocity V_p of the lamina and the azimuthal velocity of propagation V_φ of the curl as shown in Fig. 2B. When two curling fronts approach each other along the rim from opposite directions (irrespective of whether they arise from the same or different curling points) they describe the characteristic cardioid or leaflike shape of biomorphs because of the continuous reorientation of the growth edge induced by the accumulation of angles β' , β'' , and β''' , whose origin is thus explained (Fig. 2, B to F).

This simple curl triggers a morphogenetic mechanism that explains the whole variety of 3D morphologies displayed by silica biomorphs. The parameters involved in the morphogenesis are the following (Fig. 2A): (i) The relative directionality of the curling, either right- (D) or left- (L) handed; (ii) the relative values of the azimuthal velocities V_φ of the two approaching curled rims, as well as those relative to the radial velocity V_p of the uncurled sheet; and (iii) the relative height H of the two approaching curls. The following characteristic biomorph forms emerge as specific cases of this mechanism.

1) Morphogenesis of leaflike shapes (L_1L_2 or D_1L_2 ; $H_1 = H_2$; $V_{\varphi 1} \approx V_{\varphi 2} < V_p$). To form a regular leaf, the two approaching curling fronts must bend with different handedness and their curling height must be of the same size. Thus, when the two curling rims meet, their growth fronts seal in a single cusp. The overall contour of the leaflike shape and the existence of a bilateral symmetry (a mirror plane across the cusp) depend on the relative rates of azimuthal growth (Fig. 2).

2) Morphogenesis of helicoids of constant width (L_1L_2 or D_1D_2 ; $H_1 = H_2$; $V_{\varphi 1} \approx V_{\varphi 2} > V_p$). The two approaching curled rims have the same handedness and similar heights. In addition, the azimuthal growth rates of both rims are similar and are similar to the rate of growth of the uncurled sheet. A perfect helicoid is formed, which advances linearly with time (Fig. 3).

3) Morphogenesis of helicoids of decreasing width (L_1L_2 or D_1D_2 ; $H_1 \approx H_2$; $V_{\varphi 1} \approx V_{\varphi 2} > V_p$). The two approaching curled rims have the same handedness and similar heights, but the azimuthal velocity of the rims is faster than the rate of growth of the uncurled sheet. The resulting

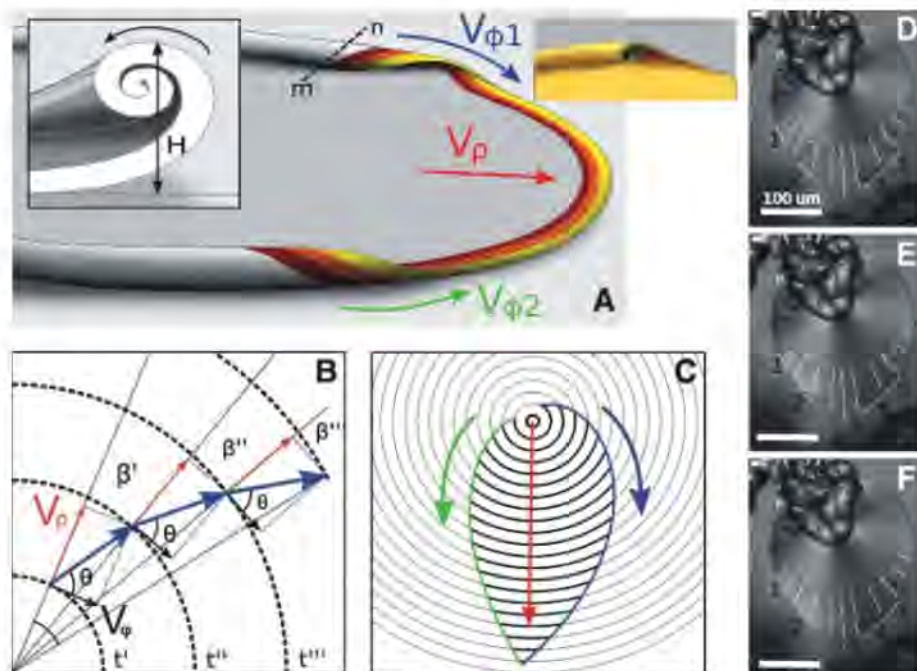
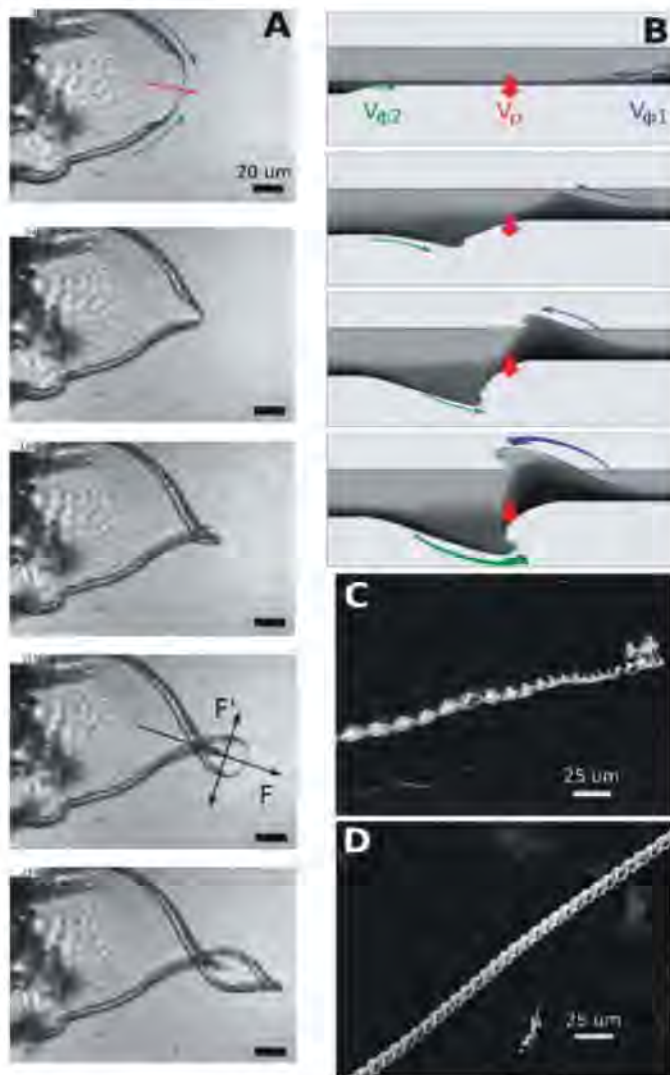


Fig. 2. Morphogenesis of the leaf and curl parameters described in the text. (A) shows an artist's view of two opposite-handed curls counterpropagating along the rim of a growing lamina. The inset shows a cross section of the curl (dashed line m-n) with the parameter H described in the text. The colors indicate the time history of the growth of the aggregate, and the yellow rim shows the current growth front. (B and C) show a scheme of the origin of the leaflike morphology as a result of the propagation of the curled front along the rim. The actual shape is determined by the ratio of the velocities $V_{\varphi 1}$, $V_{\varphi 2}$ of each moving curl and V_p that fixes the angle θ , and the specific point in space and time at which the curls originated. This is illustrated by frames D to F of movie S7, where the velocities were measured to be $V_p = 0.91(3) \mu\text{m/min}$ along the radial white paths, and $V_{\varphi 2} = 2.0(3) \mu\text{m/min}$ (paths labeled 1 and 2) and $V_{\varphi 1} = 2.8(3) \mu\text{m/min}$ (paths labeled 3 and 4).

Fig. 3. Formation of helicoids. When two counter-propagating curls with the same handedness approach each other, the flat lamina continues to grow outward with velocity V_p . As the curls approach each other, the lamina bends, following the sense of the curls. (A) displays a series of frames of movie S8, showing the formation of a helicoid. (B) is a front-view illustration of two like-handed curls twisting to produce a helix. Different types of helicoidal morphologies are produced, depending on the relative growth rates. For equal or nearly equal azimuthal velocities of the two curled fronts, comparable with the radial growth rate V_p , the lamina and the two curled rims are locked into a coupled growth process, in which the curls propagate along the rims of a central lamina, leading to continuous twisting with the sense along the direction F indicated in (A). Because the growth of the central lamina in the direction F perpendicular to F is hindered by the propagation of the curlings along its rim, a helicoid of approximately constant width sprouts from the site of the lamina where the approaching curls meet. (C and D) show scanning electron microscopy views of a helicoid with constant width and of a braid, respectively.



helicoids display constant pitch but have linearly decreasing diameter. If V_{p1} and V_{p2} are different but still larger than V_p , the diameter of the helicoids decreases asymmetrically (movie S2).

4) Morphogenesis of braids (L_1L_2 or D_1D_2 ; $H_1 \approx H_2$; $V_{p1} \approx V_{p2} > V_p$). The azimuthal growth rates of the two rims are much faster than the radial velocity of the uncurled lamina. Therefore, the uncurled lamina is overtaken by a braid that forms because the two curls of the same handedness coil onto each other (Fig. 3D).

5) Morphogenesis of wormlike structures (L_1L_2 or D_1D_2 or L_1D_2 ; $H_1 \gg H_2$; V_{p1} ; V_{p2} ; V_p). If the height and azimuthal growth rate of one of the curls is much larger than the other, regardless of the handedness of the rims, upon interaction it ends up coiling on itself. That in-folding can grow forward or backward, yielding the wormlike morphologies displayed by some silica biomorphs (movies S3 to S5).

It is worth noticing that all the twisted shapes result when the two curls have the same hand-

edness. Because either enantiomorph has an equal probability of forming, no chiral bias can be expected, and silica biomorphs are by nature racemic.

The proposed growth mechanism explains a number of symmetry properties of silica biomorphs that have remained a puzzle for several years. The leaf shape, so characteristic of silica biomorphs, is an inevitable result of the opposing and mutually interacting surfing curls. Further, regular forms, with uniform curvature distributions over their surface (such as twisted spheres and generic twisted surfaces), are less common than irregular shapes because geometric regularity in this sense requires fixed ratios of growth rates over extended times. This mechanism also explains the absence of chirality in silica biomorphs, because the handedness of the helical structures depends on the relative sign of curl, which is arbitrary. Finally, this mechanism explains the failure to induce chirality in silica biomorphs with the use of chiral molecules: The origin of the curling is at a much larger length

scale and is therefore uncoupled from molecular chemistry.

The combined curling and radial growth phenomenology outlined here produces the variety of curvilinear forms observed in biomorphs, without the presence of biomolecular agents, such as proteins, to steer growth via surface adsorption. It follows that complex curved shapes are not exclusive to biology. This morphogenetical mechanism may contribute to the morphogenesis of other exotic inorganic precipitates (20–23). It also shows that evidence for nanobacteria (24) and ancient terrestrial (3, 25) and Martian (26–28) life remnants cannot rest on morphology alone.

References and Notes

1. I. Sunagawa, *Crystals: Growth, Morphology and Perfection* (Cambridge Univ. Press, Cambridge, 2005).
2. D. W. Thompson, *On Growth and Form* (Cambridge Univ. Press, Cambridge, 1942).
3. J. M. García-Ruiz *et al.*, *Science* **302**, 1194 (2003).
4. J. M. García-Ruiz, *Geology* **26**, 843 (1998).
5. S. T. Hyde, A. M. Carnerup, A. Larsson, A. G. Christy, J. M. García-Ruiz, *Physica A* **339**, 24 (2004).
6. T. Terada, S. Yamabi, H. Imai, *J. Cryst. Growth* **253**, 435 (2003).
7. J. M. García-Ruiz, *J. Cryst. Growth* **73**, 251 (1985).
8. Materials and methods are available as supporting material on Science Online.
9. F. Lippmann, *Sedimentary Carbonate Minerals* (Springer, Berlin, 1973).
10. E. Bittarello, D. Aquilano, *Eur. J. Mineral.* **19**, 345 (2007).
11. A. E. Voinescu *et al.*, *J. Cryst. Growth* **306**, 152 (2007).
12. J. M. García-Ruiz, J. L. Amorós, *J. Cryst. Growth* **55**, 379 (1981).
13. H. D. Keith, F. J. Padden, *J. Appl. Phys.* **34**, 2409 (1963).
14. N. Goldenfeld, *J. Cryst. Growth* **84**, 601 (1987).
15. P. Phillips, in *Handbook of Crystal Growth* (Elsevier, Amsterdam, 1993), vol. 2, chap. 18, pp. 1169–1216.
16. R. K. Iler, *The Chemistry of Silica* (Wiley, New York, 1979).
17. C.-C. Li, J.-H. Jean, *J. Am. Ceram. Soc.* **85**, 2977 (2002).
18. D. P. Grigoriev, *Ontogeny of Minerals* (Israel Program for Scientific Translation, Jerusalem, Israel, 1965).
19. M. N. Maleev, *Tschermak's Mineral. Petrogr. Mitt.* **18**, 1 (1972).
20. H. Cölfen, *Curr. Opin. Colloid Interface Sci.* **8**, 23 (2003).
21. H. Cölfen, M. Antonietti, *Angew. Chem. Int. Ed.* **44**, 5576 (2005).
22. L. B. Gower, D. J. Odom, *J. Cryst. Growth* **210**, 719 (2000).
23. S. Mann, G. A. Ozin, *Nature* **382**, 313 (1996).
24. J. Martel, D. J. Young, *Proc. Natl. Acad. Sci. U.S.A.* **105**, 5549 (2008).
25. J. M. García-Ruiz, A. Carnerup, A. G. Christy, N. J. Welham, S. T. Hyde, *Astrobiology* **2**, 353 (2002).
26. F. Poulet *et al.*, *Nature* **438**, 623 (2005).
27. J. F. Mustard *et al.*, *Nature* **454**, 305 (2008).
28. F. Westall, *Space Sci. Rev.* **135**, 95 (2008).
29. C. B. Andersen, *J. Geosci. Edu.* **50**, 389 (2002).
30. We are grateful to N. J. Welham (Australian National University, now at the University of Ballarat) for some of the videomicroscopy recordings. This work was supported by the Spanish Ministry of Education and Science (project MAT2006-11701) and is part of the Consolider-Ingenio 2010 project Factoría Española de Cristalización. E.M.-G. acknowledges financial support from the program Juan de la Cierva (Ministerio de Innovación y Ciencia). S.T.H. acknowledges the Australian Research Council for a Federation Fellowship.

Supporting Online Material

www.sciencemag.org/cgi/content/full/323/5912/362/DC1
Materials and Methods

References

Movies S1 to S9

2 September 2008; accepted 26 November 2008
10.1126/science.1165349

Broadband Ground-Plane Cloak

R. Liu,^{1*} C. Ji,^{2*} J. J. Mock,¹ J. Y. Chin,³ T. J. Cui,^{3†} D. R. Smith^{1†}

The possibility of cloaking an object from detection by electromagnetic waves has recently become a topic of considerable interest. The design of a cloak uses transformation optics, in which a conformal coordinate transformation is applied to Maxwell's equations to obtain a spatially distributed set of constitutive parameters that define the cloak. Here, we present an experimental realization of a cloak design that conceals a perturbation on a flat conducting plane, under which an object can be hidden. To match the complex spatial distribution of the required constitutive parameters, we constructed a metamaterial consisting of thousands of elements, the geometry of each element determined by an automated design process. The ground-plane cloak can be realized with the use of nonresonant metamaterial elements, resulting in a structure having a broad operational bandwidth (covering the range of 13 to 16 gigahertz in our experiment) and exhibiting extremely low loss. Our experimental results indicate that this type of cloak should scale well toward optical wavelengths.

Transformation optics is a method for the conceptual design of complex electromagnetic media, offering opportunities for the control of electromagnetic waves (1, 2). A wide variety of conventional devices can be designed by the transformation optical approach, including beam shifters (3), beam bends (4), beam splitters (3), focusing and collimating lenses (5), and structures that concentrate electromagnetic waves (6, 7). Whereas all of these devices have properties that are unique to the class of transformation optical structures, one of the most compelling and unprecedented concepts to emerge has been that of a medium that can conceal objects from detection by electromagnetic waves. The prospect of electromagnetic cloaking has proven a tantalizing goal, with numerous concepts currently under investigation (1, 2, 8–14).

In the transformation optical approach, one imagines warping space so as to control the trajectories of light in a desired manner. As an example of this approach, a cloak can be designed by performing a coordinate transformation that squeezes the space from within a sphere to within a shell having the same outer radius. Waves do not interact with or scatter from the core because it is simply not part of the transformed space. The form invariance of Maxwell's equations implies that the coordinate transformation can instead be applied to the permittivity and permeability tensors, yielding the prescription for a medium that will accomplish the desired functionality. The resulting medium is highly complex, being anisotropic and with spatial gradients in the components of the permittivity and permeability tensors.

Such complicated gradient-index media are difficult to create with conventional materials but

are much easier to build with artificially structured metamaterials, in which spatial variations of the material parameters can be achieved by modifying the geometry and placement of the constituent element. Even so, the large number of elements required in an arbitrary cloak medium can represent a substantial computational burden resulting in long design cycles. To address this time-consuming design step, we have developed a systematic algorithm that is applied once the spatial distribution of the constitutive parameters has been determined by the transformation. Previously, metamaterial structures requiring spatial gradients have been obtained by designing one unit cell at a time until a library of unique metamaterial elements, whose constitutive parameters span the range required by the transformation optical design, is generated. In contrast, the algorithm we use (15) requires only a comparatively small number of simulations of the metamaterial element, relying on a regression scheme to generate the functional dependence of the constitutive parameters on the unit cell geometry. The reduced number of simulations vastly speeds the metamaterial cloak-design process and makes the design of complex media possible.

The specification of a ground-plane cloak can be determined in the manner described in (16). If waves are restricted to a single plane of incidence, with the polarization of the waves being transverse electric (electric field perpendicular to the plane of incidence or parallel to the ground plane), then the cloak parameters need only be determined across a two-dimensional (2D) plane. The domain of the problem is thus a 2D space, filled with a uniform dielectric with refractive index value n_b and bounded by a conducting sheet. A family of coordinate transformations that will map a given nonplanar conducting surface to a planar surface can be found; however, such transformations generally lead to an anisotropic medium with values of n_x and n_y that vary as a function of the spatial coordinate. Yet, given the restricted geometry, it is possible to find a coordinate map that minimizes the anisotropy in the permeability components. Defining an anisotropy factor as $\alpha = \max(n_x/n_y, n_y/n_x)$, transformations

can be found for which α is near unity so that the isotropic refractive index value varies throughout the space. If n_b in the original space is sufficiently greater than unity, then the values for the refractive index of the cloaking structure are also greater than unity. Under these conditions, nonresonant metamaterial elements can be used, and the cloak can exhibit a broad frequency bandwidth (15).

In our particular design, we followed the optimization technique (16) for the transformation region, in which a quasi-conformal coordinate map is generated by minimizing the Modified-Liao functional (17, 18) with slipping boundary conditions. The Jacobian matrix Λ that relates the physical and virtual systems is then computed numerically, from which the index distribution $n^2 = \frac{1}{\sqrt{|\Lambda^T \Lambda|}}$ of the cloak is found (here, T is the transpose of the Jacobian matrix). In our final design, $\alpha = 1.04$, which is treated as negligible (that is, we assume $n_x = n_y$).

A photograph of the fabricated sample, a color map indicating the transformed space, and the associated refractive index distribution are presented in Fig. 1. We assume that the entire cloak is embedded in a background material with refractive index $n_b = 1.331$. Under these assumptions, the transformation leads to refractive index values for the ground-plane cloak that range from $n = 1.08$ to 1.67 (values that can be achieved with the use of nonresonant metamaterial elements). On the right and left side of the sample in Fig. 1B, the refractive index distribution is uniform ($n_b = 1.331$), taking the value of the background material. Because the cloak is designed to be embedded in a higher dielectric region, we add an impedance matching layer (IML) that surrounds the entire structure, for which the index changes gradually and linearly from that of air to that of the background index (15). This step is taken to minimize reflection from the cloak surface when illuminated by a microwave beam within the scattering chamber, which exists in an $n = 1.0$ (air) environment. The procedure for designing the IML layer is described in (15). Because of the index gradient coupled with the cloak, we expect no amplitude scattering and only a slight offset of the wave reflected from the ground-plane structure due to the refractive index change. The effect should be similar to observing a mirror through a layer of glass; objects on the top of the mirror, within the cloaked region, remain hidden from detection (visualized by ray tracing in Fig. 1D). It is important to note that this type of cloaking phenomena is distinct from current scattering suppression technologies because it both eliminates backscattering and restores the reflected beam.

To implement the cloak defined by the index distribution presented in Fig. 1C and the associated background material and IML in Fig. 1B, the continuous theoretical constitutive parameter distribution must be approximated by a discrete number of metamaterial elements. In our design, the entire sample region is divided into 2-by-2-mm squares, requiring more than 10,000 elements, about 6000 of which are unique.

¹Center for Metamaterials and Integrated Plasmonics, Department of Electrical and Computer Engineering, Duke University, Durham, NC 27708, USA. ²Department of Statistical Science, Duke University, Durham, NC 27708, USA. ³State Key Laboratory of Millimeter Waves, Southeast University, Nanjing 210096, China.

*These authors contributed equally to this work.

†To whom correspondence should be addressed. E-mail: tjui@seu.edu.cn (T.J.C.); drsmith@duke.edu (D.R.S.)

The elements chosen to achieve the design are all variations of the structure shown in Fig. 2. By changing the dimension a , we are able to span the required index range of $n = 1.08$ to 1.67. After a

well-established retrieval process, modified to include the effects of the finite unit cell size relative to the wavelength (19, 20), the effective permittivity and permeability for a given element

can be found via numerical simulation. A regression curve can then be made that relates the refractive index associated with a given element to the length a . Once a set of elements has been

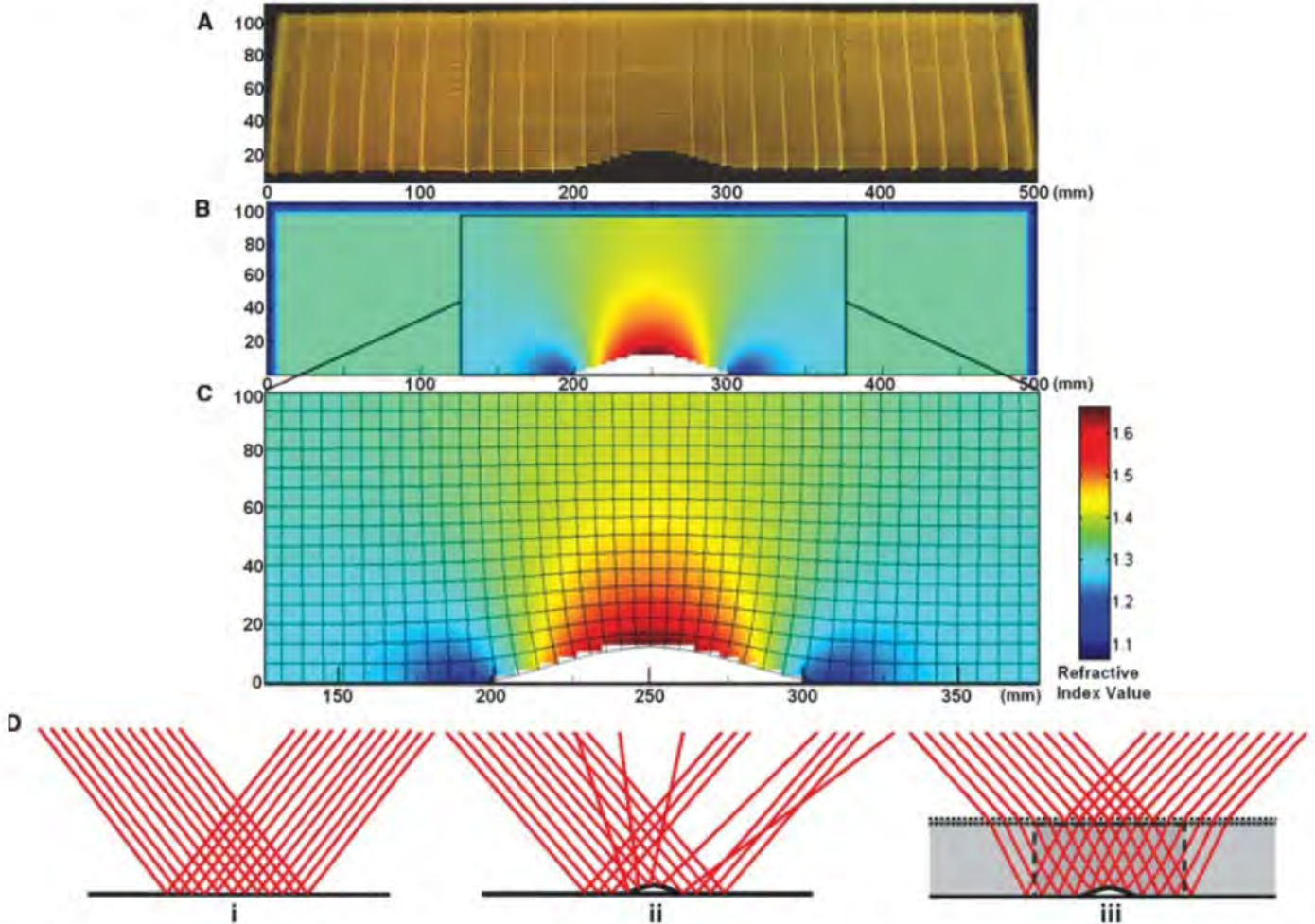
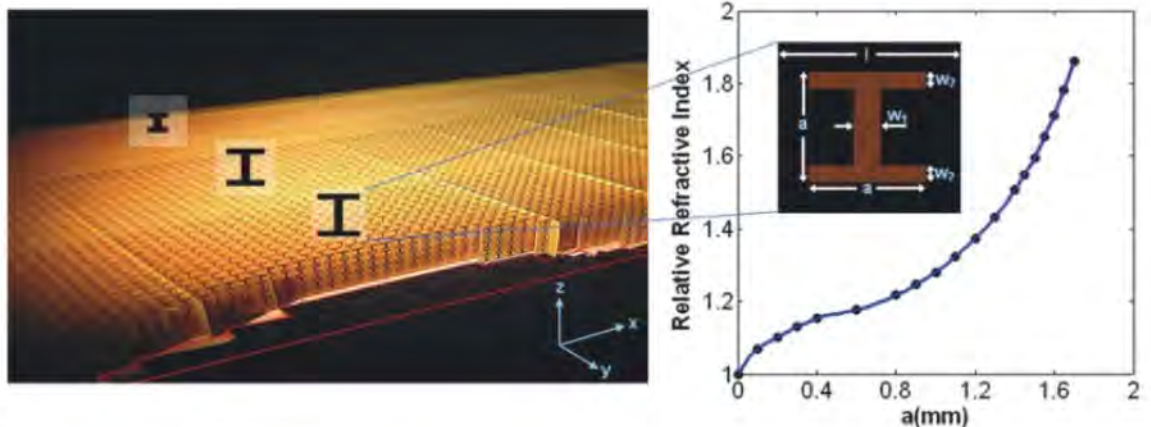


Fig. 1. The transformation optical design for the ground-plane cloak. The metamaterial cloak region is embedded in a uniform higher index background with gradients introduced at the edges to form impedance matching regions. (A) Photograph of the fabricated metamaterial sample. (B) Metamaterial refractive index distribution. The coordinate transformation region is shown within the box outlined in black. The surrounding material is the higher index embedding

region and the IML. (C) Expanded view of the transformation optical region in which the mesh lines indicate the quasi-conformal mapping (lateral dimensions of the unit cells are ~ 3.5 times smaller). (D) Ray tracing of a beam incident on (i) the ground, (ii) the perturbation, and (iii) the perturbation covered by a ground-plane cloak. The gray area and dashed lines in (iii) indicate the transformation region, embedded background material, and IML.

Fig. 2. The design of the nonresonant elements and the relation between the unit cell geometry and the effective index. The dimensions of the metamaterial unit cells are $l = 2$ mm, $w_1 = 0.3$ mm, $w_2 = 0.2$ mm, and a varying from 0 to 1.7 mm.



numerically simulated, all subsequent tasks in the cloak design—from the generation of the regression curve to the final layout of the elements in a mask for lithographic processing—are performed using a single Matlab program. The metamaterial elements we employ actually exhibit some degree of frequency dispersion in their constitutive parameters caused by their finite dimension with respect to the wavelength, as described in the supporting online material. In particular, the in-plane permeability and out-of-plane permittivity vary as a function of frequency such that the index stays approximately constant but the wave impedance varies considerably. Because the cell-to-cell change in impedance is minor, there is no reflection and no discernable disturbance in the cloak properties over the entire frequency range measured.

As with previous metamaterial designs implemented for microwave experiments, the final ground-plane cloak is fabricated on copper-clad printed circuit board with FR4 substrate (the substrate thickness is 0.2026 mm, with a dielectric constant of $3.85 + i0.02$). The completed sample is 500 by 106 mm with a height of 10 mm.

The center region, 250 by 96 mm, corresponds to the transformed cloaking region, whereas the rest of the sample is used for dielectric embedding and impedance matching. The cloak transformation is specifically designed to compensate a perturbation introduced on the conducting surface that follows the curve $y = 12\cos^2[(x - 125)\pi/125]$ (units in millimeters).

To verify the predicted behavior of the ground-plane cloak design, we make use of a phase-sensitive, near-field microwave scanning system to map the electric field distribution inside a planar waveguide. The planar waveguide restricts the wave polarization to transverse electric. The details of the apparatus have been described previously (21). A large area field map of the scattering region, including the collimated incident and scattered beams, is shown in Fig. 3. The waves are launched into the chamber from a standard X-band coax-to-waveguide coupler and pass through a dielectric lens that produces a nearly collimated microwave beam. The beam is arbitrarily chosen to be incident on the ground plane at an angle of 40° with respect to the nor-

mal. A flat ground plane produces a near perfect reflection of the incident beam in Fig. 3A, whereas the presence of the perturbation produces considerable scattering, as shown in Fig. 3B (note the presence of the strongly scattered secondary beam). By covering the space surrounding the perturbation with the metamaterial cloaking structure, however, the reflected beam is restored, as if the ground plane were flat in Fig. 3C. The beam is slightly bent as it enters the cloaking region because of the refractive index change of the embedding material but is bent back upon exiting. The gradient-index IML introduced into the design minimizes reflections at the boundaries of the cloaking region.

As the ground-plane cloak makes use of nonresonant elements, it is expected to exhibit a large frequency range of operation. The cloaking behavior was confirmed in our measurements from the range 13 to 16 GHz, though we expect the bandwidth to actually stretch to very low frequencies (<1 GHz) that cannot be verified experimentally because of limitations of the measurement apparatus and the beam-forming lens. We illustrate the broad bandwidth of the cloak with the field maps taken at 13 GHz in Fig. 3D, 15 GHz in Fig. 3E, and 16 GHz in Fig. 3F, which show similar cloaking behavior to the map taken at 14 GHz in Fig. 3C. The collimated beam at 16 GHz has begun to deteriorate because of multi-mode propagation in our 2D measurement chamber, which is also observed in the flat ground-plane control experiment at that frequency. However, on the basis of the predicted response of the broadband unit cells, we expect this cloak to function up to ~ 18 GHz.

To further visualize the performance of the ground-plane cloak, we illuminated the sample from the side (90° from the surface normal) with a narrow collimated beam. As the ground-plane cloaked perturbation should also be cloaked with the respect to an observer located on the ground, the wave, which should follow the metric as defined by the quasi-transformation map in Fig. 1, can be expected to detour around the perturbation and then return back to its original propagation direction. The field map for this case is shown in Fig. 4B, which corresponds with the predicted transformation extremely well (a low-resolution representation of the transformation grid is overlaid on the experimental data). For comparison, Fig. 4A shows a map of the field strongly scattered from the perturbation in the absence of the cloak.

The agreement between the measured field patterns for the ground-plane cloak and the theory (16) provides convincing evidence that metamaterials can indeed be used to construct such complex electromagnetic media. Although this cloak is not able to hide objects from detection that do not lie under the conducting curtain formed by the perturbation of the ground plane, its broadband and low-loss properties are compelling and offer a path toward realization of some forms of cloaking at frequencies approach-

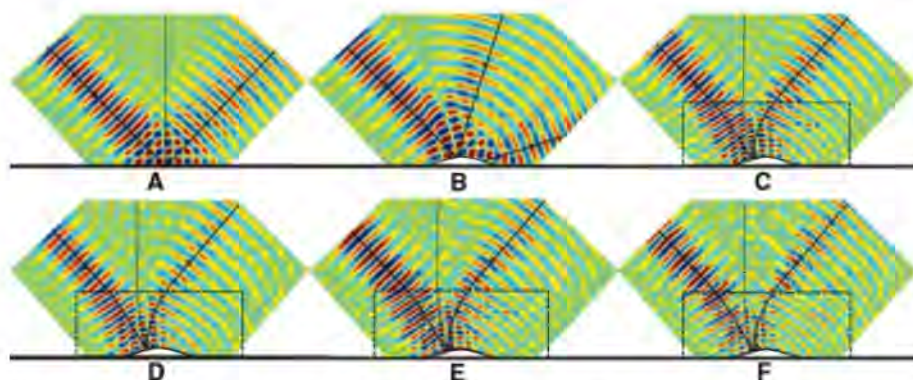


Fig. 3. Measured field mapping (E-field) of the ground, perturbation, and ground-plane cloaked perturbation. The rays display the wave propagation direction, and the dashed line indicates the normal of the ground in the case of free space and that of the ground-plane cloak in the case of the transformed space. (A) Collimated beam incident on the ground plane at 14 GHz. (B) Collimated beam incident on the perturbation at 14 GHz (control). (C) Collimated beam incident on the ground-plane cloaked perturbation at 14 GHz. (D) Collimated beam incident on the ground-plane cloaked perturbation at 15 GHz. (E) Collimated beam incident on the ground-plane cloaked perturbation at 15 GHz. (F) Collimated beam incident on the ground-plane cloaked perturbation at 16 GHz.

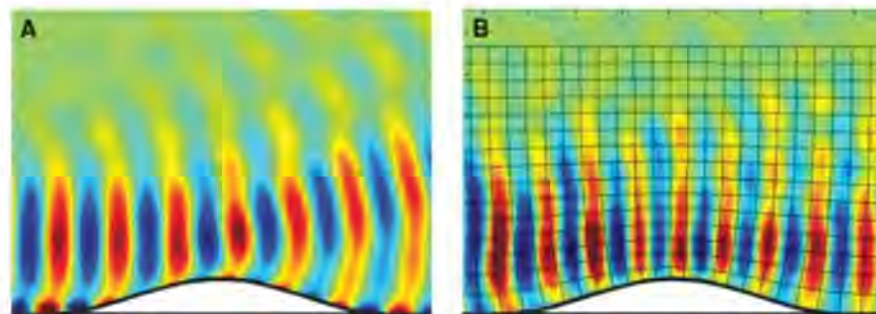


Fig. 4. 2D field mapping (E-field) of the perturbation and ground-plane cloaked perturbation, illuminated by the waves from the left side (A) perturbation and (B) ground-plane cloaked perturbation. The grid pattern indicates the quasi-conformal mapping of the transformation optics material parameters.

ing the optical. By merging the nascent technique of transformation optics with traditional gradient-index optics, we have shown that more functional hybrid structures can be developed that enable us to access previously unseen electromagnetic behavior while mitigating some of the inherent limitations. Though transformation optical designs are highly complex, metamaterial implementations can be rapidly and efficiently achieved using the algorithms and approach described in this report.

References and Notes

1. J. B. Pendry, D. Schurig, D. R. Smith, *Science* **312**, 1780 (2006); published online 24 May 2006 (10.1126/science.1125907).
2. U. Leonhardt, *Science* **312**, 1777 (2006), published online 24 May 2006; 10.1126/science.1126493.
3. M. Rahm, S. A. Cummer, D. Schurig, J. B. Pendry, D. R. Smith, *Phys. Rev. Lett.* **100**, 063903 (2008).
4. M. Rahm *et al.*, *Opt. Express* **16**, 11555 (2008).
5. A. V. Kildishev, V. M. Shalaev, *Opt. Lett.* **33**, 43 (2008).
6. M. Rahm *et al.*, *Phot. Nano. Fund. Appl.* **6**, 87 (2008).
7. W. X. Jiang *et al.*, *Appl. Phys. Lett.* **92**, 264101 (2008).
8. Z. Ruan, M. Yan, C. W. Neff, M. Qiu, *Phys. Rev. Lett.* **99**, 113903 (2007).
9. A. Hendi, J. Henn, U. Leonhardt, *Phys. Rev. Lett.* **97**, 073902 (2006).
10. D. Schurig *et al.*, *Science* **314**, 977 (2006); published online 18 October 2006 (10.1126/science.1133628).
11. W. Cai, U. K. Chettiar, A. V. Kildishev, V. M. Shalaev, *Nat. Photon.* **1**, 224 (2007).
12. H. Chen, B. I. Wu, B. Zhang, J. A. Kong, *Phys. Rev. Lett.* **99**, 063903 (2007).
13. A. Alu, N. Engheta, *Phys. Rev. Lett.* **100**, 113901 (2008).
14. W. X. Jiang *et al.*, *Phys. Rev. E Stat. Nonlin. Soft Matter Phys.* **77**, 066607 (2008).
15. See the supporting material on Science Online.
16. J. Li, J. B. Pendry, *Phys. Rev. Lett.* **101**, 203901 (2008).
17. J. F. Thompson, B. K. Soni, N. P. Weatherill, *Handbook of Grid Generation* (CRC Press, Boca Raton, FL, 1999).
18. P. Knupp, S. Steinberg, *Fundamentals of Grid Generation* (CRC Press, Boca Raton, FL, 1994).
19. D. R. Smith, D. C. Vier, Th. Koschny, C. M. Soukoulis, *Phys. Rev. E Stat. Nonlin. Soft Matter Phys.* **71**, 036617 (2005).
20. R. Liu, T. J. Cui, D. Huang, B. Zhao, D. R. Smith, *Phys. Rev. E Stat. Nonlin. Soft Matter Phys.* **76**, 026606 (2007).
21. B. J. Justice *et al.*, *Opt. Express* **14**, 8694 (2006).
22. This work was supported by a gift from Raytheon Missile Systems (Tucson), and the rapid design approach was supported by a Multiple University Research Initiative supported by the Air Force Office of Scientific Research, contract no. FA9550-06-1-0279. T.J.C. acknowledges the support from InnovateHan Technology, National Science Foundation of China (60871016 and 60671015), National Basic Research Program (973) of China (2004CB719802), Natural Science Foundation of Jiangsu Province (BK2008031), and the 111 Project (111-2-05). We thank C. Harrison, N. Kundtz, and J. Allen for assistance for the experimental apparatus; A. Degiron for careful reading of the manuscript; Q. Cheng for the nonresonant element metamaterials technique development; and H. Schmitt, D. Barker (Raytheon Missile Systems), and M. West for helpful discussions.

Supporting Online Material

www.sciencemag.org/cgi/content/full/323/5912/366/DC1
SOM Text
Figs. S1 to S6
Movies S1 to S5

8 October 2008; accepted 5 December 2008
10.1126/science.1166949

Coherent Intrachain Energy Migration in a Conjugated Polymer at Room Temperature

Elisabetta Collini and Gregory D. Scholes*

The intermediate coupling regime for electronic energy transfer is of particular interest because excitation moves in space, as in a classical hopping mechanism, but quantum phase information is conserved. We conducted an ultrafast polarization experiment specifically designed to observe quantum coherent dynamics in this regime. Conjugated polymer samples with different chain conformations were examined as model multichromophoric systems. The data, recorded at room temperature, reveal coherent intrachain (but not interchain) electronic energy transfer. Our results suggest that quantum transport effects occur at room temperature when chemical donor-acceptor bonds help to correlate dephasing perturbations.

Numerous systems, such as natural photosynthetic proteins and artificial polymers, organize light-absorbing molecules (chromophores) to channel photon energy to create electronic or chemical gradients. The excitation energy from the absorbed light is either transferred through space or shared quantum mechanically among several chromophores (1). The interplay among these classical and quantum limits of electronic energy transfer (EET) dynamics is dictated by the way the chromophores communicate with each other via long-range Coulombic interactions, as well as by the strength of perturbations from the bath of fluctuating nuclear motions in the molecular architecture and surrounding external medium (2–6).

An elusive intermediate EET regime is of particular interest because the excitation moves in space—which is a deterministic, classical attribute—

yet a preferred path can be adopted through wave function delocalization and associated interference effects, which introduce quantum characteristics to the dynamics (7). Together these attributes may in principle allow phase information to be transferred through space, with the electronic Hamiltonian of the entire system thereby steering EET. By learning how to observe the intermediate coupling case and thereafter to understand its properties, we could learn how to control excitation waves in a complex, multichromophoric system. Here, we present the results of an ultrafast spectroscopy experiment specifically designed to probe quantum coherent EET in the intermediate coupling case.

Rapid decoherence—the loss of memory of the initial electronic transition frequency distribution in an ensemble, caused by random fluctuations due to interaction of the system with its surroundings—is the primary reason for the scarcity of reports of coherent EET in complex condensed-phase systems. In the following, $|0\rangle$ designates the ground state, $|d\rangle$ is the donor, and $|a\rangle$ is the acceptor. According to theory, the evolution of

the acceptor probability density in EET can be written as a product of forward ($|d\rangle$ to $|a\rangle$) and reverse propagations of the system [e.g., (2)], which allows us to describe how the competition between electronic interaction and decoherence determines the EET dynamics. In the strong coupling case, the electronic coupling period dominates over decoherence; therefore, forward and reverse donor-acceptor paths tend to be almost identical. Phase is preserved over each path, and a kind of standing wave connects the two states so that their evolution is intimately entangled in a quantum state. In the weak coupling case, the fluctuations of the electronic transition frequency of a chromophore occur faster than the characteristic time of the donor-acceptor coupling. Owing to the tremendous number of different possible trajectories of transition energy fluctuations that can occur, the forward and reverse donor-acceptor propagations differ, so that decoherence dominates and the excitation is localized on the donor or acceptor at any one time—but not on both simultaneously—and the EET dynamics follow classical rate laws.

The rate of EET is often measured by transient absorption spectroscopy, where an ultrafast laser pulse photoexcites the donor chromophores and a probe pulse monitors the probability that the excitation has been transferred to an acceptor as a function of pump-probe delay time T . When the donor and acceptor chromophores have similar excitation energies, they cannot be spectrally distinguished, so we instead record anisotropy as a function of T . This technique has been extensively exploited to study EET in various kinds of multichromophoric systems (8–10). The anisotropy decay is caused by any process that changes the orientation of the chromophores probed relative to those initially photoexcited. For instance, electronic excitation could pass between two segments that are oriented at an angle in space. Alternatively, an excited chromophore could physically

Department of Chemistry, Institute for Optical Sciences, and Center for Quantum Information and Quantum Control, University of Toronto, Toronto, Ontario M5S 3H6, Canada.

*To whom correspondence should be addressed. E-mail: gscholes@chem.utoronto.ca

rotate in the laboratory frame. In the experiments reported here, this latter rotational reorientation of the chromophores, which typically occurs on time scales of tens of picoseconds or longer, is far too slow to contribute to the first few hundred femtoseconds of the anisotropy decay.

The intermediate coupling case can be distinguished by determining whether phase information is retained in the $|d\rangle$ to $|a\rangle$ propagation when excitation is transferred. An experiment sensitive only to probability density, like the pump-probe methods mentioned above, cannot elucidate this question directly because that phase information is lost when populations are formed. Instead, we measure dynamics during a coherence time period τ when the system is in a superposition of ground and excited states, and we use anisotropy to signal quantitatively that excitation coherence has been transferred. The two-time anisotropy decay (TTAD) experiment measures coherent EET directly and thereby probes the memory, or degree of coherence, characteristic of the $|d\rangle$ to $|a\rangle$ forward propagation. Whether or not this process occurs is important to establish because it is often neglected in theory (the secular approximation).

More specifically, the TTAD is recorded as a function of two different time delays (τ and T) in a three-pulse heterodyne-detected transient grating experiment. The delay T is the population time, during which excited-state dynamics such as EET occur, whereas the phase-stable delay τ , introduced between the first two pulses, scans a time period when the system is in a coherence $|0\rangle\langle d|$ between the ground and excited electronic states (11). During the τ delay, the system undergoes dephasing (free induction decay) or coherent EET from $|0\rangle\langle d|$ to $|0\rangle\langle a|$. In TTAD, coherent EET is completely discriminated from the free induction decay by monitoring anisotropy. This τ regime is the time delay scanned in photon echo experiments, which we use to investigate whether coherent EET also occurs during the population time period.

We applied the TTAD technique to study coherence EET in the prototypical conjugated polymer poly[2-methoxy,5-(2'-ethyl-hexoxy)-1,4-phenylene-vinylene] (MEH-PPV). Conjugated polymers have attracted considerable interest because they combine the ease of processing and outstanding mechanical characteristics of polymers with the versatile electrical and optical properties of functional organic molecules (12). EET within and among conjugated polymers is a practical concern as a source of electroluminescence quenching, and is also a fundamental component of how excitation evolves and migrates as a function of chain conformation and packing (13–15). Conjugated polymers are good candidate systems for seeking intermediate coupling effects because the ultrafast evolution of their excited states is governed by the interplay of delocalization and localization (16, 17); moreover, the relative orientation of chromophores is well suited for using anisotropy measurements to detect EET.

In perfectly ordered polymer chains, extensive π -electron conjugation along a rigid back-

bone confers extraordinary coherence lengths on wave functions (18). Polymers in solution, however, are disordered owing to the relatively low energy barrier for small-angle rotations around bonds along the backbone. Thus, the chain is broken into conformational subunits consisting of planar π -electron systems 2 to 12 repeat units long. These are the primary absorbing units, or chromophores, along an MEH-PPV chain (19) (Fig. 1). Neighboring chromophores are reasonably strongly coupled (20). This electronic coupling dictates how energy is transported among conformational subunits. Two basic types of EET have been identified: intrachain and interchain (20–22). The former consists of energy migration along the backbone between adjacent segments. The latter can be described as energy hopping among segments coupled through space, either because the chains are near to each other in a solid film or because the chain is folded back on itself (Fig. 1).

MEH-PPV polymer chains in two distinct conformations were investigated: (i) solutions in a good solvent (chloroform) where the polymer adopts an extended chain configuration, and (ii) aqueous suspensions of polymer nanoparticles (NPs) formed by individual collapsed chains (23). All experiments were performed in continuously flowing dilute solutions at 293 K (11). The spectra of both samples (fig. S3) exhibited the typical features known for this class of conjugated polymer (24, 25).

The conjugated polymer NPs showed little decay of anisotropy during τ (Fig. 2A), whereas the well-solvated MEH-PPV chains in chloroform

showed a striking τ dependence in the TTAD data (Fig. 2B). Owing to the experimental design, this result shows in itself that coherence EET occurs after excitation of extended-conformation MEH-PPV chains, but not in collapsed-chain NPs. Moreover, this phenomenon occurred at room temperature. A qualitative model for the τ dependence of the anisotropy decay can be derived by simulating the anisotropy according to the simplified framework discussed in (11). The anisotropy decay, depending on both τ and T , was modeled for time scales characteristic of coherence and population EET, represented as empirical rate coefficients k_τ and k_T , respectively. Finite pulse duration was taken into account by means of Gaussian field envelopes. Because coherence EET can only be measured when it is followed by population (normal) EET (11), its presence is hidden in the TTAD unless the time scales for the two processes are similar. We find that condition to be easily met when the anisotropy decay is highly nonexponential at early time, as we found for the experimental data (Fig. 2C).

Slices through the experimental surfaces at $\tau = 0$ are plotted in Fig. 3A. It is evident that the anisotropy decays during T more for NPs than for the MEH-PPV in chloroform solution because interchain interactions mediate efficient EET (20). Despite that observation, we saw no coherence anisotropy decay for NPs, which suggests that fluctuations on unconnected conformational subunits are uncorrelated (see below), as is normally assumed. In Fig. 3B, experimental data points as a function of τ are plotted for $T = 0$ and are compared to simulations (solid lines). Owing to

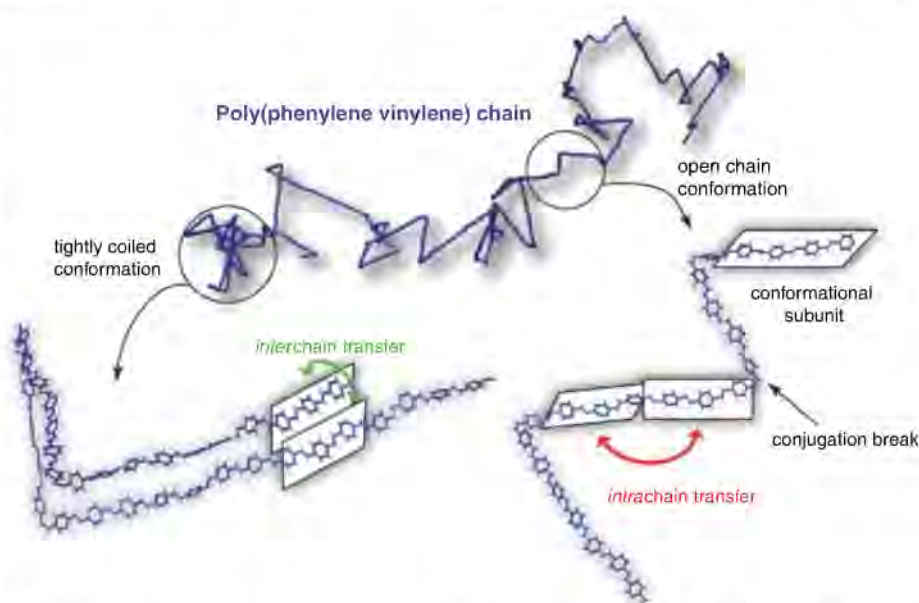


Fig. 1. Example of single-chain conformation of a poly(phenylene vinylene) conjugated polymer, referred as the defect cylinder conformation. Conformational disorder produces a chain of linked chromophores (or conformational subunits) outlined conceptually by boxes. The intrachain EET (migration along the backbone) is the predominant mechanism when the polymer chain assumes an open, extended conformation, typical for solutions in good solvents such as chloroform. On the other hand, interchain interactions (hopping between segments in close proximity) are dominant for tightly coiled configurations, polymer nanoparticles, or films.

the rapid dephasing, in particular because the measurements were performed at 293 K, it was not possible to establish the functional form of the τ dependence (the absolute signal intensities decay strongly with τ , which degrades the signal-to-noise ratio of the anisotropy measurement). Nonetheless, the value that k_τ must assume in order to fit the experimental behavior in the chloroform solution was found to be $\sim 0.05 \text{ fs}^{-1}$, corresponding to a characteristic time of $\sim 20 \text{ fs}$.

We confirmed that the TTAD does not decay for a system that cannot undergo EET by examin-

ing a dilute solution of a laser dye, rhodamine 6G in ethanol, absorbing in the same spectral region as MEH-PPV. The experimental data recorded at different τ values confirmed an anisotropy value corresponding to the expected theoretical value of 0.4 for all values of τ and T (Fig. 3B). On substantially longer time scales, the anisotropy of this single chromophore decays with T owing to rotational diffusion in the solution.

Provided that fluctuations of the electronic transition frequencies, ω_{d0} and ω_{a0} , of donor and acceptor chromophores are perfectly correlated, then coherent EET is observed in TTAD as anisotropy decay along τ . That condition is ensured when the correlation function $\xi_{dd}(\tau) \equiv \langle \omega_{d0}(\tau)\omega_{d0}(0) \rangle$ is similar to the cross-correlation function $\xi_{ad}(\tau) \equiv \langle \omega_{a0}(\tau)\omega_{d0}(0) \rangle$. However, if the fluctuations of ω_{d0} and ω_{a0} are uncorrelated (as is usually supposed), then $\xi_{ad}(\tau) = 0$ and consequently, according to Kubo's theorems for cumulants (26), coherence EET cannot contribute to the anisotropy decay we measure. Hence, anisotropy as a function of τ in TTAD decays only when coherence EET occurs, in which case $\xi_{ad}(\tau) \neq 0$. The measurement therefore incisively detects evidence for both intermediate-case EET and the necessary correlation of the fluctuations of the donor and acceptor transition frequencies.

The two polymer morphologies described above differ in their dominant energy migration pathways. Interchain EET is expected to be the leading process in the NPs because of the many close chain-chain contacts. In contrast, the relatively open and straight conformation adopted by MEH-PPV in chloroform makes intrachain EET dominant. This difference in EET mechanism helps to explain why the corresponding TTAD data (Fig. 2) are so strikingly different. For the case of the NPs, the absence of anisotropy decay during τ is likely due to the absence of correlations among the electronic transition frequencies of donor and acceptor chromophores [i.e., $\xi_{ad}(\tau) = 0$]. When these fluctuations are uncorrelated, coherent EET cannot compete with decoherence times of $\sim 10 \text{ fs}$ (27). On the other hand, the marked decay of anisotropy with τ for the extended MEH-PPV

chains (Fig. 2B) demonstrates that $\xi_{ad}(\tau) \neq 0$ —even at ambient temperature—for chromophores connected by the conjugated polymer backbone. That result implies that low-frequency vibrations characteristic of the polymer backbone have a coherence length longer than a single conformational subunit. Clearly it is not sufficient to know only the time scale and amplitude of bath fluctuations (manifest in optical line shapes); it is also important to account for the length scale of those fluctuations.

Our work is consistent with recent observations of protected coherences. Fleming and co-workers have shown, using two-dimensional photon echo (2DPE) experiments, how fluctuations at different chromophore sites in a protein at 77 K can preserve electronic coherences over time scales substantially longer than the decoherence time estimated from the correlation function of the transition frequency (28, 29). Like TTAD, 2DPE is a four-wave mixing experiment in which three laser fields interact with the sample to induce a radiated polarization. The full electric field of the signal is heterodyne-detected by spectral interferometry while T is fixed and τ is scanned. After a Fourier transform with respect to the coherence time τ and the rephasing time t (defined as the evolution time of the signal relative to the arrival time of the third pulse), the two-dimensional electronic spectrum at a given population time T is retrieved (30). The final result is a two-dimensional map in which the signal (real, imaginary, or absolute value) is plotted as a function of the coherence frequency ω_τ representing the initial excitation, and the rephasing frequency ω_τ , which can be interpreted as the ensuing emission.

Experimental and theoretical investigations have stressed that a fundamental characteristic of this technique is its sensitivity to correlations among excited levels (28, 31). We performed 2DPE experiments on MEH-PPV solutions in chloroform solvent at 293 K. These studies show that 2DPE yields incisive signatures of electronic coherences between excited states, allowing electronic coherences to be differentiated from quantum beats that are due to nuclear wave packet motion. Our observation of electronic coherences like $|d\rangle\langle a|$ in MEH-PPV, which are traditionally thought to be

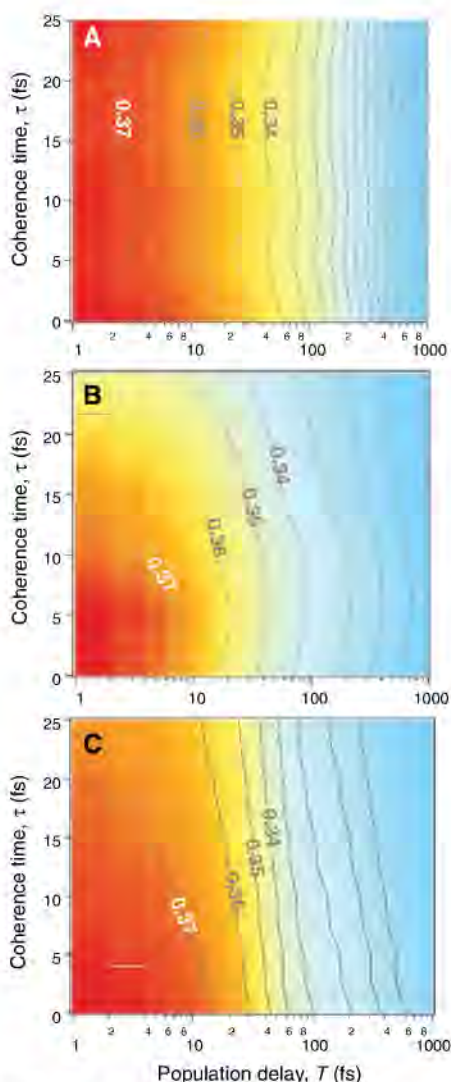


Fig. 2. Two-dimensional plots showing anisotropy decay as a function of τ and T . The color scale indicates the anisotropy, with values shown by the contour lines and corresponding labels. (A and B) Experimental results for MEH-PPV NP suspension in water (A) and MEH-PPV in chloroform solution (B). (C) Simulation results using a multiexponential model to match experimental data for the chloroform solution with $k_{T1} = 0.05$, $k_{T2} = 0.002$, and a static offset, $k_{T3} = 1.0$, $k_{T4} = 0.2$, $k_{T5} = 0.1 \text{ fs}^{-1}$. The parameters were not extracted from an optimized fit but were found to provide a reasonable simulation of the data.

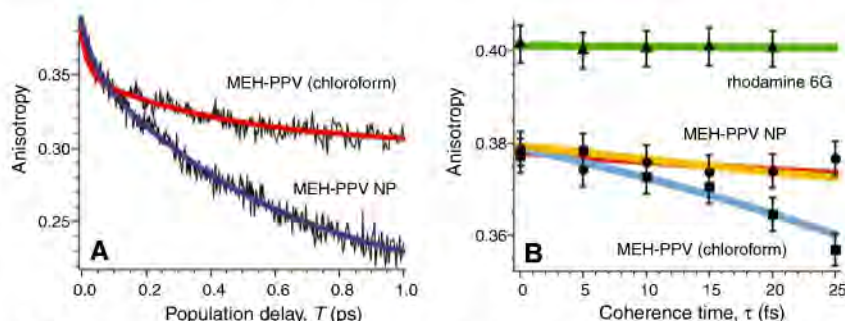
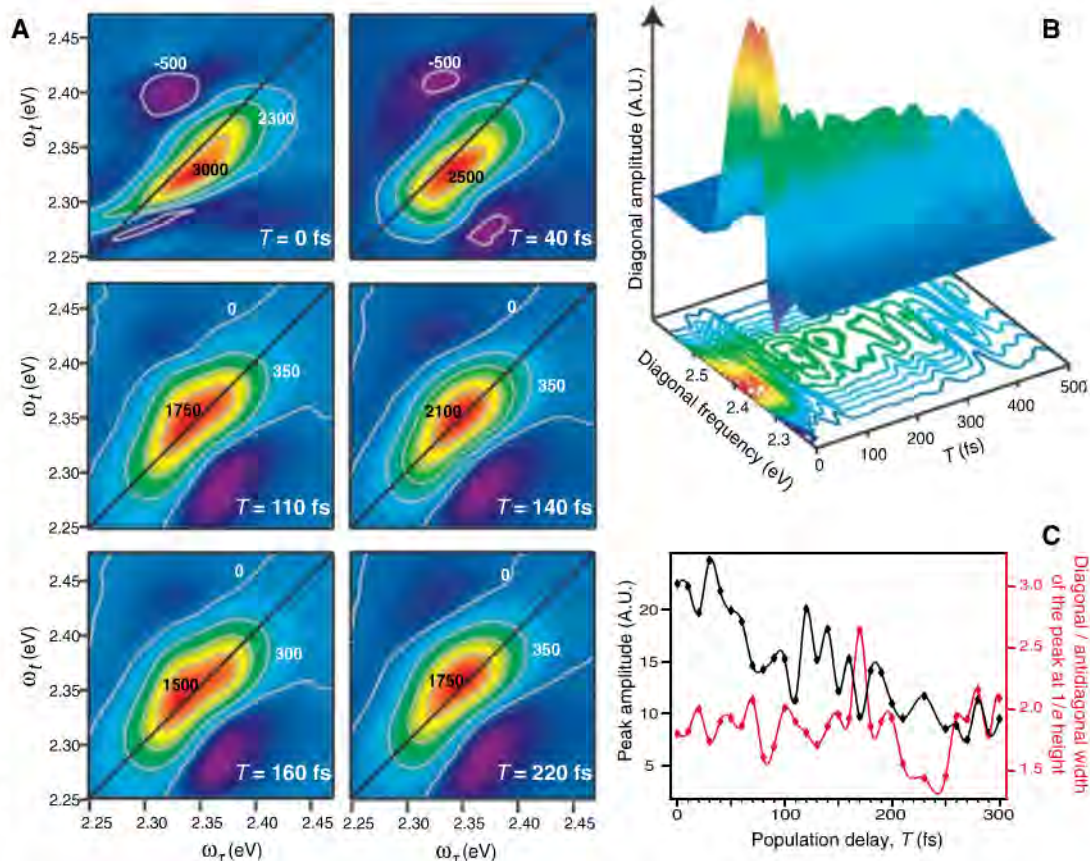


Fig. 3. (A) Comparison between the conventional ($\tau = 0$) anisotropy decay dynamics in chloroform solution (red) and NP suspension (blue). (B) Anisotropy values calculated at $T = 0$ as a function of coherence time for rhodamine 6G (triangles), polymer solution in chloroform (squares), and aqueous NP suspension (circles). The data points are averages; error bars were estimated as SDs of at least nine repeated measurements. The green solid line is a linear fit of the experimental points for rhodamine 6G, whereas the orange, red, and cyan lines represent slices at $T = 0$ of simulations.

Fig. 4. (A) Selected 2DPE spectra (real part) of MEH-PPV in chloroform solution at $T = 0, 40, 110, 140, 160$, and 220 fs, demonstrating the oscillation in the amplitude and in the shape of the diagonal peak. The color scale indicates the signal value; deep blue denotes zero, and other values (arbitrary units) are shown by the contour lines and corresponding labels. (B) Three-dimensional plot of the amplitude of the spectra along the diagonal line as a function of frequency and population time. A cubic spline interpolation is used to connect the experimental points and generate a smooth surface. (C) Comparison between the amplitude of the diagonal peak (left axis, black line) and the ratio between the diagonal and antidiagonal widths of the peak at $1/e$ height (right axis, red line). These data are an average of three independent experiments. The lines show the characteristic anticorrelation theoretically predicted for oscillations caused by electronic coherences.



very short-lived owing to decoherence, complement our interpretation of the TTAD data by supporting the condition that $\xi_{\text{rad}}(\tau) \neq 0$.

The principal feature in the 2DPE spectra of MEH-PPV solutions in chloroform (Fig. 4A) is a diagonally elongated peak. This diagonal shape, where the radiated signal frequencies (ω_r) are correlated with the initial transition dipole oscillation frequency (ω_t), is related to the linear absorption spectrum of MEH-PPV. The comparison between 2DPE spectra measured at different T values reveals the presence of an oscillation in the amplitude and in the shape of this main peak, which becomes rounder as it gets stronger. The presence of this oscillation is more evident in the plot of amplitude of the spectra along the diagonal line as a function of frequency and T (Fig. 4B). The electronic origin of these beats is confirmed by the characteristic anticorrelation of the amplitude and the peak shape, defined as the ratio of diagonal to antidiagonal widths of the peak (Fig. 4C). According to previous experimental and theoretical studies, that anticorrelation is a signature of electronic coherences rather than vibrational coherences (28, 31). These electronic beats persist for at least 250 fs, a time period vastly longer than the generally assumed decoherence time of ~ 10 fs (27).

2DPE is sensitive to coherence effects during T , and therefore it measures the coherent buildup and decay of population while EET is occurring, evidenced by the coherent oscillations in the data.

It establishes that long-lived electronic coherences persist for at least 250 fs after photoexcitation of MEH-PPV in solution at 293 K. The TTAD technique shows unequivocally that coherent EET occurs during τ , which suggests that the electronic coherences observed in the 2DPE data can assist energy migration, predominantly in the case of intrachain EET. It is probable that the common structural framework of the macromolecule introduces correlation in the energy gap fluctuations, which in turn preserves the coherence and permits coherent EET even at room temperature. It remains unclear whether these are predominantly fluctuations affecting the site (diagonal) energies of the conformational subunits, or fluctuations of the electronic couplings (off-diagonal). Physically the former case corresponds to preservation of delocalization by nuclear motions with length scales longer than one conformational subunit. The latter case is more intrinsically related to the formation of conformational subunits, perhaps originating from fluctuations that partially restore a conjugation break.

Our results show that quantum transport effects occur at ambient temperature along conjugated polymer chains. We conclude that chemical bonds connecting chromophores, such as in polymers, macromolecules, and supramolecular systems, play an important role in introducing quantum effects in EET dynamics. This observation extends the paradigm of protein-protected coherences proposed by Fleming and co-workers to chemically bonded chromophores in nanoscale materials at

ambient temperatures. In the case of conjugated polymers, this phenomenon may assist formation of the semiconductor band character of the electronic states.

References and Notes

- G. D. Scholes, *Annu. Rev. Phys. Chem.* **54**, 57 (2003).
- S. Rackovsky, R. Silbey, *Mol. Phys.* **25**, 61 (1973).
- H. Haken, P. Reineker, *Z. Phys.* **249**, 253 (1972).
- V. M. Kenkre, R. S. Knox, *Phys. Rev. B* **9**, 5279 (1974).
- V. Chernyak, S. Mukamel, *J. Chem. Phys.* **105**, 4565 (1996).
- A. Kimura, T. Kakitani, *J. Phys. Chem. B* **107**, 14486 (2003).
- J. Klafter, R. Silbey, *Phys. Lett.* **76A**, 143 (1980).
- T. Goodson, *Annu. Rev. Phys. Chem.* **56**, 581 (2005).
- S. Akimoto, M. Mimuro, *Photochem. Photobiol.* **83**, 163 (2007).
- C. R. Gochanour, M. D. Fayer, *J. Phys. Chem.* **85**, 1989 (1981).
- See supporting material on Science Online.
- G. Hadzioannou, G. G. Malliaras, Eds., *Semiconducting Polymers: Chemistry, Physics and Engineering* (Wiley-VCH, Weinheim, Germany, ed. 2, 2007).
- J. L. Brédas, D. Beljonne, V. Coropceanu, J. Cornil, *Chem. Rev.* **104**, 4971 (2004).
- A. Ruseckas et al., *Phys. Rev. B* **72**, 115214 (2005).
- S. Heun et al., *J. Phys. Condens. Matter* **5**, 247 (1993).
- G. D. Scholes, G. Rumbles, *Nat. Mater.* **5**, 683 (2006).
- N. S. Sariciftci, Ed., *Primary Excitations in Conjugated Polymers: Molecular Excitation Versus Semiconductor Band Model* (World Scientific, Singapore, 1997).
- F. Dubin et al., *Nat. Phys.* **2**, 32 (2006).
- H. Bässler, B. Schweizer, *Acc. Chem. Res.* **32**, 173 (1999).
- D. Beljonne et al., *Proc. Natl. Acad. Sci. U.S.A.* **99**, 10982 (2002).

21. T.-Q. Nguyen, J. Wu, S. H. Tolbert, B. J. Schwartz, *Adv. Mater.* **13**, 609 (2001).
22. J. Yu, D. Hu, P. F. Barbara, *Science* **289**, 1327 (2000).
23. C. Szymanski et al., *J. Phys. Chem. C* **109**, 8543 (2005).
24. B. J. Schwartz, *Annu. Rev. Phys. Chem.* **54**, 141 (2003).
25. L. J. Rothberg et al., *Synth. Met.* **80**, 41 (1996).
26. R. Kubo, *J. Phys. Soc. Jpn.* **17**, 1100 (1962).
27. O. V. Prezhdo, P. J. Rossky, *Phys. Rev. Lett.* **81**, 5294 (1998).
28. G. S. Engel et al., *Nature* **446**, 782 (2007).
29. H. Lee, Y.-C. Cheng, G. R. Fleming, *Science* **316**, 1462 (2007).
30. T. Brixner, T. Mancal, I. V. Stiopkin, G. R. Fleming, *J. Chem. Phys.* **121**, 4221 (2004).
31. A. V. Pislakov, T. Mancal, G. R. Fleming, *J. Chem. Phys.* **124**, 234505 (2006).
32. Supported by an E. W. R. Steacie Memorial Fellowship (G.D.S.) and by the Natural Sciences and Engineering Research Council of Canada. We thank Y.-C. Cheng, G. R. Fleming, and R. J. Silbey for their comments on the manuscript.

Supporting Online Material

www.sciencemag.org/cgi/content/full/323/5912/369/DC1

Materials and Methods

SOM Text

Figs. S1 to S4

Table S1 and S2

References

31 July 2008; accepted 19 November 2008
10.1126/science.1164016

A Mouse Speciation Gene Encodes a Meiotic Histone H3 Methyltransferase

Ondrej Mihola,^{1*} Zdenek Trachtulec,^{1*} Cestmir Vlcek,¹ John C. Schimenti,² Jiri Forejt^{1†}

Speciation genes restrict gene flow between the incipient species and related taxa. Three decades ago, we mapped a mammalian speciation gene, hybrid sterility 1 (*Hst1*), in the intersubspecific hybrids of house mouse. Here, we identify this gene as *Prdm9*, encoding a histone H3 lysine 4 trimethyltransferase. We rescued infertility in male hybrids with bacterial artificial chromosomes carrying *Prdm9* from a strain with the “fertility” *Hst1*^f allele. Sterile hybrids display down-regulated microorchidia 2B (*Mor2b*) and fail to compartmentalize γ H2AX into the pachynema sex (XY) body. These defects, seen also in *Prdm9*-null mutants, are rescued by the *Prdm9* transgene. Identification of a vertebrate hybrid sterility gene reveals a role for epigenetics in speciation and opens a window to a hybrid sterility gene network.

Hybrid sterility is one of the postzygotic reproduction isolating mechanisms that play an important role in speciation. Hybrid sterility is defined as a situation where parental forms, each fertile inter se, produce infertile offspring (1, 2). Hybrid sterility follows Haldane’s rule by affecting predominantly the heterogametic sex (XY or ZW) in crosses where one sex of the progeny is sterile or missing (3). Identification of speciation genes has not been particularly successful. Despite decades of effort, only two hybrid sterility genes have been isolated, both from *Drosophila* species (4, 5).

Here, we report identification of a hybrid sterility gene in a vertebrate species. Hybrid sterility 1 (*Hst1*) is one of several genes responsible for spermatogenic failure in *Mus m. musculus*-*Mus m. domesticus* (*Mmm*-*Mmd*) hybrids (6, 7). It was genetically mapped to mouse chromosome 17 (Chr17) in hybrids between the *Mmm*-derived PWD/Ph inbred strain (8) and several classical laboratory strains, mostly of *Mmd* origin (9). Whereas most laboratory inbred strains, including C57BL/6J (B6), carry the *Hst1*^s (sterility) allele, a few strains, such as C3H/DiSnPh (C3H) or P/J, carry the *Hst1*^f (fertility) allele (table S1) (10). In sterile male hybrids, the *Hst1* interacts, among other genes, with *Hst1*^{ovs} locus on Chr17 of

Mmm subspecies. However, it remains to be determined whether *Hst1* and *Hst1*^{ovs} are identical genes.

A series of high-resolution genetic mapping experiments (11–13) and haplotype analyses (14, 15) localized *Hst1* to a 255-kb single-copy candidate region on Chr17, harboring six protein-coding genes (*Dill1*, *Pgcc1*, *Psmbl1*, *Tbp*, *Pdcd2*, and *Prdm9*) and six pseudogenes (Fig. 1A). To narrow the *Hst1* critical region, we attempted rescue of the hybrid sterility phenotype by transgenesis with bacterial artificial chromosomes (BACs) derived from the C3H/HeJ strain carrying the “fertility” *Hst1*^f allele. Four overlapping BAC clones (CHORI-34-45F17; hereafter BAC5, CHORI-34-255E14 -BAC19, CHORI-34-289M8 -BAC21, and CHORI-34-331G23-BAC24) (16, 17) were transfected into embryonic stem (ES) cells of (129 × B6)F₁, predominantly of *Mmd* origin. The mice with BAC19 did not transmit the BAC to progeny and were not studied further. The other three BACs were transmitted, and as expected, none of them interfered with fertility after outcrossing to the B6

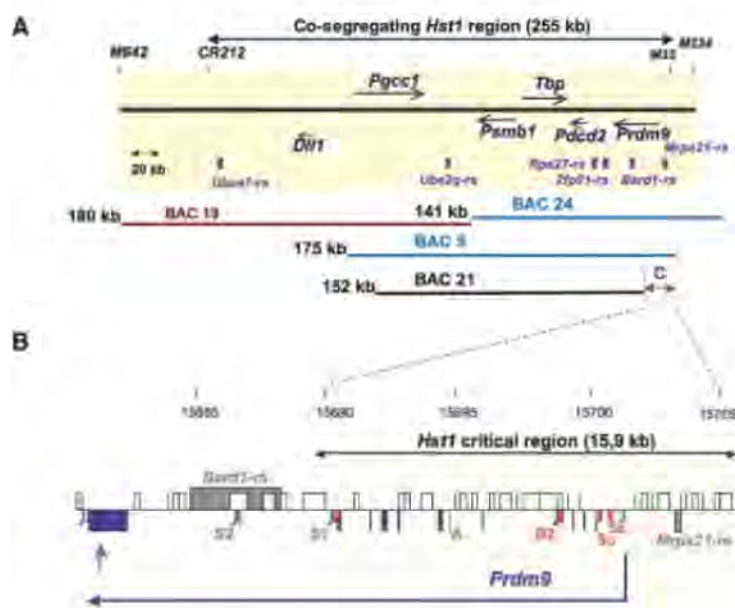


Fig. 1. The *Prdm9* gene encodes *Hst1*. (A) The cosegregating *Hst1* region is defined by the markers CR212 and M33 (table S2). The arrows point in the direction of gene transcription; the boxes denote pseudogenes. The C3H BAC clones used for transgenesis are shown as horizontal lines with their sizes on the left. The BAC19 chimeras did not transmit the transgene (red line). The blue lines show the BACs rescuing hybrid sterility, whereas BAC21 did not rescue sterility; the C region is necessary for the rescue. (B) The *Hst1* critical region. Dark blue boxes: coding exons; light blue box: untranslated region; red boxes: alternative exons (marked 5a, 5u, B2, A, S1, and S2); gray boxes: putative pseudogenes; empty boxes or vertical black lines: repetitive sequences; and asterisks: polyadenylation sites. The vertical arrow points to the site of insertion of a zinc-finger in the last exon of *Prdm9* in the C3H mouse strain. The numbers at the top indicate the positions on Chr17 (in kb, NCBI m37 assembly).

¹Institute of Molecular Genetics, Academy of Sciences of the Czech Republic, Videnska 1083, 142 20 Prague, Czech Republic. ²Center for Vertebrate Genomics, Department of Biomedical Sciences, College of Veterinary Medicine, Cornell University, T9014A Vet Research Tower, Ithaca, NY 14853, USA.

*These authors contributed equally to this work.

†To whom correspondence should be addressed. E-mail: jforejt@img.cas.cz

laboratory strain. However, in crosses to PWD (*Mmm*) females, BAC5 and BAC24 fully restored male fertility of the F_1 hybrid males,

whereas BAC21 transgenic F_1 hybrid males remained sterile (Table 1). *Psmbl*, *Tbp*, and *Pdcd2* were excluded as *Hst1* candidates based on their

Table 1. The effect of BAC transgenes on male fertility phenotypes. TW, wet weight of paired testes; OFM, offspring per female per month; ND, not determined; F, fertile; S, sterile.

Tg line*	Tg	Genetic background†	TW (mg)	N	Sperm count ($\times 10^{-6}$)	N	OFM	N	Fertility
BAC5	—	B6 \times (B6 \times 129)	199 \pm 41	5	4.5 \pm 1.1	5	ND		F
BAC5	+	B6 \times (B6 \times 129)	212 \pm 22	7	4.6 \pm 1.1	7	6.3 \pm 1.2	3	F
BAC5	—	PWD \times (B6 \times 129)	63 \pm 7	15	0	15	0	5	S
BAC5	+	PWD \times (B6 \times 129)	145 \pm 25	22	2.4 \pm 0.9	22	6.5 \pm 1	7	F
BAC21	—	PWD \times (B6 \times 129)	54 \pm 5	12	0	12	ND		S
BAC21	+	PWD \times (B6 \times 129)	55 \pm 6	12	0	12	0	2	S
BAC24	—	PWD \times (B6 \times 129)	63 \pm 8	12	0	6	ND		S
BAC24	+	PWD \times (B6 \times 129)	211 \pm 16	18	6.9 \pm 1.2	14	7.3	2	F
None	—	B6 \times PWD	152 \pm 13	9	1.0	2	3.6	2	F
None	—	PWD \times B6	60 \pm 4	12	0	6	ND		S
None	—	PWD \times C3H	128 \pm 2	2	1.0	2	4.2 \pm 0.7	5	F

*Transgenic (Tg) lines carried two BAC copies in BAC5 and BAC21 lines, and six in BAC24. †B6 (*Mmd*) or PWD (*Mmm*) females were crossed with male BAC carriers on a mixture of B6 and 129 genetic background (*Hst1*²). The C3H strain and BAC clones carry the *Hst1* allele. The presence of BAC (Tg +) was tested with an SSLP (microsatellite) polymorphic marker. B6 \times PWD, reciprocal hybrid (PWD male).

expression in BAC5 (rescuing) as well as in BAC21 (nonrescuing) transgenic lines (see below). *Pgcc1* was excluded because of its absence in rescuing BAC24. Previous sequencing of *Dll1*, *Pgcc1*, *Psmbl*, *Tbp*, and *Pdcd2* alleles suggested that they are unlikely candidates for *Hst1* (13, 14). Thus, the newly defined *Hst1* critical region was restricted to the 15.9-kb interval [Chr17-15689705-15705634, National Center for Biotechnology Information (NCBI) Build 37.1] shared by rescuing BAC24 and BAC5 but absent in BAC21. This region is occupied by the 5' end of the PR-domain 9 (*Prdm9*) gene and the *Mrps21-rs* pseudogene (Fig. 1B).

To exclude the possibility that BAC21 did not rescue hybrid sterility because its genes were silenced in the BAC integration site, we analyzed the BAC transgenics for the expression of the genes within the *Hst1* candidate region. The C3H allele-specific transcript of *Tbp* was found in adult testis, proving its activity in the BAC transgene (fig. S1). *Psmbl* and *Pdcd2* could not be tested owing to the lack of suitable polymorphism, but the dosage-dependent increase of their testicular expression (Fig. 2A) suggested that the genes within the BAC21 were active but unable to rescue the meiotic arrest. A dosage-dependent increase in *Prdm9* expression was seen in the BAC5 and BAC24 hybrids but was absent in BAC21 hybrids, confirming that the *Prdm9* transcript from the *Hst1* allele was not present in the latter (Fig. 2A). The analysis of prepubertal fertile and sterile hybrids revealed no significant differences in mRNA expression in any of the six *Hst1* candidate genes (fig. S2). These results further corroborated *Prdm9* as the only candidate gene. Previously unknown testicular mRNA isoforms of *Prdm9* were found (fig. S3); however, none of them exhibited reproducible differential expression between prospectively fertile and sterile prepubertal hybrid testis (fig. S4).

Next, we sequenced the 25-kb region containing the C3H allele of *Prdm9* including the 5' flanking region (GeneBank EU719625) and found 57 differences between the B6 and C3H strains: 35 microsatellite length polymorphisms, 21 single-nucleotide polymorphisms, and one zinc-finger-encoding repeat variant. All except the zinc-finger variant were in noncoding regions. Whereas PRDM9^{B6} contained 13 C₂H₂ zinc fingers, we found that PRDM9^{C3H} contains 14 of them (fig. S5). The pseudogene *Mrps21-rs* is not polymorphic between C3H and B6. Thus, *Prdm9* remains the only candidate for *Hst1*.

The *Prdm9* gene, also known as Meisetz, is expressed in testis and ovaries (18). It encodes a histone 3 lysine 4 (H3K4) trimethyltransferase. Trimethylation of histone H3K4 at promoters leads to the transcriptional activation of genes. The *Prdm9*-null mice show arrest of spermatogenesis and oogenesis at pachynema, impairment of double-strand break repair, chromosome asynapsis, and disrupted sex-body formation (18). To further verify *Prdm9* as *Hst1*, we compared the phenotypes of the sterile *Hst1*^{ns}/*Hst1*^{ns}

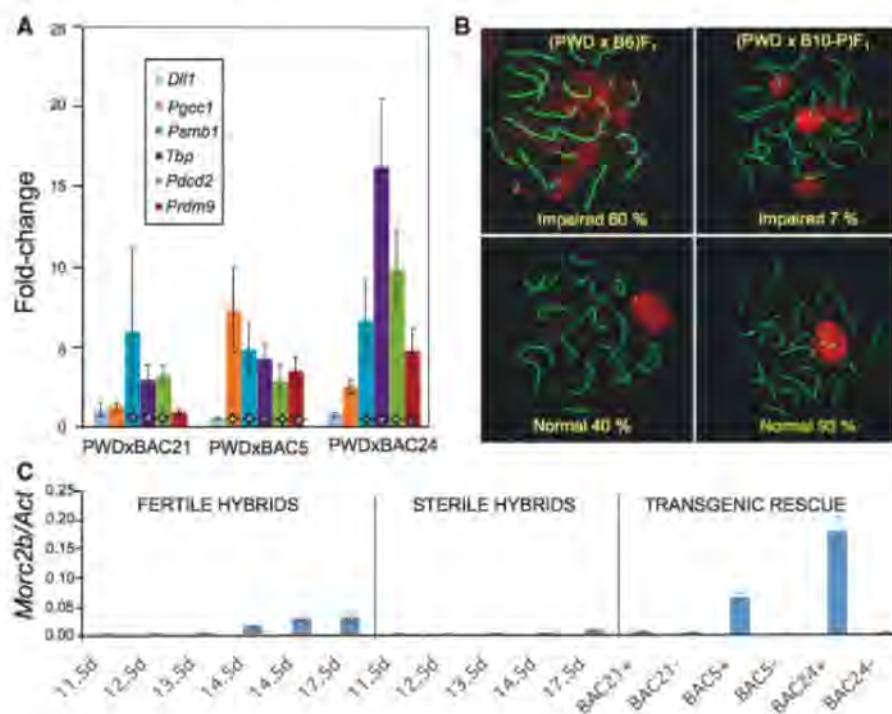
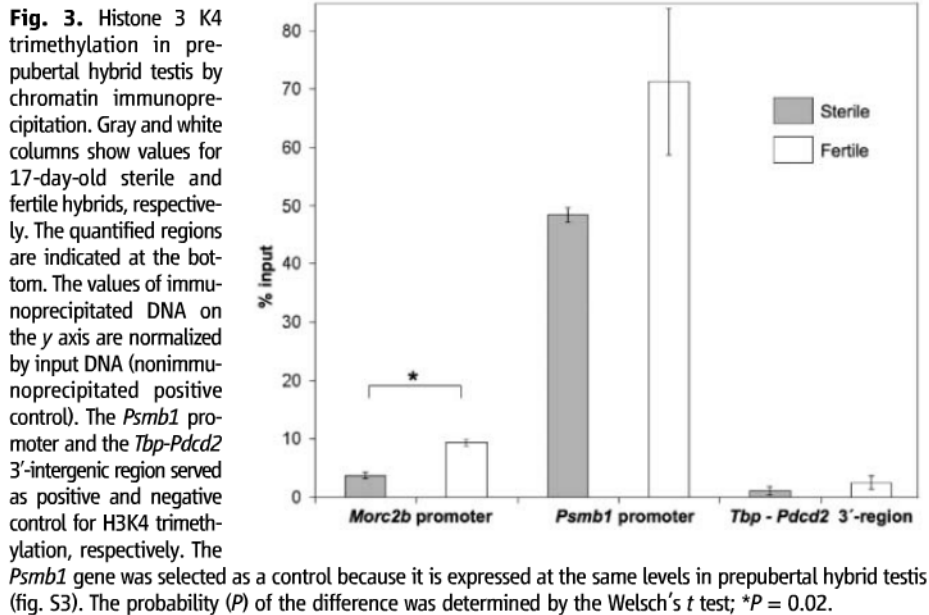


Fig. 2. The effect of BAC transgenes on gene expression in testes of hybrid males. (A) Fold change of gene expression in the *Hst1* critical region in BAC carriers versus their wild-type littermates. Stars indicate the presence of an intact gene within the BAC. *Psmbl* and *Pdcd2*, predominantly expressed in spermatogonia and pachynema, show dosage-dependent increase in expression (BAC21, two copies; BAC5, two copies; BAC24, six copies). (B) Indirect immunofluorescence of γ H2AX (red) and SCP1 (synaptonemal complexes, green) in pachytene spermatocytes. Most pachytene spermatocytes of fertile hybrids (*Hst1*^{ns}/*Hst1*^{ns}, right) display γ H2AX within the sex body. In the sterile hybrids (*Hst1*^{ns}/*Hst1*^{ns}, left), the patches of γ H2AX are scattered over the autosomes in most of the examined cells. Three hundred pachytene spermatocytes of each genotype were analyzed. Congenic strain B10.P carries the *Hst1* allele on C57BL/10 background. (C) Transcription of *Morc2b* is induced in prepubertal fertile (PWD \times B6.C3H-*Hst1*²) testes but is missing in (PWD \times B6)F₁ sterile hybrids. The expression at day 17.5 is rescued in a dosage-dependent manner in (PWD \times BAC) hybrids by BAC5 and BAC24, but not by BAC21. The fertility status of F₁ hybrids of various combinations of inbred mouse strains is shown in table S1.



(PWD \times B6)F₁ males with the published phenotypes of *Prdm9*^{-/-} mutants. Sterile hybrids have small testes with spermatogenic arrest predominantly during pachytene and no sperm in the seminiferous tubules (6, 19, 20) (Table 1). Rare surviving primary spermatocytes at diakinesis–metaphase I manifest two to six univalents and frequent X–Y dissociation (6), resembling the impairment of synapsis between homologous chromosomes in the *Prdm9*^{-/-} mutants. Both sterile hybrids and *Prdm9*^{-/-} mice display abnormal sex-body formation in pachytene spermatocytes (Fig. 2B). *Prdm9*^{-/-} pachytene spermatocytes lack a sex body and exhibit patches of γ H2AX over the synaptonemal complexes (18). We observed a comparable failure of sex-body formation with scattered γ H2AX in 60% of pachytene spermatocytes in sterile (PWD \times B6)F₁ hybrids versus 7% in fertile hybrid controls (Fig. 2B).

The microorchidia 2b gene, *Morc2b*, or 493241A10Rik, encoding a gonad-specific protein, is directly induced by *Prdm9*. Similar to *Prdm9*^{-/-} testis (18), we found that *Morc2b* mRNA is barely detectable in sterile hybrids. The *Morc2b* expression in hybrid males was restored by the *Prdm9*-containing BACs (Fig. 2C). Transcription from *Morc2b* corresponds to the amounts of histone H3K4 trimethylation controlled by the enzymatic activity of PRDM9 (18). Chromatin immunoprecipitation revealed decreased H3K4 trimethylation of *Morc2b* in sterile hybrid testis (Fig. 3).

Two differences were observed between sterile hybrids and *Prdm9*-null mutants. Following Haldane's rule (3), hybrid sterility is male-limited, yet meiotic arrest of *Prdm9*^{-/-} mice affects both sexes. This discordance could be explained by incompatible *domesticus-musculus* epistatic interaction(s) of the *Prdm9* gene in sterile hybrids in contrast to the complete silencing of *Prdm9* in the knockout. Similar meiotic effects, sterility of both

sexes or dominant male-limited sterility, have been described for the null and missense mutations of the *Dmcl* gene (21), respectively. Second, the *Prdm9*-null mutation acts independently, whereas meiotic arrest in F₁ hybrids results from the epistatic interaction of the *Hst1* gene (*Hst*^{MS}/*Hst*^{LS}) with several independently segregating genes (10). Hybrids between the consomic strain B6.PWD–Chr17 and B6 (22), as well as hybrids (B6 female \times PWD male, Table 1), carry the “sterile” *Hst*^{MS}/*Hst*^{LS} genotype but are fertile due to their lack of an interaction of *Hst1* with other hybrid sterility genes (10, 23).

The parallel between the role of *Hst1* in mouse hybrid sterility and the role of *Lhr* in hybrid male inviability of *Drosophila* is striking. In both cases, a variant form able to rescue hybrid incompatibility was found within a species. It behaved as an autosomal locus, *Hst1*^f within *Mmd* and *Lhr* in the case of *D. simulans*, and interacted with an X-linked genetic factor (7, 23, 24). Finally, both in the mouse and *Drosophila*, the two loci were necessary but not sufficient to reconstitute the hybrid incompatibility phenotype.

Our data show that *Prdm9*, known to activate genes essential for meiosis by methylation of histone H3 at lysine 4, is the only candidate for *Hst1*. It is the only known gene located within the newly defined 15.9-kb hybrid sterility 1 critical region, expressed at the right tissue and at the right time of germ cell differentiation (primary spermatocytes). The perturbation of *Prdm9* function observed in sterile hybrid males corresponds to the phenotype of the *Prdm9*^{-/-} mutants.

The genes that reduce hybrid fitness because of their divergent evolution can be the cause or the consequence of speciation, depending on whether they evolved before or after the complete reproductive isolation of the studied taxa (25, 26). The advantage of our mouse model is that reproductive isolation of *Mmm* and *Mmd* is still incom-

plete. Thus, *Prdm9* may be an essential component of a Dobzhansky–Muller incompatibility that is part of an incipient speciation event. It can lead us to the Dobzhansky–Muller incompatibility gene(s) that interferes with the normal meiotic function of histone H3K4 methyltransferase. The meiosis-specific function of *Prdm9* can explain the breakdown of meiotic cells with no effect on somatic tissues in intersubspecific hybrids. Uncovering *Prdm9* as a hybrid sterility gene will permit us to search for the epigenetically regulated downstream genes and their role in the hybrid sterility gene network.

References and Notes

1. T. Dobzhansky, in *Genetics and the Origin of Species* (Columbia Univ. Press, New York, 1951).
2. H. A. Orr, *Proc. Natl. Acad. Sci. U.S.A.* **102** (suppl. 1), 6522 (2005).
3. J. Haldane, *J. Genet.* **12**, 101 (1922).
4. C.-T. Ting, S. Tsaur, M. Wu, C. Wu, *Science* **282**, 1501 (1998).
5. J. P. Masly, C. D. Jones, M. A. Noor, J. Locke, H. A. Orr, *Science* **313**, 1448 (2006).
6. J. Forejt, P. Ivanyi, *Genet. Res.* **24**, 189 (1974).
7. J. M. Good, M. A. Handel, M. W. Nachman, *Evolution Int. J. Org. Evolution* **62**, 50 (2008).
8. S. Gregorova, J. Forejt, *Folia Biol. (Praha)* **46**, 31 (2000).
9. H. Yang, T. A. Bell, G. A. Churchill, F. Pardo-Manuel de Villena, *Nat. Genet.* **39**, 1100 (2007).
10. J. Forejt, *Trends Genet.* **12**, 412 (1996).
11. S. Gregorova et al., *Mamm. Genome* **7**, 107 (1996).
12. Z. Trachtulec et al., *Mamm. Genome* **8**, 312 (1997).
13. Z. Trachtulec et al., *Biol. J. Linn. Soc. London* **84**, 637 (2005).
14. O. Mihola, J. Forejt, Z. Trachtulec, *BMC Genomics* **8**, 20 (2007).
15. Z. Trachtulec et al., *Genetics* **178**, 1777 (2008).
16. K. Osogawa et al., *Genome Res.* **10**, 116 (2000).
17. Materials and methods are available as supporting material on Science Online.
18. K. Hayashi, K. Yoshida, Y. Matsui, *Nature* **438**, 374 (2005).
19. J. Forejt, in *Current Trends in Histocompatibility*, R. Reisfeld, S. Ferrone, Eds. (Plenum, New York, 1981), vol. 1, pp. 103–131.
20. A. Yoshiki, K. Moriwaki, T. Sakakura, M. Kusakabe, *Dev. Growth Differ.* **35**, 271 (1993).
21. L. A. Bannister et al., *PLoS Biol.* **5**, e105 (2007).
22. S. Gregorova et al., *Genome Res.* **18**, 509 (2008).
23. R. Storchova et al., *Mamm. Genome* **15**, 515 (2004).
24. N. J. Briede et al., *Science* **314**, 1292 (2006).
25. R. Lewontin, *The Genetic Basis of Evolutionary Change* (Columbia Univ. Press, New York, 1974).
26. H. A. Orr, D. C. Presgraves, *Bioessays* **22**, 1085 (2000).
27. We thank M. Nachman (University of Arizona), K. Paigen (The Jackson Laboratory), and D. Barbash (Cornell University) for valuable comments. We are grateful to P. Jansa for advice with the immunofluorescence and P. Flachs for assistance. This work was funded by the Czech Science Foundation, the Grant Agency of the Academy of Sciences of the Czech Republic and the Ministry of Education, Youth and Sports of the Czech Republic (J.F. and Z.T.), and a grant from NIH (J.C.S.). J.F. was an International Fellow of the Howard Hughes Medical Institute.

Supporting Online Material

www.sciencemag.org/cgi/content/full/1163601/DC1

Materials and Methods

Figs. S1 to S5

Tables S1 and S2

References

22 July 2008; accepted 21 October 2008

Published online 11 December 2008;

10.1126/science.1163601

Include this information when citing this paper.

A Single Gene Causes Both Male Sterility and Segregation Distortion in *Drosophila* Hybrids

Nitin Phadnis* and H. Allen Orr

A central goal of evolutionary biology is to identify the genes and evolutionary forces that cause speciation, the emergence of reproductive isolation between populations. Despite the identification of several genes that cause hybrid sterility or inviability—many of which have evolved rapidly under positive Darwinian selection—little is known about the ecological or genomic forces that drive the evolution of postzygotic isolation. Here, we show that the same gene, *Overdrive*, causes both male sterility and segregation distortion in F_1 hybrids between the Bogota and U.S. subspecies of *Drosophila pseudoobscura*. This segregation distorter gene is essential for hybrid sterility, a strong reproductive barrier between these young taxa. Our results suggest that genetic conflict may be an important evolutionary force in speciation.

Segregation distorters (also called transmission ratio distorters) are selfish genetic elements that manipulate Mendelian transmission to their own advantage. Because they are inherited by more than 50% of functional gametes, such distorters can spread rapidly through populations. Natural selection, however, favors the suppression of distortion, especially if the distorter locus resides on a sex chromosome and biases sex ratios. Theory predicts that mutations suppressing segregation distortion will invade populations once distorter alleles are at a high frequency or are fixed (1, 2). Bouts of distortion and suppression could occur repeatedly and often. If suppressors of distortion are less than fully dominant, segregation distortion may reappear in F_1 hybrids between species. And because segregation distorters often act by destroying gametes (3), such reexpression could result in hybrid sterility (4, 5). The idea that intragenomic conflict involving segregation distorters may cause hybrid sterility is controversial (4–9). Although it can explain both the observed rapid evolution of most hybrid incompatibility genes (10–15) and the preferential sterility of the heterogametic sex [an aspect of Haldane's rule (16)], direct empirical evidence is scarce [(17) but see (8)].

Drosophila pseudoobscura pseudoobscura and *Drosophila pseudoobscura bogotana* (hereafter USA and Bogota, respectively) are allopatric subspecies that diverged just 155,000 to 230,000 years ago (18). Crosses between Bogota females and USA males produce F_1 hybrid males that are nearly completely sterile, whereas all other F_1 hybrids are fertile (19). Hybrid sterility appears to involve a single complex genetic incompatibility, in which several loci are essential for the expression of full sterility. Bogota alleles at loci on the right and left arms of the X chromosome (XR and XL, respectively) interact with dominant

USA alleles on the second and third autosomes to cause hybrid sterility (20). Because these genes are essential for hybrid sterility, they could not have evolved after the attainment of complete reproductive isolation. These genes may therefore be important components of ongoing speciation.

When aged, F_1 hybrid males (previously thought to be completely sterile) become weakly fertile. These hybrid males produce progeny that are almost all daughters (21). This sex-ratio distortion is not caused by hybrid inviability but by an overrepresentation of X-bearing sperm among functional gametes; consequently, X-bearing sperm from F_1 hybrid males fertilize more eggs than do Y-bearing sperm (21). The precise mechanism of

segregation distortion may involve true meiotic drive (which acts during meiosis) or gamete killing or inactivation (which acts after meiosis); in either case, the X chromosome carrying this segregation distorter enjoys a selective advantage.

Male sterility and segregation distortion in Bogota-USA hybrids both map to the same chromosomal regions, and these regions show a similar pattern of complex epistasis for both phenotypes (20, 21). A region on the Bogota XR that is tightly linked to the visible mutation *sepia* (*se*, XR-156.6) was identified as playing a large and essential role in both hybrid male sterility and hybrid segregation distortion. We tested if the same genes cause hybrid sterility and hybrid segregation distortion by genetically dissecting the *sepia* region.

We generated 175 independent introgression lines in which the USA *sepia* region was moved into an otherwise pure Bogota background by backcrossing to the Bogota subspecies for 28 generations (14 of which involved recombination) (Fig. 1A) (22). The resulting introgression lines have genomes that derive almost entirely from Bogota, except for a small chromosomal region near *sepia*. We tested each introgression line for hybrid sterility and segregation distortion by crossing females from these introgression lines with USA males. The resulting hybrid males should be genetically identical to F_1 hybrid males, except for the small chromosomal region introgressed from USA. All 175 lines yielded hybrid males that were both fertile and produced normal (~50:50) sex ratios (Fig. 1B and figs. S1 and S2). This suggests that hybrid sterility and hybrid segregation distortion are caused either by

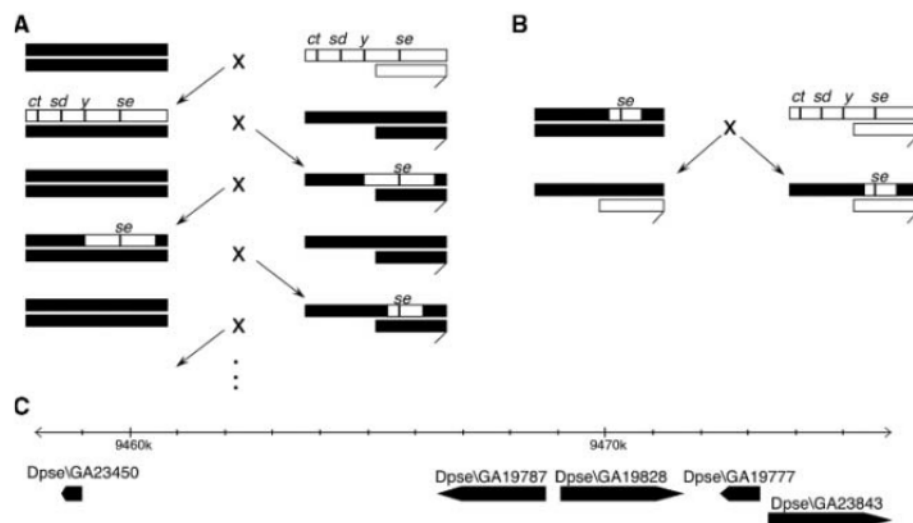


Fig. 1. (A) The *sepia* region of the USA X-chromosome was introduced into an otherwise pure Bogota background by using a crisscross design; recombination occurs in females, and the visible marker *sepia* was selected in males. Bogota material is black and USA material is white. Females have two X chromosomes, and males have one X chromosome and one Y chromosome (denoted by a hook). (B) When crossed with USA males, heterozygous introgression females produce two types of hybrid males. All *sepia* introgression hybrid males were fertile and showed normal segregation, whereas control F_1 hybrid males were mostly sterile and showed segregation distortion, as expected. (C) Hybrid sterility and segregation distortion both mapped to a region spanning ~20 kb that included five predicted genes, of which *GA19777* is the fastest evolving.

Department of Biology, University of Rochester, Rochester, NY 14627-0211, USA.

*To whom correspondence should be addressed. E-mail: pdns@mail.rochester.edu

tightly linked genes or by the same genes (or genes) in the region.

We genotyped all introgression lines using 41 microsatellite and 44 single-nucleotide polymorphism-based diagnostic markers [supporting online material (SOM) text]. The introgression breakpoints defined a region around *sepia* that harbors the hybrid sterility and hybrid segregation distortion genes (or genes). To isolate recombinants between the *sepia* locus and the hybrid sterility locus (recombinants that we did not recover above), we crossed Bogota females heterozygous for an introgression with USA males and tested *se*⁺ males for their ability to produce progeny. We found one such fertile *se*⁺ male. Analysis of flies derived from this recombinant showed that such males produce ~50:50 male:female progeny (fig. S3). Genotyping revealed that the gene (or genes) causing hybrid sterility and hybrid segregation distortion is located to the left of *sepia*. Together, the introgression and fertile *se*⁺ recombinant lines (which provided left and right breakpoints, respectively) localized the gene (or genes) causing hybrid sterility and hybrid segregation distortion to a ~20-kb region that contains five predicted genes (Fig. 1C).

No functional data are available from *Drosophila melanogaster* for the homologs of these genes. We sequenced the entire ~20-kb region from

the Bogota subspecies and compared it to the homologous USA sequence from the *D. pseudoobscura pseudoobscura* genome (23). We found no duplication, deletion, or obvious rearrangement differences between the subspecies in this region. But one of the predicted genes in the region, *GA19777*, shows eight nonsynonymous changes, which is surprising given its small coding region [591 base pairs (bp), excluding one 74-bp intron] (table S1). Given that genes causing reproductive isolation often evolve rapidly, *GA19777*, which contains a DNA-binding motif, represented our best candidate for the cause of hybrid sterility and/or hybrid segregation distortion.

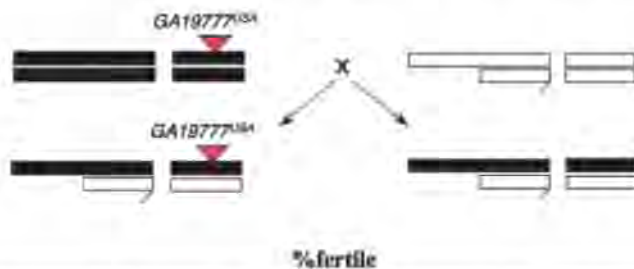
To determine whether *GA19777* causes these hybrid phenotypes, we first attempted to rescue the fertility of F₁ hybrid males with a transgenic copy of the (fertile) USA allele of *GA19777* (*GA19777*^{USA}). We cloned *GA19777*^{USA} along with ~0.2 kb of upstream and ~1.2 kb of downstream sequence into a *CaSpeR-4* P-element vector. The plasmid *P*₁^{w⁺}; *GA19777*^{USA}, which carries a *D. melanogaster* miniwhite gene, was injected in Bogota-ER white embryos, and transformants were identified by wild-type eye color. When crossed with USA white males, Bogota females heterozygous for *P*₁^{w⁺}; *GA19777*^{USA} produced two types of hybrid sons: those that inherited a transgenic *GA19777*^{USA} along with the endogenous Bogota

allele of *GA19777* (*GA19777*^{BOG}) (genotype *GA19777*^{BOG}/Y; *GA19777*^{USA}) and those that inherited only the endogenous *GA19777*^{BOG} allele (genotype *GA19777*^{BOG}/Y). The strength of fertility rescue in these experiments, if any, would thus depend on dominance relations between *GA19777*^{BOG} and the *GA19777*^{USA} transgene. Sperm motility assays showed that hybrid males that inherited the *GA19777*^{USA} transgene were more fertile than those that inherited only the endogenous *GA19777*^{BOG} regardless of the transgenic line studied (Fig. 2). We also crossed males with Bogota white females and found that hybrid males that inherited the *GA19777*^{USA} transgene produced progeny significantly more often than males that inherited only the endogenous *GA19777*^{BOG}, although fertility rescue was weak (Table 1). On the basis of these results, we conclude that *GA19777* plays a role in hybrid male sterility.

Surprisingly, *GA19777*^{USA} transgenic hybrids still produced almost all daughters (Table 1). *GA19777*^{USA} transgenes do not, therefore, suppress segregation distortion. This result can be explained in at least two ways: *GA19777* might cause hybrid sterility but not hybrid segregation distortion, or *GA19777* might cause both hybrid sterility and hybrid segregation distortion but each phenotype has different penetrance or degree of dominance (for example, with *GA19777*^{BOG} having more dominant effects on hybrid segregation distortion and more recessive effects on hybrid sterility).

To distinguish these possibilities, we performed a second transgenic experiment. In particular, we tested whether transgenic *GA19777*^{BOG} can induce segregation distortion. To do so, we cloned *GA19777*^{BOG} to the same length and coordinates as *GA19777*^{USA} and transformed USA and Bogota white strains with *P*₁^{w⁺}; *GA19777*^{BOG}. As expected, no sterility or segregation distortion appeared in our transformed pure subspecies strains because such individuals lack the partner genes required for the hybrid incompatibility.

We tested whether *P*₁^{w⁺}; *GA19777*^{BOG} can cause segregation distortion in hybrid sons produced by crossing introgression females to USA males. These sons carry all partner loci necessary for the appearance of hybrid problems (Bogota XL and USA autosomes) except for the Bogota factor (or factors) linked to *sepia* and are therefore fertile and nondistorting. We used females from a single introgression line (line104), which carries the smallest USA introgression near *sepia*. When crossed with USA males carrying *P*₁^{w⁺}; *GA19777*^{BOG}, introgression females produced two types of hybrid sons: those that inherited a transgenic *GA19777*^{BOG} along with the endogenous *GA19777*^{USA} (genotype *GA19777*^{USA}/Y; *GA19777*^{BOG}) and those that inherited only endogenous *GA19777*^{USA} (genotype *GA19777*^{USA}/Y) (Fig. 3). Hybrid males that inherited the *GA19777*^{BOG} transgene produced a strikingly female-biased sex ratio when crossed with Bogota white females, whereas control males that inherited only endogenous *GA19777*^{USA} produced normal (~50:50) sex ratios (Fig. 3).



	%fertile			
USA1-1	74 (N =155)	25 (N =130)	P = 7.18E-55	
USA1-2	91 (N =113)	24 (N =111)	P = 1.16E-62	
USA1-7	79 (N =128)	20 (N =123)	P = 4.43E-67	

Fig. 2. *P*₁^{w⁺}; *GA19777*^{USA} rescues fertility in F₁ hybrid males, as measured blind in a sperm motility assay. Three independent transgenic strains were tested; the total number of males tested per genotype is denoted by *N*. The two genotypes are identical except for the presence or absence of the construct. *P* values were calculated using χ^2 tests with one degree of freedom. Red triangles indicate the inserted transgene.

Table 1. *P*₁^{w⁺}; *GA19777*^{USA} rescues hybrid fertility but does not suppress segregation distortion. The transgene strains we used were the same as in Fig. 2. The two genotypes shown for each line are identical except for the presence or absence of the construct. Hybrid males producing one or more progeny (or no progeny) were classified as fertile (or sterile). We used a χ^2 test with one degree of freedom. SE values are shown in parentheses.

Line	Genotype	Fertile	Sterile	P value	Mean progeny	Females (%)
USA1-1	w ⁺	80	140	2.37E-42	2.123 (0.33)	95.37 (1.5) n = 80
	w	7	174		0.304 (0.13)	90.80 (6.91) n = 7
USA1-2	w ⁺	87	147	1.60E-62	2.490 (0.42)	94.90 (1.10) n = 87
	w	0	254		0.000	n = 0
USA1-7	w ⁺	56	146	6.02E-58	1.327 (0.24)	94.77 (2.01) n = 56
	w	2	206		0.024 (0.04)	75.00 (25.07) n = 2

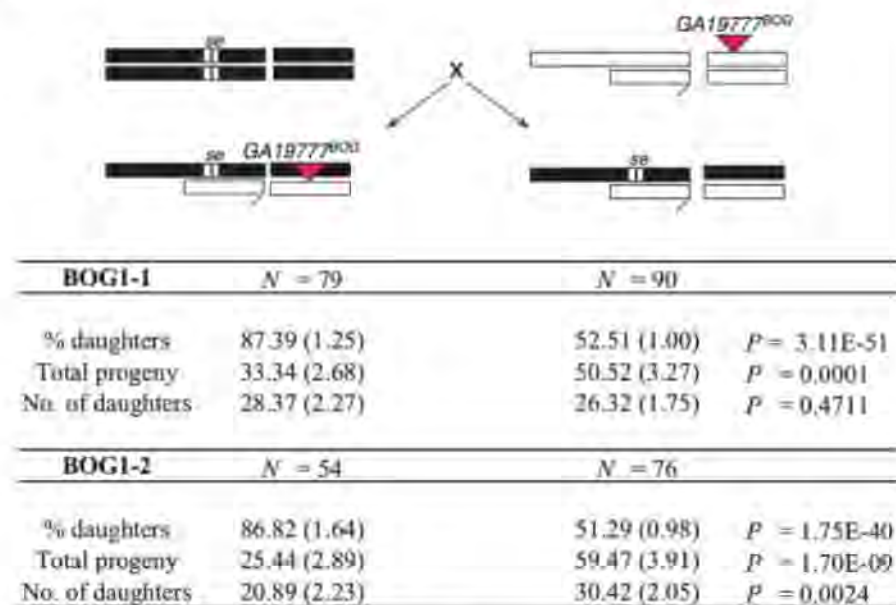


Fig. 3. $P\{w^+; GA19777^{BOG}\}$ induces segregation distortion in *sepia* introgression hybrid males. *Sepia* introgression hybrid males that inherit the $P\{w^+; GA19777^{BOG}\}$ transgene show significantly female-biased progeny as compared with those of males that do not inherit the transgene (when crossed with *Bogota white* females). The two genotypes are identical except for the presence or absence of the construct. Segregation distortion is also accompanied by a reduction in the total number of progeny and, in the case of BOG1-2, in the number of daughters produced. Two independent transgenic strains (BOG1-1 and BOG1-2) were tested; N denotes the number of fathers tested per genotype; mean values along with SE (in parentheses) are reported. P values were calculated using analysis of variance. Transgene males were inferred from the presence of w^+ individuals among F_1 and F_2 progeny. We modified the cross for the transgenic *Bogota* strain (BOG1-2): We first crossed introgression females with *Bogota* males carrying $P\{w^+; GA19777^{BOG}\}$ and collected female progeny. When crossed with USA *white* males, these females produced two types of hybrid sons: those that inherit a transgenic $GA19777^{BOG}$ along with endogenous $GA19777^{USA}$ and those that inherit only endogenous $GA19777^{USA}$. With both BOG1-1 and BOG1-2, transgenic hybrid males produced (rare) *white* and wild-type sons in roughly equal numbers, showing that sex ratio distortion is not due to transgene-induced male lethality.

Thus, *GA19777* plays a role in hybrid segregation distortion.

GA19777 is predicted to encode a polypeptide with a single Myb/SANT-like domain in Adf-1 (MADF) DNA-binding domain near its C terminus end. Reverse transcription polymerase chain reaction revealed that *GA19777* is expressed in the testes of both pure subspecies males and in sterile F_1 hybrid males (fig. S4). The constructs from the transgene experiments caused sex-chromosome segregation distortion and rescue of fertility even when located on autosomes, showing that transgenes have an effect in *trans* with respect to the sex chromosomes (table S2). *GA19777* therefore appears to act through its encoded product and not through *cis* chromosome effects. Further controls (fig. S5) showed that the segregation distortion/sterility effects of transgenes are not an artifact of gene dosage but depend on the species identity of the transgene.

The segregation distortion effect of *GA19777^{BOG}* appears to reflect single-nucleotide substitutions that have occurred since the *Bogota* and USA subspecies split. In contrast, other known distorter genes involve gene duplications (24–26). The segregation distortion caused by *GA19777* is suppressed in pure *Bogota* individuals not be-

cause such individuals carry an insensitive Y chromosome [the *Bogota* Y can in fact be driven (21)] but because they are homozygous for recessive autosomal suppressors (21). Given its role in both segregation distortion (meiotic drive) and hybrid sterility, we named *GA19777 Overdrive (Ovd)*.

To study *Ovd*'s evolutionary history, we sequenced nine additional lines of *Bogota* and 16 of USA and found that seven of the eight nonsynonymous differences initially identified are fixed in the sample, whereas the remaining one (at position 61) is polymorphic within *Bogota*. Because *Bogota* strains lacking this segregating difference produce hybrids that are mostly sterile with segregation distortion (21), the change at position 61 does not seem essential for hybrid sterility or segregation distortion. We tested if *GA19777* experienced recurrent positive selection by performing a McDonald-Kreitman test (27); we also tested if *GA19777* experienced a recent selective sweep by calculating Tajima's D (28). These tests showed no significant departures from the null hypothesis of neutrality (SOM text). This result may reflect a lack of power due to unusually low polymorphism in both subspecies (SOM text), little divergence between these taxa, or possibly neutral evolution at *Ovd*.

Outgroup analysis with *D. miranda* and *D. persimilis* showed that all seven nonsynonymous changes and five synonymous changes fixed between *Bogota* and USA occurred in the *Bogota* lineage. Further analysis showed that rates of nonsynonymous and synonymous evolution are accelerated in the *Bogota* lineage relative to those expected given the species tree ($P = 7.7 \times 10^{-6}$ for nonsynonymous, $P = 0.0007$ for synonymous) (SOM text). A test for accelerated evolution [ratio of nonsynonymous/synonymous DNA changes (K_a/K_s)] in the *Bogota* lineage using PAML (<http://abacus.gene.ucl.ac.uk/software/paml.html>) was, however, nonsignificant ($P = 0.89$) (table S3), probably reflecting accelerated evolution at both nonsynonymous and synonymous sites in *Bogota*.

Our results show that the same gene, *Ovd*, affects both F_1 segregation distortion and hybrid sterility in evolutionarily young taxa that obey Haldane's rule. Although our results do not prove a history of segregation distortion in *D. pseudoobscura*, our results are consistent with and suggestive of such a history, especially given the burst of substitutions at *Ovd* in the *Bogota* lineage. Although evolutionary biologists usually explain the evolution of reproductive isolation as a side effect of adaptation to the ecological environment, our findings support the idea that genetic conflict, a form of adaptation to the internal genomic environment, may also be an important force in the evolution of postzygotic isolation.

References and Notes

1. D. L. Hartl, *Theor. Popul. Biol.* **7**, 168 (1975).
2. D. W. Hall, *Evolution* **58**, 925 (2004).
3. T. W. Lytle, *Annu. Rev. Genet.* **25**, 511 (1991).
4. S. A. Frank, *Evolution* **45**, 262 (1991).
5. L. D. Hurst, A. Pomiankowski, *Genetics* **128**, 841 (1991).
6. B. Charlesworth, J. A. Coyne, H. A. Orr, *Genetics* **133**, 421 (1993).
7. J. A. Coyne, H. A. Orr, *Evolution* **47**, 685 (1993).
8. Y. Tao, D. L. Hartl, C. C. Laurie, *Proc. Natl. Acad. Sci. U.S.A.* **98**, 13183 (2001).
9. S. Henikoff, K. Ahmad, H. S. Malik, *Science* **293**, 1098 (2001).
10. D. A. Barbash, D. F. Siino, A. M. Tarone, J. Roote, *Proc. Natl. Acad. Sci. U.S.A.* **100**, 5302 (2003).
11. J. Wittbrodt, R. Lammers, B. Malitschek, A. Ullrich, M. Scharl, *EMBO J.* **11**, 4239 (1992).
12. C. T. Ting, S. C. Tsaur, M. L. Wu, C. I. Wu, *Science* **282**, 1501 (1998).
13. D. C. Presgraves, L. Balagopalani, S. M. Abmayr, H. A. Orr, *Nature* **423**, 715 (2003).
14. J. P. Masly, C. D. Jones, M. A. F. Noor, J. Locke, H. A. Orr, *Science* **313**, 1448 (2006).
15. N. J. Bideau et al., *Science* **314**, 1292 (2006).
16. J. B. S. Haldane, *J. Genet.* **12**, 101 (1922).
17. J. A. Coyne, H. A. Orr, *Speciation* (Sinauer Associates, Sunderland, MA, 2004).
18. S. W. Schaeffer, E. L. Miller, *Proc. Natl. Acad. Sci. U.S.A.* **88**, 6097 (1991).
19. S. Prakash, *Genetics* **72**, 143 (1972).
20. H. A. Orr, S. Irving, *Genetics* **158**, 1089 (2001).
21. H. A. Orr, S. Irving, *Genetics* **169**, 671 (2005).
22. Materials and methods are available as supporting material on Science Online.
23. S. Richards et al., *Genome Res.* **15**, 1 (2005).
24. C. Merrill, L. Bayraktaroglu, A. Kusano, B. Ganetzky, *Science* **283**, 1742 (1999).
25. Y. Tao et al., *PLoS Biol.* **5**, 2576 (2007).
26. C. Montchamp-Moreau, D. Ogereau, N. Chaminade, A. Colard, S. Aulard, *Genetics* **174**, 1365 (2006).

27. J. H. McDonald, M. Kreitman, *Nature* **351**, 652 (1991).
 28. F. Tajima, *Genetics* **123**, 585 (1989).
 29. We thank C. Aquadro, J. Fry, R. Glor, H. Malik, D. Presgraves, Y. Tao, and the Orr lab for discussions; D. Lambert for advice on molecular techniques; H. Malik and N. Elde for help with PAML; and S. Schaeffer for fly stocks. Financial support was provided by NIH (GM51932). All sequences are available at GenBank

(accession numbers FJ349335 to FJ349342 and FJ418600 to FJ418631). The authors declare no conflict of interest.

Supporting Online Material

www.sciencemag.org/cgi/content/full/1163934/DC1
 Materials and Methods
 SOM Text

Figs. S1 to S7
 Tables S1 to S9
 References

29 July 2008; accepted 7 November 2008
 Published online 11 December 2008;
 10.1126/science.1163934
 Include this information when citing this paper.

The Dynamics and Time Scale of Ongoing Genomic Erosion in Symbiotic Bacteria

Nancy A. Moran,^{1*} Heather J. McLaughlin,¹ Rotem Sorek²

Among cellular organisms, symbiotic bacteria provide the extreme examples of genome degradation and reduction. However, only isolated snapshots of eroding symbiont genomes have previously been available. We documented the dynamics of symbiont genome evolution by sequencing seven strains of *Buchnera aphidicola* from pea aphid hosts. We estimated a spontaneous mutation rate of at least 4×10^{-9} substitutions per site per replication, which is more than 10 times as high as the rates previously estimated for any bacteria. We observed a high rate of small insertions and deletions associated with abundant DNA homopolymers, and occasional larger deletions. Although purifying selection eliminates many mutations, some persist, resulting in ongoing loss of genes and DNA from this already tiny genome. Our results provide a general model for the stepwise process leading to genome reduction.

Obligate symbionts and pathogens, which have evolved repeatedly from free-living bacterial ancestors, show striking convergence in fundamental genomic features. In several symbionts of insects, most ancestral genes are eliminated by deletion, resulting in some of the smallest known cellular genomes (1–4). Symbionts also display rapid evolution at both the DNA and peptide sequence levels and have highly biased nucleotide base com-

positions, with elevated frequencies of adenine and thymine (A+T). Because these genomes are asexual and do not acquire foreign DNA, each gene loss is irreversible (2, 5–7). These genomic features have been ascribed to increases in genetic drift associated with a host-restricted life-style (8, 9) and, potentially, to an increased mutation rate and biased mutational profile stemming from the loss of DNA-repair genes, which are among the gene categories most depleted in symbiont genomes (1, 10).

Although numerous sequenced examples of reduced genomes in obligate symbionts or pathogens are available, these are too distantly related to permit stepwise reconstruction of genomic changes. As a result, the dynamics of

ongoing genomic erosion, the extent to which mutation rate is elevated, the effectiveness of natural selection in purging mutations, and the nature of the mutational events that lead to further loss of DNA and metabolic functions are unclear. To illuminate these evolutionary processes, we sequenced several closely related genomes of the obligate symbiont *Buchnera aphidicola* from a single host species, the pea aphid *Acyrtosiphon pisum* (*Buchnera-Ap*). A previously sequenced genome of *Buchnera-Ap* showed a gene set typical for an obligate symbiont (1) lacking most ancestral genes, including genes underlying transcriptional regulation, biosynthesis of cofactors present in hosts, DNA repair, and other processes. The 607 retained genes encode machinery for replication, transcription, translation, and other essential processes, as well as biosynthetic pathways for essential amino acids required by hosts (1).

A. pisum is native to Eurasia, but has been introduced worldwide. It was first detected in North America in the 1870s (11). We sequenced the genomes of seven *Buchnera-Ap* strains descended from two colonizers of North America (and hence diverging up to 135 years ago), including two strains diverging in the laboratory for 7.5 years. Solexa sequencing was combined with verification by Sanger sequencing (12), to determine genomic sequences of these seven strains (Table 1). A total of 2392 positions (0.3% of sites on the 641-kb chromosome) showed a nucleotide substitution. These single-nucleotide polymorphisms (SNPs) were distributed approximately evenly around the chromosome (fig. S1). We also detected a total of 149 insertion or deletion events (indels): 134

¹Department of Ecology and Evolutionary Biology, University of Arizona, Tucson, AZ 85721, USA. ²Department of Molecular Genetics, Weizmann Institute of Science, Rehovot 76100, Israel.

*To whom correspondence should be addressed. E-mail: nmoran@email.arizona.edu

Table 1. Description of sequence data.

	Tuc7	9-2-1	8-10-1	8-10-1	A2A	5AR	5A	7A
Source locality, year	Tucson AZ, 1999	Cayuga Co NY, 2001	Cayuga Co NY, 2001	Cayuga Co NY, 2001	Logan UT, 2003	Derived from 5A, 2000	Madison WI, 1999	Cayuga Co NY, 2000
Average read size	39	36	39	36	39	36	39	39
No. of initial reads	3,185,491	11,293,714	9,064,851	20,653,949	9,224,134	9,615,693	8,227,047	18,234,517
No. of reads mapped	1,024,330	6,731,726	4,432,760	12,977,253	7,088,978	6,944,135	4,448,342	12,150,323
Percent reads mapped*	32.16	59.61	48.90	62.83	76.85	72.22	54.07	66.63
Fold genome coverage (average)	57.9	369.9	259.4	700.5	412.2	374.6	256.0	661.1

*Unmapped reads represent contaminating DNA, largely from the host genome.

single-base indels, 12 indels of 2 to 16 bases, and 3 large deletions (220 to 1131 bases), also dispersed around the genome (fig. S1).

Parsimony analysis of SNPs yielded a single phylogenetic tree with no homoplasy, as expected for clonal lineages if each base substitution is a singular event (Fig. 1A). Indels showed almost no homoplasy; all but two mapped as single events (Fig. 1B). The newly sequenced genomes comprised two tight clusters that were divergent from each other and even more divergent from the reference strain, Tokyo1998 (Fig. 1A). Rooting the phylogeny on the branch leading to Tokyo1998 enabled us to assign direction of change for both base changes and indels on the lineages leading to the two clusters.

We inferred that the two clusters consist of descendants of two separate female colonizers, each arriving in North America sometime after 1870, by constructing a phylogeny on the basis of a 1.1-kb DNA fragment from 38 *Buchnera-Ap* samples collected in America, Asia, and Europe (12). The clades corresponding to these two clusters contain the large majority of North American samples, but are absent (Cluster 2) or rare (Cluster 1) among samples from Eurasia, where diverse lineages are present (fig. S2). Thus, we dated the common ancestor of each cluster representing an introduced matriline to a maximum of 135 years ago. Averaging the pairwise divergences through the ancestral node of each cluster, we calculated rates of nucleotide substitution of 19 SNPs per genome per

270 years for each U.S. haplotype cluster (divergence times are doubled to derive the rate along a single evolving lineage). After pooling the observed changes, we estimated the rate as 0.70 substitutions per genome per decade [95% confidence interval (CI): 0.51 to 0.97 substitutions per genome per decade], or 1.1×10^{-7} substitutions per site per year (95% CI: 0.8 to 1.5×10^{-7} substitutions per site per year). The rate is doubled (2.2×10^{-7} ; 95% CI: 1.4 to 3.3×10^{-7} substitutions per site per year) if calculated on the basis of changes at intergenic spacers and synonymous sites, that is, genomic sites that generally can tolerate mutations with little effect on fitness and that are thus expected to approximate the mutation rate (Table 2) (12). Adjusting for *Buchnera* replications per year [by estimating *Buchnera* divisions per aphid generation and aphid generations per year (13)] gives an estimate of 4×10^{-9} substitutions per site per replication.

Our estimated mutation rate for base changes was unexpectedly high: more than 10 times the previous estimates of mutation rate in *Buchnera*, from genome pairs diverging 60 million years ago, were lower, those calculations were unreliable because intergenic spacers were too divergent to allow alignment and because silent sites underwent too many substitutions for accurate estimation of divergence (5).

This rate calibration can be used to estimate divergence times of older lineages of *Buchnera-Ap* used in this study. If the root of the tree is on the branch leading to the Tokyo1998 strain, we calculated that the lineage leading to the two clusters we sequenced (showing an average divergence of 1617 substitutions per genome) diverged from the Tokyo1998 strain 11,489 (95% CI: 8340 to 15,790) years ago. Calculations made only on the basis of intergenic spacers and synonymous changes gave similar estimates [12,555 (95% CI: 8292 to 20,030) years].

We next considered trends in nucleotide-composition bias. A distinctive feature of most small bacterial genomes is an elevated A+T content, reflecting biased mutational patterns. Our data show no evidence of continued evolution toward increased A+T content in *Buchnera-Ap*. The 50 substitutions in the terminal branches of the tree had little effect on base composition, with 21 increasing, 31 decreasing, and 6 not affecting A+T content (Fig. 1A). For the 1423 substitutions on the branches leading to the two clusters, base composition was in near-equilibrium, with 47% decreasing and 48% increasing overall G+C content. This implies that the overall genomic base composition near 25% G+C is an approximate equilibrium, consistent with a mutation rate from G/C to A/T that is three times as high as that for A/T to G/C (Fig. 2C) (14). However, this equilibrium could be disturbed if additional DNA repair functions are lost.

To estimate the effect of purifying selection on the ongoing evolution of *Buchnera-Ap* genomes, we analyzed base substitutions in coding regions. On the basis of the genome-wide frequencies of mutation types acting on each base (Fig. 2C) and codon frequencies calculated for the entire *Buchnera-Ap* genome, mutations causing amino acid replacements are expected to arise 4.5 times as often as those affecting only codon choice (12). But only 36% of observed substitutions were replacement substitutions, giving a per-site ratio of replacement to silent changes (dN/dS) of 0.125 and implying that most mutations affecting polypeptide sequence are purged by selection. Purifying selection was also evident from the concentration of indels in intergenic spacers, which are largely selectively neutral regions sometimes recognizable as eroding pseudogenes (5). Of 146 small indels, 134 (92%) occur in intergenic spacers, which constitute only 13.5% of the genome. The SNP-to-indel ratio is 3.1 in spacers and 166.4 in coding regions (Table 2). This paucity of indels within coding genes reflects the fact that most indels cause frameshifts, leading to dysfunctional protein products, and are eliminated by selection. Indeed, 11 of 12 indels observed in coding regions imposed frameshifts. Thus, during the evolution of these *Buchnera-Ap* lineages, an estimated 82% of new indels have been purged by selection.

To determine whether genome erosion is ongoing in the closely related genomes that we sequenced, we addressed whether the 146 detected indels contributed to genome reduction. Our findings indicate that small indels do not directly cause DNA loss in *Buchnera*, because

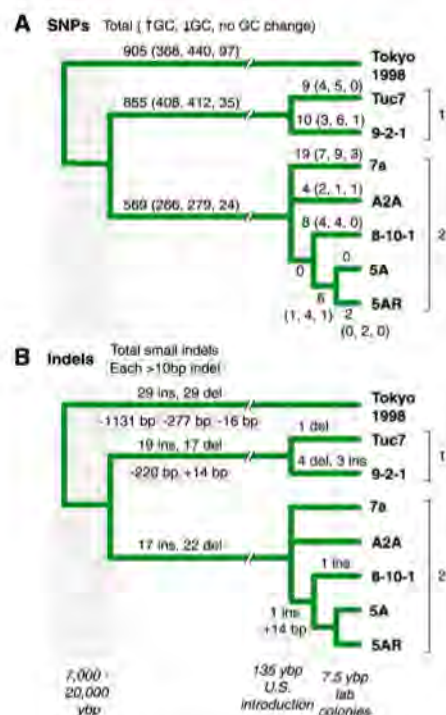


Fig. 1. A maximum-parsimony tree showing the evolutionary reconstruction of phylogenetic relationships and changes in the genomes of *Buchnera-Ap* strains. (A) Single-nucleotide substitutions. (B) Small and large insertion and deletions.

Table 2. Mutational patterns in genomes of *Buchnera* symbionts of pea aphids, from all base changes and insertion/deletion events, of Fig. 1.

	SNPs	SNPs/kb	Small indels	Indels/kb	SNP/indel ratio
Protein-coding	1997	3.6	12	0.02	166.4
Intergenic spacer	395	4.6	130	1.50	3.1
Total	2392	3.7	142	0.22	16.8

small deletions were balanced by small insertions on all branches of the tree, regardless of root position (Fig. 1B). But three large deletions did effect a net DNA loss: (i) a 220-base pair (bp) deletion in the *znuC-pyxA* spacer in the lineage leading to Cluster 1; (ii) a 277-bp deletion in the *gapA-fidA* spacer in the lineage leading to Tokyo1998; and (iii) a 1131-bp deletion corresponding to part of the gene *yaeT* and the entire sequence of the gene *fabZ*, also in the lineage leading to Tokyo1998. All large deletions corresponded to positions of extra genes (*znuA-yebA*, *queF*, and *fabZ*) in the *Buchnera-Schizaphis graminum* genome (5), suggesting that the detected deletions eliminated relics of these genes from the *Buchnera-Ap* genomes. No large insertions were identified, consistent with previous evidence that *Buchnera* does not acquire foreign genes (2, 5, 6). Together these three deletions account for a loss of 1625 nucleotides (Fig. 1B). This corresponds to DNA loss at a rate of roughly 1 kb per 10,000 years, although this estimate is subject to a high error rate due to the small number of large deletions observed.

We next studied whether ongoing loss of functional genes has occurred during the divergence of the *Buchnera-Ap* genomes. We observed 16 genes that appear to be inactivated, either through a 1- to 2-base indel causing a frameshift (11 genes), a base substitution generating a stop codon (three genes), or a large deletion (one event, two genes) (table S1). Functions of these genes include DNA repair (*ung*, *sbcB*), biosynthesis potentially affect-

ing host amino acid or vitamin nutrition (*argC*, *trpB*, *ghyA*, *ribD2*), fatty acid biosynthesis (*fabZ*), or cell envelope production (*murF*), and genes involved in transport (*ynfM*) or secretion (*fliK*, *flgB*) (table S1). Genes in these functional categories have been noted to undergo degradation or loss in distantly related strains of *Buchnera* and other obligate symbionts (2, 5, 6). Such losses could influence further genomic evolution (by affecting mutation), as well as the ability to provision hosts. Genes with frameshift mutations may retain partial functionality, through production of some in-frame transcripts due to slippage of RNA polymerase (15), but the notable concentration of indels in intergenic spacers implies that most frameshifts adversely affect gene function.

As indicated above, SNPs are about three times as common among new mutations as are small indels (Table 2), but indels mediated most inferred gene inactivations. Small indels were heavily concentrated in mononucleotide runs ("homopolymers" (15), with 93% of single-base indels linked to runs of at least five and 66% in runs of at least seven consecutive A's or T's (Fig. 2, A and B). [Solexa sequencing resolves homopolymer length with low error and without bias (12).] The incidence of indels per run was highest in the longest runs (10 and above), but because the longest runs were rare, most indels were found in runs of 7 to 9 bases (Fig. 2A, B).

Together, the evolutionary trends observed in *Buchnera-Ap* converged to a model describing a stepwise process of symbiont genome erosion (Fig. 3). The shift toward high A+T content that is common in host-restricted bacteria leads to increased occurrence of A/T homopolymers. These, in turn, are hot-spots for small indels, which are elevated in homopolymers due to replication slippage, and which are further increased when certain DNA repair pathways are compromised (16). Our data imply that many new indels disrupt reading frames and that most are removed by selection. However, a minority persists, leading to inactivated genes. The resulting pseudogenes undergo rapid sequence evolution due to the

lack of purifying selection and are eventually removed by large deletions. Because large deletions do not precisely excise inactivated genes, intergenic spacers often persist in the positions of former genes.

This process fits well with previous observations comparing more distantly related symbiont genomes [e.g., (5–7)]; however, those studies lacked the precision needed to detect the critical role of homopolymers and frameshifts in gene inactivation. Our model predicts that the initial step leading to genome reduction is a shift in nucleotide composition toward higher A+T content. Loss of DNA-repair functions has been proposed as the cause for this shift (17). A consequence of high A+T content is an excess of homopolymers and a resulting high incidence of small indels (Fig. 2, A and B) leading to gene inactivations. Indeed, A+T-biased genomes, including *Buchnera* genomes, show higher frequencies of A/T homopolymers than expected by chance alone (18), reflecting mutational patterns that yield longer A/T runs through replication slippage or other processes (16).

Most sequenced insect symbiont genomes are between 0.6 and 1 megabases in size and contain more than 500 genes, similar to the smallest known pathogen genomes and consistent with previous suggestions that cellular genomes have a minimal size threshold (1, 5, 6, 19, 20). This study, as well as the recent discovery of symbiont genomes containing only 182 to 450 genes (2–4), suggests instead that the process of gene loss has no clearly defined limit. We identified a surprisingly high rate of new mutations, including both base changes and indels, in the genomes of *Buchnera-Ap*. Although most mutations impairing gene function are removed by selection, others persist, leading to the permanent inactivation of genes and the subsequent loss of the corresponding DNA through larger deletions.

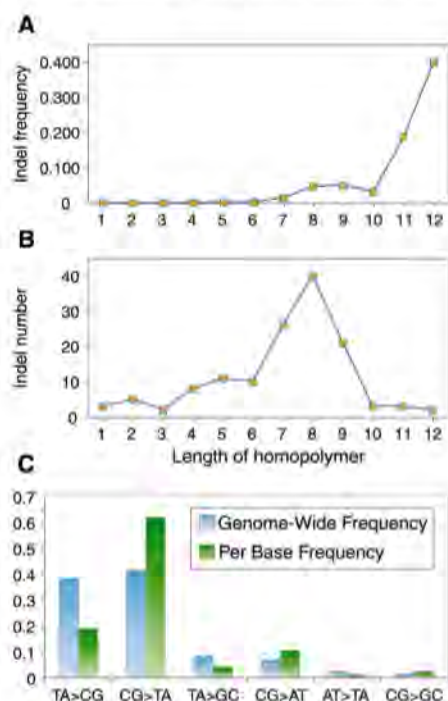


Fig. 2. Observed mutations in *Buchnera-Ap*. Frequencies of single-base indels in homopolymers of different lengths (A) per homopolymer and (B) genome-wide. (C) Relative frequencies of base substitutions genome-wide and per nucleotide base.

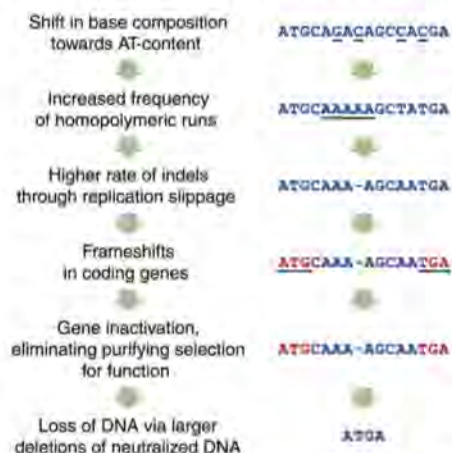


Fig. 3. Model of symbiont genome erosion, from mutational patterns revealed by sequencing the complete genomes of seven *Buchnera-Ap* strains.

References and Notes

1. S. Shigenobu, H. Watanabe, M. Hattori, Y. Sakaki, H. Ishikawa, *Nature* **407**, 81 (2000).
2. V. Perez-Brocal et al., *Science* **314**, 312 (2006).
3. J. P. McCutcheon, N. A. Moran, *Proc. Natl. Acad. Sci. U.S.A.* **104**, 19392 (2007).
4. A. Nakabachi et al., *Science* **314**, 267 (2006).
5. I. Tamas et al., *Science* **296**, 2376 (2002).
6. R. C. H. J. van Ham et al., *Proc. Natl. Acad. Sci. U.S.A.* **100**, 581 (2003).
7. P. H. Degnan, A. B. Lazarus, J. J. Wernegreen, *Genome Res.* **15**, 1023 (2005).
8. N. A. Moran, *Proc. Natl. Acad. Sci. U.S.A.* **93**, 2873 (1996).
9. T. Hosokawa et al., *PLoS Biol.* **4**, e337 (2006).
10. N. A. Moran, J. P. McCutcheon, A. Nakabachi, *Annu. Rev. Genet.* **42**, 165 (2008).
11. A. M. Harper, J. P. Miska, G. R. Mangiltz, B. J. Irwin, E. J. Armbrust, in *Special Publication 50* (Agricultural Experimental Station, University of Illinois, Urbana-Champaign, 1978), pp. 1–89.
12. Materials and methods are available as supporting material on Science Online.
13. H. Ochman, S. Elwyn, N. A. Moran, *Proc. Natl. Acad. Sci. U.S.A.* **96**, 12638 (1999).
14. N. Sueoka, *Proc. Natl. Acad. Sci. U.S.A.* **85**, 2653 (1988).
15. I. Tamas et al., *Proc. Natl. Acad. Sci. U.S.A.* **105**, 14934 (2008).

16. B. O. Parker, M. G. Marinus, *Proc. Natl. Acad. Sci. U.S.A.* **89**, 1730 (1992).
17. N. A. Moran, *Cell* **108**, 583 (2002).
18. T. Coenye, P. Vandamme, *DNA Res.* **12**, 221 (2005).
19. L. Akman *et al.*, *Nat. Genet.* **32**, 402 (2002).
20. D. Wu *et al.*, *PLoS Biol.* **4**, e188 (2006).
21. We thank staff at the Joint Genome Institute for the Solexa sequencing runs, E. Rubin for support and facilities, and H. Ochman for comments on the manuscript. Aphid samples

were donated by G. Powell and J. C. Simon. K. Hammond maintained insect cultures, and B. Nankivell prepared figures. Funding was provided by NSF award 0723472 (to N.A.M.), the Y. Leon Benozio Institute for Molecular Medicine (to R.S.), and the U.S. Department of Energy (to the Joint Genome Institute supporting the sequencing). GenBank accession numbers are CP00158 and CP00161 for the genomic sequences and FJ357501 to FJ357538 for sequences used for the phylogeny of fig. S2.

Supporting Online Material

www.sciencemag.org/cgi/content/full/323/5912/379/DC1
Materials and Methods
Figs. S1 and S2
Table S1
References

13 October 2008; accepted 19 November 2008
10.1126/science.1167140

A Polymorphism in *npr-1* Is a Behavioral Determinant of Pathogen Susceptibility in *C. elegans*

Kirthi C. Reddy,^{1*} Erik C. Andersen,^{2,3*} Leonid Kruglyak,^{2,3†} Dennis H. Kim^{1†}

The nematode *Caenorhabditis elegans* responds to pathogenic bacteria with conserved innate immune responses and pathogen avoidance behaviors. We investigated natural variation in *C. elegans* resistance to pathogen infection. With the use of quantitative genetic analysis, we determined that the pathogen susceptibility difference between the laboratory wild-type strain N2 and the wild isolate CB4856 is caused by a polymorphism in the *npr-1* gene, which encodes a homolog of the mammalian neuropeptide Y receptor. We show that the mechanism of NPR-1-mediated pathogen resistance is through oxygen-dependent behavioral avoidance rather than direct regulation of innate immunity. For *C. elegans*, bacteria represent food but also a potential source of infection. Our data underscore the importance of behavioral responses to oxygen levels in finding an optimal balance between these potentially conflicting cues.

Microbes, including commensal organisms and pathogens, profoundly influence the immune and metabolic physiology of host organisms (1). We used the nematode *Caenorhabditis elegans* as an experimental host to dissect the molecular basis of interactions between host species and microorganisms. *C. elegans* exhibits diverse behaviors in response to bacteria provided as a nutrient source (2–4). Feeding behavior can be modulated by environmental conditions, including oxygen concentration (5). Some bacterial species are pathogenic to *C. elegans* (6), and *C. elegans* responds by activating conserved innate immune pathways (7–9) and avoiding pathogens (10–12).

We found that the standard laboratory strain N2 (isolated in Bristol, England) and strain CB4856 (isolated in Hawaii, USA) exhibited a marked difference in susceptibility to the human opportunistic pathogen *Pseudomonas aeruginosa* strain PA14 (Fig. 1A) (13). The mean time to 50% lethality (LT₅₀) for CB4856 was shorter (50 ± 7.8 hours) than that for N2 (90 ± 13 hours). Using a collection of recombi-

nant inbred lines (14), we mapped the pathogen susceptibility trait to a 774-kb region of the X chromosome (LGX) containing *npr-1*, which encodes a G protein-coupled receptor related to the mammalian neuropeptide Y receptor (Fig. 1B). The 215V *npr-1* allele in N2 has increased NPR-1 activity relative to the 215F *npr-1* allele in CB4856, and the 215V allele confers behavioral differences that are dominant to those conferred by the 215F allele (15). To test the possibility that *npr-1* causes the difference in pathogen susceptibility between the N2 and CB4856 strains, we used *npr-1* loss-of-function mutants isolated in the N2 background. Like the CB4856 strain, the *npr-1* presumptive null alleles *ad609* and *ky13*, along with the reduction-of-function alleles *ur89* and *n1353*, had enhanced susceptibility to killing by PA14 (Fig. 1C and fig. S1). The enhanced susceptibility of *npr-1(ky13)* mutants was rescued by a transgene containing N2 wild-type (WT) copies of *npr-1*, and an N2 *npr-1* null mutation failed to complement the pathogen susceptibility phenotype of CB4856 (Fig. 1C). Thus, the enhanced susceptibility to pathogen of CB4856 is caused by the ancestral 215F allele of *npr-1*. This finding is consistent with a recent report by Styer *et al.* (16) that showed that loss-of-function mutations in the *npr-1* gene in the N2 background result in enhanced susceptibility to pathogen killing.

The 215F *npr-1* allele in CB4856 and loss-of-function mutations in *npr-1* confer a constellation of related behavioral phenotypes that have been termed “social feeding”—the animals associate

together in groups (clumping) and are often found at the edge of the bacterial lawn (bordering) (15). The characterization of aerotaxis behavior in *C. elegans* revealed that CB4856 and *npr-1* loss-of-function mutants prefer the decreased oxygen concentrations found at the edge of the live bacterial lawn, which drives the bordering phenotype (5, 17, 18). We hypothesized that differences in behavior, instead of in innate immune responses as recently proposed (16), might underlie the observed pathogen susceptibility differences caused by the *npr-1* polymorphism. By spending more time on the bacterial lawn, CB4856 and *npr-1* mutants would receive an increased dose of the pathogenic bacteria, leading to higher mortality. Multiple independent experiments support our hypothesis.

First, mutations in the oxygen-sensing guanylate cyclase *gcy-35* and the neuronal signaling genes *ocr-2* and *osm-9*, which are necessary for *npr-1*-mediated bordering and aerotaxis behaviors (5, 19, 20), also suppressed the pathogen susceptibility of *npr-1* mutants (fig. S2, A and B). These data suggest that the clumping and bordering behaviors mediated by responses to oxygen concentration are necessary for the enhanced susceptibility to the pathogen.

Second, we altered the standard slow-killing pathogenesis assay (21) by spreading the PA14 lawn to the edges of the agar plate. In this “big lawn” assay, there is no region of the plate in which the animals can avoid pathogen. Under these conditions, N2 displayed increased susceptibility equivalent to both CB4856 and *npr-1(ad609)*, whereas the susceptibilities of *npr-1(ad609)* and *npr-1(ky13)* were equivalent in both assays (Fig. 2A and figs. S3 and S4). These data demonstrate that the pathogen susceptibility difference arises not from differential activation of immune pathways, but rather from the aberrant aerotaxis behavior of the N2 strain in the presence of the pathogenic lawn that results in lower exposure to the pathogen.

Third, we carried out the standard pathogenesis assay at 10% oxygen concentration, which suppresses bordering and aerotaxis behaviors in CB4856 and *npr-1* mutants (5, 18). We observed that this reduced oxygen concentration also suppressed the pathogen susceptibility phenotypes of CB4856 and *npr-1(ad609)*. Allowing CB4856 and *npr-1* mutants to disperse off of the bacterial lawn results in survival that is equivalent to that observed for N2.

In addition, we found that three dauer-defective mutants that weakly aggregate and bor-

¹Department of Biology, Massachusetts Institute of Technology, Cambridge, MA 02139, USA. ²Howard Hughes Medical Institute, Lewis-Sigler Institute for Integrative Genomics, Princeton University, Princeton, NJ 08544, USA. ³Department of Ecology and Evolutionary Biology, Princeton University, Princeton, NJ 08544, USA.

*These authors contributed equally to this work.

†To whom correspondence should be addressed. E-mail: leonid@genomics.princeton.edu (L.K.); dhkim@mit.edu (D.H.K.)

der on the bacterial lawn in an *npr-1*-independent manner (20) were more susceptible to PA14 killing than N2 (fig. S6), indicating that social feeding behaviors are sufficient to cause increased susceptibility. Also, we examined five transcriptional targets of the *pmk-1* p38 MAPK immune signaling pathway (22) and observed no differences between the WT and *npr-1* mutant strains (fig. S7). The behavioral differences between N2 and *npr-1* mutant strains precluded the analysis of gene expression changes on worms exposed to the pathogen because different degrees of pathogen exposure, and not direct NPR-1-mediated regulation of innate immunity, control infection and immunity-related transcriptional changes.

We analyzed the kinetics of pathogen accumulation using green fluorescent protein (GFP)-labeled PA14 and red fluorescent beads, showing that CB4856 and *npr-1* mutants have a greater intake in the standard slow-killing assay as compared with N2 (Fig. 3, A to F). Whereas the increased accumulation of PA14-GFP could be attributed either to increased exposure and intake or to diminished intestinal immune responses, the concomitant accumulation of fluorescent-labeled

beads suggests that the increased accumulation is due to increased exposure. We also observed that N2, CB4856, and *npr-1* mutants have equivalent rates of PA14-GFP accumulation under big lawn assay conditions (Fig. 3, G to I), fully consistent with the equivalent survival that we observe under these assay conditions (Fig. 2A).

These experiments show that the increased exposure to pathogen, mediated by the behavior of the animals, is necessary and sufficient for susceptibility to *P. aeruginosa* PA14. Our data contradict the claim of the recent report by Styer *et al.* (16) that the pathogen susceptibility phenotype of *npr-1* mutants results from direct neuronal regulation of the intestinal immune response. Styer *et al.* also observed that N2 worms died faster on plates completely covered with PA14 and that *npr-1(ad609)* was more resistant to PA14 at a lower oxygen concentration. However, they reported residual differences in survival between N2 worms and *npr-1(ad609)* in both of these assays and interpreted these residual differences as evidence of direct neuronal regulation of innate immunity. We see similar survival among N2, CB4856, and *npr-1* mutant worms on the big

lawn and at lower oxygen concentrations. Small residual effects are difficult to rule out due to possible differences between strains and assay conditions, but we would interpret any such effects as more likely to represent subtle uncontrolled variation in behavior than the presence of a nonbehavioral resistance mechanism. Our results are internally consistent between two laboratories (fig. S3). Additionally, our interpretation of a behaviorally mediated difference in susceptibility is supported by our observations of faster accumulation of both GFP-labeled PA14 and fluorescent beads by CB4856 and *npr-1* mutants in the standard assay but equal accumulation of PA14 by these strains and N2 on the big lawn.

Our data underscore that behavioral avoidance can confer dramatic effects on survival in the presence of pathogenic bacteria. The physiological interplay between mechanisms of aerotaxis and pathogen survival is intriguing given the molecular connection between responses to changes in oxygen and innate immunity in mammals (23). The N2 allele of *npr-1* causes animals to spend less time in regions of low oxygen concentration in the presence of bacteria, thereby

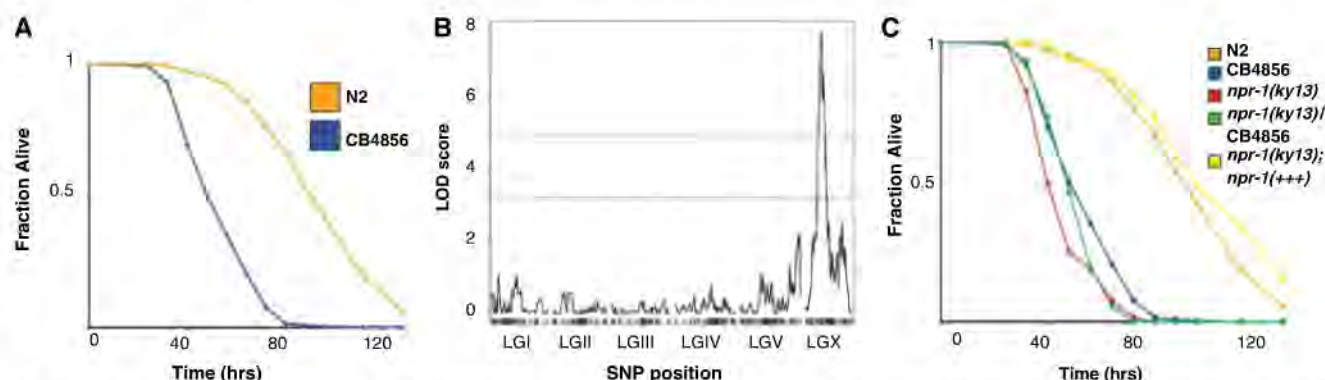


Fig. 1. The enhanced pathogen susceptibility of CB4856 is caused by the 215F allele of *npr-1*. (A) Fraction alive versus time for N2 (orange) and CB4856 (blue) fed PA14 using standard assays (19). Means from 27 independent experiments for each strain are shown. (B) Logarithm of the odds ratio (LOD) score for linkage between LT50 and 1454 single-nucleotide polymorphisms (SNPs) in 126 recombinant inbred lines showing one major

quantitative trait locus on LGX. Dotted and solid lines show 5 and 0.1% genome-wide significance levels, respectively, determined from 1000 permutations. (C) Fraction alive versus time for N2 (orange), CB4856 (blue), the *npr-1* loss-of-function mutant *ky13* (red), a complementation test between *npr-1(ky13)* derived from the N2 background and *npr-1* derived from the CB4856 background (green), and rescue of the *npr-1(ky13)* allele (yellow).

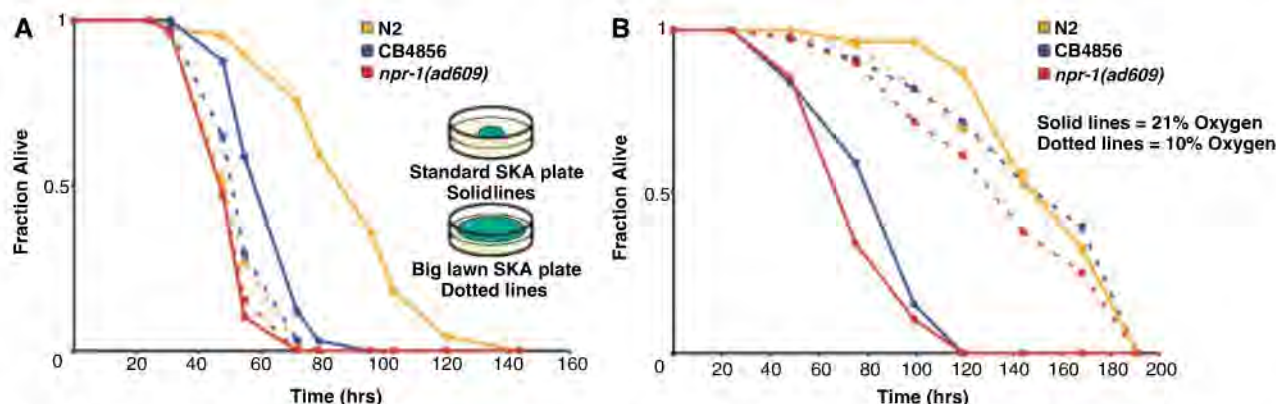


Fig. 2. *npr-1*-mediated behaviors determine the susceptibility of *C. elegans* to PA14. (A) Fraction alive versus time for N2 (orange) and CB4856 (blue) fed PA14 on standard plates (solid lines) and big lawn

plates (dotted lines). (B) Fraction alive versus time for N2 (orange), CB4856 (blue), and the *npr-1* loss-of-function allele *ad609* (red) at 21% oxygen (solid lines) and 10% oxygen (dotted lines).

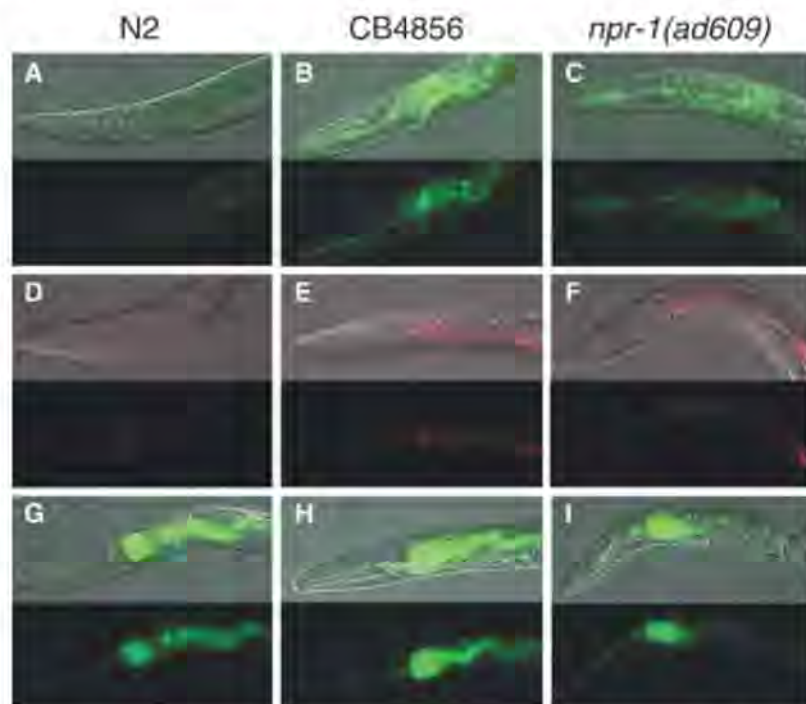


Fig. 3. *npr-1*-mediated behaviors cause increased exposure to bacteria. Differential interference contrast and fluorescence microscopy of N2, CB4856, and *npr-1(ad609)* animals fed GFP-labeled PA14 for 24 hours on a standard lawn (A to C) or fed a 50:1 mixture of unlabeled PA14 and 0.2- μ m fluorescent beads (D to F) or on a big lawn of GFP-labeled PA14 (G to I).

decreasing their exposure to bacterial pathogens and leading to greater survival. Whether this trade-off would be beneficial in nature is debatable, as increased avoidance of potentially pathogenic bacteria may also decrease consumption of bacterial food. We speculate that the maintenance of the 215V allele of *npr-1* may have depended on laboratory propagation of N2 in plentiful sources of bacterial food that can be pathogenic,

whereas in the wild, maximizing consumption of scarce food might be the preferred strategy.

References and Notes

1. L. Dethlefsen, M. McFall-Ngai, D. A. Relman, *Nature* **449**, 811 (2007).
2. L. Avery, *Genetics* **133**, 897 (1993).
3. E. R. Sawin, R. Ranganathan, H. R. Horvitz, *Neuron* **26**, 619 (2000).
4. C. Trent, N. Tsuing, H. R. Horvitz, *Genetics* **104**, 619 (1983).
5. J. M. Gray et al., *Nature* **430**, 317 (2004).

6. C. Darby, in *WormBook* (The *C. elegans* Research Community, 2005).
7. D. H. Kim et al., *Science* **297**, 623 (2002).
8. G. V. Mallo et al., *Curr. Biol.* **12**, 1209 (2002).
9. H. R. Nicholas, J. Hodgkin, *Curr. Biol.* **14**, 1256 (2004).
10. Y. Zhang, H. Lu, C. I. Bargmann, *Nature* **438**, 179 (2005).
11. E. Pradel et al., *Proc. Natl. Acad. Sci. U.S.A.* **104**, 2295 (2007).
12. N. Pujol, J. J. Ewbank, in *Toll and Toll-Like Receptors: An Immunologic Perspective* (Springer, New York, 2007).
13. Materials and methods are available as supporting material on Science Online.
14. H. S. Seidel, M. V. Rockman, L. Kruglyak, *Science* **319**, 589 (2008); published online 10 January 2008 (10.1126/science.1151107).
15. M. de Bono, C. I. Bargmann, *Cell* **94**, 679 (1998).
16. K. L. Styer et al., *Science* **322**, 460 (2008); published online 18 September 2008 (10.1126/science.1163673).
17. A. J. Chang, N. Chronis, D. S. Karow, M. A. Marletta, C. I. Bargmann, *PLoS Biol.* **4**, e274 (2006).
18. B. H. Cheung, M. Cohen, C. Rogers, O. Albayram, M. de Bono, *Curr. Biol.* **15**, 905 (2005).
19. B. H. Cheung, F. Arellano-Carbajal, I. Rybicki, M. de Bono, *Curr. Biol.* **14**, 1105 (2004).
20. M. de Bono, D. M. Tobin, M. W. Davis, L. Avery, C. I. Bargmann, *Nature* **419**, 899 (2002).
21. M. W. Tan, S. Mahajan-Miklos, F. M. Ausubel, *Proc. Natl. Acad. Sci. U.S.A.* **96**, 715 (1999).
22. E. R. Troemel et al., *PLoS Genet.* **2**, e183 (2006).
23. J. Rius et al., *Nature* **453**, 807 (2008).
24. We thank the *Caenorhabditis* Genetics Center, C. Bargmann, M. de Bono, and D. Omura for strains; S. Skrovanek for technical assistance; L. Dietrich for facilitating the oxygen assay; E. Alvarez-Saavedra, J. Shapiro, and members of our laboratories for advice; and C. Bargmann for comments on the manuscript. This work was supported by grants from NIH (GM084477 to D.H.K., HG004321 to L.K., and GM071508 to the Lewis-Sigler Institute), the Burroughs Wellcome Fund (to D.H.K.), the Jane Coffin Childs Fund for Medical Research (to K.C.R.), the James S. McDonnell Foundation (to L.K.), and the Howard Hughes Medical Institute (to L.K.).

Supporting Online Material

www.sciencemag.org/cgi/content/full/323/5912/382/DC1
Materials and Methods
Figs. S1 to S7
References

29 September 2008; accepted 20 November 2008
10.1126/science.1166527

The Structure of Rat Liver Vault at 3.5 Angstrom Resolution

Hideaki Tanaka,^{1*} Koji Kato,^{1*} Eiki Yamashita,¹ Tomoyuki Sumizawa,² Yong Zhou,³ Min Yao,³ Kenji Iwasaki,^{1,4} Masato Yoshimura,⁵ Tomitake Tsukihara^{1,6,†}

Vaults are among the largest cytoplasmic ribonucleoprotein particles and are found in numerous eukaryotic species. Roles in multidrug resistance and innate immunity have been suggested, but the cellular function remains unclear. We have determined the x-ray structure of rat liver vault at 3.5 angstrom resolution and show that the cage structure consists of a dimer of half-vaults, with each half-vault comprising 39 identical major vault protein (MVP) chains. Each MVP monomer folds into 12 domains: nine structural repeat domains, a shoulder domain, a cap-helix domain, and a cap-ring domain. Interactions between the 42-turn-long cap-helix domains are key to stabilizing the particle. The shoulder domain is structurally similar to a core domain of stomatin, a lipid-raft component in erythrocytes and epithelial cells.

Vaults are large barrel-shaped ribonucleoprotein particles that are highly conserved in a wide variety of eukaryotes (1). Although several functions have been proposed for vaults since their discovery in 1986 (2–10), in-

cluding roles in multidrug resistance, cell signaling, and innate immunity, their cellular function remains unclear. Most vault particles are present in the cytoplasm, but a few of them localize to the nucleus (11,12). Rat liver vault comprises a small

untranslated RNA consisting of 141 bases (vRNA) (13) and three proteins. The sequences of these proteins are known for the human vault. The 99-kD major vault protein (MVP, Swiss-Prot entry Q14764) is the major structural protein and can self-assemble to form vault-like particles (14); the 193-kD vault poly(adenosine diphosphate-ribose) polymerase (VPARP, Swiss-Prot entry Q9UKK3) presumably ribosylates substrates (15); and the

¹Institute for Protein Research, Osaka University, 3-2 Yamadaoka, Suita, Osaka 565-0871, Japan. ²University of Occupational and Environmental Health, 1-1 Iseigaoka, Yahatanishi, Kitakyushu, Fukuoka 807-8555, Japan. ³Faculty of Advanced Life Sciences, Graduate School of Life Sciences, Hokkaido University, Sapporo, Hokkaido 060-0810, Japan. ⁴Bio-multisome Research Team, Structural Physiology Research Group, RIKEN Harima Institute, Mikazuki Sayo, Hyogo 679-5148, Japan. ⁵National Synchrotron Radiation Research Center, 101 Hsin-Ann Road, Hsinchu Science Park, Hsinchu 30076, Taiwan. ⁶Department of Life Science, University of Hyogo, 3-2-1 Koto, Kamigori, Akoh, Hyogo 678-1297, Japan.

*These authors contributed equally to this work.

†To whom correspondence should be addressed. E-mail: tsuki@protein.osaka-u.ac.jp

290-kD telomerase-associated protein 1 (TEP1, Swiss-Prot entry Q99973) (16) is important for stabilization of vRNA (17). Molecular composition of the vault has been roughly estimated as 96 MVPs, eight VPARPs, two TEP1s, and at least six copies of vRNA (18).

Electron microscopy and x-ray crystal structural analysis at 9 Å resolution (19,20) have revealed a cage-like structure with two protruding caps and an invaginated waist. On the basis of the x-ray structure, which was of an empty vault built from a cysteine-tagged construct of MVP [termed cpMVP vaults; Protein DataBank entry (PDB) 2QZV], the cpMVP vault was proposed to comprise 96 MVP molecules, each folding into 14 domains. Forty-eight MVP molecules were proposed to extend between the middle and each tip of the vault, so that the cpMVP vault exhibited 48-fold dihedral symmetry. The resolution, however, was too low to determine the main chain fold. Nuclear magnetic resonance (NMR) spectroscopy of an MVP fragment from human (domains 3 to 4; PDB 1Y7X) reveals that each domain contains a three-stranded antiparallel β sheet and loops (21). Our previously published crystallographic analysis of rat liver vault, at 10 Å resolution, demonstrated that the particle exhibits 39-fold dihedral symmetry, instead of 48-fold dihedral symmetry (22). Here, we report the determination of the x-ray crystal structure of rat liver vault at 3.5 Å resolution.

Vault complexes containing all components were purified and crystallized as described previously (22,23). The initial electron density of a vault was obtained by the molecular replacement (MR) method, by using the cryo-EM (cryo-EM) map (22) as a starting model of noncrystallographic symmetry (NCS) averaging. Phase extension was performed by NCS averaging about the 3-fold axis contained within the 39-fold symmetry, by using a mask generated by the EM structure (22). Judging from the *R* factor, correlation coefficient between observed and calculated structure factors (F_{obs} and F_{calc}), and the soundness of the electron density distributions of helical region and β barrels, a phase extension by the 3-fold axis at ($\omega = 19.83^\circ$, $\varphi = 0.00^\circ$) resulted in the best electron density map of the crystal. The *R* factor, $\Sigma ||F_{\text{obs}}| - |F_{\text{calc}}|| / \Sigma |F_{\text{obs}}|$, and the correlation coefficient of structure factors, $\Sigma (|F_{\text{obs}}| - \langle |F_{\text{obs}}| \rangle)(|F_{\text{calc}}| - \langle |F_{\text{calc}}| \rangle) / [\Sigma (|F_{\text{obs}}| - \langle |F_{\text{obs}}| \rangle)^2 \Sigma (|F_{\text{calc}}| - \langle |F_{\text{calc}}| \rangle)^2]^{1/2}$, were 0.137 and 0.971, respectively, where $\langle |F_{\text{obs}}| \rangle$ and $\langle |F_{\text{calc}}| \rangle$ were the averaged values of $|F_{\text{obs}}|$ and $|F_{\text{calc}}|$, respectively. The 3.5 Å resolution map showed that a vault comprises 78 MVP chains with 39-fold dihedral symmetry coming from the 39 MVP chains in each half-vault (Fig. 1). Each MVP monomer folds into 12 domains: nine structural repeat domains, a shoulder domain, a cap-helix domain, and a cap-ring domain (Fig. 2).

After preparing a molecular mask from the atomic model of MVP, we performed further phase refinement by 39-fold NCS averaging.

NCS parameters of each MVP domain were refined during the phase extension. The averaged value for the correlation coefficient of electron density for domains 3 to 9, the shoulder domain, and the cap-helix domain were ~0.95, whereas domain 1, domain 2, and the cap-ring domain had smaller correlation coefficients, ~0.92. The electron density distribution was significantly improved in all regions of the MVP molecule compared with densities obtained by NCS averaging of three-fold symmetries. Bulky electron density maps of aromatic residues are clearly shown in the regions with higher correlation coefficients (~0.95). An electron density map of each

domain, together with the structural model, is depicted in fig. S1, A to D.

Refinement statistics of the whole structure are summarized in Table 1. The final round of refinement, using the program CNS (24), reduced the *R* factor to 31.1% and *R*_{free} factor to 33.0% for reflections in the resolution range 204.0 to 3.5 Å. The refined vault structure converged well to root-mean-square deviations (RMSDs) from the ideal bond lengths and angles of 0.010 Å and 1.48°, respectively. Of the nonglycine residues, 80.0% were in the most favorable region of the Ramachandran plot (25), 19.7% in the allowed region, and 0.3% in the disallowed region. Out of

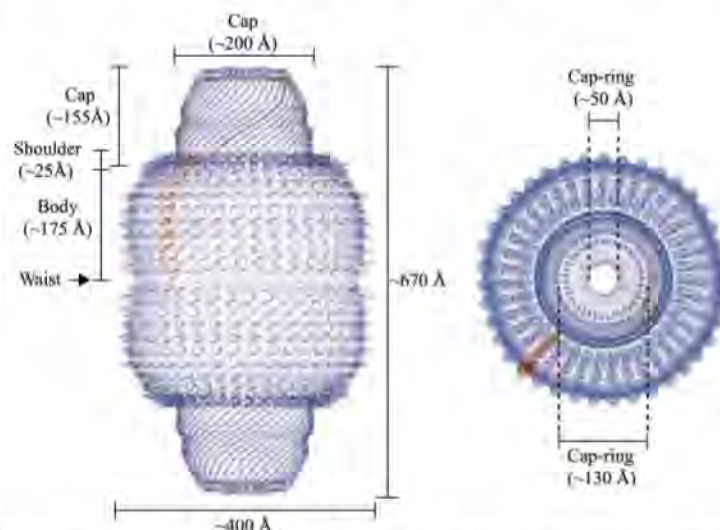


Fig. 1. Overall structure of the vault shell. One molecule of MVP is colored in tan, and the others are colored in purple. **(Left)** Side view of the ribbon representation. The whole vault shell comprises a 78-oligomer polymer of MVP molecules. The size of the whole particle is ~670 Å from the top to the bottom and ~400 Å in maximum diameter. The particle has two protruding caps, two shoulders, and a body with an invaginated waist. Two half-vaults are associated at the waist with N-terminal domains of MVP. **(Right)** Top view of the ribbon representation. The maximum diameter of the cap is ~200 Å. The outer and the inner diameters of the cap-ring are shown.

Table 1. Refinement statistics.

Refinement statistics	
Resolution (Å)	204–3.5
Reflection used	1,436,395
Number of protein residues	31,668
<i>R</i> factor (%) ^a	0.311
<i>R</i> _{free} factor (%) ^a	0.330
RMSD from ideal	
Bond length (Å)	0.010
Bond angles (°)	1.48
Ramachandran plot statistics	
Residues in most favored region (%)	80.0
Residues in additionally allowed region (%)	18.3
Residues in generously allowed region (%)	1.4
Residues in disallowed region (%)	0.3
Averaged <i>B</i> -factor	
Main chain (Å ²)	110.2
Side chain (Å ²)	133.1
Overall (Å ²)	121.4

^a*R* is conventional crystallographic *R* factor, $\Sigma ||F_{\text{obs}}| - |F_{\text{calc}}|| / \Sigma |F_{\text{obs}}|$, where F_{obs} and F_{calc} are the observed and calculated structure factors, respectively. Five percent of the reflections that were excluded from the refinement were used in the *R*_{free} calculation.

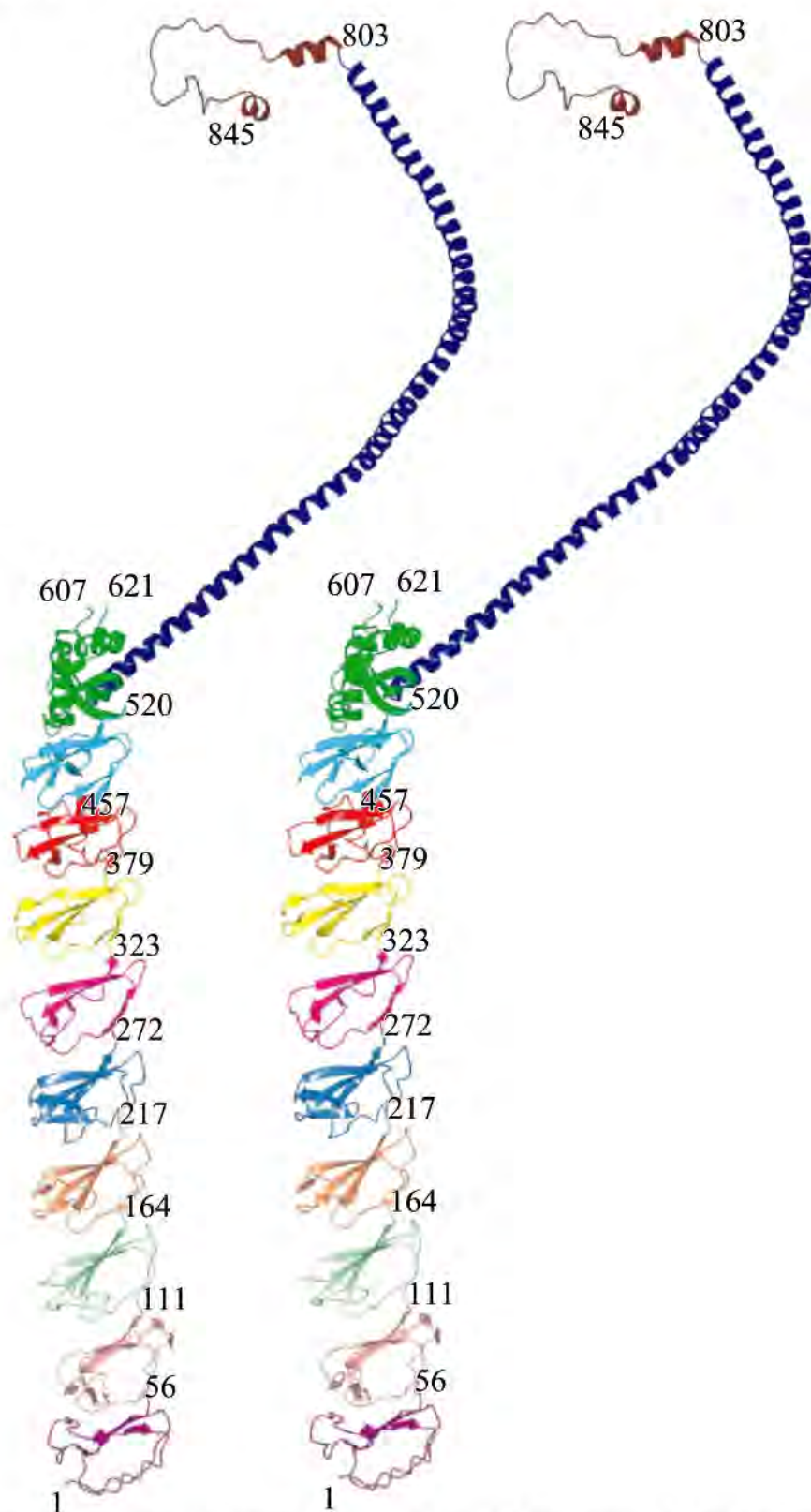


Fig. 2. Stereoscopic ribbon drawing of the overall fold of an MVP monomer. The MVP monomer is folded into nine structural repeat domains, a shoulder domain, a cap-helix domain, and a cap-ring domain. Each domain is depicted in a different color: domain 1 (Met¹-Pro⁵⁵), purple; domain 2 (Arg⁵⁶-Thr¹¹⁰), pink; domain 3 (Pro¹¹¹-Ile¹⁶³), light green; domain 4 (Gln¹⁶⁴-Val²¹⁶), coral; domain 5 (Asp²¹⁷-Val²⁷¹), light blue; domain 6 (Pro²⁷²-Asp³²²), magenta; domain 7 (Val³²³-Gln³⁷⁸), yellow; domain 8 (Ala³⁷⁹-Arg⁴⁵⁶), red; domain 9 (Val⁴⁵⁷-Gly⁵¹⁹), cyan; shoulder domain (Pro⁵²⁰-Val⁶⁴⁶), green; cap-helix domain (Asp⁶⁴⁷-Leu⁸⁰²), purple; and cap-ring domain (Gly⁸⁰³-Ala⁸⁴⁵), dark red.

861 total amino acid residues, we determined the tertiary structures, including side-chain structures, of 782 residues from Met¹ to Pro⁸¹⁵. Residues Leu⁴²⁹-Pro⁴⁴⁸, Met⁶⁰⁸-Pro⁶²⁰, and Phe⁸⁴⁶-Lys⁸⁶¹ could not be determined, and only the C α trace could be determined for the residues Glu⁸¹⁶-Ala⁸⁴⁵.

Although the vault sample prepared for crystallization contained all the protein components and vRNA as shown in fig. S2, only MVP could be definitively assigned in the electron density map. A cylindrical region with ~25 Å diameter and ~25 Å height at the top center of the cap exhibited significant electron density both in the NCS averaged map (fig. S1D) and a σ -A weighted $2F_{\text{obs}} - F_{\text{calc}}$ map, but was unlikely to be part of MVP, because it did not have 39-fold symmetry. The probable candidate for this density is TEP1, because it is located in the cap (18), and the size is reasonable for its molecular weight of 290 kD. Molar ratios of VPARP, TEP1, and vRNA to MVP are less than one to eight (18), so these proteins would likely not have 39-fold symmetry and, thus, may not be observed in the region exhibiting 39-fold symmetry.

The vault shell measures ~670 Å in length and ~400 Å in maximum diameter (Fig. 1). The barrel wall of only 15 to 25 Å in thickness encloses an internal cavity with the length of ~620 Å, and the maximum diameter of ~350 Å, large enough to enclose most objects found within the cell. The body consists of 78 copies of the nine MVP structural repeat domains (39 copies in each half-vault), with the waist formed by end-to-end association of structural domain 1. The nine structural repeat domains can be classified into two subgroups by their topological arrangements of antiparallel β strands. Structural repeat domains 8 and 9 consist of five antiparallel β strands termed S1, S2, S3, S4, and S5 (fig. S3, A and C). The other seven structural repeats have two antiparallel β strands (S2a and S2b) inserted between S2 and S3 (fig. S3, B and D). The latter structure is consistent with the domain structure determined by the NMR method (21).

The shoulder region is ~25 Å in height along the 39-fold axis and ~315 Å in diameter. Each shoulder domain (Pro⁵²⁰ to Val⁶⁴⁶) folds into a single α/β globular domain with a four-stranded antiparallel β sheet on one side and four α helices on the other side (Fig. 3). The ~155 Å high cap is formed by the cap-helix domains (Asp⁶⁴⁷ to Leu⁸⁰²) that form a 42-turn-long α helix that exhibits a quarter turn of superhelical structure (Fig. 2) and the cap-ring domains (Gly⁸⁰³ to Ala⁸⁴⁵) that form a U-shaped structure at the top of the cap. The inner and outer diameters of the cap-ring are ~50 Å and ~130 Å, respectively (Fig. 1).

Details of intersubunit interactions are provided in the supplementary online text and table S1 (A, B, and C). Out of 74 total interactions observed between two adjacent MVP subunits, 41 interactions were between cap-helix domains; this suggests that these interactions promote self-assembly of the particle. In the cap-helix domain,

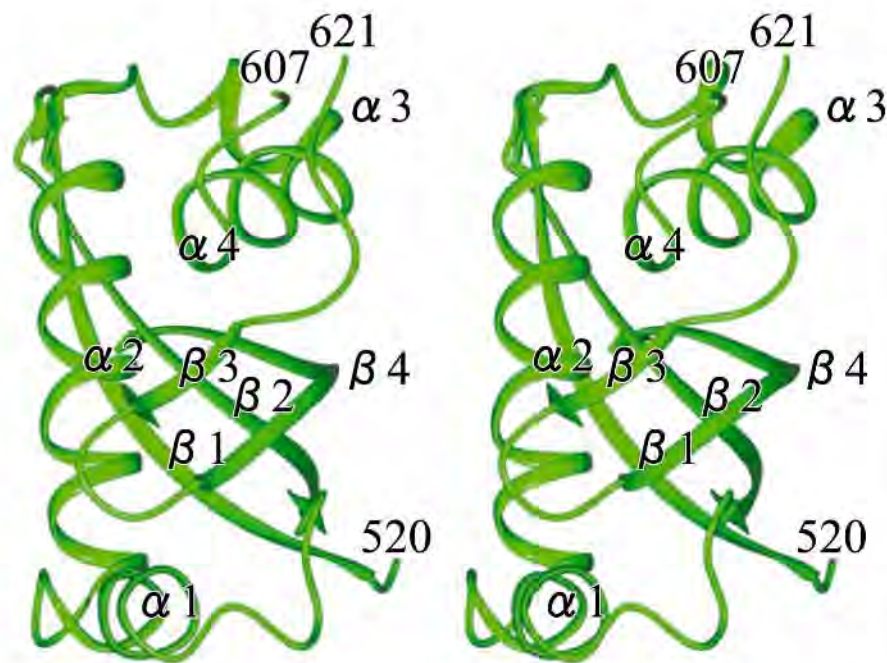


Fig. 3. A stereoscopic ribbon representation of the shoulder domain, along with secondary structure notations. The secondary structures are $\beta 1$, $\beta 2$, $\alpha 1$, $\alpha 2$, $\alpha 3$, $\alpha 4$, $\beta 3$, and $\beta 4$ from the N-terminal side to the C-terminal side.

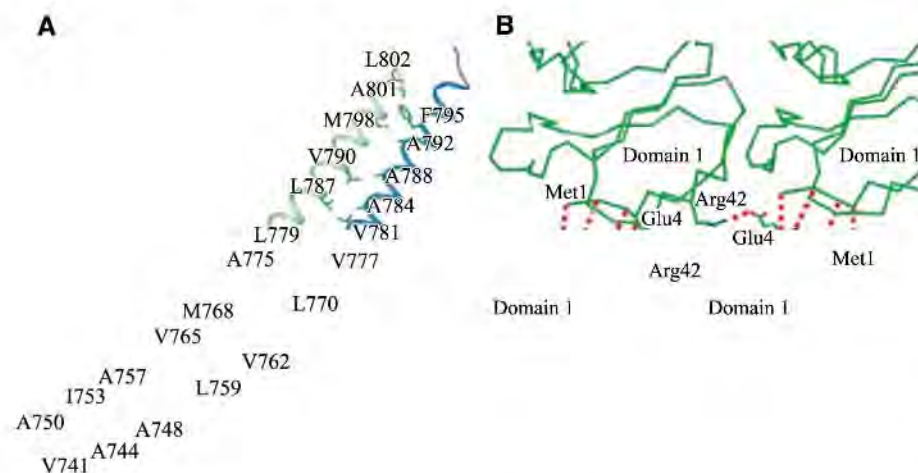


Fig. 4. (A) Hydrophobic interactions for the cap-helix domain. In the cap-helix domain most of the hydrophobic residues appear at the interface between two helices to form hydrophobic interactions. These side-by-side interactions of the cap-helix domain play key roles in self-assembly of the particle. (B) Intermolecular interactions between two half-vaults. N-terminal residues of domain 1, Met¹-Glu⁴, formed an intermolecular antiparallel β sheet with those of the two-fold symmetry-related molecule. An ionic bond of Glu⁴-Arg⁴² was another specific interaction between two half-vaults. In contrast to the association of C-terminal cap domains, N-terminal associations were abundant in hydrophilic interactions.

most polar residues are exposed to inner or outer surfaces of the particle, and hydrophobic residues appear on the interface between two helices to form hydrophobic interactions (fig. S4). Specific ionic pairs and hydrophobic interactions for the cap-helix domain are depicted in fig. S5 and Fig. 4A, respectively. N-terminal residues of MVP domain 1 form an intermolecular antiparallel β sheet around the two-fold axis (Fig. 4B). Using an electron microscopic method, Kedersha *et al.*

(26) have observed flowerlike structures, each of which is composed of petals surrounding the central ring. This observation is consistent with our structure. Because interactions stabilizing the dimer of half-vaults are weaker than interactions stabilizing the cap structure, it is reasonable that the particle may separate into half-vaults with MVP structural repeat domains separated and appearing as petals around the central ring formed by the cap structure.

A search for three-dimensional structures similar to the shoulder domain using the DALI server (27) revealed that the shoulder domain is structurally similar to the core domain of stomatin from *Pyrococcus horikoshii* (PhSto^{CD}) (28) (PDB 3BK6) and the flotillin-2 band-7 domain (Flot^{BD7}) (PDB 1WIN). The structure of the shoulder domain is superimposed on those of PhSto^{CD} and Flot^{BD7} with RMSDs of 2.1 and 2.2 Å, respectively (fig. S6, A and B). The core domain of stomatin is evolutionarily conserved and falls within the stomatin-prohibitin-flotillin-HflK-C (SPFH) domain family (29). Although the physiological function of stomatin is not yet clearly understood, the SPFH domain is known to be involved in lipid raft association (30). Human stomatin, which has 40.3% and 18.4% sequence identities with PhSto^{CD} and Flot^{BD7}, respectively, is a major integral membrane protein of human erythrocytes. Podocin from mouse and mechanosensory protein 2 from *Caenorhabditis elegans* have SPFH domains that bind cholesterol but not phosphatidylcholine (31). Cholesterol binding of the SPFH domain is likely an important factor in lipid raft association. Thus, the structural similarity between the shoulder domain and SPFH domain family supports the report proposing that MVP is recruited to lipid rafts, e.g., when human lung epithelial cells are infected with *Pseudomonas aeruginosa* (10).

References and Notes

- N. L. Kedersha, M. C. Miquel, D. Bittner, L. H. Rome, *J. Cell Biol.* **110**, 895 (1990).
- Z. Yu *et al.*, *J. Biol. Chem.* **277**, 40247 (2002).
- S. Kolli, C. I. Zito, M. H. Mossink, E. A. Wiemer, A. M. Bennett, *J. Biol. Chem.* **279**, 29374 (2004).
- C. Yi *et al.*, *Cancer Res.* **65**, 5835 (2005).
- E. Steiner *et al.*, *J. Cell Sci.* **119**, 459 (2006).
- E. Kim *et al.*, *FEBS J.* **273**, 793 (2006).
- G. L. Scheffer *et al.*, *Nat. Med.* **1**, 578 (1995).
- G. L. Scheffer, A. B. Schroeijs, M. A. Izquierdo, E. A. Wiemer, R. J. Scheper, *Curr. Opin. Oncol.* **12**, 550 (2000).
- S. C. Gopinath, A. Matsugami, M. Katahira, P. K. Kumar, *Nucleic Acids Res.* **33**, 4874 (2005).
- M. P. Kowalski *et al.*, *Science* **317**, 130 (2007).
- D. R. Hamill, K. A. Suprenant, *Dev. Biol.* **190**, 117 (1997).
- D. C. Chugani, L. H. Rome, N. L. Kedersha, *J. Cell Sci.* **106**, 23 (1993).
- V. A. Kickhoefer *et al.*, *J. Biol. Chem.* **268**, 7868 (1993).
- A. G. Stephen *et al.*, *J. Biol. Chem.* **276**, 23217 (2001).
- V. A. Kickhoefer *et al.*, *J. Cell Biol.* **146**, 917 (1999).
- V. A. Kickhoefer, A. G. Stephen, L. Harrington, M. O. Robinson, L. H. Rome, *J. Biol. Chem.* **274**, 32712 (1999).
- V. A. Kickhoefer *et al.*, *J. Cell Biol.* **152**, 157 (2001).
- L. B. Kong, A. C. Siva, V. A. Kickhoefer, L. H. Rome, P. L. Stewart, *RNA* **6**, 890 (2000).
- Y. Mikyas *et al.*, *J. Mol. Biol.* **344**, 91 (2004).
- D. H. Anderson, V. A. Kickhoefer, S. A. Sievers, L. H. Rome, D. Eisenberg, *PLoS Biol.* **5**, e318 (2007).
- G. Kozlov *et al.*, *J. Mol. Biol.* **356**, 444 (2006).
- K. Kato *et al.*, *Acta Crystallogr. D* **64**, 525 (2008).
- Materials and methods are available as supporting material on Science Online.
- A. T. Brunger *et al.*, *Acta Crystallogr. D* **54**, 905 (1998).
- C. Ramakrishnan, G. N. Ramachandran, *Biophys. J.* **5**, 909 (1965).
- N. L. Kedersha, J. E. Heuser, D. C. Chugani, L. H. Rome, *J. Cell Biol.* **112**, 225 (1991).

27. L. Holm, C. Sander, *Science* **273**, 595 (1996).
28. H. Yokoyama, S. Fujii, I. Matsui, *J. Mol. Biol.* **376**, 868 (2008).
29. N. Tavernarakis, M. Driscoll, N. C. Kypides, *Trends Biochem. Sci.* **24**, 425 (1999).
30. E. Umlauf et al., *J. Biol. Chem.* **279**, 23699 (2004).
31. T. B. Huber et al., *Proc. Natl. Acad. Sci. U.S.A.* **103**, 17079 (2006).
32. We thank T. Tomizaki for help in the diffraction data collection on X10SA (PX II) at the Swiss Light Source (Villigen, Switzerland). This work was supported in part by a Grant-in-Aid for Scientific Research in a Priority Area (10188101 and 10179101) and the Global Center of Excellence (GCOE) program (A-041) from the Ministry of Education, Culture, Sports, Science, and Technology of Japan (to T.T.) and by a Ground-Based Research Announcement for Space Utilization provided by the Japan Space Forum (T.T.). This work was also supported in part by a Grant-in-Aid for Young Scientists (B) 19770082 (H.T.) and Grant-in-Aids for Scientific Research in a Priority Area 16048216 (H.T.) and 20051001 (M.Y.) from the Ministry of Education, Culture, Sports, Science, and Technology of Japan. Coordinates and structure factors have been deposited with the PDB under accession codes 2ZUO, 2ZV4, and 2ZV5. The three entries were made because the number of coordinates exceeded the limits of

a PDB file. A PDB formatted file that contains whole coordinates and structure factors is available from www.protein.osaka-u.ac.jp/crystallography/mvp/.

Supporting Online Material

www.sciencemag.org/cgi/content/full/323/5912/384/DC1
Materials and Methods
Figs. S1 to S11
Tables S1 and S2
References and Notes

21 August 2008; accepted 3 December 2008
10.1126/science.1164975

Draxin, a Repulsive Guidance Protein for Spinal Cord and Forebrain Commissures

Shahidul M. Islam,^{1,2*} Yohei Shinmyo,^{1,2*} Tatsuya Okafuji,^{1†} Yuhong Su,^{1,2,3} Iftekhar Bin Naser,^{1,2,3} Giasuddin Ahmed,^{1,2,3} Sanbing Zhang,^{1,2,3} Sandy Chen,¹ Kunimasa Ohta,¹ Hiroshi Kiyonari,⁴ Takaya Abe,⁴ Satomi Tanaka,⁵ Ryuichi Nishinakamura,^{3,5} Toshio Terashima,⁶ Toshio Kitamura,⁷ Hideaki Tanaka^{1,2,3‡}

Axon guidance proteins are critical for the correct wiring of the nervous system during development. Several axon guidance cues and their family members have been well characterized. More unidentified axon guidance cues are assumed to participate in the formation of the extremely complex nervous system. We identified a secreted protein, draxin, that shares no homology with known guidance cues. Draxin inhibited or repelled neurite outgrowth from dorsal spinal cord and cortical explants in vitro. Ectopically expressed draxin inhibited growth or caused misrouting of chick spinal cord commissural axons in vivo. *draxin* knockout mice showed defasciculation of spinal cord commissural axons and absence of all forebrain commissures. Thus, draxin is a previously unknown chemorepulsive axon guidance molecule required for the development of spinal cord and forebrain commissures.

Although axon guidance proteins, including netrins, semaphorins, ephrins, and Slits (also slits), and morphogens, such as sonic hedgehog (Shh), Wnts, and bone morphogenic proteins (BMPs), are known to play roles in the correct wiring of the nervous system during development (1–3), the immense complexity of the nervous system makes it likely

that there are more unidentified axon guidance cues to be discovered. In our search for novel axon guidance proteins, we performed signal sequence trap screening, which enabled us to identify secreted and transmembrane proteins (table S1). With this method, we have identified a molecule named draxin (dorsal repulsive axon guidance protein, fig. S1A) from a cDNA library of enriched motoneurons, floor plate, and roof plate of chick embryos. Chick *draxin* mRNA was expressed transiently during development of the brain and spinal cord (Fig. 1A), especially in the roof plate and the dorsal lip of the dermomyotome (Fig. 1B). Mouse *draxin* mRNA was expressed in a manner similar to that of the chick (fig. S2, A and B). We examined the expression of *draxin* in the brain by β -galactosidase (β -gal) staining of heterozygous mice (fig. S3). Mouse *draxin* expression was observed in many brain regions, including the olfactory bulb, cortex, mid-brain, cerebellum, and pontine nuclei in postnatal day 0 (P0) mice (Fig. 1D and fig. S2, D and E).

The deduced draxin amino acid sequence (fig. S1A) indicates that chick draxin consists of 349 amino acids with a putative signal peptide sequence at the N-terminal end but no membrane anchoring sequence, which suggests that draxin is a secreted protein. We confirmed this hypoth-

esis via detection of the recombinant protein in conditioned medium of COS7 cells transfected with chick *draxin* expression vector (fig. S1B). Immunohistochemistry using antibodies against draxin (anti-draxin) revealed an interesting attribute of the draxin protein. In addition to its detection in mRNA-positive regions, draxin protein was detected at the dorsolateral basement membrane of the spinal cord (Fig. 1C and fig. S2C), indicating that the protein diffuses from its site of production and has high affinity for basement membranes.

To examine whether draxin has guidance activity for commissural axons in the spinal cord, we cultured dorsal spinal cord explants from stages 19 and 20 chick embryonic spinal cords, obtained from the thoracic level, in collagen gels. Netrin-1 (4) was added to the cultures to stimulate neurite outgrowth of commissural neurons from the explants. Neurites emerged from dorsal spinal cord explants, and dissociated cells were stained with chick TAG-1 antibody (chick anti-TAG-1), a marker for commissural axons (fig. S4), suggesting that they were commissural axons. Neurite outgrowth from dorsal spinal cord explants was greatly inhibited in draxin-conditioned medium (Fig. 2B), whereas there was robust neurite outgrowth in the control mock-transfected conditioned medium (Fig. 2A). After replacing draxin-conditioned medium with fresh culture medium, we observed robust neurite growth within 24 hours (Fig. 2C). These data excluded the possibility of a secondary effect of cell death in the presence of draxin-conditioned medium and indicated that draxin did indeed inhibit neurite outgrowth from dorsal spinal cord explants. Purified recombinant chick draxin also inhibited neurite outgrowth from dorsal spinal cord explants in a dose-dependent manner (Fig. 2, D, E, and P). We co-cultured the dorsal spinal cord explants with COS7 cell aggregates expressing chick draxin in collagen gels. Explants were dissected without adjacent roof plate tissue for radial outgrowth of neurites (5). When explants were co-cultured with mock-transfected cell aggregates, neurites grew radially from all sides of the explants (Fig. 2, F and Q). In contrast, when co-cultured with cell aggregates expressing draxin, neurites did not grow out of the proximal side to the COS7 cell aggregates; rather, they grew out of the distal side (Fig. 2, G and Q). To test whether draxin could induce growth cone

¹Division of Developmental Neurobiology, Graduate School of Medical Sciences, Kumamoto University, 1-1-1 Honjo, Kumamoto 860-8556, Japan. ²21st Century COE (Center of Excellence) Cell Fate Regulation Research and Education Unit, Kumamoto University, 2-2-1 Honjo, Kumamoto 860-0811, Japan. ³Global COE Cell Fate Regulation Research and Education Unit, Kumamoto University, 2-2-1 Honjo, Kumamoto 860-0811, Japan. ⁴Laboratory for Animal Resources and Genetic Engineering, Center for Developmental Biology (CDB), RIKEN Kobe, 2-2-3 Minatogima-minamimachi, Chuo-ku, Kobe 650-0047, Japan. ⁵Division of Integrative Cell Biology, Institute of Molecular Embryology and Genetics, Kumamoto University, 2-2-1 Honjo, Kumamoto 860-0811, Japan. ⁶Division of Anatomy and Neurobiology, Kobe University Graduate School of Medicine, Kobe 650-0017, Japan. ⁷Division of Cellular Therapy, Institute of Medical Science, The University of Tokyo, 4-6-1 Shirokanedai, Minato-ku, Tokyo 108-8639, Japan.

*These authors contributed equally to this work.

†Present address: Department of Genetics, Trinity College Dublin, Dublin 2, Ireland.

‡To whom correspondence should be addressed. E-mail: hitanaka@kumamoto-u.ac.jp

collapse, we cultured chick embryonic dorsal spinal cord explants on a laminin-coated dish without netrin-1 addition. Purified draxin protein was added to the culture medium after neurites had grown out from the explants (Fig. 2H), and growth cones were followed by time-lapse video microscopy. Growth cone collapse was observed within 30 min after the addition of purified draxin (Fig. 2I), and the neurites gradually retracted (movie S1). About 70% of the growth cones collapsed, and the remaining seemed to be insensitive to draxin. These results indicated that draxin might directly bind to the neurites and growth cones. We confirmed draxin binding to the neurites and growth cones by a binding assay using alkaline phosphatase (AP)-tagged draxin protein (Fig. 2, J and K). Importantly, draxin did not bind to and did not repel the neurites of dorsal root ganglion (Fig. 2, L and M). Next, we checked whether the above three events—neurite outgrowth inhibition, growth cone collapse, and draxin binding—were correlated in terms of dose dependency. We used draxin-AP protein for this analysis (6) and observed that these three events were correlated with each other (Fig. 2S). We also examined whether mouse draxin had repulsive activity against cortical neurites. Cortical explants from E17 mouse brains were co-cultured with COS7 cell aggregates expressing mouse draxin. Draxin repelled neurites from mouse cortical explants (Fig. 2, N, O and R). These results indicated that draxin might function as a repulsive axon guidance molecule for subpopulations of neurons *in vivo*.

To understand the function of draxin *in vivo*, we overexpressed myc-tagged draxin in the chick spinal cord at stages 14 and 15 at the thoracic level by *in ovo* electroporation. Embryos were fixed at stages 23 to 25, when many commissural axons cross the floor plate. Anti-myc signals from ectopic draxin were detected in the electroporated side (fig. S5, A to C). Anti-myc signals were also detected in the dorsolateral basement membrane of the control side (fig. S5B arrowhead). This result further supported the diffusible nature of draxin and its tendency to deposit in the dorsolateral basement membrane of the spinal cord. Immunohistochemical analyses using chick anti-TAG-1 showed partial inhibition of commissural axon growth in the experimental side (Fig. 3D and fig. S5G) compared with the control side or after expression of enhanced green fluorescent protein (EGFP) alone (Fig. 3B and fig. S5G). Next, we analyzed the effects of draxin on high-level ectopic expression by constructing an expression vector for a membrane-bound form of draxin. Anti-myc signals were localized only in the EGFP-expressing area, and there was no diffusion of the ectopic protein to the control side (fig. S5, D to F). Anti-TAG-1 staining showed a stronger effect of ectopic membrane-bound draxin compared with native draxin on commissural axon growth, which was almost completely inhibited on the experimental side in the presence of the membrane-bound form (Fig. 3F and fig. S5G). This result suggests that the signal induced

by membrane-bound draxin is stronger than that of the ectopically expressed native draxin. Moreover, this result suggests that membrane-bound draxin inhibited axonogenesis in the same way as bath application of draxin in the context of explant culture. However, overexpression of membrane-bound draxin at stages 19 and 20, after substantial commissural axonal growth initiation, resulted in the growth of many TAG-1-positive axons into the lumen of the central canal of the cord (Fig. 3H arrowheads). Whole-mount immunohistochemistry and EGFP fluorescence in open-book configuration after expression of EGFP alone showed the following: clear commissural axonal growth with parallel axons and a ventral funiculus along the floor plate after crossing over (fig. S5H arrowheads) and thick dorsal

funiculi of the dorsal root ganglia (fig. S5I). In the case of membrane-bound draxin expression, EGFP-positive parallel axons and the ventral funiculus were not observed (fig. S5, J and L). Commissural axonal growth was completely inhibited on the experimental side; however, these axons grew normally toward the floor plate in the control side. The dorsal funiculi formed normally on both sides (fig. S5, K and M). Anti-TAG-1 staining of the electroporated side showed a clear stage difference in the effects of ectopic draxin expression, which is consistent with the data obtained from staining of the sections (Fig. 3, F and H). Earlier electroporation of membrane-bound draxin substantially inhibited commissural axonal growth (fig. S5K); however, later electroporation did not inhibit axonal growth itself, and

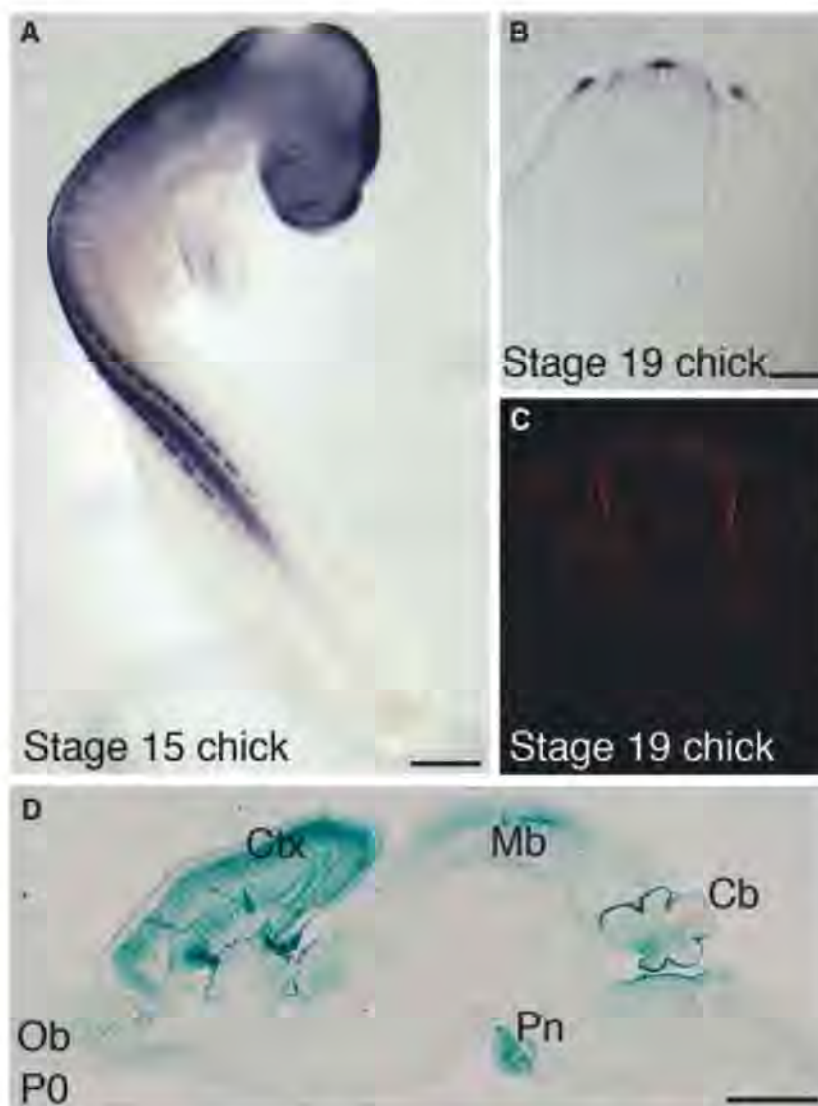


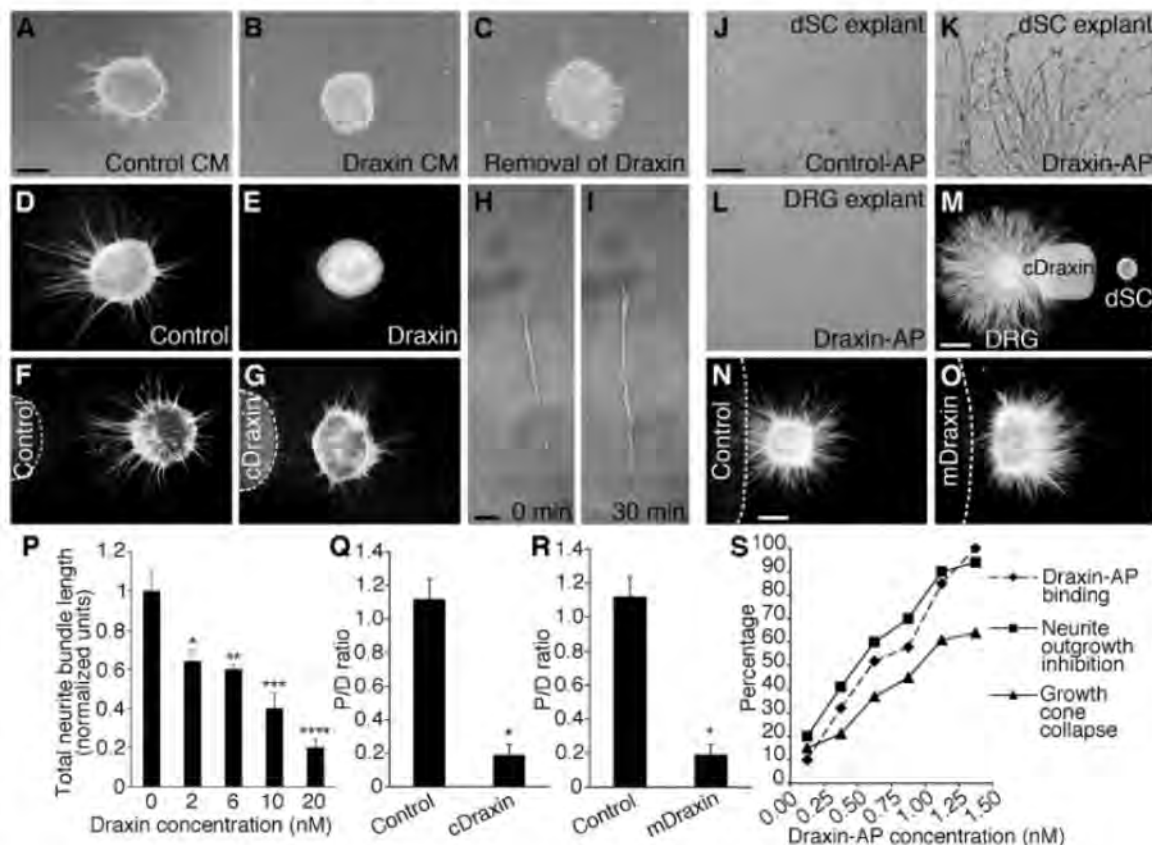
Fig. 1. Expression of *draxin* transcripts and protein during nervous system development. (A to C) *draxin* mRNA expression [(A) and (B)] and protein distribution (C) in chick embryos. *draxin* is expressed in the brain and spinal cord. (D) *draxin* expression by β -gal staining in a sagittal section of *draxin* heterozygous P0 mouse brain. *draxin* is expressed in the cortex (Ctx), midbrain (Mb), cerebellum (Cb), olfactory bulb (Ob), and pontine nuclei (Pn). Scale bars in (A) and (D) indicate 1 mm; in (B) and (C), 100 μ m.

axons were distributed in such a disorganized manner that the staining density was much higher than that in the control side (fig. S5M).

Next, we examined whether postcrossing commissural axons are affected by draxin. We co-cultured spinal cord explants, including the

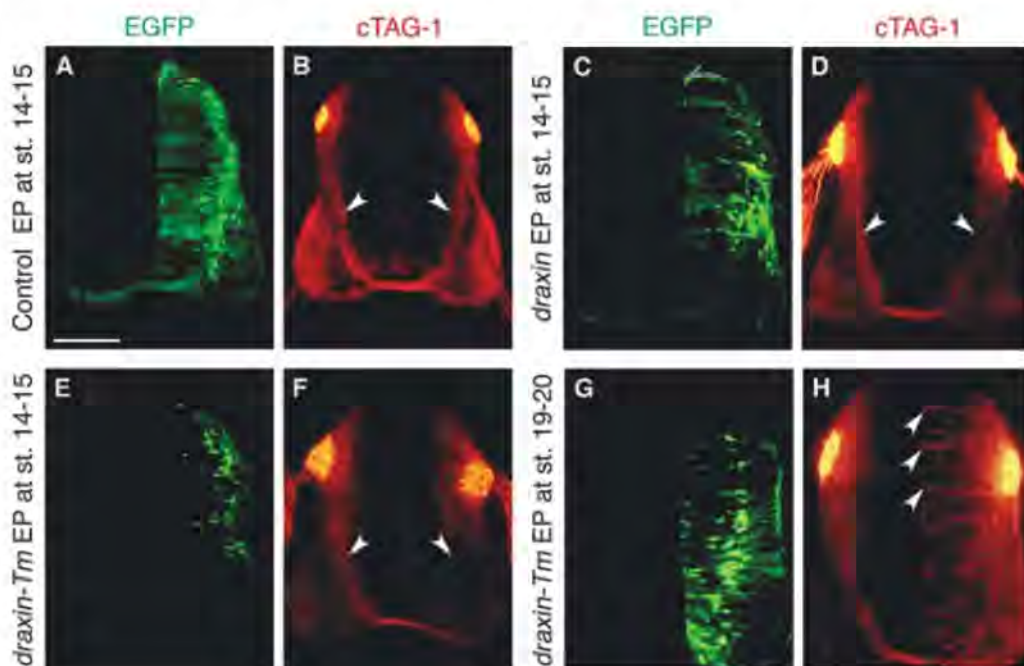
floor plate, from stages 25 and 26 chick embryos and COS7 cell aggregates in collagen gel. We did not observe any significant difference in the in-

Fig. 2. Draxin inhibits neurite outgrowth. (A to E) Inhibition of neurite outgrowth by draxin in conditioned medium (B) or purified [(E), 20 nM] form from dorsal spinal cord (dSC) explants of chick embryos. (F and G) Repulsion of neurite growth from chick dorsal spinal cord explants by draxin. (H and I) Growth cone collapse induced by draxin ($n = 15$). The black spots are landmarks in (H) and (I). (J to L) Draxin-AP binding to neurites from dorsal spinal cord and dorsal root ganglion (DRG) explants. (M) Co-culture of dorsal root ganglion explant, dorsal spinal cord explant, and draxin COS7 cell aggregates were performed at least three times. (N and O) Repulsion of neurite outgrowth by draxin from mouse cortical explants. (P) Quantification of neurite outgrowth inhibition (mean \pm SEM, $^*P = 0.009$, $^{**}P = 0.005$, $^{***}P = 0.001$, $^{****}P < 0.001$, t test, $n = 8$, P values were calculated by comparing with control). (Q) Quantification of repulsive activity observed in (F) and (G) measured as previously described (16) (mean \pm SEM, $^*P < 0.001$, t test, $n = 10$). (R)



Quantification of repulsive activity observed in (N) and (O), measured as described in (Q) (mean \pm SEM, $^*P < 0.001$, t test, $n = 15$). (S) Dose-dependent activity of draxin (6). CM, conditioned medium. Scale bars in (A) to (G), (N), and (O), 200 μ m; in (H) and (I), 10 μ m; in (J) to (L), 100 μ m; and in (M), 500 μ m.

Fig. 3. Ectopic draxin inhibits growth and disrupts the routing of commissural axons in vivo. (A to H) Transverse sections of chick spinal cord, fixed at stages 23 and 24 after electroporation. Commissural axon (TAG-1-positive) growth was normal when the control vector was electroporated [compare arrowheads in (B)]. In contrast, their growth was partially inhibited by secreted draxin [compare arrowheads in (D)]. They were completely inhibited [compare arrowheads in (F)] or severely misrouted [arrowheads in (H)] ($n = 12$) by membrane-bound draxin. *draxin-Tm* indicates membrane-bound draxin. EP, electroporation. Scale bar, 100 μ m.

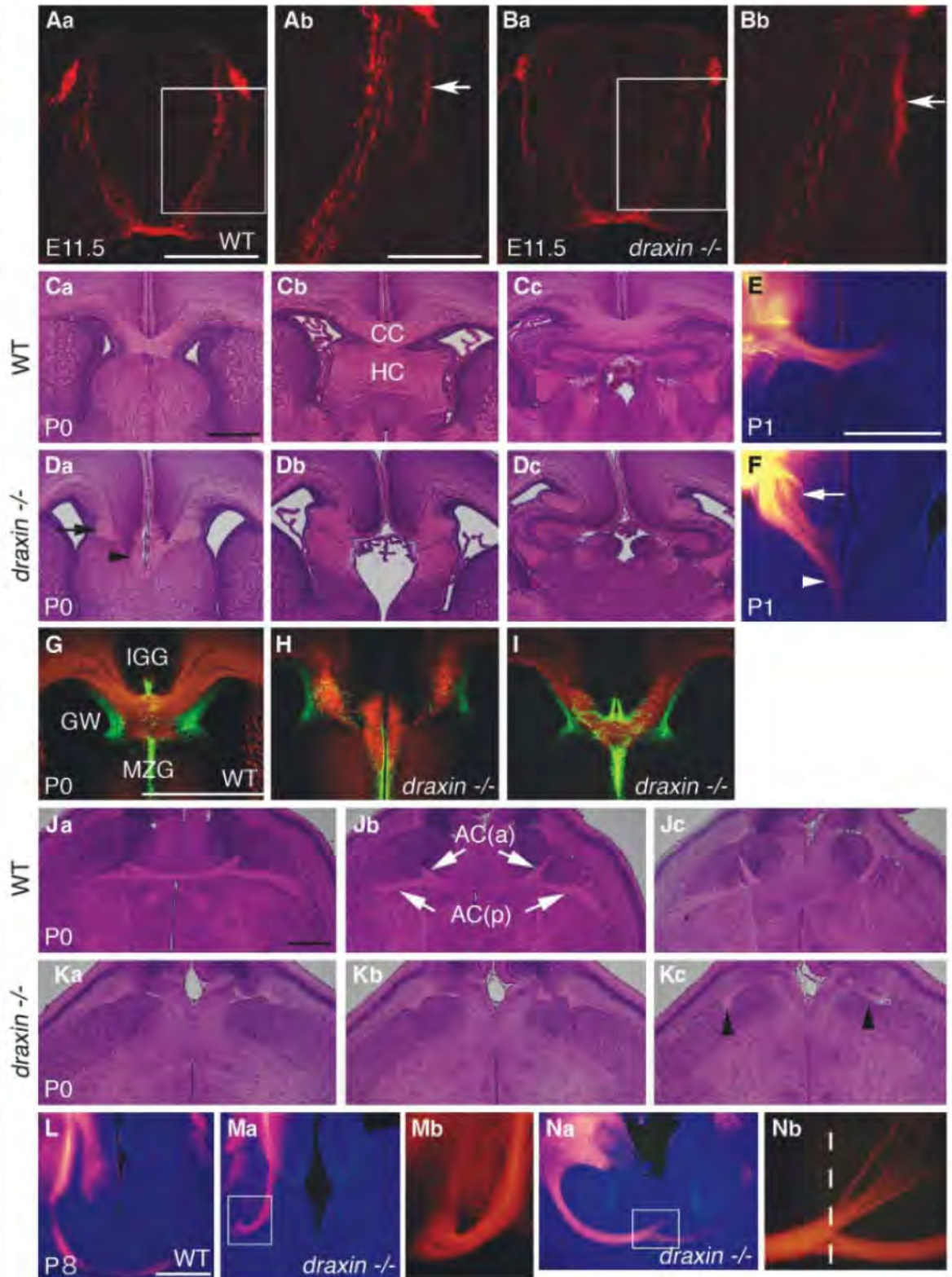


tensity of growth of postcrossing axons toward the COS7 cell aggregates transfected with control vector or chick *draxin* (fig. S6, A to C). We also labeled commissural axons with 1,1'-dioctadecyl-3,3,3',3'-tetramethylindocarbocyanine perchlorate

(DiI) after electroporation of membrane-bound *draxin* at stages 19 and 20. From the control side, labeled axons crossed the floor plate and turned to the anterior direction in a normal manner within the ectopic *draxin* environment, whereas

projection patterns of precrossing axons were severely disrupted in the electroporated side (fig. S6, G to I). In the case of control vector electroporation, projection patterns of both precrossing and postcrossing axons were normal (fig.

Fig. 4. Abnormal development of spinal cord and forebrain commissures in *draxin* deficient mice. (**Aa** to **Bb**) Transverse section at the upper thoracic level of E11.5 spinal cord stained with anti-TAG-1. Boxed areas in (**Aa**) and (**Ba**) are shown at high magnification in (**Ab**) and (**Bb**), respectively. The arrow in (**Bb**) indicates an axon bundle along the basement membrane that is thicker than that in the wild type [arrow in (**Ab**)]. Serial coronal [(**Ca**) to (**Dc**)] and horizontal [(**Ja**) to (**Kc**)] sections of P0 brains stained with hematoxylin and eosin. Coronal [(**E**) and (**F**)] and horizontal [(**L**) to (**Nb**)] sections of brains after injection of DiI into the neocortex [(**E**) and (**F**)] or olfactory bulb [(**L**) to (**Nb**)]. The corpus callosum (CC) and hippocampal commissure (HC) failed to cross the midline in the knockout mice [(**Da**) to (**Dc**)]. Arrow and arrowhead in (**Da**) and (**F**) indicate tangled corpus callosum axons and misprojected corpus callosum axons, respectively. (**G** to **I**) Coimmunostaining for GFAP and L1 in coronal sections of wild-type mice (**G**) and strongly (**H**) and weakly (**I**) affected mice at P0 to visualize the glial wedge (GW), indusium griseum glia (IGG), and midline zipper glia (MZG). Note the absence of indusium griseum glia in the strongly affected mice (**H**). The boxed areas in (**Ma**) and (**Na**) are shown at higher magnification in (**Mb**) and (**Nb**), respectively. Arrowheads in (**Kc**) indicate rudiments of anterior [AC(a)] and posterior [AC(p)] of the anterior commissure that never cross the midline. The dotted white line in (**Nb**) indicates the midline of the forebrain. Scale bars in (**Aa**) and (**Ba**), 200 μ m; in (**Ab**) and (**Bb**), 100 μ m; in (**Ca**) to (**Dc**) and (**Ja**) to (**Kc**), 500 μ m; and in (**E**) to (**F**), (**G**) to (**I**), (**L**), (**Ma**), and (**Na**), 1 mm.



S6, D to F). These data suggest that postcrossing commissural axons are not sensitive to draxin.

To examine the function of draxin by *in vivo* loss-of-function analysis, we established *draxin* knockout mice (fig. S3). Homozygous *draxin* ($-/-$) mice are viable and fertile. We analyzed projection patterns of spinal commissural axons by TAG-1 staining at embryonic day 11.5 (E11.5). In homozygous *draxin* ($-/-$) mice, commissural axons projected in a defasciculated manner toward the floor plate (Fig. 4, Ba and Bb, and fig. S7, A and B), resulting in expansion of the TAG-1-positive area medially, whereas they projected in a tightly fasciculated form in wild-type (Fig. 4, Aa and Ab, and fig. S7, A and B) and heterozygous mice. In addition, thick bundles of TAG-1-positive axons along the basement membrane were observed more frequently in homozygous *draxin* ($-/-$) mice than in wild-type littermates (compare arrows in Fig. 4, Ab and Bb). Whole-mount anti-TAG-1 immunohistochemistry of a dissected spinal cord in open-book configuration also showed the defasciculation of commissural axons in homozygous *draxin* ($-/-$) mice (fig. S7, E and F) compared with those in wild-type mice (fig. S7, C and D). Postcrossing commissural axon projections seemed normal in homozygous *draxin* ($-/-$) mice (fig. S8, A and B).

We next examined whether the projections of brain commissures were impaired in the *draxin* knockout mice with use of hematoxylin-eosin staining (Fig. 4, Ca to Dc and Ja to Kc) and immunostaining for the axonal marker L1 (fig. S9, A' to D"). All homozygous *draxin* ($-/-$) mice showed abnormal development of the corpus callosum, hippocampal commissure, and anterior commissure. We classified these phenotypes into two groups, depending on their severity. Severely affected mice had complete agenesis of these commissures (Fig. 4, Da to Dc and Ka to Kc and fig. S9, C' to D"), and weakly affected ones had partial defects in the formation of these commissures (table S2). About half of the heterozygous *draxin* mice showed abnormalities in corpus callosum and hippocampal commissure formation, and some showed complete agenesis (table S2). Anterograde tracing by Dil injection into the cortex revealed that, in the *draxin* knockout mice, corpus callosum axons failed to cross the midline and instead abnormally directed ventrally before they reached the midline (Fig. 4F), whereas corpus callosum axons in control mice crossed the midline (Fig. 4E). Previous studies have described that midline glial structures are intermediate targets of corpus callosum axons (7). To examine these structures, we immunostained with an antibody against glial fibrillary acidic protein (anti-GFAP) in wild-type and knockout mice at P0. All three midline glial populations—the glial wedge, indusium griseum glia, and midline zipper glia—were present in wild-type (Fig. 4G, $n = 8$) and weakly affected *draxin* knockout mice (Fig. 4I, $n = 4$). In contrast, indusium griseum glia was absent in strongly affected knockout mice (Fig. 4H, $n = 6$). This result suggests that the lack of indusium griseum glia might correlate with the severe defect in corpus callosum development. In

the anterior parts of the anterior commissure, the axons in control mice turned to the midline and crossed toward the contralateral side, and this was confirmed by Dil injection into the olfactory bulb (Fig. 4L). The anterior commissure axons in strongly affected knockout mice turned to the lateral side but not the midline (Fig. 4, Ma and Mb), whereas the majority of anterior commissure axons in weakly affected knockout mice took a normal course toward the midline but misprojected rostrally at the midline (Fig. 4, Na and Nb). In addition, anterior commissure neurons were retrogradely labeled in the olfactory bulb contralateral to the injection site in wild-type mice (Fig. 4L); however, such labeled neurons were not detected in the corresponding area of strongly affected knockout mice (Fig. 4Ma). In contrast to the severe defects in the forebrain commissure, the posterior commissure and habenular commissure appeared to develop normally in the *draxin* knockout mice (fig. S8, D and F).

We next investigated *draxin* expression during development of the spinal cord and forebrain commissures by β -gal staining of heterozygous mice. β -gal expression was detected in the dorsal spinal cord and commissural axons (fig. S10, A to F). Antidraxin staining revealed draxin protein expression in the same area and heavy deposition in the lateral basement membrane (fig. S10, G to L). In the case of forebrain commissures, β -gal expression was observed in the regions that surround the corpus callosum, hippocampal commissure, and anterior commissure, such as the midline glial cells, indusium griseum glia, and glial wedge, whereas β -gal expression was not detected in these commissural axons (fig. S11). Antidraxin staining and draxin-AP binding on sections revealed the presence of draxin proteins and its receptors in the forebrain commissural axons (fig. S12).

Spinal cord commissural axonal growth has been well studied and found to be guided by the attractive cues netrin-1 (8, 9) and Shh (10), which emanate from the floor plate, and also by the repulsive cues BMP7 and growth differentiation factor 7 (GDF7), which emanate from the roof plate (11, 12). Our *in vitro* and *in vivo* gain-of-function data suggest that draxin is a chemorepulsive guidance protein for commissural axons. The homozygous *draxin* ($-/-$) mouse showed defasciculated projections of commissural axons toward the floor plate (Fig. 4 and fig. S7). This defasciculation might be due to the deficient repulsive activity of environmental draxin, mainly in the lateral basement membrane. Immunohistochemical analyses indicate expression of *draxin* mRNA and protein in commissural axons (fig. S10). The importance of this expression is unknown, although draxin may function in an autocrine manner to regulate the sensitivity of commissural axon to draxin in the surrounding milieu.

The data presented here demonstrate that draxin is required for the midline crossing of forebrain commissures (Fig. 4 and fig. S9). *draxin* is expressed in midline glial cells, which have been thought to act as intermediate guideposts for corpus callosum axons via the expression of axon guidance mole-

cules (13), such as Slit2 (14) and Wnt5a (15). In addition, draxin repels neurite outgrowth from cortical explants at E17 (Fig. 2O), when corpus callosum axons cross the midline. These results suggest that draxin is a chemorepulsive molecule that is responsible for corpus callosum development in midline glial cells. We speculate that misprojection of corpus callosum axons at the midline, observed in almost all of the knockout mice (Fig. 4F), is caused by the deficient draxin repulsive activity from the glial wedge. A similar presumption probably applies to the draxin roles in anterior commissure and hippocampal commissure development, as judged from analyses of the *draxin* expression and the mutant phenotypes. Thus, we propose that draxin repulsion from the regions surround the trajectories of forebrain commissures is essential for proper guidance of their commissural axons, preventing them from misprojecting before reaching the midline. Because all forebrain commissures were frequently misprojected at the midline in the knockout mice, midline cells expressing *draxin* may be particularly critical for the midline crossing. Furthermore, corpus callosum axons in the knockout mice are defasciculated in the ipsilateral side (Fig. 4F). *draxin* is expressed in deep cortical layers and cingulate cortex, in addition to the midline glial cells. Because most of corpus callosum axons arise from neurons in layers 2/3 and 5, some of the projecting neurons may express *draxin*. Thus, draxin is required for the fasciculation of corpus callosum axons in a paracrine and/or autocrine manner, which may be consistent with draxin functions on spinal commissural axons. It is also important to note that indusium griseum glia is missing only in the severely affected knockout mice (Fig. 4H). This result suggests that not only the deficient repulsive activity from the glial cells but also the lack of indusium griseum glia might be involved in the disruption of the corpus callosum formation. Further investigation is needed to clarify draxin functions on the formation of indusium griseum glia and its involvement on the commissure formation.

References and Notes

1. M. Tessier-Lavigne, C. S. Goodman, *Science* **274**, 1123 (1996).
2. B. J. Dickson, *Science* **298**, 1959 (2002).
3. Y. Zou, A. Lyuksyutova, *Curr. Opin. Neurobiol.* **17**, 22 (2007).
4. T. Serafini *et al.*, *Cell* **78**, 409 (1994).
5. M. Placzek, M. Tessier-Lavigne, T. M. Jessell, J. Dodd, *Development* **110**, 19 (1990).
6. Materials and methods are available as supporting material on Science Online.
7. T. Shu, L. J. Richards, *J. Neurosci.* **21**, 2749 (2001).
8. T. E. Kennedy, T. Serafini, J. de la Torre, M. Tessier-Lavigne, *Cell* **78**, 425 (1994).
9. T. Serafini *et al.*, *Cell* **87**, 1001 (1996).
10. F. Charron, E. Stein, J. Jeong, A. P. McMahon, M. Tessier-Lavigne, *Cell* **113**, 11 (2003).
11. A. Augsburger, A. Schuchardt, S. Hoskins, J. Dodd, S. Butler, *Neuron* **24**, 127 (1999).
12. S. J. Butler, J. Dodd, *Neuron* **38**, 389 (2003).
13. C. Lindwall, T. Fothergill, L. J. Richards, *Curr. Opin. Neurobiol.* **17**, 3 (2007).
14. T. Shu, V. Sundaresan, M. McCarthy, L. J. Richards, *J. Neurosci.* **23**, 8176 (2003).
15. T. R. Keeble *et al.*, *J. Neurosci.* **26**, 5840 (2006).
16. Y. Liu *et al.*, *Nat. Neurosci.* **8**, 1151 (2005).

17. We thank D. S. Campbell for careful reading of the manuscript, C. Krull for the pMES-internal ribosome entry site (IRES)-EGFP vector, J. G. Flanagan for APTag-2 vector, H. Fujisawa for helpful discussions, and the Developmental Studies Hybridoma Bank for antibodies. This work was supported by grants-in-aid from the Ministry of Education, Science, Sports, and Culture of

Japan (MEXT), by the 21st Century COE Program and by the Global COE Program (Cell Fate Regulation Research and Education Unit), MEXT, Japan.

Supporting Online Material

www.sciencemag.org/cgi/content/full/323/5912/388/DC1
Materials and Methods

Figs. S1 to S12
Tables S1 and S2
Movie S1

27 August 2008; accepted 2 December 2008
10.1126/science.1165187

Recombination of Retrotransposon and Exogenous RNA Virus Results in Nonretroviral cDNA Integration

Markus B. Geuking,^{1,†} Jacqueline Weber,^{1,‡} Marie Dewannieux,² Elieser Gorelik,³ Thierry Heidmann,² Hans Hengartner,¹ Rolf M. Zinkernagel,^{1,§} Lars Hangartner^{1,†§}

Retroviruses have the potential to acquire host cell-derived genetic material during reverse transcription and can integrate into the genomes of larger, more complex DNA viruses. In contrast, RNA viruses were believed not to integrate into the host's genome under any circumstances. We found that illegitimate recombination between an exogenous nonretroviral RNA virus, lymphocytic choriomeningitis virus, and the endogenous intracisternal A-type particle (IAP) retrotransposon occurred and led to reverse transcription of exogenous viral RNA. The resulting complementary DNA was integrated into the host's genome with an IAP element. Thus, RNA viruses should be closely scrutinized for any capacity to interact with endogenous retroviral elements before their approval for therapeutic use in humans.

Lymphocytic choriomeningitis virus (LCMV) is an ambisensed RNA virus belonging to the Arenaviridae family with no known reverse transcriptase (RT) activity. Nevertheless, DNA complementary to the small genomic RNA of LCMV, which encodes for the viral glycopro-

tein (GP) and nucleoprotein (NP), is found in vitro and in vivo after infection (1).

Intracisternal A-type particle (IAP) elements, retrotransposons that belong to the retroviral family, are found in ~1000 copies per haploid genome of the mouse (*Mus musculus*). Only a fraction

of these is assumed to be actively transposing (2). Their retrotransposition has frequently been associated with oncogenesis or aberrant cytokine expression (3–7) reviewed in (8). IAP expression has been associated with tumor control (9) or major histocompatibility complex class I down-regulation (10). Transcription of IAP genes, and probably the transposition of IAP, occurs during spermatogenesis and in the thymus (11, 12). To date, the biological role of IAP elements and other endogenous retroviruses remains unclear.

¹Institute of Experimental Immunology, University Hospital Zürich, Schmelzbergstrasse 12, 8091 Zürich, Switzerland.

²CNRS Unité Mixte de Recherche 8122, Unité des Rétrovirus Endogènes et Éléments Rétroviraux des Eucaryotes Supérieurs, Institut Gustave Roussy, 94805 Villejuif Cedex and Université Paris-Sud 91405 Orsay, France. ³University of Pittsburgh Cancer Institute, Hillman Cancer Center, Room 1.46, Pittsburgh, PA 15232, USA.

*Present address: Department of Medicine, McMaster University, 1200 Main Street West, Hamilton, ON L8N 3Z5, Canada.

†To whom correspondence should be addressed. E-mail: hangartner.lars@virology.uzh.ch (L.H.); geuking@mcmaster.ca (M.B.G.); rolf.zinkernagel@usz.ch (R.M.Z.)

‡Present address: Institut für Molekulare Biomedizin, ETH Zürich, Wagistrasse 27, 8952 Schlieren, Switzerland.

§These authors contributed equally to this work.

||Present address: Institute of Medical Virology, University of Zurich, Gloriastrasse 30, 8006 Zurich, Switzerland.

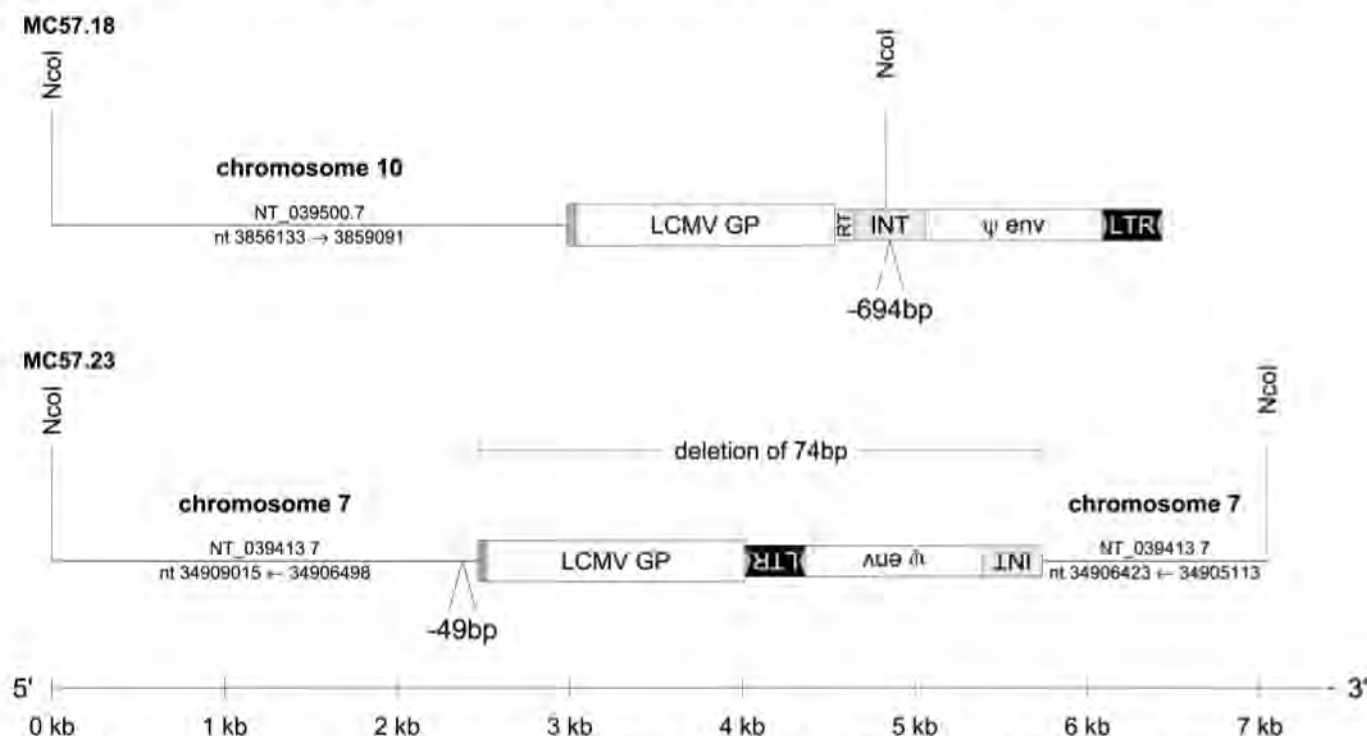


Fig. 1. DNA complementary to LCMV-GP integrated into the genome in conjunction with sequences derived from a retrotransposon. Schematic maps of cGP and flanking sequences in clone MC57.18 and MC57.23

derived from LCMV infected MC57G cells. Genes, open or gray boxes; IAP LTRs, black boxes with the inverted repeats indicated as gray triangles. Positions of deletions and restriction sites are indicated.

Here, we show that endogenous IAP elements promoted reverse transcription and integration of LCMV RNA after infection. These findings impinge on the design of RNA vectors and indicate alternative mechanisms for the coevolution between host, endogenous retroviral elements, and exogenous viruses.

Formation of DNA complementary to the LCMV RNA genome (cLCMV) after infection of MC57G cells can be detected in about 1 in 10³ to 10⁴ cells (1). To analyze the events leading up to cLCMV formation, we serially subcloned LCMV-infected MC57G cells to derive two stable cell lines (MC57.18 and MC57.23) that contained genetic material complementary to LCMV GP (cGP) (Fig. 1) (13). It is important to note that LCMV could not be detected in the supernatants of these cell cultures after the subcloning procedure (14).

Using a combination of long-range and inverse polymerase chain reaction (PCR) (13), we isolated the LCMV-GP-derived genetic material, including the flanking sequences from both clones (Fig. 1). In both cell lines, the virus-derived genetic material consisted of a full-length cGP gene that was joined at the 3' end to sequences derived from murine IAP retrotransposon (Fig. 1). In both cases, homology with IAP ended within the 3' region of the IAP polymerase/integrase gene, albeit at different locations and in opposite orientations. The 5' cGP-flanking sequences of MC57.18 shared 99% homology with the C57BL/6 mouse chromosome 10 (NT_039500.7, nucleotides 3856133 to 3859091). The 5' and 3' cGP flanking sequences of MC57.23 were 99% homologous to chromosome 7 from C57BL/6 mice (NT_039413.7, nucleotides 34906498 to 34909015 and 34905113 to 34906423, respec-

tively), with an internal deletion of 49 base pairs near the integration site.

Analysis of the homologies between the cGP sequences and the small genomic RNA of LCMV revealed that both the 3' and 5' homology breakpoints were almost at the same position [\pm 1 nucleotide (nt)] (fig. S1, A and B). At the 5' end, homology with LCMV always ended in the 5' untranslated region. Both 3' homology breakpoints were located within the stop codon of the LCMV-GP open reading frame. No target site duplication was found at the site of integration in MC57.23, suggesting that integration of the cLCMV/IAP sequences was not catalyzed by a classical retroviral integrase activity. In addition, the multiple deletions shown in Fig. 1 indicate that integration of the cLCMV/IAP recombination product might have occurred at sites of DNA damage [supporting online material (SOM) text 1].

From these results, we hypothesized that IAP elements were catalyzing the reverse transcription and subsequent integration of the cGP genes. To obtain more formal proof, we transfected a series of plasmids encoding for functional IAP retrotransposons (213P12, 440N1, 92L23, and 262J2) (15) into LCMV-infected cell lines from four different species (human, green monkey, dog, and Chinese hamster) that do not display cGP formation (1) after LCMV infection (Table 1). As a control, we transfected a plasmid encoding enhanced green fluorescence protein (EGFP) or we left the cells untreated. Three days later, we isolated genomic DNA and tested for the presence of cGP by nested PCR (Table 1).

Untransfected or LCMV-infected cells transfected with the control EGFP plasmid did not make cGP [0 out of 34 independent transfection experiments (0/34)]. Transfection of noninfected cells with the panel of IAP elements also failed to produce cGP sequences (0/47). In contrast, transfection of LCMV-infected cells with IAP-expressing plasmids resulted in the formation of cGP sequences with a frequency of 70.2% (33/47). Some IAP variants (e.g., 262J21 and 440N1) mediated cGP formation more efficiently (\geq 80%) than others (e.g., 92L23, with 40% efficiency), confirming that expression of functional IAP elements is required for the formation of LCMV cDNA.

IAP elements lacking (440N1 Δ RT) or having a nonfunctional (440N1LinkerStopRT) *pol* gene failed to mediate cGP formation in LCMV-infected Vero cells (Table 2). We also found that in the absence of gag, cGP formation did not occur (0/2).

Table 1. Correlation between IAP expression and LCMV cDNA formation. Human (HeLa), green monkey (Vero), canine (MDCK), and Chinese hamster (CHO) cells were infected with LCMV at a multiplicity of infection of 0.001 (+) or left untreated (–). One day later, plasmids expressing the indicated functional IAP element (15) or a control plasmid expressing EGFP were transfected. The number of cultures displaying cGP formation per total number of cultures tested is indicated.

Virus/cell line	Plasmids containing functional wild-type IAP elements								Negative controls			
	213P12		440N1		92L23		262J21		pEGFP-N3		Mock	
	–	+	–	+	–	+	–	+	–	+	–	+
LCMV	–	–	–	–	–	–	–	–	–	–	–	–
HeLa	0/3	3/3	0/3	3/3	0/3	2/3	0/5	4/5	0/5	0/5	0/5	0/5
Vero	0/2	0/2	0/2	1/2	0/2	0/2	0/5	4/5	0/5	0/5	0/5	0/5
MDCK	0/3	2/3	0/3	2/3	0/3	0/3	0/5	5/5	0/5	0/5	0/5	0/5
CHO	0/2	2/2	0/2	2/2	0/2	2/2	0/2	1/2	0/2	0/2	0/2	0/2
Total	0/10	7/10	0/10	8/10	0/10	4/10	0/17	14/17	0/17	0/17	0/17	0/17
% cGP+	0%	70%	0%	80%	0%	40%	0%	82%	0%	0%	0%	0%

Table 2. IAP-derived RT activity is required for LCMV GP cDNA formation. Vero cells were infected with LCMV at a multiplicity of infection of 0.001 (+) or left untreated (–). One day later, plasmids containing a functional IAP element (440N1), RT-deficient IAP elements (440N1 Δ RT and LinkerStopRT), or the HIV-1 Gag-Pol plasmid pCMV Δ R8 were transfected. Mock transfection was performed as an additional negative control. The number of cultures displaying cGP formation per total number of cultures tested is indicated.

Virus/cell line	Functional		No functional IAP RT				HIV-1 Gag-Pol		Control	
	440N1		440N1 Δ RT		LinkerStopRT		HIV-1 pCMV Δ R8		Mock	
	–	+	–	+	–	+	–	+	–	+
LCMV	–	–	–	–	–	–	–	–	–	–
Vero	0/10	11/14	0/1	0/16	0/4	0/8	0/4	1/18	0/8	0/12
% cGP+	0%	78.6%	0%	0%	0%	0%	0%	5.6%	0%	0%

Fig. 2. cNP/IAP and cGP/IAP recombinations detected in vitro and in vivo in mice after LCMV infection. Recombination products for cNP/IAP (A) and cGP/IAP (B) amplified from genomic DNA of the indicated source and sample number. Genes are shown as labeled open boxes, gray boxes indicate insertion sequences derived from the intergenic region of the small genomic RNA of LCMV, black boxes indicate IAP LTR-derived sequences, and a gray triangle indicates the inverted repeats of the IAP LTR. Gray normal-faced letters represent nucleotides derived from the LCMV intergenic region, and bold-faced ones represent the direct repeat of the IAP LTR. Red boxes and letters indicate sequences derived from tRNA^{Phe}.

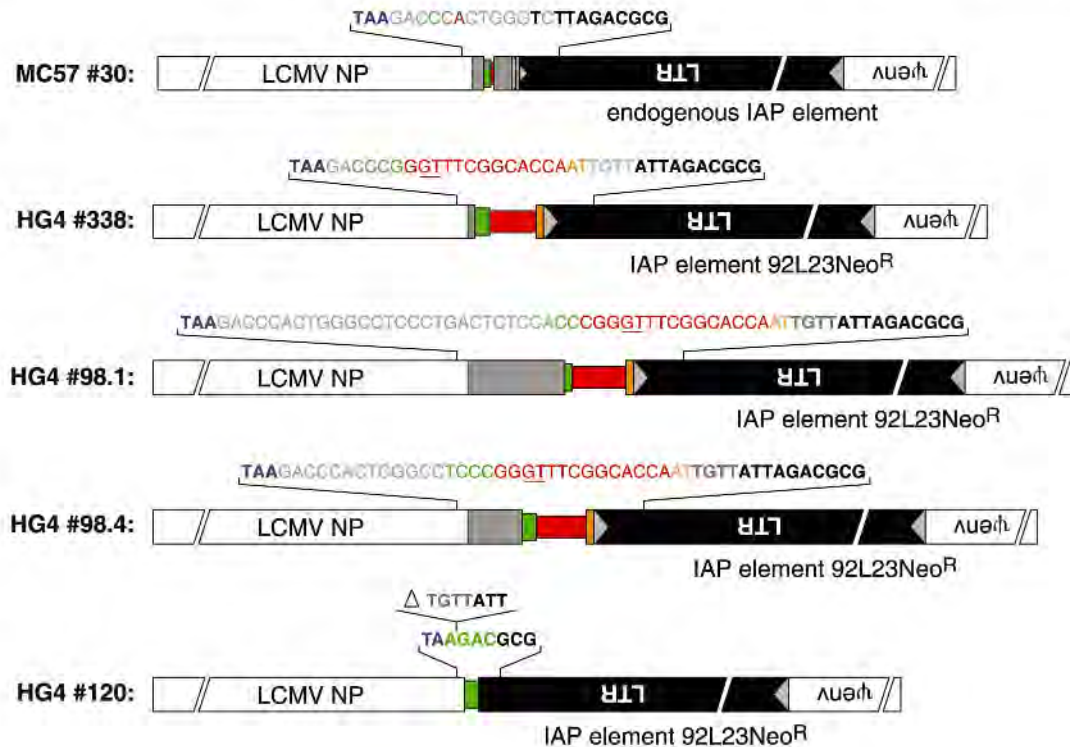
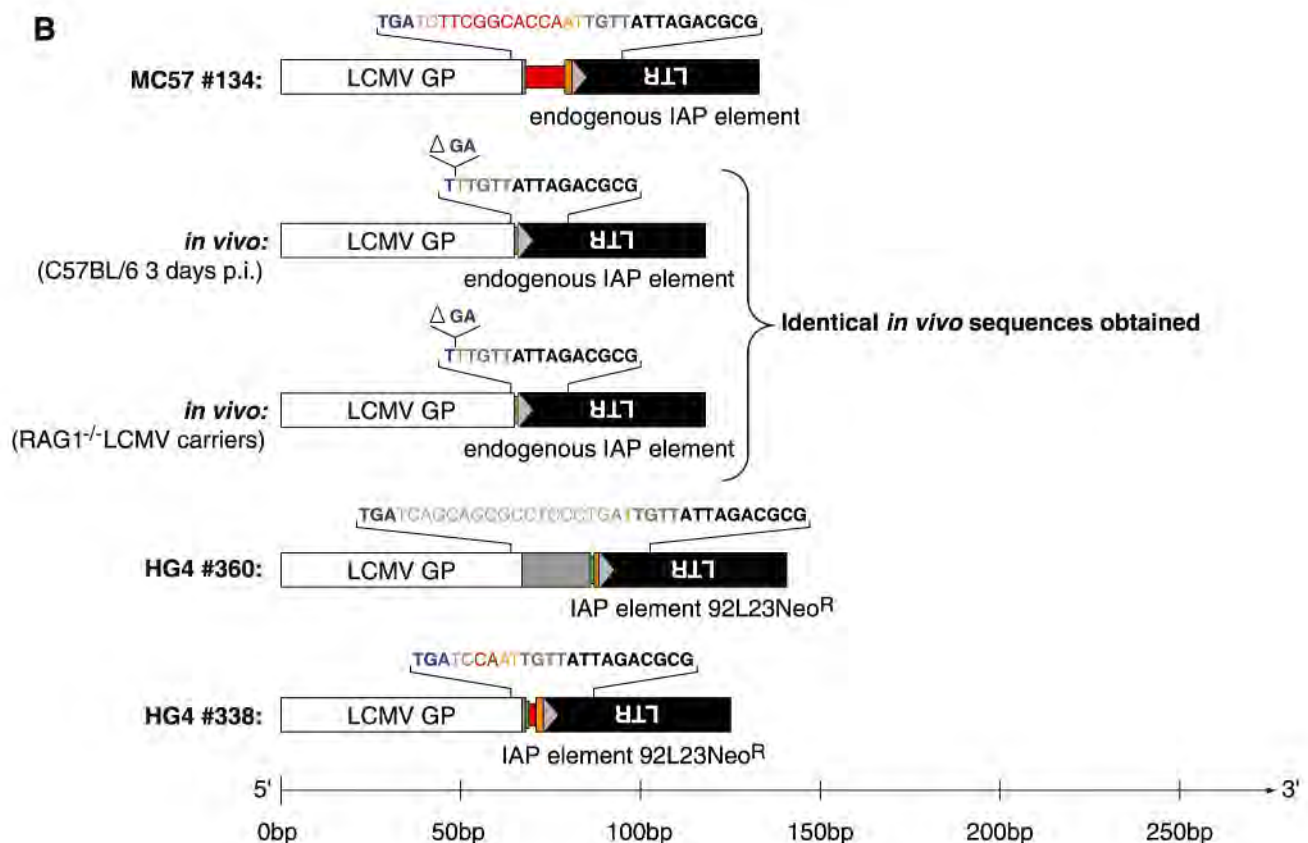
The underlined nucleotides GT are only found in the tRNA^{Phe} and not in the IAP primer-binding site. Blue bold letters indicate the NP and GP stop codons. Orange letters and boxes indicate the nucleotides bridging between the IAP LTR and the primer-binding site (fig. S2). Green letters and boxes indicate nucleotides at the homology break points that cannot unambiguously be assigned to either tRNA^{Phe}/IAP LTR or LCMV small RNA. The center of the maps showing the recombination site is proportional to the depicted ruler, but large portions of the LCMV NP, IAP LTR, and IAP ψ env genes were omitted because of limited space and are indicated by interrupted gene symbols (A).

When we compared the ability of gag/pol proteins derived from IAP to mediate cGP formation with that of gag/pol proteins derived from another retrovirus (HIV-1, pCMVΔR8) (16), we found that

the IAP element 440N1 was more efficient (11 out of 14 = 78.6%) than HIV-1 (1 out of 18 = 5.6%) (Table 2) in catalyzing cGP formation. Moreover, the guinea pig cell line CCL158 fails to form

cLCMV, despite high levels of RT activity (1). Thus, the efficiency of the endogenous retrovirus derived from the natural host in mediating cLCMV formation probably reflects their evolutionary history.

A

**B**

To further investigate the detailed molecular events giving rise to LCMV/IAP hybrid DNA formation, we designed nested PCR approaches that detect recombined cLCMV/IAP hybrid sequences (13). We were able to amplify both cNP/IAP and cGP/IAP recombination events directly from infected murine MC57G cells (Fig. 2). We also detected cGP/IAP recombination events *in vivo* in splenocytes of an acutely infected C57BL/6 mouse and in peripheral blood mononuclear cells of RAG1^{-/-} mice persistently infected with LCMV (Fig. 2B), demonstrating that recombination between IAP retrotransposons and LCMV was not an artifact of immortalized cells but also occurred spontaneously *in vivo*.

The abundance of IAP elements in the murine genome (2) makes a detailed interpretation of sequence data difficult, as the exact sequence of the IAP element involved in LCMV hybrid formation is not known. We generated a recombinant HeLa cell line (HG4) in which all the IAP elements were derived from a single molecular clone 92L23Neo^R (15) and that reliably formed cLCMV upon infection.

Three days after LCMV infection of HG4 cells we amplified several different cNP/IAP and cGP/IAP recombination events involving the 92L23Neo^R IAP element (Fig. 2). All amplified recombination products were sequenced and analyzed for homologies to 92L23Neo^R and the LCMV genome. In contrast to the sequences obtained from the subcloned infected MC57G cell lines MC57.18 and MC57.23, where IAP and LCMV sequences were directly joined to each other (Fig. 1), we observed insertions of additional nucleotides at the site of recombination in cLCMV/IAP hybrid DNA amplified from infected HG4 and MC57G cells (Fig. 2). These insertions, consisting of up to 14 nts displayed homology to the 3' end of the 76-nt-long phenylalanine tRNA (tRNA^{Phe}, GenBank accession number K02684), which has previously been shown to act as primer for the reverse transcription of IAP elements (SOM text 2) (17).

We showed that endogenous retroviral elements can recombine with exogenous nonretroviral RNA viruses presumably by copy choice during reverse transcription (SOM text 2) to yield cDNA complementary to both the endogenous retrovirus and the exogenous RNA virus. Such recombinant cDNA has the potential to integrate into the genome of the infected cell, and because IAP elements have been shown to transpose most efficiently in the thymus and in the LCMV-sanctuaries (18) of the testicles (11, 12), such recombinations theoretically could lead to germline transmission of viral genes from RNA viruses. Therefore, nonretroviral RNA viruses may have contributed more substantially and directly to the evolution of mammalian genomes than has been assumed so far (SOM text 3). However, extensive database analysis of the murine genome, which was determined with DNA from LCMV-free mice, did not yield substantial homologies

to the LCMV-genome. In humans, there is some evidence to suggest that at least one subgroup of the human endogenous retrovirus-K family may be active (19, 20). Thus, the potential risk of somatic integration into host cells during human gene therapy using RNA virus vectors should be experimentally assessed by nested PCR.

References and Notes

1. P. Kleenerman, H. Hengartner, R. M. Zinkernagel, *Nature* **390**, 298 (1997).
2. E. L. Kuff, K. K. Lueders, *Adv. Cancer Res.* **51**, 183 (1988).
3. E. L. Kuff *et al.*, *Nature* **302**, 547 (1983).
4. E. Canaan *et al.*, *Proc. Natl. Acad. Sci. U.S.A.* **80**, 7118 (1983).
5. K. B. Leslie, F. Lee, J. W. Schrader, *Mol. Cell. Biol.* **11**, 5562 (1991).
6. H. Ishihara, I. Tanaka, H. Wan, K. Nojima, K. Yoshida, *J. Radiat. Res. (Tokyo)* **45**, 25 (2004).
7. X. Y. Wang, L. S. Steelman, J. A. McCubrey, *Cytokines Cell. Mol. Ther.* **3**, 3 (1997).
8. I. A. Maksakova *et al.*, *PLoS Genet.* **2**, e2 (2006).
9. E. Braun, E. Rorman, K. K. Lueders, A. Bar-Sinai, J. Hochman, *Virology* **277**, 136 (2000).
10. M. Li *et al.*, *J. Gen. Virol.* **77**, 2757 (1996).
11. A. Dupressoir, T. Heidmann, *Mol. Cell. Biol.* **16**, 4495 (1996).
12. E. L. Kuff, J. W. Fewell, *Mol. Cell. Biol.* **5**, 474 (1985).
13. Materials and methods are available as supporting material on Science Online.
14. F. Lehmann-Grube, *Virology Monographs* (Springer, New York, 1971).

15. M. Dewannieux, A. Dupressoir, F. Harper, G. Pierron, T. Heidmann, *Nat. Genet.* **36**, 534 (2004).
16. L. Naldini *et al.*, *Science* **272**, 263 (1996).
17. M. Ono, H. Ohishi, *Nucleic Acids Res.* **11**, 7169 (1983).
18. M. Reher *et al.*, *Nat. Med.* **13**, 1316 (2007).
19. N. Bannert, R. Kurth, *Proc. Natl. Acad. Sci. U.S.A.* **101**, 14572 (2004).
20. R. Belshaw *et al.*, *J. Virol.* **79**, 12507 (2005).
21. We are very grateful to K. K. Lueders for providing plasmids and critically reading the manuscript. We thank A. Macpherson, K. McCoy, and D. Burton for their support. We would also like to thank K. McCoy for critically reading the manuscript and for helpful comments. This study was supported by the Swiss National Science Foundation and the Canton of Zurich. M.B.G. planned and performed the experiments and wrote the paper together with L.H.; J.W. performed experiments; M.D., E.G., and T.H. provided reagents, cell lines, or plasmids; H.H. and R.M.Z. were involved in the planning and discussions of experiments, helped to write the paper, and provided the infrastructure used for this study; and L.H. initiated and supervised the study, planned and conducted experiments, and wrote the paper together with M.B.G. Sequences depicted in Fig. 1 are available from GenBank under accession numbers FJ460582 (MC57.18) and FJ460583 (MC57.23).

Supporting Online Material

www.sciencemag.org/cgi/content/full/323/5912/393/DC1

Materials and Methods

SOM Text

Figs. S1 to S3

Tables S1 and S2

References

20 October 2008; accepted 19 November 2008

10.1126/science.1167375

Molecular Mechanisms of HipA-Mediated Multidrug Tolerance and Its Neutralization by HipB

Maria A. Schumacher,^{1*} Kevin M. Piro,¹ Weijun Xu,¹ Sonja Hansen,² Kim Lewis,² Richard G. Brennan^{1*}

Bacterial multidrug tolerance is largely responsible for the inability of antibiotics to eradicate infections and is caused by a small population of dormant bacteria called persisters. HipA is a critical *Escherichia coli* persistence factor that is normally neutralized by HipB, a transcription repressor, which also regulates *hipBA* expression. Here, we report multiple structures of HipA and a HipA-HipB-DNA complex. HipA has a eukaryotic serine/threonine kinase-like fold and can phosphorylate the translation factor EF-Tu, suggesting a persistence mechanism via cell stasis. The HipA-HipB-DNA structure reveals the HipB-operator binding mechanism, ~70° DNA bending, and unexpected HipA-DNA contacts. Dimeric HipB interacts with two HipA molecules to inhibit its kinase activity through sequestration and conformational inactivation. Combined, these studies suggest mechanisms for HipA-mediated persistence and its neutralization by HipB.

Bacteria that are resistant or tolerant to antibiotics are an increasing threat to human health. Indeed, ~60% of infections in the developed world are caused by biofilms, which exhibit multidrug tolerance (MDT) (1, 2). MDT is caused by the presence of dormant bacterial cells called persisters, which account for only 10⁻⁶ to 10⁻⁴ cells in a growing population, making MDT difficult to study (3–5). Persisters are not mutants but phenotypic variants of wild-type cells that evade killing by somehow adopting a transient dormant state (6, 7). Dormancy provides protection because bactericidal antibiotics kill by

corrupting their active targets into producing toxic byproducts. These protected persisters can then switch back to the growth phase after the removal of antibiotics, allowing the bacterial population to survive. The first high-persistence allele, *hipA7*

¹Department of Biochemistry and Molecular Biology, University of Texas, M. D. Anderson Cancer Center, Unit 1000, Houston, TX 77030, USA. ²Department of Biology and Antimicrobial Discovery Center, Northeastern University, Boston, MA 02115, USA.

*To whom correspondence should be addressed. E-mail: rgbrenna@mdanderson.org (R.G.B.); maschuma@mdanderson.org (M.A.S.)

(*high-persistence A*), was identified in *Escherichia coli* and increased the frequency of persistence by 10,000 fold (8–10). *E. coli* *hipA* encodes a 440-residue protein, HipA, which is cotranscribed with a smaller upstream gene, *hipB*. HipB is an 88-residue protein that represses the *hipBA* operon by binding cooperatively to four operators upstream of *hipBA* (11, 12). HipB forms a complex with HipA, and because wild-type HipA cannot be expressed in the absence of HipB because of its deleterious effects on cell growth, *hipBA* has been categorized as a toxin/antitoxin (TA) module in which HipA, the toxin, is neutralized by the antitoxin, HipB (13, 14). Toxin proteins from chromosomally encoded TA modules, of which more than 10 have been identified in *E. coli*, appear to promote cell dormancy and may play roles in the development of persistence under certain conditions (5, 7). Chromosomal TA modules can be grouped into three main superfamilies based on whether the toxin has a ribonuclease (RNase)/gyrase-like fold, RNase barnase-like structure, or a PilT N-terminus (PIN) domain (14). The corresponding antitoxins contain DNA binding domains and C termini that are largely unfolded until bound by the toxin (14). HipA and HipB show no homology to any member of these TA superfamilies. Moreover, HipA is one of the few validated biofilm tolerance factors. Indeed, it has been demonstrated that overexpression of the HipA protein leads to MDT in *E. coli* (2). However, the mechanism of HipA-mediated MDT is unknown.

To delineate the functions of HipA and HipB in MDT, we carried out biochemical and structural studies on HipA and HipA-HipB-DNA complexes. Because of wild-type HipA-mediated persistence, we used the HipA mutant Asp³⁰⁹→Gln³⁰⁹ (D309Q) (referred to as HipA), which can be produced in large quantities in the absence of HipB (15). The structure of HipA was solved to 1.54 Å resolution and refined to an $R_{\text{work}}/R_{\text{free}}$ of 19.5/23.2% (table S1 and fig. S1) (16–18). The HipA structure has a globular fold with 15 β strands and 15 α helices and can be divided into an N-terminal α/β domain and an all- α -helical C-terminal domain (Fig. 1A). Density is missing for residues 185 to 195, which are near the active site and probably correspond to the activation loop of other kinases. Structure-based homology searches revealed that HipA is most similar to human CDK2/cyclin A kinase (19). The structural homology between HipA and CDK2 was highest in the C-terminal region that contains CDK2 catalytic residues, suggesting that HipA functions as a protein kinase, as reported (15). Although HipA is most similar to CDK2, the proteins superimposed with a large root mean square deviation (RMSD) of 3.9 Å for 150 corresponding C α atoms, indicating that HipA represents a previously unknown class of protein kinase (20).

HipA contains all the catalytic residues found in protein kinases, including the putative catalytic base Asp³⁰⁹ (20). The D309Q mutation abrogates persistence, strongly suggesting that kinase func-

tion is key to HipA-mediated MDT (15). Indeed, we found that HipA binds adenosine triphosphate (ATP) with a dissociation constant (K_d) of 18.0 ± 2.0 μ M, which is similar to the dissociation constants obtained for ATP binding to other serine/threonine kinases (fig. S2) (20). To delineate the

ATP binding mechanism of HipA, we determined the structure of the HipA-ATP-Mg²⁺ complex to 1.66 Å resolution and refined the structure to an $R_{\text{work}}/R_{\text{free}}$ of 18.4/21.7%. Density for ATP is observed in the cleft between the HipA N and C domains (fig. S1). HipA binds ATP with high

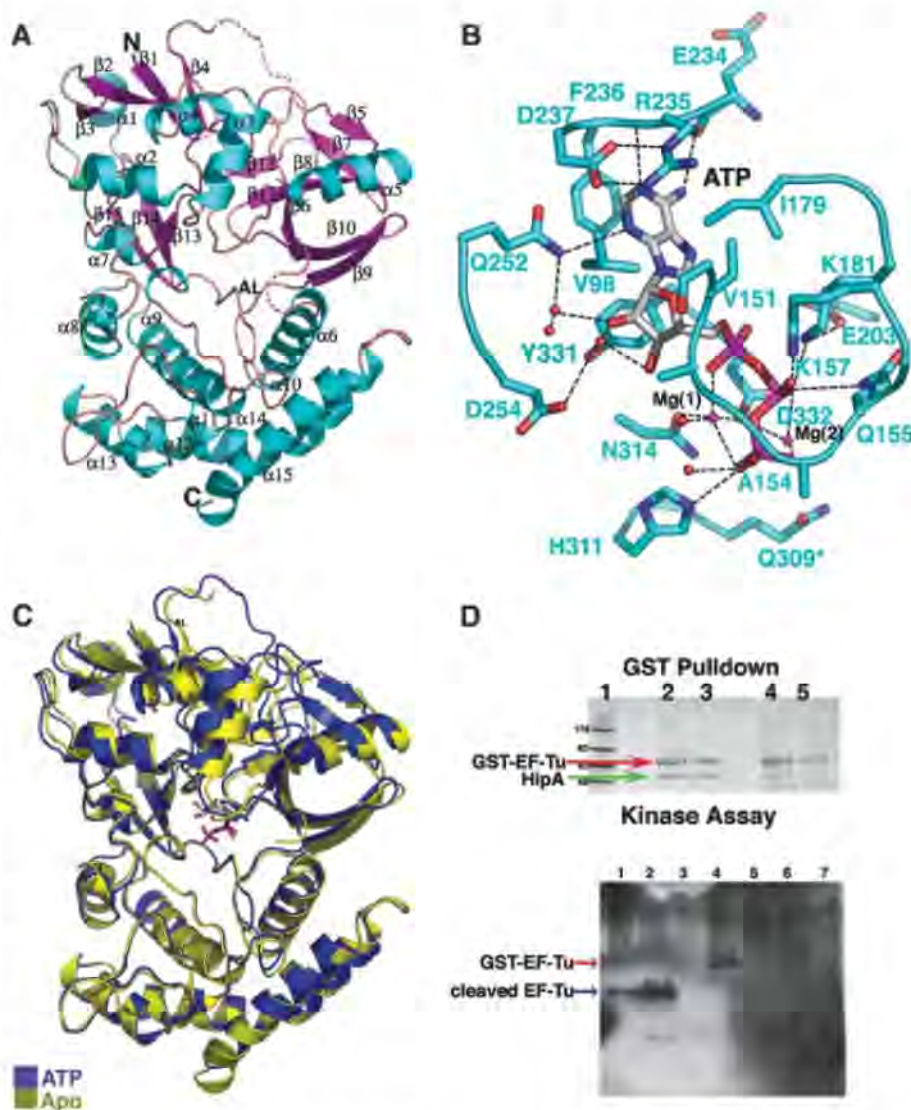


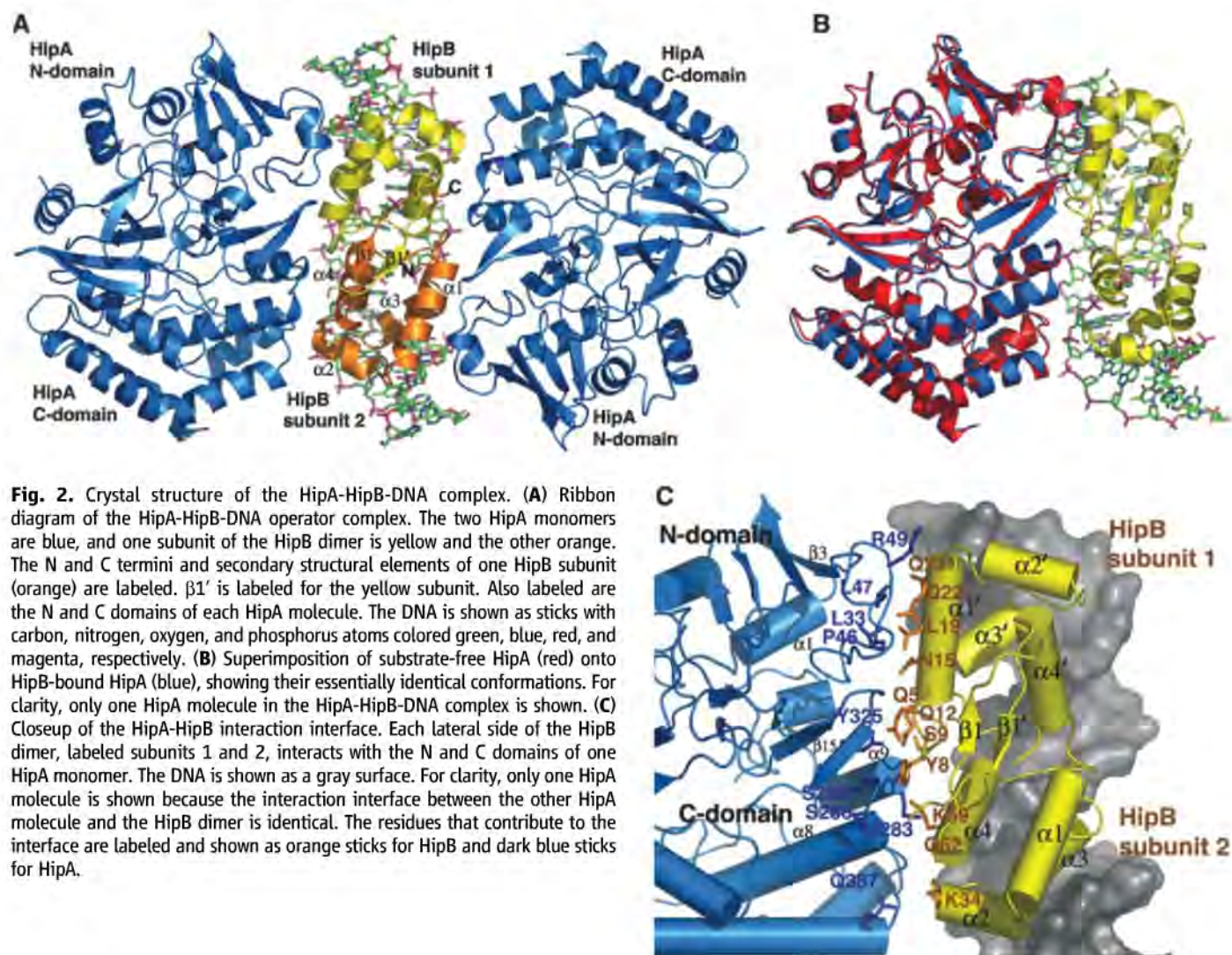
Fig. 1. HipA is a protein kinase that phosphorylates EF-Tu. (A) The *E. coli* apoHipA structure. β sheets and α helices are colored magenta and cyan, respectively. Secondary structural elements and the N and C termini are labeled. Disordered loops, including the putative activation loop (labeled AL), are indicated by dashed lines. (A) to (C) and Figs. 2, A to C; 3, B to D; and 4, A to D were made using PyMOL (31). (B) The ATP-binding pocket of HipA. Shown are ATP molecules (sticks), Mg²⁺ ions (magenta spheres), water molecules (red spheres), and hydrogen bonds (dashed black lines). (C) Superimposition of the C domains of apoHipA (yellow) and HipA-ATP-Mg²⁺ (blue) reveals only a small rotation upon ATP binding. ATP in the HipA-ATP structure is shown as sticks. (D) (Top) HipA-(GST-EF-Tu) pull-down (SDS-PAGE, stained with Coomassie brilliant blue). Lanes are as follows: 1, molecular weight ladder; 2, glutathione agarose (bead) retentate after addition of GST-EF-Tu, HipA, ATP, and GDP; 3, bead retentate after addition of GST-EF-Tu, HipA, ATP, and GDP, and washing; 4, bead retentate after addition of GST-EF-Tu, HipA, and no GDP or ATP; 5, bead retentate after addition of GST-EF-Tu, HipA, and no GDP or ATP, and washing. (Bottom) Wild-type HipA kinase assay using EF-Tu as a substrate (immunoblot). The positions of GST-EF-Tu and X_a-cleaved EF-Tu are indicated by red and blue arrows, respectively. Lanes are as follows: 1, EF-Tu (cleaved) + wild-type HipA + ATP + GTP; 2, EF-Tu (cleaved) + wild-type HipA + ATP + GDP; 3, EF-Tu (cleaved) + inactive HipA (D309Q) + ATP + GDP; 4, EF-Tu (uncleaved) + wild-type HipA + ATP + GDP; 5, EF-Tu (uncleaved) + wild-type HipA + ATP + GTP; 6, wild-type HipA + ATP; 7, native EF-Tu (cleaved) + ATP + GDP.

selectivity (Fig. 1B). Specifying contacts are provided to the adenine N6, N1, and N3 atoms by the carbonyl oxygen of Glu²³⁴, the amide nitrogen of Phe²³⁶, and the side chain Nε of Gln²⁵², respectively. The adenine ring stacks with Phe²³⁶ and Tyr³³¹, whereas Val⁹⁸, Val¹⁵¹, Ile¹⁷⁹, and the side-chain methylene carbons of salt-bridged residues Asp²³⁷ and Arg²³⁵ provide hydrophobic interactions. The γ phosphate hydrogen-bonds to both the side chain of His³¹¹ and the amide groups of Gly¹⁵³ and Ala¹⁵⁴, which form part of a loop analogous to the Gly loops of other protein kinases (Fig. 1B). Residues 152 to 156 of this loop are less ordered in the substrate-free HipA (apoHipA) structure, indicating that nucleotide binding is required for its stabilization. Two Mg²⁺ ions are also present in the HipA-ATP structure and probably function analogously to other protein kinases in facilitating phosphotransfer by accelerating substrate association and product dissociation (20, 21).

Comparison of the HipA-ATP and apoHipA structures revealed that binding ATP causes the N and C domains to undergo only a small rotation (~4°) relative to each other (Fig. 1C). However,

by analogy to other kinases, a more pronounced closure of the HipA domains upon binding the protein substrate is expected (20). The findings of a specialized kinase fold and high-affinity ATP binding strongly supported the hypothesis that HipA mediates persistence by phosphorylating one or more target proteins. To identify possible HipA targets, we carried out *in vitro* pulldown assays on candidate *E. coli* proteins. One protein, EF-Tu, was found to interact strongly with HipA in the presence of ATP-Mg²⁺ and guanosine diphosphate (GDP) (Fig. 1D). EF-Tu, the most abundant protein in *E. coli*, belongs to the guanosine triphosphatase superfamily and plays an essential role in translation by catalyzing aminoacyl-transfer RNA (tRNA) binding to the ribosome (22). Upon guanosine triphosphate (GTP) hydrolysis to GDP, EF-Tu undergoes a conformational change to an open form, which cannot bind the ribosome. Previous studies showed that EF-Tu is phosphorylated on residue Thr³⁸² by an unknown kinase or kinases (23, 24). The side chain of Thr³⁸² contacts Glu¹¹⁷ to stabilize the GTP-bound closed state of EF-Tu. Phosphorylation of Thr³⁸² favors the GDP-bound open form because it would lead to

repulsion of Glu¹¹⁷ and prevent EF-Tu from adopting the GTP-bound closed conformation. Thr³⁸²-phosphorylated EF-Tu cannot bind aminoacyl-tRNA and is therefore inactive in translation (23, 24). To test whether EF-Tu is a HipA substrate, we used an *in vitro* transcription/translation system to produce the toxic wild-type HipA enzyme (fig. S3). Immunoblotting studies, using antibodies to pThr/pSer/pTyr, indicated that HipA could phosphorylate EF-Tu in a manner stimulated by GDP (Fig. 1D). Moreover, fluorescence polarization studies revealed that HipA bound the EF-Tu peptide, IREGGRTVGA (25), encompassing Thr³⁸² (shown in bold here) with a *K_d* of 15 ± 5 μM (fig. S4). Subsequently, we solved a crystal structure of the HipA-(AMP-PNP)-IREGGRTVGA complex to 3.5 Å resolution. The structure revealed that the activation loop, residues 185 to 195, was now folded and density was observed for the peptide near the active site and close to the activation loop (fig. S4). These combined data suggest that HipA may phosphorylate Thr³⁸² to block aminoacyl-tRNA binding by EF-Tu. However, given that HipA affects multiple *E. coli* processes, other cellular targets are likely (9, 10).



Under normal cellular conditions, the persistence function of HipA is somehow masked by its tight interaction with HipB (11, 12). HipB also functions as a transcriptional autoregulator of the *hipBA* operon by cooperatively binding four operators with the consensus sequence TATCCN₈GGATA (where N indicates any nucleotide), located in the *hipBA* promoter region (11, 12). HipB binds these operators with high affinity, which is enhanced by the addition of HipA to the complex (12). To delineate the mechanism of HipB-mediated inhibition of HipA, the structure of the HipA-HipB complex bound to a 21-base pair *hipB* operator (top strand ACTATCCCCCTTAAGGGGATAG) was solved and refined to an $R_{\text{work}}/R_{\text{free}}$ of 22.5/28.1% to 2.68 Å resolution (table S1) (Figs. 2 and 3).

HipB forms a compact dimer that specifically interacts with DNA through major groove contacts, whereas two HipA molecules sandwich the HipB-DNA complex by contacting the sides of the HipB dimer (Fig. 2). HipB binds far from the HipA active sites and, unlike other TA inhibition mechanisms, does not occlude the active site. The HipB dimer interface is extensive and buries 2700 Å² of accessible surface area (ASA), which accounts for over 36% of the total dimer ASA. HipB contains one β strand and four α helices with topology α1-α2-α3-α4-β1. Helices 2 and 3 form a canonical helix-turn-helix (HTH) motif. The first 3 and last 16 residues of each HipB subunit are disordered and located near a small β sheet that is composed of β1 and β1' (from the other subunit) and forms a "β lid" (Fig. 2A). The

HipB subunit structure showed significant homology to 434 Repressor, 434 Cro, and the restriction-modification controller protein C. AhdI from *Aeromonas hydrophila*, with RMSDs of 1.56, 1.60, and 1.51 Å for 59, 56, and 59 corresponding Cα atoms, respectively, thus placing it in the Xre-HTH family of transcriptional regulators (26). The homology between HipB and these proteins is confined to the four-helix bundle region because the β lid is found only in HipB. Despite the similarities in DNA binding domains, these proteins bind their DNA sites differently because 434 Cro does not significantly distort its DNA site, and biochemical data indicate that C. AhdI bends its DNA site by 47° (27, 28). In contrast, HipB induces a large, 70° bend in its operator (Fig. 3D). This bending may play a role in the cooperative binding of HipB to its four operator sites, which is predicted to involve DNA wrapping (11, 12). Indeed, the *hipBA* promoter also contains a binding site for the architectural protein IHF, which could further aid in DNA condensation.

HipB-induced DNA distortion aligns the recognition helices for specific binding to consecutive major grooves. Contacts from the HTH motif completely specify the nucleotides of the HipB signature motif, T₂A₃T₄C₅C₆ (Fig. 3, A and B). Ser²⁹ from α2 makes hydrophobic contacts with the Thy2 methyl group. Residues of the recognition helix provide the remaining base-specifying contacts whereby two hydrogen bonds from Gln³⁹ read Ade3, whereas two hydrophobic contacts from Ala⁴⁰ and Ser⁴³ specify Thy4. Finally, Lys³⁸ makes hydrogen bonds with the guanine O6 oxygens of base pairs 5 and 6. HipB also makes 11 phosphate contacts to each half site. Deoxyribonuclease I protection studies showed that HipA binding to the HipB-DNA complex leads to an increase in protection and binding affinity (12). This is explained by the finding that HipA provides four phosphate backbone contacts to each half site from Lys³⁷⁹ and Arg³⁸² (Fig. 3, A and C).

In the HipA-HipB-DNA complex, the HipB dimer is sandwiched on each side by one HipA molecule, and the complex is formed from noncontiguous regions of both HipA and HipB (Figs. 2 and 3C). This type of interaction contrasts sharply with structures of other TA modules in which the toxin interacts with a C-terminal region of the antitoxin that typically is structured only in the presence of toxin. Specifically, for the HipA-HipB pair, the HipA N domains interact with one HipB subunit, whereas the HipA C domains interact primarily with the other HipB subunit (Fig. 2C). This interaction interface is extensive, burying ~5000 Å² of ASA, and involves both nonpolar and polar interactions. In the HipA N-domain-HipB interface, HipB residues from the turn before α1 interact with residues on HipA β15, and residues on HipB α1 make extensive contacts with HipA residues located on a long 3₁₀-like loop between β3 and α1. The formation of the HipA C-domain-HipB interface primarily involves HipB residues from α2 and the turn between α4

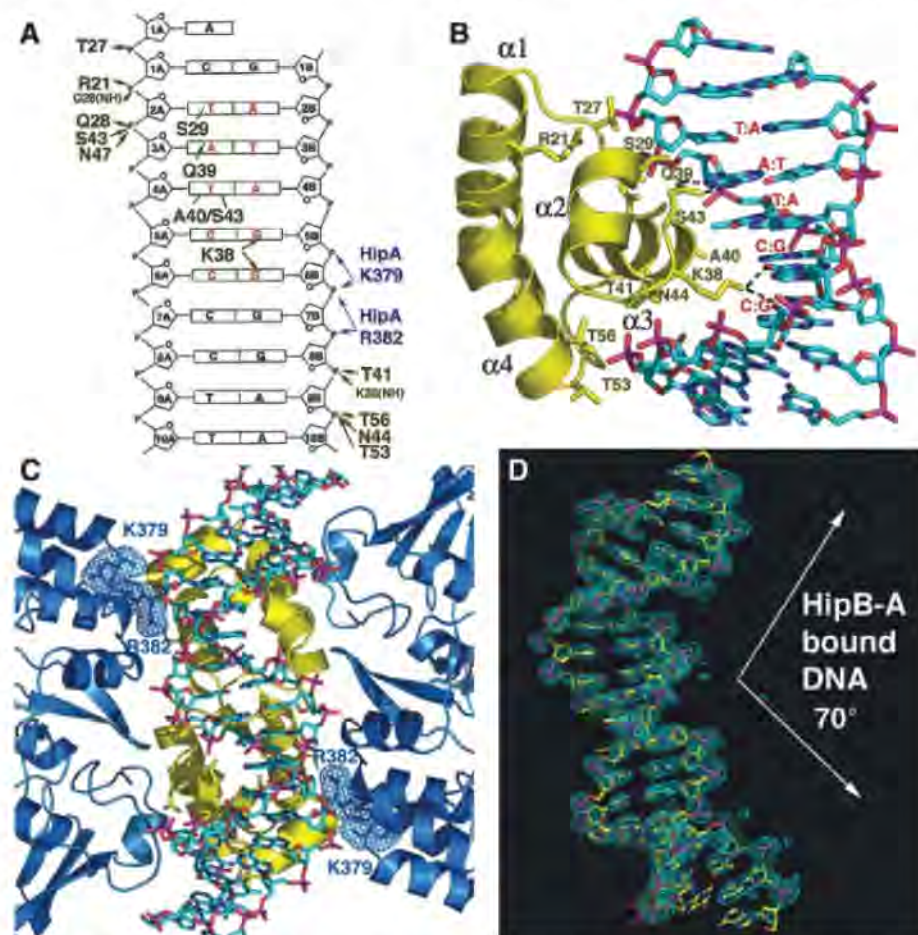


Fig. 3. HipB and HipA interactions with the *hipB* operator DNA. (A) Schematic representation of HipB-HipA-DNA interactions. Only one half site of the 21-oligomer duplex is shown because the identical contacts are made with each half site. The strands are labeled 1A to 10A and 1B to 10B. Bases are represented as rectangles and labeled according to sequence. The ribose groups are shown as pentagons. The operator signature motif sequence, TATCC, is red. HipB-DNA contacts are shown. Hydrophobic contacts are indicated by lines and hydrogen bonds are indicated by arrows. Blue arrows indicate HipA-phosphate contacts. (B) HipB-DNA interactions. Only one HipB subunit-DNA half site is shown. The DNA and residues making side-chain contacts are shown as sticks. The signature motif sequence, TATCC, is labeled in red. For clarity, only the four-helix bundle is shown and labeled. (C) HipA-DNA contacts. The HipB dimer (yellow) is shown for reference. The location of the two DNA-interacting residues from HipA, K379 and R382, are shown as blue sticks and highlighted by mesh surface representations. The DNA is shown as sticks and colored as in (B). (D) HipA-HipB bound DNA is bent. This is an omit $F_o - F_c$ map in which the DNA was omitted from refinement to 2.68 Å resolution. The map is contoured at 2.8 σ . The DNA is shown as sticks and the bend angle is indicated.

and $\beta 1$. These residues interact primarily with HipA residues in the loop between $\alpha 8$ and $\alpha 9$ and the N terminus of $\alpha 9$. In addition, "cross-subunit" contacts are made between HipB residues Gln¹² and HipA C-domain residue Gly²⁸⁴, and between HipB residue Tyr⁸ and HipA C-domain residue Ser²⁸⁶. These cross contacts, combined with the numerous interactions of each subunit in the HipB dimer with the N and C domains of HipA, lock HipA in an open and probably inactive conformation (Fig. 2C).

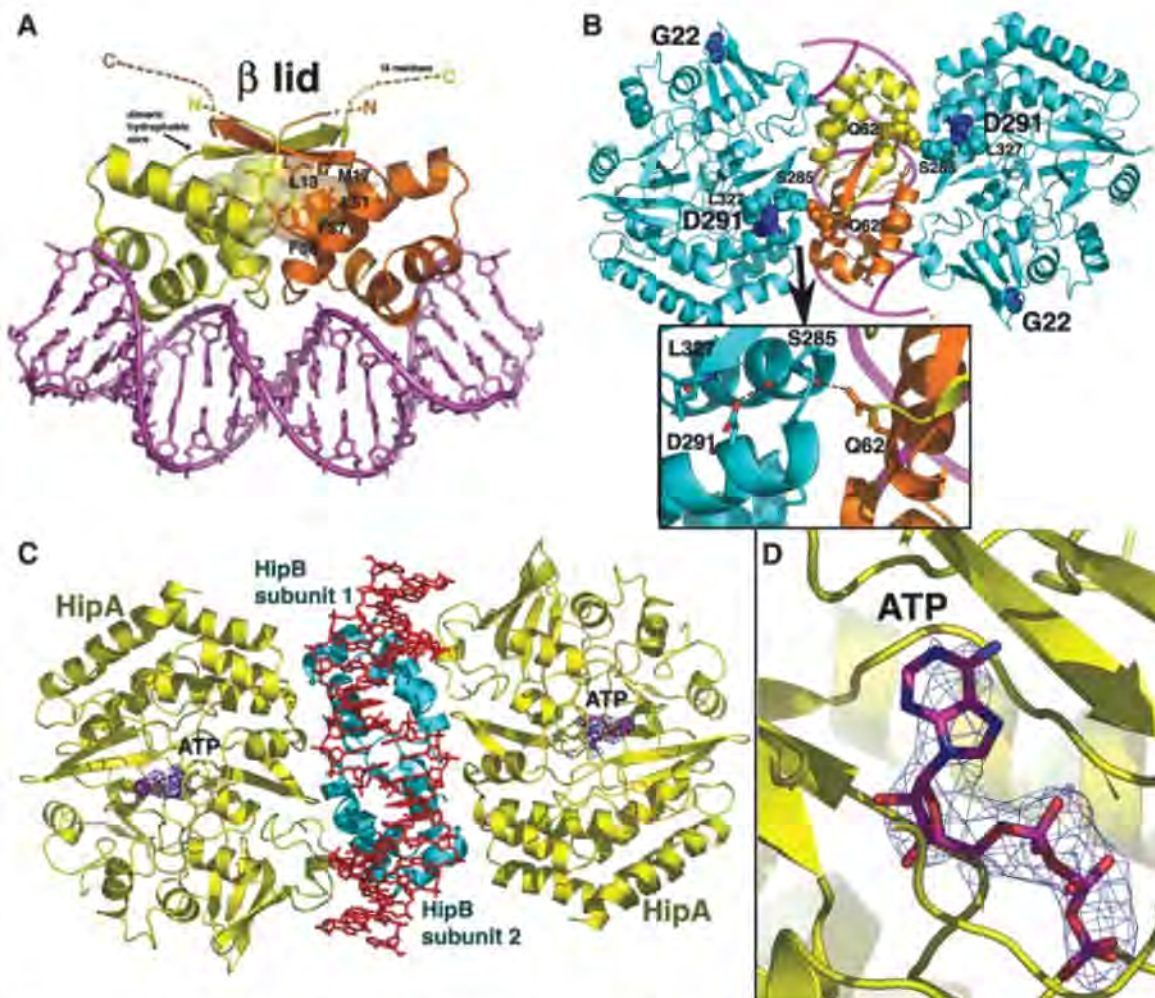
To activate HipA for persistence and free it from its DNA tether, HipB must be removed or degraded. Unlike most antitoxins, HipB interacts with HipA using residues from noncontiguous, well-ordered domains and not loops. Proteases that degrade toxins typically bind and tug on disordered regions to unfold the substrate. HipB contains an exposed and flexible 16-residue C terminus attached to the small β lid that covers the hydrophobic core of the protein and would appear to be an excellent candidate for protease attack (Fig. 4A). The structure of the HipA-HipB-DNA complex also provides insight into

the mechanism of increased persistence of the HipA7 protein. HipA7, which contains two substitutions, G22S and D291A, confers a high-persistence phenotype on *E. coli* cells independent of HipB. Subsequent data revealed that the D291A mutation alone was sufficient for this phenotype (29). The HipA-HipB-DNA structure indicates that this phenotype probably results from a weakened HipA-HipB interaction, which unleashes HipA kinase activity. Specifically, Asp²⁹¹ makes key contacts to stabilize the HipA-HipB interface, including hydrogen bonds to the side chain of Ser²⁸⁵, which positions the Ser²⁸⁵ carbonyl oxygen to interact with HipB residue Gln⁶², and hydrogen bonds to the amide nitrogen of Leu³²⁷, which buttresses the HipA C-terminal region that interacts with HipB (Fig. 4B).

HipA undergoes only a small conformational change upon binding ATP, suggesting that HipA could bind ATP when in complex with HipB-DNA. Indeed, HipA(ATP)-HipB-DNA crystals isomorphous to HipA-HipB-DNA crystals could be grown de novo. Alternatively, ATP could be soaked into preformed HipA-HipB-DNA crys-

tals. In both cases, difference $F_o - F_c$ electron density maps revealed clear density for ATP in the HipA active site (Fig. 4, C and D). In addition, isothermal titration calorimetry studies revealed a K_d of 15.0 ± 1.0 μ M for ATP-Mg²⁺ binding to HipA in the HipA-HipB-DNA complex, which is essentially identical to that obtained for ATP-Mg²⁺ binding to HipA alone (fig. S2). If the HipA active site is not blocked for ATP binding, then how does HipB binding neutralize HipA? Data from other protein kinase structures indicate that although ATP binding causes only small domain movements such as those we observed in HipA, the binding of protein substrates causes substantial domain closure (20, 21). This large-scale movement brings the two substrates into proximity for catalysis and precludes bulk solvent from the active site. HipB binding would appear to prevent this conformational change in HipA by locking the enzyme into an inactive open conformation by its extensive interactions with the HipA N and C domains. Finally, the recent finding that *E. coli* EF-Tu is localized primarily to the cytosolic and membrane fractions, which is far from the

Fig. 4. HipB is a vulnerable antitoxin that neutralizes HipA. **(A)** The HipB dimer is shown as ribbons with one yellow and one orange subunit. The DNA is shown as pink sticks. Hydrophobic core residues are shown as sticks and transparent surfaces. The β lid is composed of a short two-stranded β sheet. Disordered C-terminal residues extend from the lid and are depicted as colored dashes. **(B)** Mutation sites (G22S and D291A) in the HipA7 protein mapped onto HipA proteins of the HipA-HipB-DNA complex. The HipA molecules are cyan, the HipB subunits are yellow and orange, and the DNA is a pink ribbon. Residues G22 and D291 are shown as blue Corey, Pauling, Koltan structures (CPKs). HipB residue Q62 and HipA residues S285 and L327 are also shown as CPKs. A closeup of the interactions involving HipA residue D291 is shown (inset). Hydrogen bonds are indicated by dashed lines. **(C)** Structure of the HipA(ATP)-HipB-DNA complex. HipA molecules are yellow, the HipB dimer is cyan, and the DNA and ATP are shown as sticks. The blue mesh represents a 2.98 Å resolution $F_o - F_c$ map, contoured at 4.0 σ , in



which the ATP was omitted. **(D)** Closeup view of the ATP-binding pocket and omit map. Carbon, nitrogen, oxygen, and phosphorus atoms are colored magenta, blue, red, and purple, respectively.

nucleoid where the HipA-HipB-DNA complex would reside, suggests that HipB-DNA binding may also inactivate HipA by its sequestration (30).

These studies have provided important insight into the mechanisms by which HipA mediates persistence and HipB neutralizes HipA. The high conservation of HipA among Gram-negative bacteria indicates its central role in the development of persistence. Thus, inhibitors that specifically target the substrate-binding sites of HipA, may prove effective against persistence and MDT.

References and Notes

1. K. Lewis, *Nat. Rev. Microbiol.* **5**, 48 (2007).
2. K. Lewis, *Curr. Top. Microbiol. Immunol.* **322**, 107 (2008).
3. N. Q. Balaban, J. Merrin, R. Chait, L. Kowalik, S. Leibler, *Science* **305**, 1622 (2004).
4. J. W. Bigger, *Lancet* **244**, 497 (1944).
5. I. Keren, D. Shah, A. Spoering, N. Kaldalu, K. Lewis, *J. Bacteriol.* **186**, 8172 (2004).
6. I. Keren, N. Kaldalu, A. Spoering, Y. Wang, K. Lewis, *FEMS Microbiol. Lett.* **230**, 13 (2004).
7. D. Shah *et al.*, *Biomed. Cent. Microbiol.* **12**, 6 (2006).
8. R. Scherrer, H. S. Moyed, *J. Bacteriol.* **170**, 3321 (1988).
9. H. S. Moyed, S. H. Broderick, *J. Bacteriol.* **166**, 399 (1986).
10. H. S. Moyed, K. P. Bertrand, *J. Bacteriol.* **155**, 768 (1983).
11. D. S. Black, B. Irwin, H. S. Moyed, *J. Bacteriol.* **176**, 4081 (1994).
12. D. S. Black, A. J. Kelly, M. J. Mardis, H. S. Moyed, *J. Bacteriol.* **173**, 5732 (1991).
13. K. Gerdes, S. K. Christensen, A. Løbner-Olesen, *Nat. Rev. Microbiol.* **3**, 371 (2005).
14. L. Buts, J. Lah, M.-H. Dao-Thi, L. Wyns, R. Loris, *Trends Biochem. Sci.* **30**, 672 (2005).
15. F. F. Correia *et al.*, *J. Bacteriol.* **188**, 8360 (2006).
16. T. C. Terwilliger, J. Berendzen, *Acta Crystallogr. D Biol. Crystallogr.* **55**, 849 (1999).
17. A. T. Brünger *et al.*, *Acta Crystallogr. D Biol. Crystallogr.* **54**, 905 (1998).
18. T. A. Jones, J. Y. Zou, S. W. Cowan, M. Kjeldgaard, *Acta Crystallogr. A* **47**, 110 (1991).
19. R. Honda *et al.*, *EMBO J.* **24**, 452 (2005).
20. M. Huse, J. Kuriyan, *Cell* **109**, 275 (2002).
21. D. R. Knighton *et al.*, *Science* **253**, 407 (1991).
22. J. Nyborg, A. Liljas, *FEBS Lett.* **430**, 95 (1998).
23. C. Lippmann *et al.*, *J. Biol. Chem.* **268**, 601 (1993).
24. C. Alexander *et al.*, *J. Biol. Chem.* **270**, 14541 (1995).
25. Single-letter abbreviations for the amino acid residues are as follows: A, Ala; C, Cys; D, Asp; E, Glu; F, Phe; G, Gly; H, His; I, Ile; K, Lys; L, Leu; M, Met; N, Asn; P, Pro; Q, Gln; R, Arg; S, Ser; T, Thr; V, Val; W, Trp; and Y, Tyr.
26. R. Wintjens, M. Rooman, *J. Mol. Biol.* **262**, 294 (1996).
27. C. Wolberger, Y. C. Dong, M. Ptashne, S. C. Harrison, *Nature* **335**, 789 (1988).
28. I. Papapanagiotou, S. D. Streeter, P. D. Cary, G. G. Kneale, *Nucleic Acids Res.* **35**, 2643 (2007).
29. S. B. Korch, T. M. Hill, *J. Bacteriol.* **188**, 3826 (2006).
30. C. Archambaud, E. Gouin, J. Pizarro-Cerda, P. Cossart, O. Dussurget, *Mol. Microbiol.* **56**, 383 (2005).
31. W. L. Delano, the PyMOL Molecular Graphics System (Delano Scientific, San Carlos, CA, 2002).
32. We thank C. R. Knudsen for her generous gift of the GST-EF-Tu expression construct. Coordinates and structure factor amplitudes for the apoHipA, HipA-ATP, HipA-HipB-DNA, and HipA(ATP)-HipB-DNA complexes have been deposited in the Protein Data Bank, Research Collaboratory for Structural Bioinformatics, Rutgers University, New Brunswick, NJ (www.rcsb.org/) under accession codes 3DNU, 3DNT, 3DNV, and 3DNW, respectively. We acknowledge support from Burroughs Wellcome Career Development Award 992863 and NIH grant GM074815 (to M.A.S.), NIH grant GM061162 (to K.L.), and the Robert A. Welch Foundation (grant G0040) and NIH grant AI048593 (to R.G.B.).

Supporting Online Material

www.sciencemag.org/cgi/content/full/323/5912/396/DC1

Materials and Methods

Figs. S1 to S4

Table S1

25 July 2008; accepted 18 November 2008

10.1126/science.1163806

Chromatin-Associated Periodicity in Genetic Variation Downstream of Transcriptional Start Sites

Shin Sasaki,^{1*} Cecilia C. Mello,² Atsuko Shimada,³ Yoichiro Nakatani,¹ Shin-ichi Hashimoto,⁴ Masako Ogawa,⁴ Kouji Matsushima,⁴ Sam Guoping Gu,² Masahiro Kasahara,¹ Budrul Ahsan,¹ Atsushi Sasaki,¹ Taro Saito,¹ Yutaka Suzuki,⁵ Sumio Sugano,⁵ Yuji Kohara,⁶ Hiroyuki Takeda,³ Andrew Fire,^{2†} Shinichi Morishita^{1,7†}

Might DNA sequence variation reflect germline genetic activity and underlying chromatin structure? We investigated this question using medaka (Japanese killifish, *Oryzias latipes*), by comparing the genomic sequences of two strains (Hd-rR and HNI) and by mapping ~37.3 million nucleosome cores from Hd-rR blastulae and 11,654 representative transcription start sites from six embryonic stages. We observed a distinctive ~200-base pair (bp) periodic pattern of genetic variation downstream of transcription start sites; the rate of insertions and deletions longer than 1 bp peaked at positions of approximately +200, +400, and +600 bp, whereas the point mutation rate showed corresponding valleys. This ~200-bp periodicity was correlated with the chromatin structure, with nucleosome occupancy minimized at positions 0, +200, +400, and +600 bp. These data exemplify the potential for genetic activity (transcription) and chromatin structure to contribute to molding the DNA sequence on an evolutionary time scale.

Mutation and repair characteristics of DNA sequence in experimental systems have been shown in a number of cases to reflect structures in chromatin. For one well-studied experimental system, ultraviolet-irradiated yeast (*Saccharomyces cerevisiae*), repair rates for a set of DNA nucleosome core regions are lower than in the surrounding linker regions (1–4). Correlations between chromatin structure and mutation rates have also been suggested in analysis of human and yeast genomes (5–7). The draft genome sequences of two inbred medaka strains, Hd-rR and HNI (8), provide a remarkable opportunity for extensive comparison

between genomic variation and structural features in the genome. The two strains are cross-fertile, yet their genomes are substantially different [~3.42% single-nucleotide polymorphism (SNP)] (8). For analysis of chromatin and transcriptional effects on genetic variation, tissue samples including totipotent (germline tissue) would be most relevant, as mutational events in the germ line would uniquely contribute to shaping the genome over evolutionary time (9–11).

To characterize transcriptional activity patterns from the medaka genome at embryonic stages, we collected 25-nucleotide (nt) 5'-end mRNA tags for 1-, 2-, 3-, 5-, 10-, and 14-day Hd-rR medaka

embryos (12). Among a total of ~38.5 million 5'-end tags collected, ~26.2 million (68.14%) were successfully aligned to unique positions in the medaka genome (fig. S1). Starting with a rough assumption that one cell contains ~300,000 mRNA molecules (13), single-copy-per-cell RNAs would be represented by ~100 of the ~26.2 million tags. To define a set of active transcription start sites (TSSs), we used a clustering algorithm yielding 11,654 ≥100-tag clusters. More than 98.4% of neighboring clusters were separated by >100 base pairs (bp) from their nearest neighbor (fig. S3B). A reference TSS for each cluster was defined as the position with the most 5'-end tags.

The substitution and indel rates within 1000 bp of the reference TSSs in the 11,654 TSS clusters tend to reach a valley at the TSSs (Fig. 1A), suggesting relative selective constraint within promoters. This is consistent with reports of high conservation around TSS regions in mammals (14). Our analysis in medaka uncovers an additional pattern: The substitution rate (blue line) showed peaks at +100 and +300 bp and

¹Department of Computational Biology, Graduate School of Frontier Sciences, the University of Tokyo, Kashiwa, 277-0882, Japan. ²Departments of Pathology and Genetics, School of Medicine, Stanford University, Stanford, CA 94305–5324, USA. ³Department of Biological Sciences, Graduate School of Science, the University of Tokyo, Tokyo, 113-0033, Japan. ⁴Department of Molecular Preventive Medicine, School of Medicine, the University of Tokyo, Tokyo, 113-0033, Japan. ⁵Department of Medical Genome Sciences, Graduate School of Frontier Sciences, the University of Tokyo, Tokyo, 108-8639, Japan. ⁶Center for Genetic Resource Information, National Institute of Genetics, Mishima, 411-8540, Japan. ⁷Bioinformatics Research and Development (BIRD), Japan Science and Technology Agency (JST), Tokyo, 102-8666, Japan.

*Present address: Mitsubishi Research Institute, Inc., Tokyo, 100-8141, Japan.

†To whom correspondence should be addressed. E-mail: afire@stanford.edu (A.F.); moris@cb.k.u-tokyo.ac.jp (S.M.)

valleys at +200 and +400 bp around the TSSs (the same pattern was also seen in the transition and transversion rates). The indel rate [red line (Fig. 1A)] was minimal at the TSSs and maximal at +200 bp; additional peaks were evident at +400 and +600 bp. These peaks define regions where indel mutation rates were significantly greater than the average rate (0.59%) for the entire genome, with the signal weakening with increasing distance from TSSs. The indel dataset was then split into a “1-bp” category (37.46%) and the remaining “>1-bp” category of indels (fig. S4C). The peaks at +200, +400, and +600 bp are generated by the increase in the >1-bp category, whereas the 1-bp indel rate does not yield an evident periodicity (Fig. 1A). Comparisons of genetic variation to TSSs were possible in human to chimpanzee or mouse to rat, although not limited to germline or embryo TSSs (fig. S5). A limited periodicity in substi-

tution rates may be present for these genomes, albeit much smaller in magnitude than that observed with the early transcriptome TSS data from medaka.

The ~200-bp periodicity of the substitution and indel rates in medaka suggested the involvement of nucleosome structure. We isolated mononucleosome core DNAs from micrococcal nuclease-digested chromatin from blastulae [0.5-day embryos that maintain germline character in some (or all) cells (15)] and sequenced 67 million DNA ends to 36 bp (12, 16, 17). The first 25 bp were sufficient (fig. S6) to map 37.3 million ends (55.7% of sequenced reads) to unique locations in the medaka genome.

The distribution of distances between nucleosome start and end reads (fig. S7B) presents a significant peak at ~147 bp, coincident with the size of nucleosome cores and indicative of some degree of constraint in nucleosome positioning.

To assess nucleosome spacing intervals, we analyzed the distribution of distances between start positions of mapped nucleosome ends (fig. S7A) (16, 17). We observed a small peak at 165 bp, which indicated that adjacent nucleosomes in regions with conserved positioning are likely to be located at approximately 165-bp intervals (~18-bp linker), while a distinctive ~200-bp spacing (~50-bp linker) was seen downstream of TSSs (see below).

Our metric for nucleosome position at individual sites in the genome (Fig. 1B) counts the number of putative nucleosome dyads in a 23-bp “sliding window” and divides this by the total number of nucleosomes impinging on this window to obtain a localized dyad positioning score (Fig. 1B). The 23-bp window (± 1 helical turn) is used to accommodate observed variability in nuclease cleavage around nucleosome termini (see fig. S7B and S8B) (12, 17).

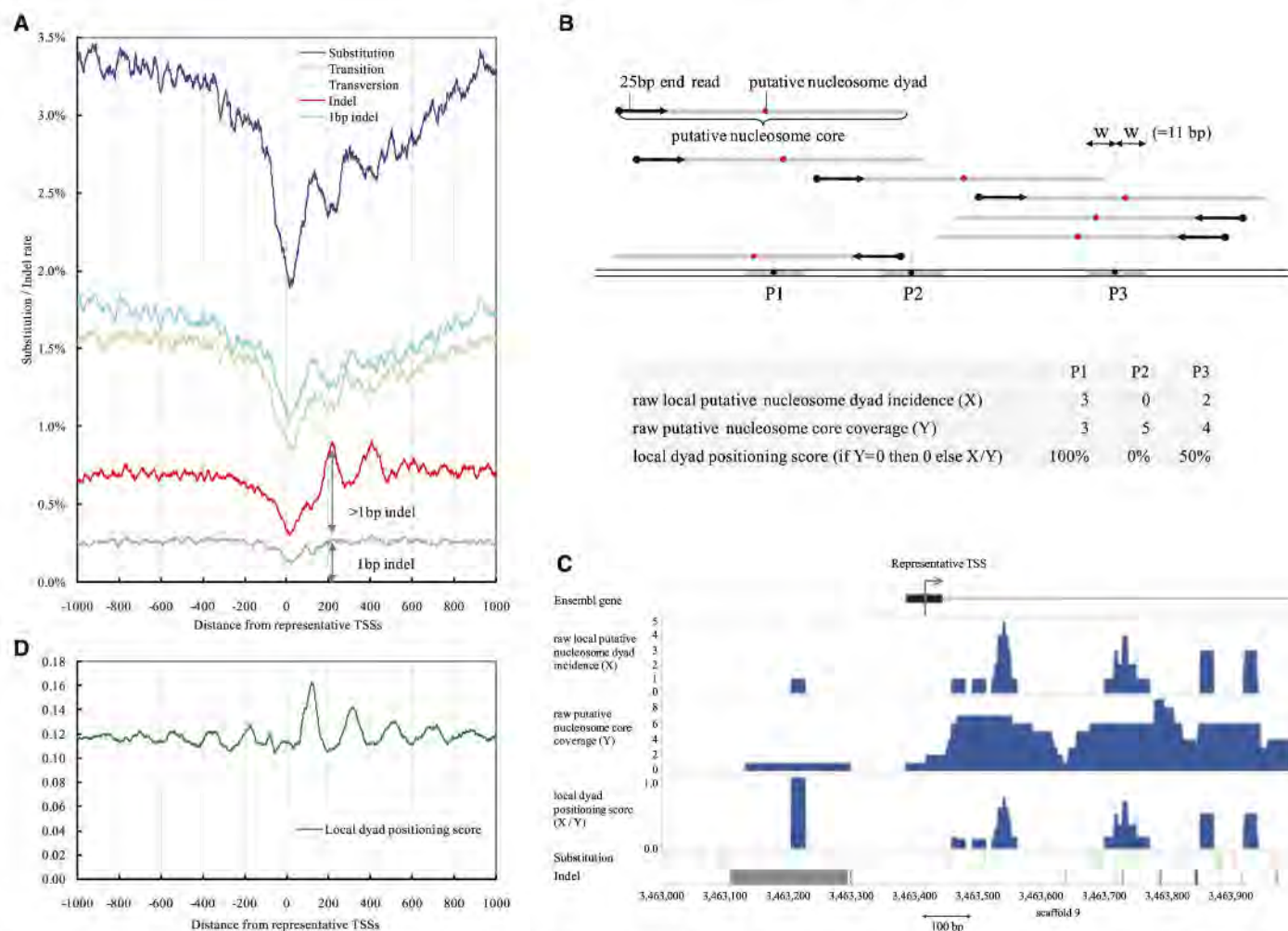


Fig. 1. Diversity rates and nucleosome positions around TSSs. (A) The x axis shows the distance from the representative TSSs in the medaka (Hd-rR) genome. Color key shows rates: blue line, mismatch mutation (substitution) rate; red line, indel mutation rate; and gray line, rate of indels of length 1 bp. For smoothing of lines, a running average over a 23-bp window (one full turn of the helix in each direction) is depicted. (B) (Top) Putative nucleosome dyads (red points, 73 bp from start of sequence read) and cores (gray bars; 147 bp).

(Bottom) The distinct meanings of the three nucleosome indicators. (C) Distribution of nucleosomes, substitutions, and indels surrounding a TSS. Black boxes, exons of the gene; blue histograms, distributions of the three nucleosome indicators; green vertical bars, substitutions between the Hd-rR and HNI genomes; red bars, deletions from the Hd-rR genome; blue bars, insertions into the Hd-rR genome; and gray bars and boxes, failure of alignment. (D) The average local dyad positioning score.

The distribution of nucleosome dyad indicators, substitutions, and indels around several TSS sites is shown in Fig. 1C and fig. S8. For global analysis, positioning scores (X/Y) were taken into account only in areas covered by multiple nucleosome reads [87.1% of genomic positions (fig. S9B); the remaining 12.9% correspond in part to repetitive sequences that occupy 17.5% of the medaka genome (8)]. In unique regions supported with multiple nucleosome core coverage, putative nucleosome dyads that occur reproducibly in a defined neighborhood allow us to define positioned nucleosomes (fig. S9C). The average local dyad positioning score has local minima at positions +200, +400, +600, and +800 bp from the TSSs (Fig. 1D, green line), which suggests the presence of phased ar-

rays of nucleosomes every ~200 bp downstream of the TSS (9–11, 18–21).

By contrast to the decreased substitution rate in nucleosome linker regions, the indel rate for medaka had peaks at positions +200, +400, and +600 bp from the TSSs, which implied that indels of length >1 bp are more likely to occur at DNA linker regions. One possible explanation is that DNA linker regions have more indel mutations than the rest of the genome; this idea is supported by the higher indel rate on a genome-wide scale (not limited to TSS regions) in the DNA linkers in regions occupied by positioned nucleosomes (Fig. 2). One might wonder if the substitution rate increases toward the positioned dyads in nonpromoter regions; however, this tendency was not observed (Fig.

2A). These observations suggest an interplay of transcription and nucleosome positioning in determining susceptibility to substitutions and indel mutations.

Transcription-coupled DNA repair (TCR), a mechanism that protects transcribed regions from mutations, may contribute to the observed sequence effects (2, 22–24). TCR is thought to work simultaneously with mRNA transcription involving RNA polymerases I and II; resulting in an asymmetric effect with an overabundance of G+T over A+C downstream from the TSSs (through an excess of C-to-T mutations over G-to-A mutations) (22, 23). A significant asymmetry of the base composition is found in examining natural variation in the medaka genome at TSSs (Fig. 3A). Examining reciprocity in frequencies of the 12 possible base substitutions in 319 transcribed loci (121.1K bp, in total; regions where ancestry could be inferred by comparison with sequence data from an outgroup species), only the C-to-T versus G-to-A in the transcribed regions downstream of TSSs showed a significant strand bias (Fig. 3B) ($P = 0.044$) (12). This is consistent with TCR as one of the factors contributing to the character of natural sequence variation in these regions.

Several possible causal and structural relationships may link sequence composition to mutagenesis rates and nucleosome positioning around TSSs. One rather simple explanation for the remarkable periodicity in mutation rates might have been an underlying bias in sequence composition in nucleosome core regions that favored certain types of mutations, whereas distinct sequence composition in linkers would favor other types of mutations. We addressed this possibility by examining sequence composition in general and around sites of genetic variation as a function of positioning relative to nucleosomes and TSSs (fig. S13) (12). This analysis gave no indication that differential mutagenesis could be accounted for by an initial sequence bias. A second intriguing possibility is that mutagenesis rates are influenced toward periodicity, not by the structural constraints of the chromatin template, but by functional constraints related to overall organismal fitness. Thus, for example, it would be conceivable that substitutions might be under-represented in a critical set of linker sequences that are essential in maintaining specific transcription complexes and nucleosome-based structures downstream of TSSs. We do not favor this explanation for the medaka data, given that indel mutations show an opposite distribution, occurring more frequently in the linker regions. Instead, the biases in genetic variation seem most likely to represent structural constraints of the chromatin template during the mutagenic processes that medaka has encountered during evolutionary time. The mechanistic points at which nucleosomes may have influenced mutagenesis and/or repair processes in medaka evolution are (by definition) not known. The ability of nucleosomes in model assay systems to block

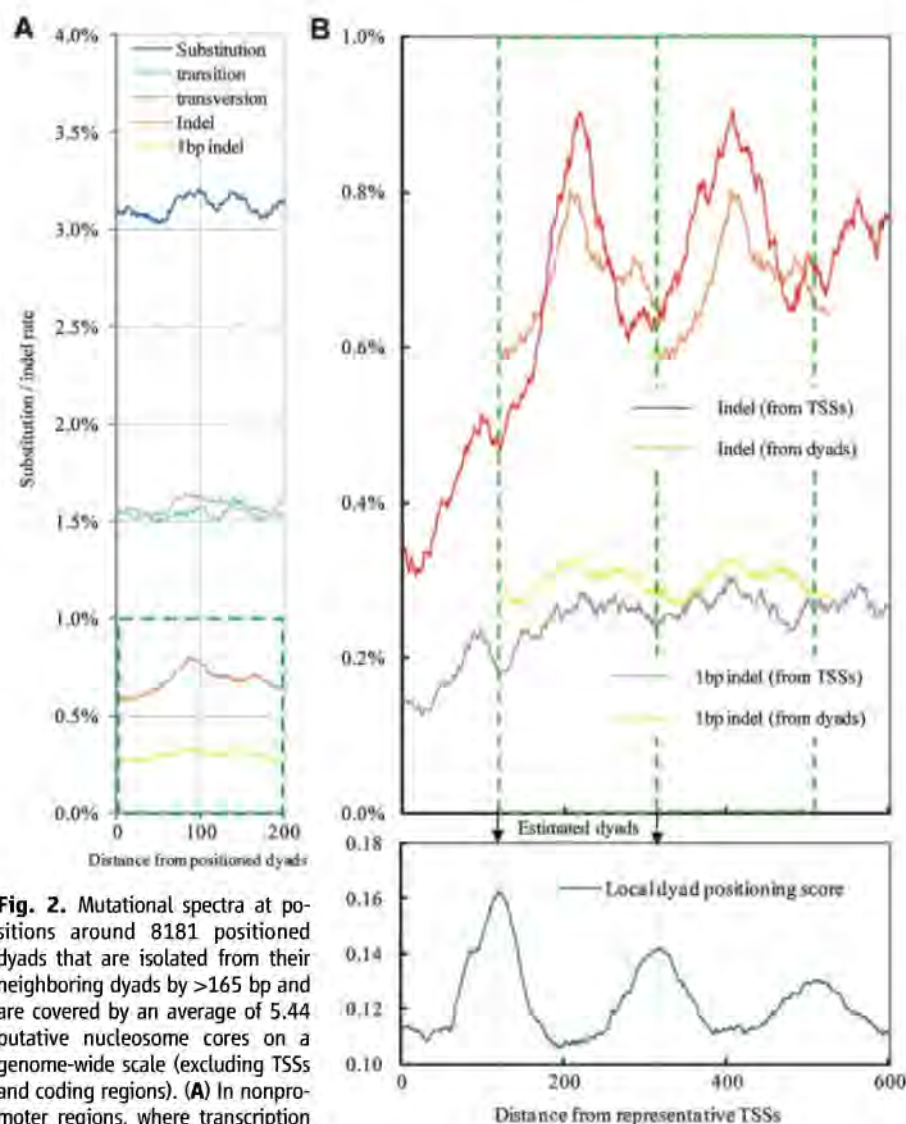
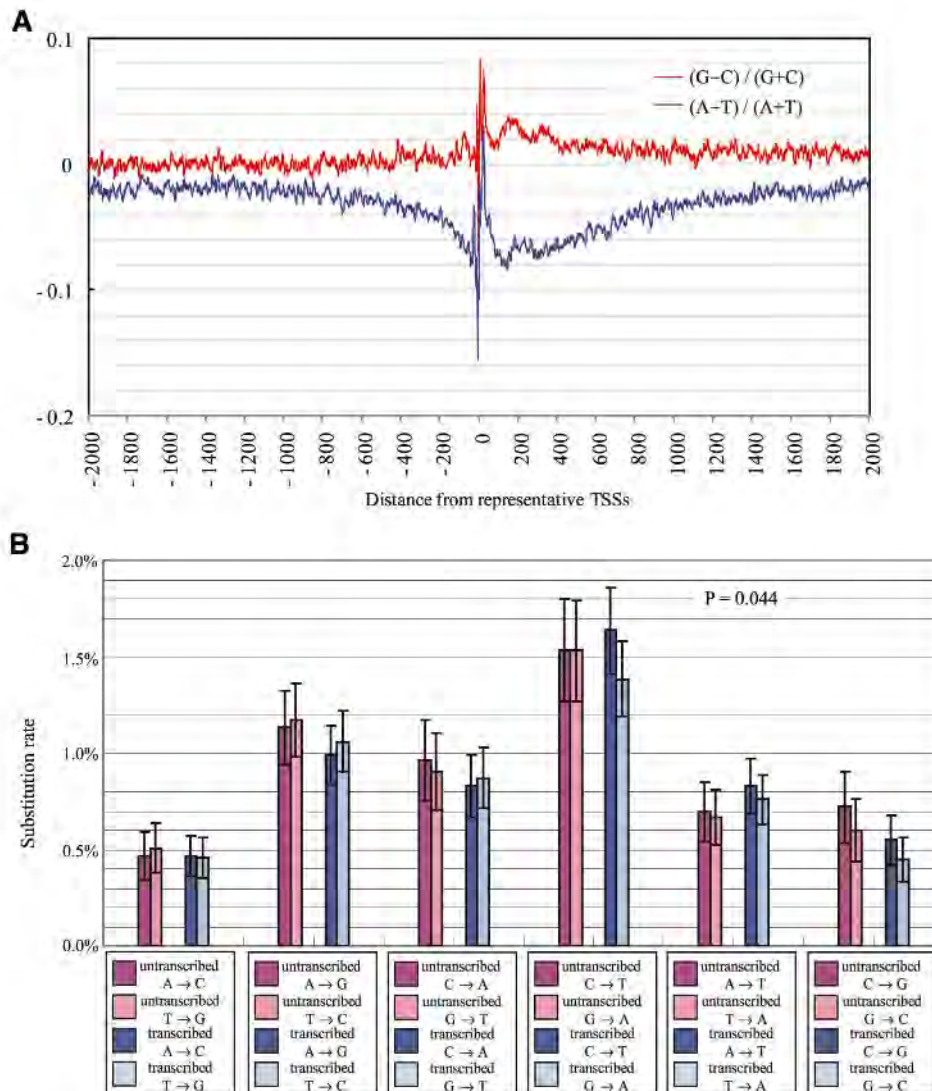


Fig. 2. Mutational spectra at positions around 8181 positioned dyads that are isolated from their neighboring dyads by >165 bp and are covered by an average of 5.44 putative nucleosome cores on a genome-wide scale (excluding TSSs and coding regions). (A) In nonpromoter regions, where transcription does not occur, the two locations in the distinct strands are positionally equivalent in a nucleosome core if they are the same distance from the dyad. The x axis presents the distance. Color key shows rates. (B) An expanded view of the indel rates enclosed in the green square in Fig. 2A is duplicated in tandem, and the two copies are overlaid for comparison with equivalent measurements relative to TSSs in Fig. 1A. (Bottom) The estimated dyads (arrows) aligned with dyad positioning score near TSSs (expanded from Fig. 1D).

Fig. 3. (A) Base composition surrounding TSSs. Red line, the difference between guanines and cytosines; blue line, the difference between adenines and thymines. **(B)** Substitution rates around TSSs. Rates for each substitution and its complement and their 95% confidence intervals are indicated side by side for untranscribed and transcribed regions that are upstream and downstream of TSSs, respectively.



repair of certain DNA lesions [e.g., (3)] certainly provides a precedent for the observed higher substitution rates in core regions. The complementary pattern of indels in medaka could reflect any of several conceivable linker and/or core differences (e.g., higher susceptibility of cores to breakage or less precise break repair in linkers).

For any species, the balance of specific mutagenic and repair processes occurring over history would have shaped the genome in potentially unique ways; thus, not all genomes would be expected to show a qualitatively or quantitatively equivalent "shadow" of germline chromatin structure. Our working model for the basis of structural variation between the genomes of these two inbred medaka strains is that chromatin structure influences mutagenesis, which in turn influences genetic variation, to provide the observed periodic pattern near the 5' ends of germ line-transcribed genomic segments. We expect the influence of chromatin structure to be a general feature of sequence evolution throughout the genome and the biosphere.

References and Notes

1. M. Tijsterman, R. de Pril, J. Tasseron-de Jong, J. Brouwer, *Mol. Cell. Biol.* **19**, 934 (1999).
 2. J. Q. Svejstrup, *Nat. Rev. Mol. Cell Biol.* **3**, 21 (2002).
 3. R. E. Wellinger, F. Thoma, *EMBO J.* **16**, 5046 (1997).
 4. B. Suter, M. Livingstone-Zatchej, F. Thoma, *EMBO J.* **16**, 2150 (1997).
 5. K. Higasa, K. Hayashi, *BMC Genomics* **7**, 66 (2006).
 6. J. G. Prendergast *et al.*, *BMC Evol. Biol.* **7**, 72 (2007).
 7. S. Washietl, R. Machné, N. Goldman, *Trends Genet.* **24**, 583 (2008).
 8. M. Kasahara *et al.*, *Nature* **447**, 714 (2007).
 9. F. Ozsolak, J. S. Song, X. S. Liu, D. E. Fisher, *Nat. Biotechnol.* **25**, 244 (2007).
 10. I. Whitehouse, O. J. Rando, J. Delrow, T. Tsukiyama, *Nature* **450**, 1031 (2007).
 11. D. E. Schones *et al.*, *Cell* **132**, 887 (2008).
 12. Materials and methods are available as supporting material on Science Online.
 13. V. Velculescu *et al.*, *Nat. Genet.* **23**, 387 (1999).
 14. M. S. Taylor *et al.*, *PLoS Genet.* **2**, e30 (2006).
 15. Y. Hong, C. Winkler, M. Schartl, *Proc. Natl. Acad. Sci. U.S.A.* **95**, 3679 (1998).
 16. S. M. Johnson, F. J. Tan, H. L. McCullough, D. P. Riordan, A. Z. Fire, *Genome Res.* **16**, 1505 (2006).
 17. A. Valouev *et al.*, *Genome Res.* **18**, 1051 (2008).
 18. I. P. Ioshikhes, I. Albert, S. J. Zanton, B. F. Pugh, *Nat. Genet.* **38**, 1210 (2006).
 19. I. Albert *et al.*, *Nature* **446**, 572 (2007).
 20. T. N. Mavrich *et al.*, *Nature* **453**, 358 (2008).
 21. M. P. Francino, L. Chao, M. A. Riley, H. Ochman, *Science* **272**, 107 (1996).
 22. P. Green *et al.*, *Nat. Genet.* **33**, 514 (2003).
 23. P. Polak, P. F. Arndt, *Genome Res.* **18**, 1216 (2008).
 24. This work was supported in part by a Grant-in-Aid for Scientific Research on Priority Areas (C) from the Monbukagakusho:MEXT, by the Japan Science and Technology Agency, and by the NIH (T32 CA09151 to C.C.M.; R01 GM37706 to A.F.). Computational time was provided by the Human Genome Center and the Information Technology Center, the University of Tokyo. We thank A. Sidow, A. Valouev, S. Johnson, J. Ford, and J. Cai for specific advice over the course of this work, and our colleagues at each institution for their help and suggestions. All sequence data are deposited at NCBI Short Read Archive (accession number SRA002449).
- ### Supporting Online Material

www.sciencemag.org/cgi/content/full/1163183/DC1

Materials and Methods
Figs. S1 to S14
Tables S1 to S3
References

14 July 2008; accepted 26 November 2008
Published online 11 December 2008;
10.1126/science.1163183

Include this information when citing this paper.

Supporting Online Material

www.sciencemag.org/cgi/content/full/1163183/DC1

Materials and Methods

Figs. S1 to S14

Tables S1 to S3

References

14 July 2008; accepted 26 November 2008

Published online 11 December 2008;

10.1126/science.1163183

Include this information when citing this paper.

New Products Focus: Sample Handling/Storage

Multipurpose Rotator

A new rotator accepts a variety of tube sizes and mixes them horizontally, vertically, or in any position in between. The system's interchangeable rotisseries accept tubes from 1.5 ml to 50 ml. Each rotisserie is split into two halves that can be exchanged to mix more than one tube type at the same time. Each rotisserie half can be rotated independently from a center point on the shaft. Placing the halves in line with the shaft produces an end-over-end tumbling motion, as for mixing blood samples. Placing the rotisserie at a right angle to the shaft produces a gentle mixing motion, suitable for hybridization. Rotation speed is fixed at 18 rpm. The rotator is small enough to be used on the bench, or in a cold room or incubator, from 4°C to 65°C.

Labnet International

For information 888-522-6381
www.labnetlink.com



DNA Amplification from Whole Blood

The Phusion Blood Direct PCR Kit for amplification of DNA from whole blood eliminates the need for DNA purification prior to polymerase chain reaction. The kit makes use of a modified Phusion Hot Start DNA Polymerase, which is highly resistant to the inhibitors in blood and retains its activity even at 40 percent blood concentration. The kit allows analysis of blood samples with different anticoagulants, under different storage conditions, and from various species. It tolerates heparin, citrate, and EDTA, and is compatible with blood stored on various types of filter paper.

Finnzymes

For information +358-9-2472-3291
www.finnzymes.com

Genomic Sequencing System

The RDT 1000 incorporates microdroplet-based technology to amplify hundreds to thousands of genomic loci with high specificity and uniformity. It leverages the sensitivity and specificity of the polymerase chain reaction while avoiding the limitations of alternative multiplex hybridization and amplification techniques. Targeted sequencing is one of the fastest growing applications for next-generation sequencing technology. Sequence enrichment is a critical step in an efficient targeted sequencing workflow. The system allows researchers to isolate specific regions of the genome for subsequent sequencing. The system can be used for simple, fast, walkaway workflow of DNA sample preparation, reagent delivery, on-chip processing, and sample recovery.

RainDance Technologies

For information 888-724-6440
www.raindancetechnologies.com

Nucleic Acid Extractor

The SPRI-TE Nucleic Acid Extractor for the automated purification of DNA and RNA prepares up to 10 samples in about 30 minutes and requires minimal user training. Prepackaged, ready-to-use extraction kits are available for preparing genomic DNA, viral nucleic acid, or formalin-fixed, paraffin-embedded nucleic acid samples. The system

features proprietary SPRI (solid phase reversible immobilization) technology, which extracts the nucleic acids without centrifugation or a vacuum manifold. This technology ensures stronger binding and higher quality purification than silica-coated beads, which can shear nucleic acids, lowering the quality of results.

Beckman Coulter

For information 714-993-8955
www.beckmancoulter.com

PCR Inhibitor Removal Kits

The OneStep and OneStep-96 PCR Inhibitor Removal Kits contain all the components necessary to remove from DNA and RNA preparations contaminants that can inhibit downstream enzymatic reactions such as polymerase chain reaction (PCR) and reverse transcription (RT). The column and plate matrices are designed to remove polyphenolic compounds, humic and fulvic acids, tannins, melanin, and more. In most commercially available kits, these inhibitory compounds can contaminate impure DNA and RNA preparations isolated from soil, plants, skin, fecal, and other samples. Sample cleanup is as simple as applying, spinning, and recovering a sample from the column or plate.

Zymo Research Corporation

For information 888-882-9682
www.zymoresearch.com

DNA and RNA from Same Soil Sample

The RNA PowerSoil DNA Elution Accessory Kit is designed to coisolate high-molecular-weight DNA for the recovery of the total nucleic acid content of the original sample. It can be used in combination with the RNA PowerSoil Total RNA Isolation Kit to isolate and elute the RNA and DNA into separate fractions. The kits include patented new technology that removes all known polymerase chain reaction inhibitors, including humic acids, polysaccharides, polyphenolics, melanin, and hematin.

Mo Bio Laboratories

For information 760-929-9911
www.mobio.com/rnapowersoilna

Electronically submit your new product description or product literature information! Go to www.sciencemag.org/products/newproducts.dtl for more information.

Newly offered instrumentation, apparatus, and laboratory materials of interest to researchers in all disciplines in academic, industrial, and governmental organizations are featured in this space. Emphasis is given to purpose, chief characteristics, and availability of products and materials. Endorsement by *Science* or AAAS of any products or materials mentioned is not implied. Additional information may be obtained from the manufacturer or supplier.

Connecting you
to the world of...
Science

Science Careers Classified Advertising

For full advertising details, go to ScienceCareers.org and click **For Advertisers**, or call one of our representatives.

UNITED STATES & CANADA

E-mail: advertise@sciencecareers.org
Fax: 202-289-6742

Joribah Able
Industry - US & Canada
Phone: 202-326-6572

Alexis Fleming
Northeast Academic
Phone: 202-326-6578

Tina Burks
Southeast Academic
Phone: 202-326-6577

Daryl Anderson
Midwest/Canada Academic
Phone: 202-326-6543

Nicholas Hintibidze
West Academic
Phone: 202-326-6533

EUROPE & INTERNATIONAL

E-mail: ads@science-int.co.uk
Fax: +44 (0) 1223 326532

Tracy Holmes
Associate Director, Science Careers
Phone: +44 (0) 1223 326525

Alex Palmer
Phone: +44 (0) 1223 326527

Dan Pennington
Phone: +44 (0) 1223 326517

Susanne Kharraz Tavakol
Phone: +44 (0) 1223 326529

Louise Moore
Phone: +44 (0) 1223 326528

JAPAN

Mashy Yoshikawa
Phone: +81 (0) 3 3235 5961
E-mail: myoshikawa@aaas.org

To subscribe to *Science*:
In US/Canada call 202-326-6417 or 1-800-731-4939.
In the rest of the world call +44 (0) 1223 326515.

Science makes every effort to screen its ads for offensive and/or discriminatory language in accordance with US and non-US law. Since we are an international journal, you may see ads from non-US countries that request applications from specific demographic groups. Since US law does not apply to other countries we try to accommodate recruiting practices of other countries. However, we encourage our readers to alert us to any ads that they feel are discriminatory or offensive.

Science Careers

From the journal *Science*



POSITIONS OPEN

MATERIALS ENGINEER

U.S. Army Research Office
Research Triangle Park, North Carolina

Applications are being solicited for a Materials Engineer, DB-0806-03 (equivalent to the GS-12/13 grade level), \$67,416 to \$104,223 per annum, or a Materials Engineer, DB-0806-04 (equivalent to the GS-14/15 grade level), \$94,733 to \$144,868 per annum. Salary within the ranges above includes a locality adjustment and depends upon individual qualifications and salary history. The position is located at the U.S. Army Research Office in Research Triangle Park, North Carolina. The incumbent creates, directs, and manages a leading extramural basic research program (experimental and theoretical) in materials science, focusing on the physical properties of materials and fostering scientific achievements relevant to future Army systems. Expertise is required in the areas of electronic, optical, magnetic, and actuator materials. Duties include: initiating new research projects in response to Army needs; stimulating proposals to respond to those needs; analyzing and evaluating proposals; communicating with grantees and contractors; reviewing and analyzing research reports and insuring their effective distribution; stimulating technology transfer to both Army and civilian users; evaluating grantee and contractor performance; disseminating program policies and research results; maintaining awareness of Army in-house R&D programs; developing and presenting briefings and research summaries that highlight projects, objectives, progress, accomplishments, and emerging opportunity areas within materials science to Army leadership and the scientific community; initiating and carrying out workshops, conferences, and symposia addressing emerging materials research initiatives; and serving as the principal Army advocate and representative for basic research activities and needs in physical properties of materials. In order to maintain scientific acumen, the incumbent may perform research at a local university for up to one day per week. Travel up to 25 percent of the time may be required. Outstanding verbal and written skills are required. Applicants must show successful completion of a full four-year course of study in an accredited college or university leading to a Bachelor's or higher degree in materials science, or a combination of education and experience equal to a GS-12/13 level position in the federal government. An advanced degree at the Ph.D. level preferred. Experience must have been in or related to the work of the position and have equipped the applicant with the knowledge, skills, and abilities to successfully perform the duties of the position.

Applicants must be U.S. citizens, be able to obtain a secret clearance, and comply with provisions of the Ethics in Government Act. Interested individuals must apply electronically following instructions at **website: <http://www.usajobs.opm.gov>** or at **website: <http://www.cpol.army.mil>**. Vacancy announcement NEAC08198679 and NEAC08198679D for the DB03 and NEAC08199486 and NEAC08199486D for the DB04.

Opening date is January 20, 2009, and closing date will be February 19, 2009. If you have questions, please contact Mrs. Paula Valdez, telephone: 301-394-2109.

THREE FACULTY POSITIONS Department of Biological Sciences North Dakota State University

An **EVOLUTIONARY DEVELOPMENTAL BIOLOGIST** and a **PHYSIOLOGICAL GENOMICIST** (both tenure track) are sought to develop an extramurally funded research program, supervise Ph.D. students, and teach courses in their area of expertise. A major's **GENERAL BIOLOGY PROGRAM COORDINATOR** (renewable non-tenure track) also is sought. Appointments are at the **ASSISTANT PROFESSOR** level and begin fall 2009. For complete description and application, see **website: <http://biology.ndsu.nodak.edu/>**. Review of applications will begin February 15, 2009. *North Dakota State University is an Equal Opportunity Institution.*

POSITIONS OPEN



**Beth Israel Deaconess
Medical Center**



A teaching hospital of
Harvard Medical School

The Department of Psychiatry at Beth Israel Deaconess Medical Center, a major teaching hospital of Harvard Medical School, is seeking exceptionally qualified **PSYCHIATRIC INVESTIGATORS** in neuroimaging research.

POSTDOCTORAL/FACULTY research opportunities are available in a dynamic new neuroimaging research initiative studying individuals in early phases of psychotic disorders or at risk for these disorders. Applicants should have an M.D., Ph.D., or equivalent degree, with at least one year of specialized postdoctoral experience in functional or structural neuroimaging, magnetic resonance spectroscopy (MRS), and/or diffusion tensor imaging, as applied to major psychiatric illnesses. Prior research experience and interest in MRS would be highly desirable. Additional qualifications include experience in research design and methodology, statistics, and quantitative data analysis. (Familiarity with one or more commonly used environments such as Matlab, SPM, IDL, FSL, et cetera would be desirable.)

In addition to contributing to the Department's expanding research initiatives, the appointee will be expected to play a significant role in our academic and training programs, including the Harvard Longwood Psychiatry Residency Training Program. Departmental startup funds commensurate with experience and scope will be available to assist with development of externally funded research. A Harvard Medical School appointment at an appropriate rank is available.

Applicants should send a statement of interest and experience; curriculum vitae; and the names, addresses, telephone numbers, and e-mail addresses of three references to: **Matcheri Keshavan, M.D., Chair, Psychiatric Neuroimaging Search Committee, c/o Ms. Audrey Coulter, Department of Psychiatry, Beth Israel Deaconess Medical Center, 330 Brookline Avenue, Boston, MA 02215.**

Correspondence by e-mail is preferred.
Address e-mail to **e-mail: neuroimaging.search@bidmc.harvard.edu**.

Women and underrepresented minorities are strongly encouraged to apply.

POSTDOCTORAL FELLOW POSITION: HIV

Immunopathogenesis. This position is available to characterize the priming of human T cells to HIV in vitro. The successful applicant must have a Ph.D. degree and should possess extensive experience in virology and immunology related to HIV infection and immunopathology. Send curriculum vitae, a one-page statement of research interests, and a list of three references to: **Dr. Charles R. Rinaldo, Department of Infectious Diseases and Microbiology, University of Pittsburgh, A419 Crabtree Hall, 130 DeSoto Street, Pittsburgh, PA 15261. E-mail: rinaldo@pitt.edu**. *The University of Pittsburgh is an Affirmative Action/Equal Opportunity Employer. Applications from qualified women, minorities, and/or disabled persons are encouraged.*

POSTDOCTORAL FELLOW POSITION: Fox

Chase Cancer Center, Philadelphia, Pennsylvania, is seeking a Postdoctoral Fellow to study B cell development, growth regulation, and transformation (leukemia). Applicants must have Ph.D./M.D. with substantial research experience, preferably in immunology and molecular biology. The role of self-antigen in generation of chronic B cell leukemia, potential cancer stem cells, and mechanism(s) of growth dysregulation will be explored. Send curriculum vitae, summary of research experience, and names of references to: **e-mail: k.hayakawa@fccc.edu**.

Equal Opportunity Employer.



NIAID

National Institute of Allergy
and Infectious Diseases

Postdoctoral Fellow

Functional Study of Natural Killer Cell Surface Receptors

A postdoctoral position is available in the Laboratory of Immunogenetics (LIG), Division of Intramural Research (DIR), National Institute of Allergy and Infectious Diseases (NIAID) to study the function of natural killer (NK) cell surface receptors. In particular, we are interested in functionally identifying potential ligands for a group of activating NK receptors to understand the role of NK cells in innate immunity.

Candidates with relevant research background are preferred. The starting salary is from \$41,200 to \$47,200, depending on experience. The research lab is located at 12441 Parklawn Drive, Room 111, Rockville, MD 20852. Interested candidates should send a detailed CV and names of three references (including email addresses and telephone numbers) to psun@nih.gov.

For more information, please contact Peter D. Sun, Ph.D., Chief, Structural Immunology Section, LIG, NIAID, NIH; telephone: (301) 496-3230; fax: (301) 402-0284; email: psun@nih.gov; Web site: <http://sis.niaid.nih.gov>.



POSTDOCTORAL POSITIONS

Two postdoctoral positions are available in the **Macromolecular Crystallography Laboratory**, National Cancer Institute (NCI), Frederick, MD, USA (<http://mdl1.ncifcrf.gov>). The Protein Structure Section (PSS, headed by **Alexander Wlodawer**) has an extensive program investigating structure-function relationships in proteolytic enzymes such as HIV and HTLV proteases, Lon, sedolisin, and VirA. It also investigates crystal structures of antiviral lectins, proteins of immunological interest, as well as proteins involved in tumor suppression and translation regulation. The Protein Engineering Section (headed by **David Waugh**) is seeking a postdoctoral fellow to spearhead the development of advanced technology for the production of recombinant proteins in eukaryotic expression systems, including yeast, insect and mammalian cells. This fellow will engage in basic research geared toward making fundamental improvements in these systems for applications in structural biology. The ideal candidate will have a sound background in eukaryotic molecular biology/genetics and expression of recombinant proteins in one or more eukaryotic systems. Familiarity with protein purification techniques would be an advantage for either position.

These positions are open to recent Ph. D's (less than 5 years since the award of doctorate) with strong background in protein crystallography. The minimum annual starting stipend at NCI is \$46,200 for new graduates, with additional increases based on previous postdoctoral experience. NCI provides full health insurance, as well as relocation benefits. Interested candidates should apply to: Dr. Alexander Wlodawer or Dr. David Waugh, Macromolecular Crystallography Laboratory, National Cancer Institute, Frederick, MD 21702, USA, Phone +1-301-846-5036, e-mail wlodawer@ncifcrf.gov (AW), Phone +1-301-846-1842, e-mail waughd@ncifcrf.gov (DW).



National Institute of General Medical Sciences Cell Biology and Biophysics Division HEALTH SCIENTIST ADMINISTRATOR

The National Institute of General Medical Sciences (NIGMS), a major research component of the National Institutes of Health (NIH) and the Department of Health and Human Services (DHHS), is seeking applications from exceptional scientists to serve as a Health Scientist Administrator in the Cell Biology and Biophysics (CBB) Division. This division supports major research grant programs in these fields. The Institute is seeking an individual with scientific, administrative, and leadership credentials who can manage and direct cell biology programs in this division. Information about the CBB can be found at: <http://www.nigms.nih.gov/About/Overview/CBB.htm>.

Applicants must possess a Ph.D., M.D. or equivalent degree in a field relevant to the position and have research experience in cell biology, leadership and managerial skills, and strong oral and written communication skills.

Salary is commensurate with qualifications, and includes a full package of benefits. A detailed vacancy announcement **NIGMS-09-313076-CR-DE** and **NIGMS-09-313076-CR-MP** with the mandatory qualifications and application procedures can be obtained via the NIGMS web page at http://www.nigms.nih.gov/about/job_vacancies.html and the NIH Home page at <http://www.jobs.nih.gov>. Questions on application procedures may be addressed to **Karen Page** at (301) 496-4232. Applications must be received by close of business **January 30, 2009**. The NIH is an equal opportunity employer.

The National Institutes of Health inspires public confidence in our science by maintaining high ethical principles. NIH employees are subject to Federal government-wide regulations and statutes as well as agency-specific regulations described at <http://ethics.od.nih.gov>. We encourage you to review this information.



National Institute of General Medical Sciences National Institutes of Health Department of Health and Human Services

The National Institute of General Medical Sciences (NIGMS) in Bethesda, Maryland is seeking applications from outstanding candidates with a strong background in genetics for one Health Scientist Administrator position in the Division of Genetics and Developmental Biology, which supports basic, non-disease oriented research and training.

The incumbent for this position will be responsible for developing and managing a portfolio of research grants that emphasizes genetics and developmental biology. The ideal candidate will have a broad background in genetics and specialized experience in one or more of the following areas: DNA replication repair, and mutagenesis and regulation of gene expression. Prior research experience in microbial genetics is also desirable.

Applicants must possess a Ph.D. or M.D. plus scientific knowledge and demonstrated expertise in at least one of the following areas: Biochemistry, microbiology, physiology, genetics, or related areas, and knowledge of the NIH peer review and grants process.

Salary is commensurate with qualifications, and includes a full package of benefits. A detailed vacancy announcement **NIGMS-09-313070-CR-DE** and **NIGMS-09-313070-CR-MP** with the mandatory qualifications and application procedures can be obtained via the NIGMS web page at http://www.nigms.nih.gov/about/job_vacancies.html and the NIH Home page at <http://www.jobs.nih.gov>. Questions on application procedures may be addressed to **Karen Page** at (301) 496-4232. Applications must be received by close of business **January 30, 2009**. The NIH is an equal opportunity employer.

The National Institutes of Health inspires public confidence in our science by maintaining high ethical principles. NIH employees are subject to Federal government-wide regulations and statutes as well as agency-specific regulations described at <http://ethics.od.nih.gov>. We encourage you to review this information.

Tenure Track Faculty Position

The Department of Physiology at The University of Texas Health Science Center at San Antonio (UTHSCSA) is continuing its major expansion. This year we seek to hire one tenure track faculty. At present, the Department of Physiology has clusters of research strength in neuroscience, cardiovascular function, ion channel biophysics, and the molecular biology of aging. Although candidates that can extend or bridge these areas are encouraged to apply, we are most interested in talented investigators using cutting edge techniques to elucidate fundamental physiological mechanisms at the molecular, cellular, or integrative levels. Investigators at all ranks are encouraged to apply. Candidates will be expected to contribute to the teaching mission that includes training medical, dental, and graduate students. Competitive start-up packages and ample resources will be offered to those selected to be a part of this exciting endeavor.

UTHSCSA is a Tier One Research Institution located in the Northwest section of San Antonio and sits as a gateway to the picturesque Texas Hill Country. San Antonio is a vibrant, dynamic, and multicultural city with much to offer including an attractive cost-of-living.

Review of applications will begin immediately and the position will remain open until filled. Candidates should submit the following as pdf files: curriculum vitae, two-page summary of description of research accomplishments/goals and three letters of reference to:

John M. Johnson, Ph.D., Professor
 Department of Physiology
 E-Mail: PhysioSearch@uthscsa.edu
 Website: www.physiology.uthscsa.edu

All faculty appointments are designated as security sensitive positions. The University of Texas Health Science Center at San Antonio is an Equal Employment Opportunity/Affirmative Action Employer.

ASSISTANT PROFESSOR OF BIOLOGY

Fall 2009 - Two Temporary, Full Time Positions Available:

First Position:

JOB DESCRIPTION: Primary teaching responsibilities include microbiology for the health sciences, both lecture and laboratories, and other courses in molecular/organismal biology.

REQUIREMENTS: Ph.D. required, college teaching experience preferred.

Supporting documentation in non-electronic format can be sent to Professor Rena Bacon, Search Committee Chair, School of Theoretical and Applied Science. **To request accommodations, call (201) 684-7734.**

Second Position:

JOB DESCRIPTION: Primary teaching responsibilities include courses in molecular/organismal biology, particularly introductory biology courses to both majors and non-majors.

REQUIREMENTS: Ph.D. required, college teaching experience preferred.

Supporting documentation in non-electronic format can be sent to Professor Susan Petro, Search Committee Chair, School of Theoretical and Applied Science. **To request accommodations, call (201) 684-7734.**

Faculty members are expected to maintain active participation in research, scholarship, college governance, service, academic advisement and professional development activities.

**All applications must be completed online at:
www.ramapo.edu/hrjobs**

Attach vita, cover letter, statement of teaching philosophy, research interests and a list of three references to your completed application. Hard copies of resumes will not be accepted. Since its beginning, Ramapo College has had an intercultural/international mission. Please tell us how your background, interest and experience can contribute to this mission, as well as to the specific position for which you are applying. Review of applications will begin immediately and continue until the positions are filled. Positions offer excellent state benefits.



**505 Ramapo Valley Road
 Mahwah, NJ 07430
 "New Jersey's Public
 Liberal Arts College"**

Ramapo College is a member of the Council of Public Liberal Arts Colleges (COPLAC), a national alliance of leading liberal arts colleges in the public sector. EEO/AFFIRMATIVE ACTION.

The University of
Montana

ASSISTANT PROFESSOR

The Division of Biological Sciences and the Center for Structural and Functional Neuroscience welcome applications for a tenure-track position at the rank of Assistant Professor.

If you are a productive and innovative biologist who can develop a creative research program in areas of interest that include but are not limited to: the genetics or molecular biology of nervous system development, the neurobiology of behavior, or the molecular/structural basis of neurophysiological mechanisms, please consider joining us at The University of Montana. Investigators who develop quantitative or predictive models in the context of experimental data are especially welcomed to apply.

The University of Montana is located in Missoula, Montana where faculty enjoy a high quality of life in a spectacular natural setting with outstanding recreational opportunities. Information about the Division of Biological Sciences and participating research centers can be found at: www.dbs.umt.edu, www.health.umt.edu/centers/cfsn, and www.cas.umt.edu/biomolecular.

Applicants should submit a curriculum vitae, a detailed statement of future research plans and teaching interests, and the names of three potential references by email to Mike Kavanaugh and Stephen Sprang, Neurobiologist Search Committee at: neurobiology.search@mso.umt.edu. Review of materials will begin on February 1, 2009 and continue until the position is filled.

UM is an EEO/AA/ADA/Veterans Preference Employer and recipient of an NSF PACE award. The Division is interested in hiring a candidate who will enhance the gender and ethnic diversity of its faculty.

ETH

**Eidgenössische Technische Hochschule Zürich
 Swiss Federal Institute of Technology Zurich**

Professor in Animal Genetics

The Department of Agricultural and Food Sciences (www.agrl.ethz.ch) at ETH Zurich invites applications for the position of a professorship in animal genetics. The future professor will be responsible for developing a leading research and teaching program in animal genetics that focuses on the identification of genes underlying important animal traits.

Candidates with expertise in QTL mapping and/or comparative genomics applied to important livestock species are especially encouraged to apply. The professorship's main research topics may include:

- Comparative genomic or QTL mapping approaches to identify key genes or chromosomal regions underlying important traits;
- Experimental approaches to understand the underlying causes of quantitative genetic variation;
- Analyses of interactions between genes;
- The influence of environmental factors on gene expression.

The Professorship is equipped with several vacant positions, has access to high-throughput genotyping facilities and to a well-equipped field station suitable for animal phenotyping.

The future professor will be expected to teach undergraduate level courses (German or English) and graduate level courses (English) - covering both basic and advanced animal genetics.

Please submit your application together with a curriculum vitae, a list of publications, a statement of research and teaching interests, and the names and contact information of three possible referees to the President of ETH Zurich, Prof. Dr. Ralph Eichler, Raemistrasse 101, 8092 Zurich, Switzerland, no later than March 31, 2009. With a view toward increasing the number of female professors, ETH Zurich specifically encourages female candidates to apply.



POSTDOCTORAL TRAINING OPPORTUNITIES

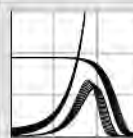
The University of Michigan is an outstanding training environment that combines world-class faculty and innovative programs of research with a rich academic tradition. For two decades Michigan has ranked among the top 10 medical schools in NIH research funding. This research effort is enhanced by 26 NIH-sponsored training programs that support Postdoctoral Scholars.

The University of Michigan recognizes the essential contributions Postdoctoral Scholars make to the University's overall research mission. We welcome inquiries from graduate students nearing completion of the Ph.D. degree regarding opportunities for postdoctoral training in the following areas:

- Alcoholism Research
- Biology of Aging
- Biology of Drug Abuse
- Cancer Biology
- Cardiovascular Research
- Cell and Molecular Dermatology
- Clinical and Basic Neuroscience
- Endocrine Dysfunction
- Endocrinology and Metabolism
- Experimental Immunology
- Genome Sciences
- Hearing, Balance and Chemical Senses
- Imaging Science in Biomedicine
- Lung Disease
- Lung Immunopathology
- Medical Rehabilitation Research
- Microbial Pathogenesis
- Molecular Hematology
- Nephrology Research
- Organogenesis
- Reproductive Sciences
- Research in Gastroenterology
- Substance Abuse
- Tissue Engineering and Regeneration
- Urology Research
- Vision Research

For more information about Sponsored Training Programs, as well as descriptions and contact information for the above programs, visit:
www.med.umich.edu/medschool/postdoc.

The University of Michigan is an equal opportunity, affirmative action employer.



Max Planck Institute for Demographic Research

Directors: Prof. James W. Vaupel – Prof. Joshua R. Goldstein

The Max Planck Institute for Demographic Research is seeking to expand further its quantitative, interdisciplinary activities in the field of

Evolutionary Biodemography / Comparative Life History Analysis

by making appointments at the

PhD, Post-Doc, and Research Scientist levels.

The research program focuses on understanding how evolution can shape age-specific mortality in tandem with age-specific fertility and other aspects of the life-history. We aim to tackle these issues by synthesizing quantitative insights from diverse disciplines including demography, life history biology, ecology, mathematics, statistics and actuarial science. As well as considering flexible, open appointments for strong candidates with appropriate backgrounds and relevant interests, the institute will make specific appointments of comparative life history biologists, phylogenetic and demographic analysts, database developers, mathematical theoreticians, programmers and statisticians to develop the

AgeLife Project,

a collaborative international network to advance understanding of lifespan and age-specific demography by comparing a wide range of organisms across the tree of life. Successful candidates will complement an existing interdisciplinary research team of more than 20 scientists and support staff within the institute. Those in the AgeLife project will have links with other partners in the network, but will principally be based in Rostock. Information about the institute, our work in Evolutionary Biodemography, and the AgeLife project can be found at www.demogr.mpg.de/agelife.

Applications should be addressed to Executive Director Prof. James W. Vaupel and should include a CV with a statement of academic interests and relevant experience, details of all qualifications including grades, a list of any publications, and the contact details of 3 referees. All material should be e-mailed to: appl-agelife@demogr.mpg.de. Review of applications will begin on 15th February 2009. We will consider applications received before the end of March. PhD positions will typically start in early September 2009, and other positions will start as soon as possible after appointment. PhD and postdoc appointments are made on doctoral and postdoctoral stipends respectively, and Research Scientist positions are on TVöD 13.

The Max Planck Society wishes to increase the share of women in areas where they are underrepresented, and strongly encourages women to apply.

The Max Planck Society is committed to employing more handicapped individuals and especially encourages them to apply.

www.demogr.mpg.de



MAX PLANCK SOCIETY

**Faculty Position in
Microbial Pathogenesis
and Immunity**



**Department of Microbiology and Immunology
Tulane University School of Medicine**

The Department of Microbiology and Immunology, Tulane University School of Medicine is recruiting a tenure-track faculty member at the rank of Assistant, Associate or Full Professor. We are primarily interested in investigators whose research complements existing strengths in host-pathogen interaction and vaccine development. The successful candidate will join a multidisciplinary department focusing on molecular, cellular, and genetic aspects of infectious disease and host-pathogen interactions. He/she will be expected to maintain an independent and dynamic, funded research program and to contribute to the teaching of medical and graduate students.

The Department of Microbiology and Immunology offers a competitive salary, attractive start-up packages, renovated laboratory space, BSL-3 and select agent laboratories, and an interactive environment. For further information about the Department and Tulane University School of Medicine visit our website at <http://www.microbiology.tulane.edu>.

Applicants should submit a curriculum vitae, a statement of research interests, and the names, addresses, email addresses, and telephone numbers of three qualified references to: **Faculty Search Committee, Department of Microbiology and Immunology, Tulane University School of Medicine, 1430 Tulane Avenue SL-38, New Orleans, LA 70112** or email to **Ms. Amy Pick (aepick@tulane.edu)**. Review of applications will begin immediately and continue until the position is filled.

Tulane University is an Equal Opportunity, Affirmative Action Employer. Women, Minorities and Veterans are encouraged to apply.



**Zhejiang University
Institute of Life Sciences**

浙江大学生命科学研究院 (筹)

Founded in 1897, Zhejiang University is committed to the highest standards of excellence in education and research, and has been at the forefront of academic scholarship in China. The newly formed Institute of Life Sciences aspires to become a top research institute in a broad range of biological and medical research.

Applications and nominations are invited for appointments as:

(1) Director of the Institute of Life Sciences

Applicants should be established scholars with a distinguished academic accomplishment and international reputation. Individuals should be able to provide leadership to the new institute and enhance the institute's profile both nationally and internationally. Experience in management would be an advantage.

(2) Principal Investigators

Applicants should have a strong research profile to establish and conduct innovative research in life sciences. Both senior and junior investigators are encouraged to apply.

The university provides state-of-the-art research facilities and strong supporting staffs. Internationally competitive start-up support, salary and benefits will be offered according to qualifications and experience.

Please login in website <http://ils.zju.edu.cn> to sign up and submit application, including a full CV, cover letter, and future plan. Application can also be sent to ils@zju.edu.cn.

Contact person: Zhu Xiaoyun, Email: zhuxy@zju.edu.cn, Fax: +86-571-88981976, Tel: +86-571-88981390

The application deadline for the director position is **February 28, 2009**, while application for the faculty position will be open.



Looking for a new dynamic medical research environment?

The Center for Primary Health Care Research (CPF) may be looking for you. The CPF is a new collaborative venture of Lund University and Region Skåne in southern Sweden.

We are located at the Clinical Research Centre, a translational research environment at Malmö University Hospital in the city of Malmö, Sweden.

Using primary health care as our arena, we will conduct world-class translational research in five program areas: • migration and neighborhoods • welfare diseases, medical epidemiology, and genetic epidemiology • research methods in family medicine and research on quality aspects of medical education • public health science and social epidemiology and • health economy, organization of health care, and evaluation of health and medical programs.

To improve the quality of our research, we will work closely with primary health care center and hospital personnel and with international collaborators at a number of universities, including Stanford and Harvard.

We are building our team and are looking for people to fill a number of positions. The CPF needs biostatisticians, postdoctoral research fellows, postdoctoral students, and doctoral students in epidemiology and physical activity. Interested? Send an informal letter to Jan. Sundquist@med.lu.se describing your qualifications and explaining why you want to be one of us. We look forward to hearing from you!

Read more about the translational research environment at the Clinical Research Centre at http://www.med.lu.se/english/crc/research_at_crc, or the new center <http://www.med.lu.se/english/cpf>

**Assistant/Associate/Full Professor in
Gene Therapy or Proteomics**

The Department of Pharmaceutical Sciences at North Dakota State University invites applications for a tenure-track faculty position at the rank of Assistant/Associate/full Professor, with appointment beginning on or after August 15, 2009. A highly competitive salary and a start-up package commensurate with qualifications and experience are available. The department of Pharmaceutical Sciences has experienced rapid recent growth and consists of twelve full-time faculty members, more than thirty doctoral students and post-doctoral fellows/research associates. The department faculty members have diverse but complementary research interests and are well funded from numerous national and other funding agencies. The department has a Center of Biopharmaceutical Research and Production (CBRP), participates in a NIH-funded (\$10.5 million) Center of Biomedical Research Excellence. Additional information about the Department and University can be obtained at <http://www.ndsu.edu/pharmsci/>.

Candidates must hold a doctoral degree in pharmacology, gene therapy, proteomics, molecular biology, or closely related field, have at least two years of postdoctoral experience either in gene therapy or proteomics with a strong record of scholarship, possess good interpersonal skills, and effective written and oral communication skills. Preference will be given to applicants with training and research expertise in areas of gene therapy or proteomics that complement existing departmental strengths in cancer and cardiovascular research. The successful candidate will be expected to establish an externally funded research program, provide service to the university, teach and mentor graduate students, and participate in team-taught pharmacology courses offered to pharmacy students. Application deadline is **March 30th, 2009**, or thereafter until the position is filled. The application portfolio containing a (1) letter of application, (2) curriculum vitae, (3) statement of teaching philosophy, (4) description of research interests and future plans, and (5) a list of references with complete address must be submitted electronically: jobs.ndsu.edu/applicants/Central?quickFind=50720. For more information, please contact Dr. Chengwen Sun (e-mail: Chengwen.Sun@ndsu.edu, Tel: 701-231-6454, Fax: 701-231-8333), Department of Pharmaceutical Sciences, North Dakota State University, Fargo, ND 58108.

NDSU is an Equal Opportunity Institution. Women and traditionally under-represented groups are encouraged to apply.



Director
Arnold O. and Mabel M. Beckman Institute
for Advanced Science and Technology

The University of Illinois at Urbana-Champaign invites applications and nominations for the position of Director of the Arnold O. and Mabel M. Beckman Institute for Advanced Science and Technology. The Beckman Institute is an interdisciplinary research institute devoted to basic research in the physical sciences, computation, engineering, biology, behavior, and cognition. The Institute's primary mission is to foster interdisciplinary work of the highest quality, transcending many of the limitations inherent in traditional university organizations and structures. Research is currently organized around four major themes, Biological Intelligence, Human Computer Intelligent Interactions, Integrative Imaging and Molecular and Electronic Nanostructures. The Institute involves about 180 faculty members from 40 different departments working with their students and postdoctoral associates in state-of-the-art research facilities. The Institute has 70 administrative staff members and a total annual budget of \$28M, which includes \$18.6M in research expenditures. More complete information is available at the website: <http://www.beckman.illinois.edu/>.

Founded in 1867, the University of Illinois is among the preeminent comprehensive public research institutions. The University of Illinois has 33 programs ranked in the top 5 and 89 programs ranked in the top 20. Illinois faculty and alumni have earned 22 Nobel Prizes and include 147 members of the American Academy of Arts and Sciences, the National Academy of Sciences and the National Academy of Engineering. They have been awarded Pulitzer Prizes and Olympic medals, have orbited the earth, and have founded and led international corporations.

The Director should be a strong leader with an exceptional record of scientific achievements that demonstrate an understanding of multi-investigator interdisciplinary activities. The Director must also have management experience leading scientific and engineering groups in academia, government or the private sector. The Director should hold a doctoral degree in a science or engineering field and have an outstanding record of scholarly accomplishments commensurate with appointment at the rank of Professor in a leading research university. Familiarity with the academic environment is essential; experience in academic administration is desirable.

Among the responsibilities of the Director are the following: Sustain and develop the vision for the Institute, in conjunction with the faculty and staff; provide research leadership for the Institute; identify new programs for inclusion in the Institute; oversee evaluations of programs and members of the Institute; work with campus units in establishing and maintaining appropriate relationships between them and the Institute; assist in attracting key faculty members to the campus; conduct development/fund raising activities; manage the Institute's physical and financial assets; mentor the Institute's faculty and assist them in acquiring external support for research; and represent the Institute beyond the campus.

This full time, twelve month appointment has a start date that is negotiable. Salary is commensurate with experience. For full consideration, nominations and applications (including a letter of interest, CV and e-mail address) should be sent by **March 15, 2009** as a single PDF document to provost@illinois.edu addressed to:

Professor Gene Robinson, Chair
Search Committee for the Director of the Beckman Institute
Office of the Provost and Vice Chancellor for Academic Affairs
University of Illinois at Urbana-Champaign
Swanlund Administration Building, Room 204
601 East John Street
Champaign, IL 61820
generobi@illinois.edu, Ph: 217/333-6843; Fax: 217/244-3499

*The University of Illinois at Urbana-Champaign is an
Affirmative Action/Equal Opportunity Employer.*



WE BELIEVE

THE CURE WILL BE FOUND RIGHT HERE

Faculty Position: Tumor Immunology

H. Lee Moffitt Cancer Center & Research Institute, an NCI-designated Comprehensive Cancer Center, is seeking candidates for the rank of Assistant/Associate/Senior Member to expand the Department of Immunology. Individuals with a research interest in any area of tumor immunology, including antigen presentation, tumor-induced immune suppression or tolerance, gene regulation, signal transduction, crosstalk between innate and adaptive immunity, immunotherapy and cancer vaccines will be considered. Successful candidates are expected to develop a strong extramurally-funded research program.

Consistently ranked in U.S. News & World Report "Best Cancer Hospitals" for the past nine years, Moffitt Cancer Center and Research Institute is a free-standing, not-for-profit cancer center. Moffitt opened on the campus of Tampa's University of South Florida in October, 1986 and became Florida's only NCI designated Comprehensive Cancer Center in 2001. There is vast opportunity within our framework for information technology, scientific research, clinical treatment and quality of life studies, as we see over 15,000 new cancer patients each year. Our environment is one of multi-modality, patient-centered care requiring highly collaborative clinical research programs.

The Cancer Center is comprised of a large ambulatory care facility, 162 inpatient beds, including a dedicated transplant unit, 12 state-of-the-art operating suites, a 30 bed intensive care unit, a high volume screening program, and a basic science research facility. The Moffitt Research Institute is comprised of approximately 140 Principal Investigators, 58 laboratories, and 306,000 square feet of research space. Our University of South Florida affiliation allows for a wide range of residency and fellowship programs, and Faculty of the Moffitt Cancer Center are eligible for academic appointments in their College of Medicine, commensurate with qualifications and experience.

Application Qualifications

The successful candidate must have an M.D. or Ph.D. with at least four years of postdoctoral experience in tumor biology or immunology and high quality publications in peer-reviewed journals. Salary and start-up packages are competitive and negotiable.

For inquiries about the position, contact Julie Djeu, Ph.D., Department Chair, at 813-745-3041 or julie.djeu@moffitt.org.

To apply, visit our website moffittcareers.org and refer to requisition number 3385.



Moffitt Cancer Center provides a tobacco-free work environment, is an equal opportunity, affirmative action employer, and a drug free workplace.

Science Careers is the forum
that answers questions.



Science Careers is dedicated to opening new doors and answering questions on career topics that matter to you. With timely feedback and a community atmosphere, our careers forum allows you to connect with colleagues and experts to get the advice and guidance you seek as you pursue your career goals.

Science Careers Forum:

- » Relevant Career Topics
- » Timely Advice and Answers
- » Community, Connections, and More!

Visit the forum and join the conversation today!



Your Future Awaits.



ScienceCareers.org



The University of Maryland School of Medicine Institute of Human Virology, in conjunction with the Marlene and Stewart Greenebaum Cancer Center, is recruiting a highly qualified **tenure track assistant or associate professor** in the field of viral oncology and AIDS-related malignancies, including investigators interested in the search for novel, human tumor viruses. The new laboratory will be a component in the growing program on HIV and Cancer and will interact with ongoing efforts in our clinical and epidemiology divisions, including the study of cancers from developing countries.

The Institute of Human Virology offers excellent laboratory facilities, competitive salary and startup packages, and access to numerous core facilities including state-of-the-art BSL3 and ABSL3 facilities in a strong academic environment. Preference will be given to candidates with established research programs and current NIH funding. The level of appointment will be commensurate with the candidate's experience.

Please submit a letter of interest, CV and three references to:

Viral Oncology Faculty Search Committee
c/o Beth Peterson

Institute of Human Virology
725 West Lombard Street, S307
Baltimore, MD 21201
bpeterson@ihv.umaryland.edu

*The University of Maryland, Baltimore is an
Equal Opportunity, Affirmative Action Employer.*

**Your
career is
our cause.**

Get help
from the
experts.

www.sciencecareers.org

- Job Postings
- Job Alerts
- Resume/CV Database
- Career Advice
- Career Forum

Science Careers

From the journal Science





Professorship in Single Molecule Biophysics

The Institute of Structural and Molecular Biology (ISMB) at UCL/Birkbeck and the London Centre for Nanotechnology (LCN) at UCL are seeking applications for a Professorship in the field of Single Molecule Biophysics, a position that will be held jointly between the two organisations. It is hoped that this post will be filled by October 2009. We wish to recruit an outstanding individual who is capable of conducting world-class, interdisciplinary research in an area of single molecule biophysics that has relevance to mainstream biomedicine. Successful applicants will be expected to develop and manage a substantial research group and make an appropriate contribution to the affiliated departmental portfolio of graduate teaching.

The ISMB (www.ismb.lon.ac.uk) is a centre of excellence, which jointly consists of the School of Crystallography at Birkbeck College and the Research Department of Structural & Molecular Biology at University College London (UCL). It was established to foster closer links between the two departments and also to provide a bridge with the Department of Chemistry at UCL. The Institute provides a scientific environment conducive to world-class research in the field of biomolecular science. The London Centre for Nanotechnology is a joint venture between University College London and Imperial College London. It has a unique operating model that accesses and focuses the combined skills of the departments of chemistry, physics, materials, medicine, electrical and electronic engineering, mechanical engineering, chemical engineering, biochemical engineering and earth sciences across the two universities.

The salary is negotiable within the University Professorial scales and will be dependent on experience and track record. A job description and details of the application procedure can be found at www.ismb.lon.ac.uk/JD1SMB.html and at the respective departmental web sites (<http://www.cryst.bbk.ac.uk/> and <http://www.london-nano.com/>). The Head of ISMB is Professor Gabriel Waksman (email: g.waksman@bbk.ac.uk) and the Head of LCN is Professor Gabriel Aeppli (email: gabriel.aeppli@ucl.ac.uk). Either can be contacted informally for general information.

The closing date for this post is 31st March, 2009. Interviews with short-listed candidates will take place during April and May 2009.

We particularly welcome female applicants and those from an ethnic minority, as they are currently under-represented within UCL at this level. This is in line with section 48 of the Sex Discrimination Act and section 38 of the Race Relations Act.



Science



Senior Editor for Science Magazine

Join the dynamic editorial team at *Science* magazine. We are seeking a Senior Editor interested in science and/or education

policy, to work in our Washington, DC, USA or Cambridge, UK office.

We are looking for an individual with broad interests including education, and a background ideally in science policy and the social or political sciences. The editor would be involved in solicitation and editing of perspectives and policy forums related to education (K-12, undergraduate, and graduate) and other policy areas. An advanced degree (PhD) is required.

Five or more years of work experience required (post-doctoral or publishing experience preferred). The ideal candidate will have an appreciation of the challenges of science communication, outstanding writing/editing skills, and an affinity for the creative use of graphics to convey technical ideas. This individual must also have the ability to work in a team and within weekly deadlines and page limits. He/she should have experience in communicating to audiences outside their specialized community.

Responsibilities include soliciting manuscripts; managing the review, selection, and editing of manuscripts; working with authors on revisions; and fostering contacts and communication with the scientific community. Candidates are expected to travel to relevant meetings.

Science is published by the AAAS, the world's largest multidisciplinary scientific membership organization. Visit us at www.sciencemag.org and www.aaas.org.

For consideration send a cover letter and resume, along with your salary requirements, to:

AAAS

Human Resources Office, Suite 101

1200 New York Ave., NW

Washington, DC 20005

or, by email, to jobs@aaas.org or, by fax, to 202-682-1630

EOE. Non-smoking work environment.



**ADDRESSING
THE CHALLENGES
OF THE LIVING WORLD**

**The French National Institute
for Agricultural Research
is recruiting**

**68
RESEARCHERS (MF)**

SCIENTIFIC EXCELLENCE	RELEVANCE	DIVERSITY
<p>INRA, the leading agricultural research institute in Europe, is focusing on the major issues involved in global sustainable development: food geared towards people's needs, competitive agriculture and a preserved environment. From fundamental research to breakthroughs, INRA scientists work together in dynamic, multidisciplinary teams open to the world that reconcile group projects and professional self-fulfillment.</p> <p>Applications from 15th of January to 27th of February 2009</p> <p>www.inra.fr</p>		

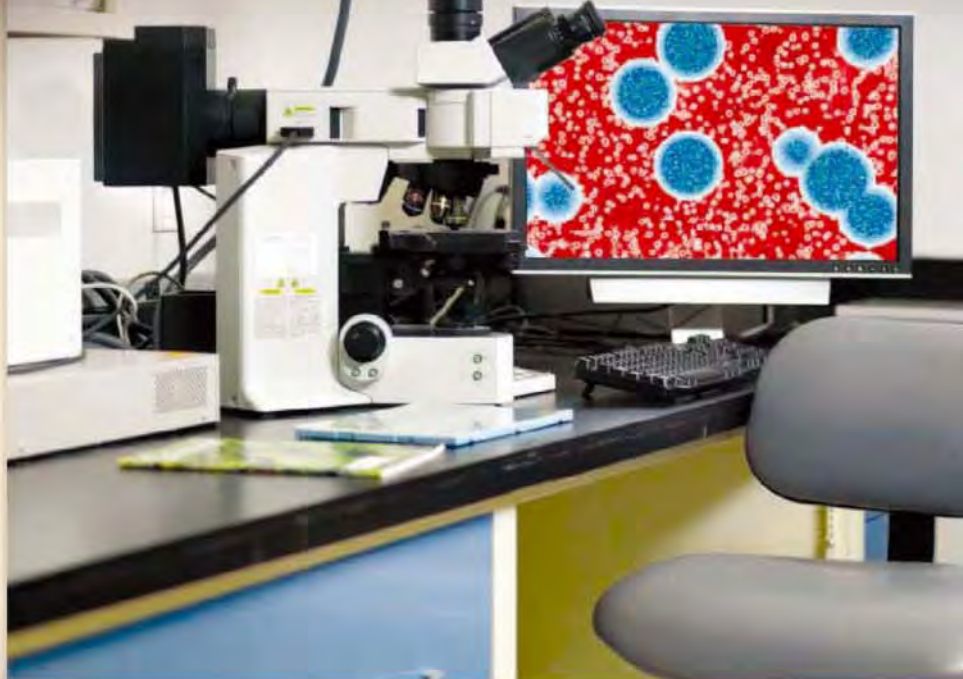
FROM SCIENTIFIC
ADVANCEMENT
TO ENVIRONMENT



orc.fr wellcom

Science Careers is the window that displays your vision.

Visit our
ENHANCED
WEBSITE!



Revealing your vision to employers is our job. We're your source for connecting with top employers in industry, academia, and government. We're the experts and entry point to the latest and most relevant career information across the globe.

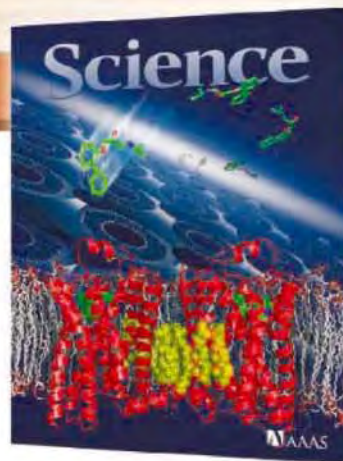
Our newly designed website offers a set of tools that reveal career opportunities and your personal potential. Whether you're seeking a new job, career advancement in your chosen field, or ways to stay current on industry trends, *Science Careers* is your window to a limitless future.

Improved Website Features:

- » Relevant Job E-mail Alerts
- » Improved Resume Uploading
- » Content Specific Multimedia Section
- » Facebook Profile

Job Search Functionality:

- » Save and Sort Jobs
- » Track Your Activity
- » Search by Geography
- » Enhanced Job Sorting

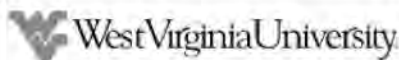


Your Future Awaits.



ScienceCareers.org

POSITIONS OPEN



The Eberly College of Arts and Sciences at West Virginia University is seeking candidates for the Eberly Family Professor of Energy Policy. The area of Energy Policy is one of the three areas of focus in West Virginia University's recently announced Advanced Energy Initiative along with Fossil Energy and Sustainable Energy. We are seeking a dynamic individual to provide scholarly leadership, at the state, national, and international levels in the general area of energy policy. Acceptable candidates must have a record of significant scholarly and educational accomplishments in the area of energy policy. The Eberly Family Professor of Energy Policy will hold tenure in one of the social science units of the Eberly College of Arts and Sciences and must have credentials expected of such a faculty appointment, including the Ph.D. degree.

Our College is recognized for its strengths in discovery, learning, and engagement in the social sciences. Our Department of Geology and Geography has an international reputation for its research contributions in the areas of energy exploration and development, remote sensing, and GIS. Equally strong programs are found in our college's School of Applied Social Sciences, incorporating Public Administration, Sociology, and Social Work, as well as in our Department of Political Science and Institute for Public Affairs. All units partner with the University's Regional Research Institute led by Professor Randy Jackson, of the Department of Geology and Geography.

West Virginia University is also well known for its basic and applied science and engineering research, particularly with respect to fossil energy sources. The institution is engaged in ongoing collaborations not only with the National Energy Technology Laboratory but also with partner universities and industries in the region focused on the effective and responsible utilization of our regions substantial fossil energy resource reserves. The Eberly College of Arts and Sciences is a strong partner in these endeavors and seeks to build strength in the area of energy policy. The Eberly Family Professor of Energy Policy will be expected to take a lead role in this development and work closely on collaborative projects with colleagues from across WVU and our partners.

Interested individuals should prepare an application package to include (1) a statement describing their qualifications and vision for the Energy Policy; (2) a complete curriculum vitae, including a record of scholarly activity and leadership experience; and (3) the names and contact information for at least five references. The search committee will begin reviewing applications on **March 1, 2009**, although the position will remain open until filled. The package should be submitted electronically to EberlyEPPProf@mail.wvu.edu. Questions regarding the position should be addressed to: **Fred L. King, Associate Dean, Eberly College of Arts and Sciences**, fred.king@mail.wvu.edu, (304) 293-4611.

West Virginia University is an Affirmative Action, Equal Opportunity Employer, dedicated to building a culturally diverse and pluralistic faculty and staff committed to working in a multicultural environment. Applications from women, minorities, individuals with disabilities and covered veterans are encouraged. Individuals that are part of dual career couples are also encouraged to apply.

ANNOUNCEMENTS



Advancing Careers. Changing Lives.

CH The Children's Hospital of Philadelphia®
Hope lives here.

Research & IT Online Career Discovery Sessions

**January 26th & 27th
8 AM-8 PM**

We invite you to join us for an online Career Discovery Session – to explore the exciting Research careers at “America's Best Children's Hospital.”

Find out why more of the nation's leading Research professionals are coming to The Children's Hospital of Philadelphia.

Discover...

- One of the nation's largest pediatric research programs with hundreds of active projects
- A system that ranks among the top two pediatric hospitals nationwide in National Institutes of Health funding
- Careers in one of the only growing areas of the U.S. economy

Register today for your online Career Discovery Session with a CHOP recruiter. Visit CHOPVirtual.com.

Must have authorization to work in the United States and the ability to pass child abuse background check. EOE

POSITIONS OPEN



An **instrumental chemistry postdoctoral position** is available immediately in the laboratories of **Dr. Nicholas E. Goeders** in the Department of Pharmacology, Toxicology & Neuroscience at the LSU Health Sciences Center in Shreveport.

This position will be part of a team investigating the neurobiology of stress and addiction, with special emphasis on the brain mechanisms involved in drug craving and drug seeking. Applicants should have training in operation and maintenance of commercial mass spectrometers and HPLC. Salary will be \$28,000-\$51,036 depending on experience. Applications should include a CV, a list of publications and the names of references familiar with the applicant's work. The LSU Health Sciences Center in Shreveport, located in northwest Louisiana, is the largest medical facility in the Tri-State area and has a reputation for excellence in medical and graduate student education and research. Excellent core facilities exist within the LSU Health Sciences Center and the adjoining Biomedical Research Institute.

Nicholas E. Goeders, Ph.D.
Professor and Head

Department of Pharmacology, Toxicology,
& Neuroscience
LSU Health Sciences Center
P.O. Box 33932
Shreveport, LA 71130-3932
NGOEDE@LSUHSC.EDU
www.sh.lsuhscc.edu

Louisiana State University is an Equal Opportunity/Affirmative Action Employer.

GRANTS



WELCOME PROGRAMME 2nd call for proposals

The newly launched FNP programme is addressed to foreign **researchers or Polish scientists abroad who wish to carry out research in Poland.**

The offered funding consists of stipends (tax exempt) for a group leader (up to 90 000* EUR/year), Master level students, PhD students, Postdocs (1300* EUR/month) and grants amounting to 250 000* EUR/year/group.

* the exact amount depending on the current exchange rate

The closing date for applications is 15 April 2009.

For further information and application forms visit:
www.fnp.eu

The programme is financed from the Operational Programme Innovative Economy 2007-2013; measure 1.2 - strengthening the human potential in the science sector



INNOVATIVE ECONOMY
NATIONAL COHESION STRATEGY



Science Careers is the stage that showcases your talent.

Visit our
ENHANCED
WEBSITE!

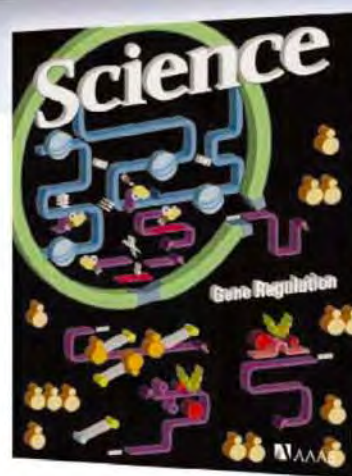
Values
- 10 %
- 20 %
- 40 %
- 80 %

EXP. DESIGN



1. Set up
2. Cell Culture
3. PCR/FACS
ANALYSIS

weeks
1 2 3



Showcasing your talent is our forte. We're your source for connecting with top employers in industry, academia, and government. We're the experts and platform for accessing the latest and most relevant career information across the globe.

Our newly designed website offers a set of tools that help you discover career opportunities and your personal potential. Whether you're seeking a new job in academia, career advancement in your chosen field, or ways to stay current on industry trends, *Science Careers* is your first stage toward a fulfilling future.

Improved Website Features:

- » Relevant Job E-mail Alerts
- » Improved Resume Uploading
- » Content Specific Multimedia Section
- » Facebook Profile

Job Search Functionality:

- » Save and Sort Jobs
- » Track Your Activity
- » Search by Geography
- » Enhanced Job Sorting

Your Future Awaits.

Science Careers

From the journal *Science*

AAAS

ScienceCareers.org

The 2nd meeting on **Molecular Mechanisms of Aging and Age-Related Diseases**

Puerto Vallarta, Mexico - March 3-6, 2009

INVITED SPEAKERS: Jeff Kelly | Reuben Shaw | Gerald Shadel | Jan Karlseder | Gérard Evan | Scott Lowe | Rick Morimoto | Rudi Tanzi | Stuart Kim | Linda Buck | Rolf Bodmer | Dan Gottschling | Richard Weindrich | Thomas Nyström | Leanne Jones | Tom Rando | Arnie Levine |

CALL FOR PAPERS: Abstracts for oral presentation and posters which fit within the theme of the meeting are invited.

ORGANIZERS: Dr. Andrew Dillin in association with Abcam

TOPICS: Diseases of aging I: metabolic syndromes
Diseases of aging II: cancer
Diseases of aging III: neurodegeneration
Organismal aging: vertebrates | The aging proteome | The aging genome

REGISTER AT: www.abcam.com/neuro2009

CONFERENCE

**Abstract Submission Deadline
February 28, 2009**



**34th FEBS
Congress**

July 4 - 9, 2009
Prague, Czech Republic



Life's Molecular Interactions

- Cells' Modular Components
- Social Life of the Cell
- Organism, the Network of Interactions



www.febs2009.org

AWARDS



Department for
Innovation,
Universities &
Skills



Invitation to nominate

The Royal Society Rosalind Franklin Award is designed to promote women in Science, Technology, Engineering and Mathematics (STEM) and is funded by the Department for Innovation, Universities and Skills (DIUS).

The award, consisting of a medal and £30,000, is made annually to an individual for an outstanding contribution to any area of STEM. As part of the nomination process nominees are asked to put forward a proposal for a project that would raise the profile of women in STEM in their host institution and/or field of expertise in the UK. The recipient of the award will be expected to spend a proportion of the £30,000 award fund on implementing their project.

There are no restrictions on the age of nominees, but it is anticipated that the award will be made to someone in their mid-career and actively involved in scientific research. Nominations are welcomed for both women and men.

For full details of the Award and guidelines for nomination, including the online nomination forms, visit royalsociety.org/franklin

Closing date for nominations: Monday 23 February 2009

POSITIONS OPEN

Stanford University School of Medicine, Department of Microbiology and Immunology, invites applications for a tenure-track faculty position at the **ASSISTANT PROFESSOR** level, although candidates at the Associate Professor level will be considered. We are looking for highly interactive candidates with an outstanding record of research achievement in the area of microbiology and/or immunology. The predominant criterion for appointment in the University tenure line is a major commitment to research and teaching.

The Department of Microbiology and Immunology (website: <http://microimmuno.stanford.edu>) is a collegial, interactive, and interdisciplinary environment that spans research areas of bacteriology, virology, parasitology, and immunology. Current faculty use a variety of classical and modern approaches to study aspects of host-microbe interactions. Applicants are expected to establish a vigorous and innovative research program that complements the current research of the Department. Responsibilities will also include teaching graduate, undergraduate, and/or medical students.

Interested applicants should submit curriculum vitae, a statement of research objectives, and a teaching statement, and arrange for three letters of reference to be sent directly to:

Chair, Search Committee
c/o Mayumi Beppu

Department of Microbiology and Immunology
Stanford University School of Medicine
Fairchild Science Building
299 Campus Drive
Stanford, CA 94305-5124

Applications will be accepted until March 2, 2009.

Stanford University is an Equal Opportunity Employer and is committed to increasing the diversity of its faculty. It welcomes nominations of and applications from women and members of minority groups as well as others who would bring additional dimensions to the University's research, teaching, and clinical missions.

FACULTY POSITIONS

Human Anatomy and Physiology

The Division of Basic Pharmaceutical Sciences (DBPS) invites applications for two 12-month, tenure-track positions at the rank of **ASSISTANT** or **ASSOCIATE PROFESSOR** starting August 2009. Candidates for these positions must have a Ph.D. in a biological or biomedical sciences field with an emphasis on human anatomy and/or physiology. The primary responsibility of both positions is to teach human anatomy and physiology lecture and laboratory courses in the Pharm.D. curriculum and to participate in other courses in the curriculum related to their expertise. The successful candidate will also be expected to establish a funded research program in his or her area of interest. Preference will be given to candidates with previous teaching experience. Applicants should submit (i) a letter of interest, (ii) curriculum vitae, (iii) a statement of teaching philosophy (including background for teaching human anatomy and/or physiology), (iv) a plan for developing research, and (v) the names and contact information for at least three references to: **Tarun K. Mandal, Ph.D., Chair, DBPS Faculty Search Committee, Xavier University College of Pharmacy, 1 Drexel Drive, New Orleans, LA 70125. E-mail: dbpsjob@xula.edu; telephone: 504-520-7650; fax: 504-520-7954.**

Xavier University of Louisiana is an Equal Opportunity and Affirmative Action Employer. Women, minorities, and persons with disabilities are encouraged to apply.

POSTDOCTORAL POSITION available in the laboratory of **Dr. Venigalla Rao**, Biology Department, the Catholic University of America, Washington, D.C., to work on the development of novel multicomponent vaccines using bacteriophage T4 display (website: <http://faculty.cua.edu/rao/>). Research involves recombinant DNA construction and protein biochemistry. Candidate will have Ph.D. in biological sciences and strong background in molecular biology and biochemistry. E-mail curriculum vitae and names of three references to e-mail: rao@cua.edu. CUA is an Equal Opportunity Employer.

POSITIONS OPEN



The U.S. Department of Agriculture, Agricultural Research Service, San Joaquin Valley Agricultural Research Center, Parlier, California, invites applications for a **RESEARCH PLANT PATHOLOGIST** GS-12/13/14 (\$67,613.00 to \$123,519.00 per annum). Incumbent conducts research independently and as part of a team on the biology of *Xylella fastidiosa* (Xf) strains that cause Pierce's disease (PD) of grapevines, almond leaf scorch, oleander leaf scorch, alfalfa dwarf, and other xylella and exotic and invasive diseases of agronomic, horticultural, and ornamental crops (announcement ARS-X9W-0090). The candidate must have the ability to formulate new concepts and hypotheses and to develop new techniques and approaches to solve problems, with particular emphasis on biotic and abiotic factors affecting pathogenesis and development of novel, biologically based control methods. This is a competitive, permanent appointment and *U.S. citizenship is required*. Vacancy announcements and where to apply can be found at website: <http://www.usajobs.com> or contact: **Drake Stenger, telephone: 559-596-2922**. Applications must be received by March 6, 2009. The USDA is an Equal Opportunity Provider and Employer.

DEPARTMENT of MEDICINE University of California, San Francisco

The Department of Medicine at the University of California, San Francisco is recruiting for physician-scientists engaged in basic science research. Candidates must have demonstrated potential to lead a first-rate, independent research program and be American Board of Internal Medicine-certified. Successful candidates will be eligible for faculty membership in the Biomedical Sciences Graduate Program and for membership in the recently created Institute for Molecular Medicine. Outstanding research space and generous startup packages will be provided. Appointment will be made at the **ASSISTANT/ASSOCIATE/PROFESSOR** level in any relevant division of the Department depending on seniority and experience of the successful candidate.

Send curriculum vitae, a brief statement of your research plans, and three letters of reference to **Dean Sheppard, M.D., Chair, Search Committee, Director, Lung Biology Center**. Send materials to e-mail: dean.sheppard@ucsf.edu and/or by mail to **University of California San Francisco, P.O. Box 2922, San Francisco, CA 94143-2922**. UCSF seeks candidates whose experience, teaching, research, or community service has prepared them to contribute to our commitment to diversity and excellence. UCSF is an Equal Opportunity/Affirmative Action Employer. The University undertakes affirmative action to assure equal employment opportunity for underrepresented minorities and women, for persons with disabilities, and for covered veterans. All qualified applicants are encouraged to apply, including minorities and women.

FACULTY POSITION

Molecular Biology and Genetics

The Department of Biochemistry and Molecular Biology at the Penn State University College of Medicine invites applications for a full-time, tenure-track position at any level. Research programs should address fundamental questions in molecular biology and genetics, epigenetics, and/or genomics. For additional information, please visit website: <http://www.hmc.psu.edu/college/faculty/index.htm>. Applicants should submit curriculum vitae and a brief statement of research plans and should arrange to have three letters of reference sent to: **Judith S. Bond, Ph.D., Professor and Chair, Department of Biochemistry and Molecular Biology H171, The Penn State University College of Medicine, Hershey, PA 17033. E-mail: jbond@psu.edu**. Applications will be evaluated as received; submissions are encouraged by March 15, 2009. Penn State is committed to Affirmative Action, Equal Opportunity, and diversity.

POSITIONS OPEN

RESEARCH ASSISTANT PROFESSOR Department of Infectious Diseases and Microbiology University of Pittsburgh Graduate School of Public Health

The Department of Infectious Diseases and Microbiology in the University of Pittsburgh's Graduate School of Public Health invites applications for a Research Assistant Professor in the area of viral immunology. Applicants must have a Ph.D. or M.D. degree or equivalent. The Department is searching for an individual with extensive expertise in T cell mediated immunity to HIV and HCV antigens, as well as flow cytometry-based assays. The selected individual will be required to plan and direct immunological experiments to test T cell mediated reactivity to viral epitopes in human subjects, demonstrate extensive knowledge of multicolor flow cytometry, and supervise technical personnel and students. Special consideration will be given to those candidates with extensive experience in writing manuscripts and grant applications. The candidate will have flexibility to develop his/her own collaborative project with the principal investigator. Applicants should submit, to e-mail: fjenkins@pitt.edu, curriculum vitae, statement up to three pages of research interests and future plans, and names and contact details of three references to: **Dr. Frank Jenkins, Chair, Research Assistant Professor Search Committee, Department of Infectious Diseases and Microbiology, A419 Crabtree Hall, Graduate School of Public Health, University of Pittsburgh, 130 DeSoto Street, Pittsburgh, PA 15261**. Review of applications will commence upon receipt and will continue until the position is filled. The University of Pittsburgh is committed to Affirmative Action, Equal Opportunity, and the diversity of its work force.

Two **POSTDOCTORAL POSITIONS** are available to study oxidative stress signaling in cell survival and death. First position will investigate Nrf2 and Irf2 (Keap1) signaling in oxidative stress, cell survival, and cancer. It involves studying oxidative stress-induced modifications of Nrf2 and Irf2 by serine/threonine and tyrosine kinases and redox factors and generation of knockout/transgenic mice models of carcinogenesis. Second position will study stress responsive proteins NQO1 and NQO2 regulation of tumor suppressor p53 and related factors in oxidative stress and oncogenesis. It involves studying protein-protein interaction, protein modifications and degradation, apoptosis, and generation of knockout/transgenic mice models. Experience in biochemical and molecular biology techniques is essential. Applicants should submit curriculum vitae and names/e-mail addresses of three references. Contact: **Anil K. Jaiswal, Ph.D., Professor and Director, Department of Pharmacology, University of Maryland School of Medicine, 655 West Baltimore Street, Baltimore, MD 21201, or e-mail: ajaiswal@som.umaryland.edu**. UMB is an Affirmative Action/Equal Opportunity Employer.

MOLECULAR DIAGNOSTIC POSTDOCTORAL POSITION available at UCLA to study the basic and clinical sciences for molecular diagnostics using oral fluids. The UCLA Collaborative Oral Fluid Diagnostic Research Center focuses and spearheads basic and clinical research for saliva diagnostics for high impact disease detection (website: <http://hspp.dent.ucla.edu/wonglab/>). Studies include biomarker discovery and validation, biomarker characterizations. Excellent working and career development environment. Applicants with Ph.D., M.D./Ph.D., and D.D.S./Ph.D. in biology may send curriculum vitae and references to e-mail: dtw@ucla.edu.

MARKETPLACE

For COLLAGEN Detection...
Connect with Cosmo Bio

ELISAs to measure COLLAGENs: Type 1 (hu); Type 2 (hu, ms, rt, +). ELISAs to measure ANTI-COLLAGEN ANTIBODIES: Type 1 (hu); Type 2 (hu, ms, rt, +). SPECIFIC ANTIBODIES: Types 1, 2, 3, 4, 5, 6, 7, 8, 9, 10, 11, 12, 14.
Research Products from Japan
www.cosmobio.com COSMO BIO CO., LTD.
Incorporated in the United States

High Specificity with any Template Amount

SYBR® Premix Ex Taq™ II

The Perfect Real Time series introduces a new addition, the SYBR® Premix Ex Taq™ 2 reagent for Real Time PCR. This reagent has improved reaction specificity and performance and is compatible with a variety of different Real Time machines. The SYBR® Premix Ex Taq™ 2 effectively limits primer dimerization and non-specific amplification and accurately measures a wide range of concentrations from very small amounts of template. SYBR® Premix Ex Taq™ 2, the latest PCR premix from Takara, is unsurpassed for high-speed, high-specificity application results.

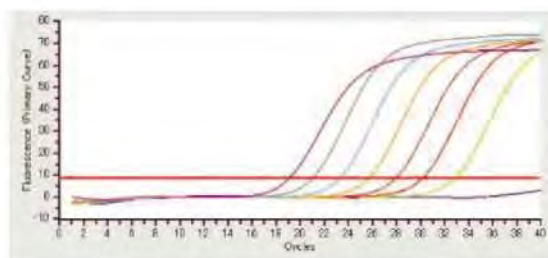
Higher Specificity: No more non-specific amplification from primer dimers, even when starting with a minute amount of template.

Wide Range of Detection: accurate quantification over 8 log of magnitude.

Simple Protocol: Ready to use premix type. Short reaction time due to the antibody mediated hot start technology.

Fast Reaction Times: Shorter reaction times due to optimized buffer. Applicable for use with Fast PCR instruments.

Versatility: Use on any qPCR instrument.



Amplification of cDNA from the Mouse gene YWHAZ using Takara's Thermal Cycler Dice® Real Time System*.
6.4 pg-100 ng of total RNA from mouse liver was used to transcribe cDNA for amplification. (*Not available in Europe)

Takara Ex Taq™ is a trademark of Takara Bio Inc. SYBR® is a registered trademark of Molecular Probes, Inc. Purchase of this product includes an immunity from suit under patents specified in the product insert to use only the amount purchased for the purchaser's own internal research. No other patent rights are conveyed expressly, by implication, or by estoppel. Further information on purchasing licenses may be obtained by contacting the Director of Licensing, Applied Biosystems, 850 Lincoln Centre Drive, Foster City, California 94044, USA. Takara Bio's Hot-Start PCR-Related products are licensed under U.S. Patent 5,338,671 and 5,587,287 and corresponding patents in other countries.

Takara

For more information
www.takara-bio.com

Japan:
Takara Bio Inc.
+81 77 543 7247
www.takara-bio.com

USA:
Takara Bio USA
A division of Clontech Laboratories, Inc.
888-251-6618
www.takarabio.com

Europe:
Takara Bio Europe S.A.S.
+33 1 3904 6880
www.takara-bio.eu

China:
Takara Biotechnology
(Dalian) Co., Ltd.
+86 411 8764 1681
www.takara.com.cn

Korea:
Takara Korea
Biomedical Inc.
+82 2 2081 2525
www.takara.co.kr



© 2009 Thermo Fisher

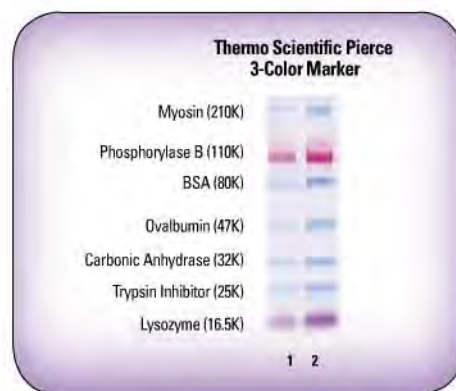
**Double the Precise, not the price:
Get two gels for the price of one.**

Thermo Scientific Precise Protein Gels are cast in a durable plastic cassette using a neutral pH buffer that prevents poly-acrylamide breakdown. The gels are individually packaged and are ready to run with no comb or tape to remove. They are available in both gradient and fixed-concentrations and in 10-, 12- and 15-well formats.

Highlights:

- Easy-to-load, large-volume wells with durable plastic dividers
- Long shelf life – 12-month guarantee ensures consistent performance
- Easy to open – no need for special tools
- Short run time – 45-minute run time provides results quickly
- 1 mm thick gels stain quickly and with high sensitivity using coomassie, fluorescent and silver stains

Visit www.thermo.com/pierce or call 800-874-3723 or 815-968-0747 for details (offer expires 3/31/2009).



Thermo Scientific Pierce MW Markers.

Single-use packaging maintains marker integrity.

Moving science forward

Thermo
SCIENTIFIC

Part of Thermo Fisher Scientific